

Biophysical Characterization of the Interactions of Nucleic Acids and Ferrocenyl Amphiphiles

By

John P. E. Muller

A dissertation submitted in partial fulfillment of
the requirements for the degree of

Doctor of Philosophy
(Chemical Engineering)

at the

UNIVERSITY OF WISCONSIN-MADISON

2012

Date of final oral examination: 10/24/12

The dissertation is approved by the following members of the Final Oral Committee:

Nicholas L. Abbott, Professor, Chemical Engineering
David M. Lynn, Professor, Chemical Engineering
Daniel J. Klingenberg, Professor, Chemical Engineering
Christos T. Maravelias, Assistant Professor, Chemical Engineering
Sandro Mecozzi, Associate Professor, Pharmaceutical Sciences

© Copyright by John P. E. Muller 2012

All Rights Reserved

Abstract

The research described in this thesis focuses on characterization of the interactions between a redox-active ferrocenyl amphiphile, (11-ferrocenylundecyl)dimethylammonium bromide (BFDMA), and nucleic acids (DNA) using a range of physicochemical techniques. It is motivated by a previous observation that, whereas multilamellar aggregates of reduced BFDMA and DNA (lipoplexes) transfect cells with high efficiency, amorphous lipoplexes of electrochemically oxidized BFDMA and DNA lead to low levels of transfection. Therefore, BFDMA provides a novel redox-based approach to the mediation of cell transfection.

The results presented herein move beyond this observation using cell transfection assays in combination with small angle x-ray and neutron scattering and cryo-TEM analysis to demonstrate and characterize the ability of BFDMA to spontaneously aggregate with dioleoylphosphatidylethanolamine (DOPE) and DNA forming serum-stable, inverse hexagonal nanostructured, lipoplexes able to mediate the delivery of DNA to mammalian cells *in vitro* in media containing physiologically relevant levels of serum.

A second study reported in this thesis demonstrates the ability of BFDMA to be chemically oxidized using Fe(III)sulfate in the presence of DNA. When excess Fe ions are chelated using EDTA, the lipoplexes of oxidized BFDMA and DNA do not transfect cells with high efficiency. However, when the chemical reducing agent,

ascorbic acid is used, the efficiency of cell transfection increased substantially, demonstrating chemical control of the oxidation state and transfection efficiency of lipoplexes of BFDMA and DNA.

Finally, this thesis reports an investigation of how self-assembly impacts the rate of electrochemical oxidation of BFDMA. BFDMA spontaneously adsorbs to Pt disk electrodes, forming an adsorbed layer blocking the electrode from exchanging electrons with BFDMA diffusing in bulk solution. In contrast, (11-ferrocenylundecyl)trimethylammonium bromide (FTMA), a similarly Pt electrode adsorbing ferrocenyl amphiphile, allows exchange of electrons with species in bulk solution across the adsorbed layer. Differential scanning calorimetry and dynamic light scattering results combined to show that the phase state, not the aggregate size, dominates the interfacial electrochemical activity of these amphiphilic redox-mediators.

The *in vitro* based studies and insight obtained from supporting physicochemical characterization presented herein provide important steps toward the development of redox-active lipid materials that permit spatial and/or temporal control over cell transfection.

*To my mother, wife and daughter,
what better representation can I give of my past, present
and future sources of support and happiness?*

Acknowledgements

The work presented in this thesis would not have been possible without the support of my family, friends, and colleagues.

I would like to thank my advisors, Professors Nick Abbott and Dave Lynn. Their input and direction have been essential elements in bringing me to the completion of my PhD. Their time spent on the review and discussion of my work has been, and always will be, greatly appreciated. I have seen them as the ideal gate keepers for the quality of my work. It is in this way that I have felt so strongly supported.

I would also like to thank my collaborators, Ishi Talmon and his group for the use of their Cryo-TEM facilities and for their hospitality during my visit to their lab, and Yuki Kondo and his group for their supply of synthesized chemicals required for my research.

I would next like to acknowledge my fellow group members, both past and present, with whom I have shared office space, coffee filters, pipettes and indeed many an intellectual discussion during my time at UW-Madison. First, the Abbott group, Aaron Lowe, Julie Last, Gaurav Pranami, Ankit Agarwal, Zhongqiang Yang, Elise Huang, I-Hsin Lin, Xiaoyang Liu, Yiqun Bai, Claribel Acevedo, Jacob Hunter, Rebecca Carlton, Daniel Abras, Rishabh Jain, Derek Ma, Dan Miller, Lie Na Tan, Matt Wang, Peter Mushenheim, Emre Bukusoglu, Ressa Abbasi, Mohit Goel, and Xiaoguang Wang and then also the Lynn group, Christopher Jewell, Nathaniel Fredin,

Bin Sun, Mike Kinsinger, Maren Buck, Eric Saurer, Ryan Flessner, Selin Aytar, Adam Broderick, Yashira Zayas-Gonzalez, Yan Yu, Matt Wang, Mike Kratochvil, and Matt Carter. This is quite the list and all within it have helped me along my way. To all of you, thank you. From this list I would like to make a few special mentions. Chris and Xiaoyang, for their help in training me on the cell based assays and electrochemical techniques that were ultimately the core of my experimental work. Without this help I would have spent a significantly longer period of time getting up to speed on my research. The person to whom I owe the most thanks on this list of illustrious Engineers is of course, Selin, my partner on my BFDMA project work. Daily, she has been my friend, my rock and my inspiration. Thank you, Selin, for your patience with my moods, dedication to our research goals, and encouragement when the way did not seem clear. Without you, this experience would not have been half the fun it was.

I would like to thank other Chemical Engineering graduate students and their partners who subsequently became great friends to me over the last five years, Ben and Stina Tillotson, Gordon Freeman and Jesse Pfammatter, and Bernardo and Tanya Yanez. It has been emotional and please do not be strangers.

And to my friends outside the walls of Engineering Hall. I have made many and to those of you who count themselves my friend, you know who you are, thanks for the good times. Special thanks to our best friends Chris Tall, Sonya Nikiforov Griffin and Jake Griffin. Where do I start? From day one in a stormy Madison on 13th August 2007, fresh off the plane, you have generously shared your homes and your

friendship and you have made Madison feel like home. For poker nights, to road trips, to always having a place for us at your Thanksgiving table, to officiating our wedding, and finally to being surrogate aunts and uncles to our daughter, thank you. We look forward to many more good times in the future.

Finally, I would like to thank my family. The hardest thing about moving from the UK to Madison, WI was to leave behind such loving and close family members. Then, the hardest thing about being here in Madison has been not being closer to my mother during her last few years. While I feel I missed many opportunities to be close with her in coming here to complete my PhD, I know for a fact she would not have had it any other way. This brings me to my girls, my wife, Erinn and daughter, Cora. Without you it just does not make sense. Thank you for allowing me the time and space to become a better Engineer, I feel it will allow me to in turn become a better husband and father in our wonderful future together.

With my sincere thanks to all,

John

Table of Contents

Abstract	i
Acknowledgments	iv
Table of Contents	vii
List of Figures, Schemes, and Tables	x
Chapter 1: Introduction	1
1.1 Background and Motivation	1
1.2 Thesis Overview	4
1.3 References	10
Chapter 2: Incorporation of DOPE into Lipoplexes formed from.....	14
a Ferrocenyl Lipid leads to Inverse Hexagonal Nanostructures	
that allow Redox-Based Control of Transfection in High Serum	
2.1 Introduction.....	14
2.2 Experimental section.....	19
2.2.1 Materials	19
2.2.2 Experimental methods	20
2.3 Results and discussion	25
2.3.1 Influence of DOPE on the transfection efficiency of.....	26
lipoplexes containing reduced BFDMA	
2.3.2 Influence of DOPE on the physical properties and	31
nanostructure of lipoplexes containing reduced BFDMA	
2.3.3 Influence of oxidation state of BFDMA on the transfection	41
efficiency, physical properties, and nanostructure of	
lipoplexes containing BFDMA and DOPE	
2.4 Conclusions	47
2.5 Acknowledgements	49
2.6 References	49
2.7 Supplemental materials	56
2.8 Supplemental materials references	70
Chapter 3: The Inverse Hexagonal Phase formed in Complexes of a Redox.....	71
Active Ferrocenyl Amphiphile, DOPE and DNA is Observed Using	
Cryo-TEM	

3.1 Introduction	71
3.2 Experimental section	73
3.2.1 Materials	73
3.2.2 Experimental methods	73
3.3 Results and discussion	76
3.3.1 Characterization of BFDMA-DOPE lipoplexes using Cryo-TEM	76
3.3.2 Characterization of BFDMA-DOPE lipoplexes using SAXS	82
3.3.3 Characterization of BFDMA and BFDMA-DOPE	86
using Cryo-TEM	
3.3.4 Treatment of lipoplexes of oxidized BFDMA and DOPE	88
with AA in the presence of cells	
3.4 Conclusions	90
3.5 Acknowledgements	91
3.6 References	92
Chapter 4: Presence of DOPE in Redox Active Ferrocenyl Amphiphile	93
Containing Lipoplexes Provides a Fusogenic Internalization Capability to Redox-based Control of Cell Transfection	
4.1 Introduction	93
4.2 Experimental section	95
4.2.1 Materials	95
4.2.2 Experimental methods	96
4.3 Results and discussion	98
4.3.1 Transgene expression of lipoplexes at 4°C and 37°C	98
4.4 Conclusions	103
4.5 Acknowledgements	104
4.6 References	104
Chapter 5: Chemical Oxidation of a Redox-Active, Ferrocene-Containing	106
Cationic Lipid: Influence on Interactions with DNA and Characterization in the Context of Cell Transfection	
5.1 Introduction	106
5.2 Experimental section	109
5.2.1 Materials	109
5.2.2 Experimental methods	110
5.3 Results and discussion	116
5.3.1 Characterization of the chemical oxidation of reduced	116
BFDMA using Fe ³⁺	
5.3.2 Characterization of cell transfection mediated by lipoplexes	119
of chemically oxidized BFDMA	
5.3.3 Characterization of the zeta potentials of lipoplexes of	123
chemically oxidized BFDMA	

5.3.4	Characterization of lipoplex nanostructures using SANS125 and cryo-TEM	125
5.3.5	Investigation of potential influences of residual Fe ²⁺ and129 Fe ³⁺ on the properties and behaviors of lipoplexes of chemically oxidized BFDMA	129
5.4	Conclusions135	135
5.5	Acknowledgements136	136
5.6	References137	137
5.7	Supplemental materials140	140
Chapter 6:	Influence of the Phase State of Self-Assembling Redox-Active142 Mediators on their Electrochemical Activity	142
6.1	Introduction142	142
6.2	Experimental section146	146
6.2.1	Materials146	146
6.2.2	Experimental methods146	146
6.3	Results and Discussion150	150
6.3.1	Bulk electrolysis of BFDMA and FTMA150	150
6.3.2	Cyclic voltammetry154	154
6.3.3	Cyclic voltammetry at a rotating disc electrode162	162
6.3.4	Investigation of the effects of heating BFDMA and FTMA168	168
6.4	Conclusions174	174
6.5	Acknowledgements175	175
6.6	References176	176
6.7	Supplemental materials180	180
6.7.1	Further discussion of CV results from Figure 6.3181	181
6.7.2	Investigation of the effects of preheating BFDMA185	185
6.8	Supplemental materials references186	186
Chapter 7:	Summary and Recommendations for Future Studies.....187	187
7.1	Summary187	187
7.2	Future Studies: <i>In vivo</i> studies of lipoplexes of BFDMA _{RED} -DOPE.191 and activation towards transgene expression in the presence of serum	191
7.3	Future Studies: Specific ion effects on the electrochemical194 activity of BFDMA	194
7.4	Future Studies: Structural variations around BFDMA198	198
7.5	References199	199
Appendix I:	Influence of Biological Media on the Structure and Behavior of.....201 Ferrocene-Containing Cationic Lipid/DNA Complexes Used for DNA Delivery	201
Appendix II:	Addition of ascorbic acid to the extracellular environment activates.....208 lipoplexes of a ferrocenyl lipid and promotes cell transfection	208

List of Figures, Schemes and Tables

Chapter 1:

Figure 1.1.....	2
Figure 1.2.....	4
Figure 1.3.	5

Chapter 2:

Figure 2.1.	16
Figure 2.2.	27
Figure 2.3.	29
Figure 2.4.	33
Figure 2.5.	36
Table 2.1.	36
Figure 2.6.	44
Figure 2.7.	56
Figure 2.8.	56
Figure 2.9.	57
Figure 2.10.	60
Figure 2.11.	61
Figure 2.12.	62
Figure 2.13.	63
Figure 2.14.	64
Figure 2.15.	65
Figure 2.16.	66
Figure 2.17.	68
Figure 2.18.	69
Table 2.2.	70

Chapter 3:

Figure 3.1.	78
Figure 3.2.	79
Figure 3.3.	84
Table 3.1.....	85
Figure 3.4.	86
Figure 3.5.	88
Figure 3.6.	90

Chapter 4:

Figure 4.1.	100
------------------	-----

Chapter 5:

Figure 5.1.	107
Figure 5.2.	118
Figure 5.3.	121
Figure 5.4.	122
Table 5.1.	123
Figure 5.5.	126
Figure 5.6.	127
Figure 5.7.	132
Figure 5.8.	133
Figure 5.9.	140
Figure 5.10.	141

Chapter 6:

Figure 6.1.	143
Figure 6.2.	152
Figure 6.3.	155
Table 6.1.	159
Figure 6.4.	161
Scheme 6.1.	162
Figure 6.5.	164
Figure 6.6.	166
Figure 6.7.	168
Table 6.2.	170
Figure 6.8.	172
Figure 6.9.	173
Figure 6.10.	180
Figure 6.11.	180
Figure 6.12.	183
Figure 6.13.	184
Figure 6.14.	185

Chapter 7:

Table 7.1.	195
Table 7.2.	196

Chapter 1: Introduction

1.1 Background and Motivation

The delivery of DNA to cells (a process known as cell transfection) using complexes formed between DNA and polymeric or lipid based vectors has been a subject of great interest over the past twenty years and has applications in a wide range of fields from *in vitro* applications within basic biological and biomedical research¹⁻¹⁰ and tissue engineering,¹¹⁻¹⁸ to *in vivo* applications such as the development of gene based therapies.¹⁹⁻³³ The majority of these complexes are, by design, able to transfect cells from the time of their formation and, thus, they do not readily permit control over ‘activation’ or ‘inactivation’ in ways that provide methods for *spatial* (the ability to limit the internalization of DNA to a sub-population of cells within a larger cell colony) and *temporal* (the ability to define the specific timing of internalization of DNA) control over delivery and/or internalization. Achieving *extracellular* control over cell transfection, i.e. designing a vector for the delivery of DNA to cells that can be triggered with spatial and/or temporal control, would therefore provide a new capability. For example, the ability to determine the timing and location of cell transfection would allow use of a lower amount of lipid and DNA, while achieving a desired or threshold level of internalization.

The research described within this thesis aims to build upon prior work, in which extracellular control over the efficiency of cell transfection was demonstrated using a novel redox-active ferrocenyl amphiphile, bis(11-ferrocenyldodecyl)-

dimethylammonium bromide (BFDMA) (Figure 1.1).³⁴⁻⁴⁰ This was achieved through control over the redox state of BFDMA (complexes of oxidized BFDMA combine with DNA to mediate low levels of cell transfection whereas complexes of reduced BFDMA combine with DNA to mediate significantly higher levels of cells transfection). These prior studies were performed *in vitro* in serum-free media.³⁴ In an effort to potentially broaden the uses of these redox-active lipoplexes to serum containing systems, and thereby enable a wider range of *in vitro* or even *in vivo* based applications, the research presented within this thesis moves to provide a system that is stable in the presence of serum, and to understand the physical properties and nanostructure of such systems through use of biophysical and structural characterization techniques.

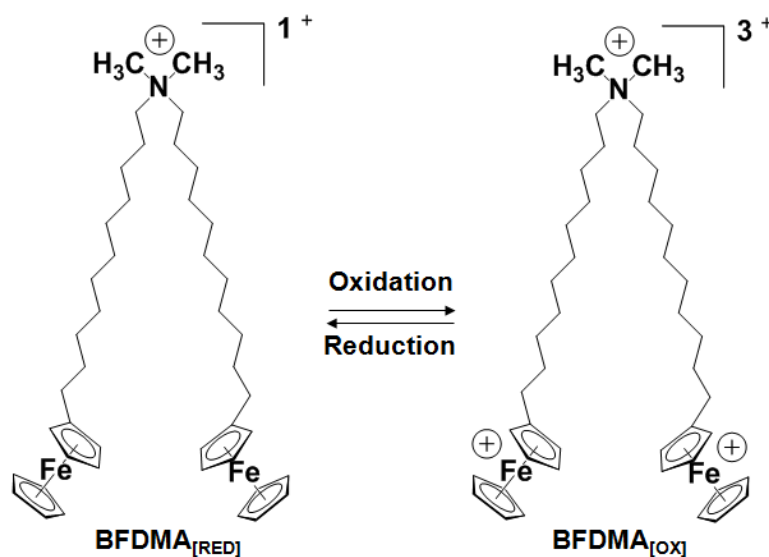


Figure 1.1. Structure of BFDMA, a redox-active cationic lipid. The charge of BFDMA can be cycled between +1 (reduced) and +3 (oxidized) by oxidation or reduction of the ferrocenyl groups at the end of each hydrophobic tail

Because ferrocenyl groups can be oxidized and reduced readily and reversibly (using either chemical or electrochemical methods),^{41, 42} BFDMA also offers a basis for active control over the ability of lipoplexes to transfect cells (e.g., by application of a chemical or electrochemical stimulus to transform the oxidation state of BFDMA). Prior studies demonstrated that it is possible to reduce the BFDMA in lipoplexes of oxidized BFDMA by treatment with chemical reducing agents (e.g., glutathione or ascorbic acid),^{36, 40} and that these treatments can be used to influence physical properties that activate these lipoplexes toward transfection. A recent publication also demonstrates that chemical reduction can be used to activate lipoplexes of oxidized BFDMA in culture media, in the presence of cells, to initiate transfection.⁴⁰ Prior studies have synthesized reduced BFDMA directly and then obtained oxidized BFDMA by subsequent electrochemical oxidation.^{34-38, 40} While this electrochemical approach is useful, complete electrochemical oxidation of BFDMA generally requires long times (e.g., 2-3 hours) at high temperatures (75 °C). The second focus of this thesis is to address these and other practical issues associated with electrochemical oxidation by investigating approaches to the chemical oxidation of BFDMA. We report that Fe(III)sulfate can be used to oxidize reduced BFDMA rapidly, quantitatively, and at ambient temperatures.

Finally, we compare and contrast the electrochemical activity of BFDMA, and a single tail analog, (11-ferrocenylundecyl) trimethylammonium bromide (FTMA)⁴³⁻⁴⁶ (Figure 1.2). It has been previously observed that the rate of oxidation of BFDMA is slow relative to FTMA.^{45, 47-50} The work reported in this study is motivated by a desire

to obtain a high degree of electrochemical control over the change in oxidation state of BFDMA as well as to understand how the differences in the self-assembled states of these amphiphilic redox-active species impact the rate of oxidation and reduction of the amphiphiles at electrodes.

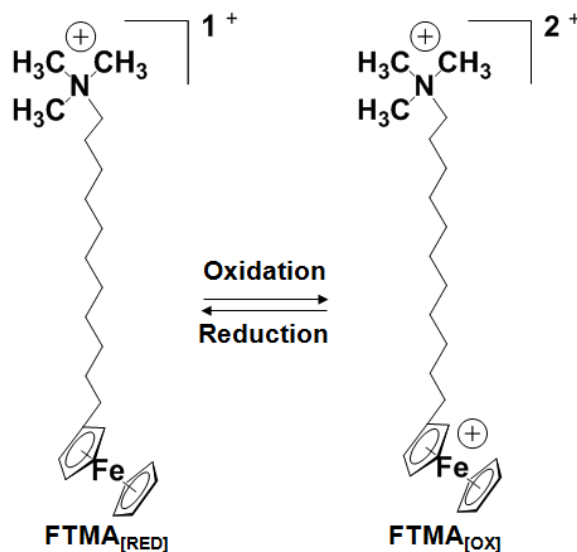


Figure 1.2. Molecular structure of FTMA ((11-ferrocenylundecyl)-trimethylammonium bromide)

1.2 Thesis Overview

The work in this thesis focuses on three research topics, all centered around a redox-active ferrocenyl amphiphile, bis(11-ferrocenylundecyl)-dimethylammonium bromide (BFDMA). The first topic focuses on the ability of BFDMA, when initially mixed with a zwitterionic lipid, dioleoylphosphatidylethanolamine (DOPE) (Figure 1.3), to form aggregates with DNA (lipoplexes) that can be used as a vector for the internalization of DNA to cells in serum-containing media. The second topic focuses on chemical oxidization of BFDMA using a chemical oxidizing agent, Fe(III)sulfate

and, subsequently, reports cell transfection data to show that control of the efficiency of transfection of cells using BFDMA-containing lipoplexes can be achieved through chemical means of control over the oxidation state of BFDMA. The third topic focuses on defining the differences in the phase states of BFDMA and a single tailed, redox-active analogue, (11-ferrocenylundecyl)trimethylammonium bromide (FTMA) and how the phase states impact rates of electrochemical oxidation and reduction of the surfactants. Each study is written in such a way as it can be understood when read alone, separately from the other studies described in the thesis.

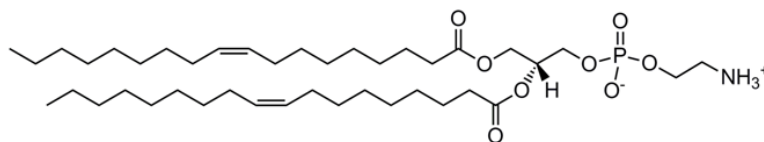


Figure 1.3. Structure of dioleoylphosphatidylethanolamine (DOPE)

Chapter 2 reports small angle X-ray and neutron scattering measurements that reveal that mixtures BFDMA and DOPE spontaneously form lipoplexes with DNA that exhibit inverse hexagonal nanostructure (H_{II}^c). In contrast to lipoplexes of DNA and BFDMA only, which exhibit a multilamellar nanostructure (L_a^c) and limited ability to transfect cells in the presence of serum proteins, we measured lipoplexes of BFDMA and DOPE with the H_{II}^c nanostructure to survive incubation in serum and to expand significantly the range of media compositions (e.g., up to 80% serum) over which BFDMA can be used to transfect cells with high efficiency. Importantly, we also measured the oxidation state of the ferrocene within the BFDMA/DNA lipoplexes to have a substantial influence on the transfection efficiency of the

lipoplexes in media containing serum. Specifically, whereas lipoplexes of reduced BFDMA and DOPE transfect cells with high efficiency, lipoplexes of oxidized BFDMA and DNA lead to low levels of transfection. Complementary measurements using SAXS reveal that the low transfection efficiency of the lipoplexes of oxidized BFDMA and DOPE correlates with the presence of weak Bragg peaks and thus low levels of H_{II}^c nanostructure in solution. Overall, these results provide support for our hypothesis that DOPE-induced formation of the H_{II}^c nanostructure of the BFDMA-containing lipoplexes underlies the high cell transfection efficiency measured in the presence of serum, and that the oxidation state of BFDMA within lipoplexes with DOPE substantially regulates the formation of the H_{II}^c nanostructure and thus the ability of the lipoplexes to transfect cells with DNA. More generally, the results presented in this chapter suggest that lipoplexes formed from BFDMA and DOPE may offer the basis of approaches that permit active and external control of transfection of cells in the presence of high (physiologically relevant) levels of serum.

Chapter 3 reports cryogenic transmission electron microscopy images that show the presence of a highly ordered H_{II}^c nanostructure in lipoplexes of BFDMA_{RED}-DOPE/DNA in both OptiMEM media and OptiMEM media with 10% (v/v) bovine serum. Analysis of lipoplexes of BFDMA_{OX}-DOPE/DNA, in contrast, show relatively poor ordering within the aggregates imaged in both media. Complementary small angle x-ray scattering analysis showed quantitative agreement with these cryo-TEM results in terms of the magnitude of the repeat structures within these ordered aggregates. Subsequent analysis of lipoplexes of BFDMA_{OX}-DOPE/DNA treated with

a ten times molar excess of ascorbic acid showed a high degree of ordered H_{II}^c structure in OptiMEM media, but significantly less ordering in OptiMEM media with 10% (v/v) bovine serum. Finally, a luciferase assay using COS-7 mammalian cells compared the cell transfection efficiency between lipoplexes of BFDMA_{RED}-DOPE/DNA, lipoplexes of BFDMA_{OX}-DOPE/DNA and lipoplexes of BFDMA_{OX}-DOPE/DNA treated with a ten times molar excess of ascorbic acid, and showed that AA activates lipoplexes of BFDMA_{OX}-DOPE/DNA towards transfection in serum free media but not in media containing 10% (v/v) bovine serum. This result suggests that the constituents of bovine serum that are preventing reformation of the ordered H_{II}^c could also be leading to this difference in efficiency of transgene expression. Overall, these observations combine to provide cryo-TEM-based evidence of H_{II}^c nanostructure of lipoplexes of BFDMA and DOPE for the first time as well as initial characterization of lipoplexes of BFDMA_{OX}-DOPE/DNA with a chemical reducing agent, ascorbic acid.

Chapter 4 also builds upon the work presented in Chapter 2 and focuses on initial investigations using temperature-dependent cell transfection assays to provide insight into the mechanism of internalization of the mixed lipid lipoplexes of BFDMA-DOPE/DNA introduced in Chapter 2. Specifically, relatively high cell transfection efficiencies are measured at 4 °C, a temperature known to greatly reduce endocytotic routes of internalization. This result is generally consistent with a fusogenic route of cell transfection, thus hinting that BFDMA may be able to be used

to exercise control over the efficiency of cell transfection when internalization is via membrane fusion.

Chapter 5 moves to the second main topic of this thesis and reports an approach to the chemical oxidation of BFDMA that provides redox-based control over the delivery of DNA to cells. We demonstrate that BFDMA can be oxidized rapidly and quantitatively by treatment with Fe(III)sulfate. This chemical approach, while offering practical advantages compared to electrochemical methods used in past studies, was found to yield BFDMA/DNA lipoplexes that behave differently in the context of cell transfection from lipoplexes formed using electrochemically oxidized BFDMA. Specifically, while lipoplexes of the latter do not transfect cells efficiently, lipoplexes of chemically oxidized BFDMA promoted high levels of transgene expression (similar to levels promoted by reduced BFDMA). Characterization by SANS and cryo-TEM revealed lipoplexes of chemically and electrochemically oxidized BFDMA to have amorphous nanostructures. These lipoplexes, however, differed significantly in size and zeta potential. Our results suggest that differences in zeta potential arise from the presence of residual Fe^{2+} and Fe^{3+} ions in samples of chemically oxidized BFDMA. Addition of the iron chelating agent EDTA to solutions of chemically oxidized BFDMA produced samples functionally similar to electrochemically oxidized BFDMA. These EDTA-treated samples could also be chemically reduced by treatment with ascorbic acid to produce samples of reduced BFDMA that do promote transfection. Our results demonstrate that entirely chemical

approaches to oxidation and reduction can be used to achieve redox-based ‘on/off’ control of cell transfection similar to that achieved using electrochemical methods.

Chapter 6 reports an investigation of how self-assembly impacts the rates of oxidation of the ferrocenyl amphiphile, FTMA and a double tailed analogue, BFDMA at Pt electrodes in contact with aqueous electrolyte (1 mM Li_2SO_4). We measure the rates of oxidation of the two amphiphiles to differ by approximately an order of magnitude. Whereas the scan-rate-dependence of cyclic voltammetry (CV) performed at stationary Pt disc electrodes revealed evidence of adsorption of both amphiphiles, at a rotating disc electrode (RDE), FTMA exhibited characteristics of a mass transfer-limited rate of oxidation whereas the rate of oxidation of BFDMA appeared to be limited by electron transfer through a population of long-lived aggregates of BFDMA on the electrode. To provide insight into this observation, we used dynamic light scattering and differential scanning calorimetry to demonstrate that phase state, not size of the assemblies, dominates the interfacial electrochemical activity of these amphiphilic redox-mediators. Specifically, differential scanning calorimetry of BFDMA revealed an endothermic event (melting) during heating from ambient to 75 °C, whereas DLS revealed only a small reduction in average size of aggregates of BFDMA (565 ± 40 nm). An order of magnitude increase in the rate of oxidation of BFDMA, however, was observed at 75 °C, consistent with a physical process wherein the change in phase state of the BFDMA aggregates provides sufficient mobility to the amphiphiles at the surface of the electrode that electron transfer across those aggregates is no longer rate-limiting. These results, when

combined, illustrate how the self-assembled states of redox-mediators impact rates of electron transfer at electrodes.

Chapter 7 provides a summary of the work presented in this thesis and a discussion of potential future directions.

1.3 References

1. Patnaik, S.; Tripathi, S. K.; Goyal, R.; Arora, A.; Mitra, K.; Villaverde, A.; Vazquez, E.; Shukla, Y.; Kumar, P.; Gupta, K. C. *Soft Matter* **2011**, *7*, 6103-6112.
2. Ziauddin, J.; Sabatini, D. M. *Nature* **2001**, *411*, 107-110.
3. Bailey, S. N.; Wu, R. Z.; Sabatini, D. M. *Drug Discovery Today* **2002**, *7*, S113-S118.
4. Chang, F. H.; Lee, C. H.; Chen, M. T.; Kuo, C. C.; Chiang, Y. L.; Hang, C. Y.; Roffler, S. *Nucleic Acids Res.* **2004**, *32*, e33.
5. Delehanty, J. B.; Shaffer, K. M.; Lin, B. C. *Anal. Chem.* **2004**, *76*, 7323-7328.
6. Yamauchi, F.; Kato, K.; Iwata, H. *Nucleic Acids Res.* **2004**, *32*, e187.
7. Yamauchi, F.; Kato, K.; Iwata, H. *Biochim. Biophys. Acta, Gen. Subj.* **2004**, *1672*, 138-147.
8. Bengali, Z.; Pannier, A. K.; Segura, T.; Anderson, B. C.; Jang, J. H.; Mustoe, T. A.; Shea, L. D. *Biotechnol. Bioeng.* **2005**, *90*, 290-302.
9. Isalan, M.; Santori, M. I.; Gonzalez, C.; Serrano, L. *Nat. Methods* **2005**, *2*, 113-118.
10. Hook, A. L.; Thissen, H.; Voelcker, N. H. *Biomacromolecules* **2009**, *10*, 573-579.
11. Green, D. W.; Mann, S.; Oreffo, R. O. C. *Soft Matter* **2006**, *2*, 732-737.

12. Saltzman, W. M.; Olbricht, W. L. *Nat. Rev. Drug Discovery* **2002**, *1*, 177-186.
13. Saltzman, W. M. *Nature Biotechnology* **1999**, *17*, 534-535.
14. Shea, L. D.; Smiley, E.; Bonadio, J.; Mooney, D. J. *Nat. Biotechnol.* **1999**, *17*, 551-554.
15. Richardson, T. P.; Peters, M. C.; Ennett, A. B.; Mooney, D. J. *Nat. Biotechnol.* **2001**, *19*, 1029-1034.
16. Richardson, T. P.; Murphy, W. L.; Mooney, D. J. *Crit. Rev. Eukaryotic Gene Expression* **2001**, *11*, 47-58.
17. Shepard, J. A.; Huang, A.; Shikanov, A.; Shea, L. D. *J. Controlled Release* **2010**, *146*, 128-135.
18. Yang, F.; Cho, S. W.; Son, S. M.; Bogatyrev, S. R.; Singh, D.; Green, J. J.; Mei, Y.; Park, S.; Bhang, S. H.; Kim, B. S.; Langer, R.; Anderson, D. G. *Proc. Natl. Acad. Sci. U.S.A.* **2010**, *107*, 3317-3322.
19. Mandal, S.; Rosso, N.; Tiribelli, C.; Scoles, G.; Krol, S. *Soft Matter* **2011**, *7*, 9424-9434.
20. Guillot-Nieckowski, M.; Eisler, S.; Diederich, F. *New Journal of Chemistry* **2007**, *31*, 1111-1127.
21. Cavazzana-Calvo, M.; Hacein-Bey, S.; Basile, C. D.; Gross, F.; Yvon, E.; Nusbaum, P.; Selz, F.; Hue, C.; Certain, S.; Casanova, J. L.; Bousso, P.; Le Deist, F.; Fischer, A. *Science* **2000**, *288*, 669-672.
22. Cavazzana-Calvo, M.; Hacein-Bey, S.; Yates, F.; de Villartay, J. P.; Le Deist, F.; Fischer, A. *J. Gene Med.* **2001**, *3*, 201-206.
23. Cavazzana-Calvo, M.; Thrasher, A.; Mavilio, F. *Nature* **2004**, *427*, 779-781.
24. Leonard, W. J. *Mol. Med. Today* **2000**, *6*, 403-407.
25. Hacein-Bey-Abina, S.; Le Deist, F.; Carlier, F.; Bouneaud, C.; Hue, C.; De Villartay, J.; Thrasher, A. J.; Wulffraat, N.; Sorensen, R.; Dupuis-Girod, S.; Fischer, A.; Cavazzana-Calvo, M.; Davies, E. G.;

- Kuis, W.; Lundlaan, W. H. K.; Leiva, L. N. *Engl. J. Med.* **2002**, *346*, 1185-1193.
26. Fischer, A.; Hacein-Bey, S.; Cavazzana-Calvo, M. *Nat. Rev. Immunol.* **2002**, *2*, 615-621.
27. Gaspar, H. B.; Howe, S.; Thrasher, A. J. *Gene Ther.* **2003**, *10*, 1999-2004.
28. Kaufman, R. J. *Hum. Gene Ther.* **1999**, *10*, 2091-2107.
29. Kohn, D. B. *J. Intern. Med.* **2001**, *249*, 379-390.
30. Dimichele, D.; Miller, F. G.; Fins, J. J. *Haemophilia* **2003**, *9*, 145-152.
31. Chamberlain, J. S. *Hum. Mol. Genet.* **2002**, *11*, 2355-2362.
32. Gregorevic, P.; Chamberlain, J. S. *Expert Opin. Biol. Ther.* **2003**, *3*, 803-814.
33. van Deutekom, J. C. T.; van Ommen, G. J. B. *Nature Rev. Genet.* **2003**, *4*, 774-783.
34. Abbott, N. L.; Jewell, C. M.; Hays, M. E.; Kondo, Y.; Lynn, D. M. *J. Am. Chem. Soc.* **2005**, *127*, 11576-11577.
35. Jewell, C. M.; Hays, M. E.; Kondo, Y.; Abbott, N. L.; Lynn, D. M. *J. Controlled Release* **2006**, *112*, 129-138.
36. Jewell, C. M.; Hays, M. E.; Kondo, Y.; Abbott, N. L.; Lynn, D. M. *Bioconjugate Chem.* **2008**, *19*, 2120-2128.
37. Pizzey, C. L.; Jewell, C. M.; Hays, M. E.; Lynn, D. M.; Abbott, N. L.; Kondo, Y.; Golan, S.; Talmon, Y. *J. Phys. Chem. B* **2008**, *112*, 5849-5857.
38. Hays, M. E.; Jewell, C. M.; Kondo, Y.; Lynn, D. M.; Abbott, N. L. *Biophys. J.* **2007**, *93*, 4414-4424.
39. Golan, S.; Aytar, B. S.; Muller, J. P. E.; Kondo, Y.; Lynn, D. M.; Abbott, N. L.; Talmon, Y. *Langmuir* **2011**, *27*, 6615-6621.

40. Aytar, B. S.; Muller, J. P. E.; Golan, S.; Hata, S.; Takahashi, H.; Kondo, Y.; Talmon, Y.; Abbott, N. L.; Lynn, D. M. *Journal of Controlled Release* **2012**, *157*, 249-259.
41. Wilkinson, G.; Rosenblum, M.; Whiting, M. C.; Woodward, R. B. *J. Am. Chem. Soc.* **1952**, *74*, 2125-2126.
42. Faulkner, B. *Electrochemical Methods; Fundamentals and Applications*; 1 ed.; John Wiley & Sons, Inc.: New York, 1980; p 718.
43. Gallardo, B. S.; Gupta, V. K.; Eagerton, F. D.; Jong, L. I.; Craig, V. S.; Shah, R. R.; Abbott, N. L. *Science* **1999**, *283*, 57-60.
44. Gallardo, B. S.; Hwa, M. J.; Abbott, N. L. *Langmuir* **1995**, *11*, 4209-4212.
45. Aydogan, N.; Abbott, N. L. *Langmuir* **2001**, *17*, 5703-5706.
46. Hays, M. E.; Jewell, C. M.; Lynn, D. M.; Abbott, N. L. *Langmuir* **2007**, *23*, 5609-5614.
47. Bennett, D. E.; Gallardo, B. S.; Abbott, N. L. *J. Am. Chem. Soc.* **1996**, *118*, 6499-6505.
48. Rosslee, C. A.; Abbott, N. L. *Anal. Chem.* **2001**, *73*, 4808-4814.
49. Liu, X. Y.; Abbott, N. L. *Anal. Chem.* **2009**, *81*, 772-781.
50. Liu, X. Y.; Abbott, N. L. *Anal. Chem.* **2011**, *83*, 3033-3041.

Chapter 2: Incorporation of DOPE into Lipoplexes formed from a Ferrocenyl Lipid leads to Inverse Hexagonal Nanostructures that allow Redox-Based Control of Transfection in High Serum[‡]

2.1 Introduction

The ability to design soft materials that deliver DNA to specific populations of cells at desired times, or to sub-populations of cells within a larger colony or tissue, would be broadly useful in a variety of *in vitro* (e.g., basic biological and biomedical research¹⁻¹⁰ or tissue engineering¹¹⁻¹⁸) and *in vivo* contexts (e.g., development of new gene-based therapies¹⁹⁻³³). Although a range of nanoscopic assemblies, including those formed from cationic lipids and polymers,³⁴⁻³⁸ have been reported to form complexes with DNA and enable the delivery of DNA to cells, the majority of these complexes are, by design, able to transfect cells from the time of their formation (and, thus, they do not readily permit control over ‘activation’ or ‘inactivation’ in ways that provide methods for spatial and temporal control over delivery and/or internalization). Several recent studies have reported on nanoscale assemblies formed from “functional” lipids that are redox-active,³⁹⁻⁴⁸ pH-responsive,^{39, 49, 50} light-sensitive⁵¹ or chemically or enzymatically cleavable.^{39, 52-54} These functional lipids respond to changes in chemical environments inside cells in ways that can help promote more efficient intracellular trafficking of DNA (e.g., endosomal escape, etc.), but these past

approaches do not, in general, provide methods for control over the activation or inactivation of lipid/DNA assemblies in *extracellular* environments. In this paper, we report the design of complexes comprised of DNA, a ferrocene-containing lipid, and a zwitterionic lipid that are stable in physiologically-relevant concentrations of serum and permit control over cell transfection *via* a change in the redox state of the ferrocene groups of the ferrocene-containing lipid (*e.g.*, whether they are present in the reduced or oxidized redox state).

The study reported in this paper builds upon past reports from our group on the characterization of lipid/DNA complexes (“lipoplexes”) formed using the ferrocene-containing cationic lipid, bis(11-ferrocenylundecyl)dimethylammonium bromide (BFDMA, Figure 2.1A).⁵⁵⁻⁶¹

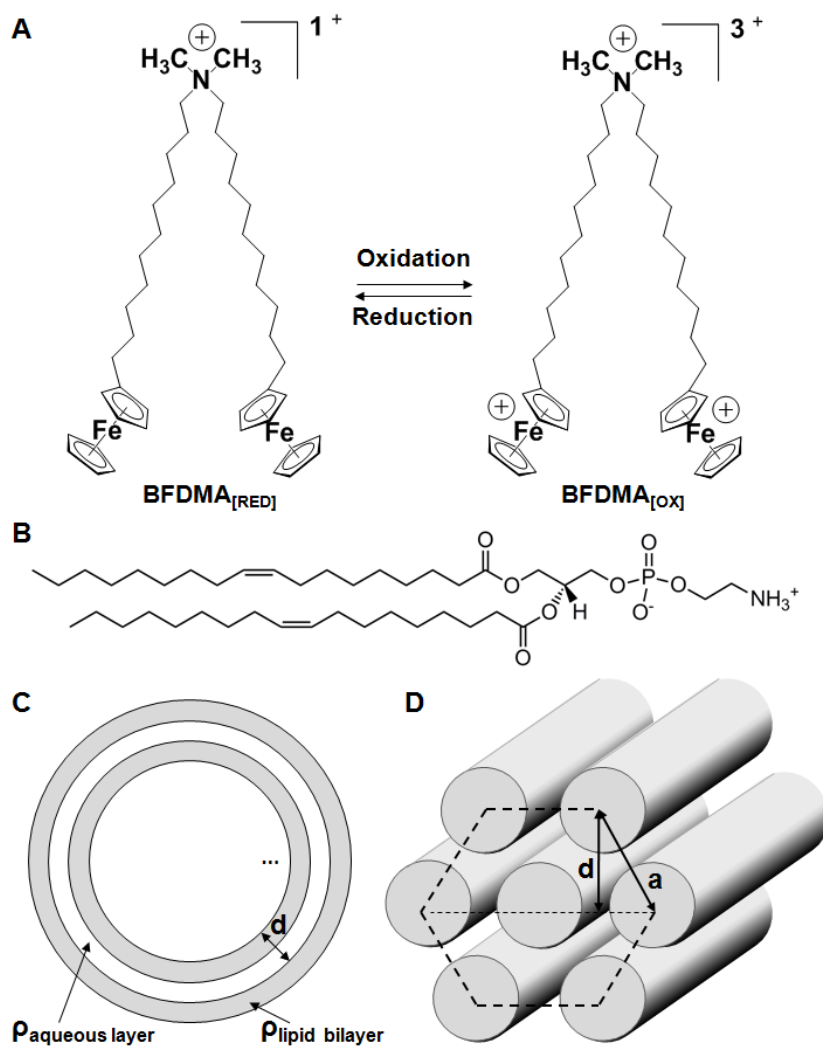


Figure 2.1. (A) Structure of BFDMA, a redox-active cationic lipid. The charge of BFDMA can be cycled between +1 (reduced) and +3 (oxidized) by oxidation or reduction of the ferrocenyl groups at the end of each hydrophobic tail; (B) Structure of dioleoylphosphatidylethanolamine (DOPE); (C) Schematic illustration of a multilamellar vesicle nanostructure; (D) Schematic illustration of a hexagonal nanostructure.

These studies demonstrated that lipoplexes formed using plasmid DNA and reduced BFDMA promote high levels of cell transfection *in vitro* when administered to mammalian cells in serum-free media.⁵⁵ In contrast, oxidation of the ferrocene groups of BFDMA to ferrocenium leads to lipoplexes that mediate low levels of transfection under otherwise identical conditions.⁵⁵ We have also demonstrated that

changes in the oxidation state of ferrocene can lead to changes in a range of different structural and physical properties of BFDMA/DNA lipoplexes that are relevant to transfection.^{55-59, 61, 62} For example, both cryo-TEM images and small angle neutron scattering (SANS)^{58, 61} spectra reveal that lipoplexes formed using reduced BFDMA and DNA possess a multilamellar, L_{α}^c nanostructure (Figure 2.1C) with a lamellar periodicity of 5.2 nm and an overall aggregate size of 50 to 150 nm. In contrast, the nanostructure of complexes formed from oxidized BFDMA and DNA have no such lamellar periodicity, *i.e.*, there is no Bragg peak in the SANS spectra and cryo-TEM images indicate the formation of loose and disordered aggregates.⁵⁸ These past results, when combined, hint at materials and methods that could ultimately enable active and external control of the transfection of cells *via* manipulation (either electrochemically or chemically) of the oxidation state of lipoplexes containing BFDMA.

Whereas our past studies were performed with lipoplexes formed from BFDMA and DNA, the study reported in this paper moves to investigate the properties and nanostructures of lipoplexes formed when BFDMA is mixed with a second lipid dioleoylphosphatidylethanolamine (DOPE; Figure 2.1B). Our investigation of BFDMA in lipoplexes formulated with DOPE was motivated by the observation that the use of mixtures of lipids, in general, provides a versatile approach for tuning a range of properties of lipoplexes that can influence transfection efficiency.⁶³ In the context of this current study, we investigated mixtures of BFDMA and DOPE because (i) incorporation of DOPE into lipoplexes has been shown in

some past studies to lead to the formation of mixed-lipid lipoplexes that promote high levels of cell transfection in media containing high levels of serum,⁶⁴⁻⁶⁸ and (ii) recent observations have revealed that serum has a deleterious influence on both the structure⁶⁰ and the transfection activity⁵⁶ of lipoplexes formed using reduced BFDMA. We hypothesized that incorporation of DOPE into lipoplexes containing BFDMA might help overcome a significant and unresolved barrier to the potential use of BFDMA in a variety of biological contexts where serum will be present. We also note here that past studies of DOPE-containing lipoplexes have reported that DOPE promotes formation of lipoplexes with an inverse hexagonal nanostructure (Figure 2.1D),^{63, 68-73} and causes fusion of lipoplexes with cell membranes,^{63, 69, 72, 74-76} observations that hint at fundamental underlying mechanisms by which DOPE, when mixed with cationic lipids, can promote high levels of transfection in the presence of serum.

The study reported in this paper explores the influence of DOPE on the nanostructure of lipoplexes containing BFDMA by using small angle X-ray scattering (SAXS) and SANS,^{71, 77} and investigates whether changes in the nanostructure of the lipoplexes induced by DOPE lead to changes in transfection efficiencies in the presence of serum at concentrations typical of several different laboratory and physiological contexts (*e.g.*, at levels commonly used in *in vitro* laboratory experiments or at levels encountered in physiological media, *i.e.*, in blood or extracellular matrices).^{78, 79} A second key goal of the study reported in this paper was to determine if changes in the oxidation state of BFDMA within lipoplexes formed

from mixtures of BFDMA and DOPE would lead to substantial changes in the transfection efficiencies of the lipoplexes (*e.g.*, as observed in our past studies of BFDMA/DNA lipoplexes in serum-free media).^{55-59, 61} To aid in the interpretation of these transfection experiments, we report the physical properties of the lipoplexes investigated in terms of their surface charge and apparent size in solution using zeta potential analysis and dynamic light scattering (DLS), respectively.

2.2 Experimental section

2.2.1 Materials

Bis-(11-ferrocenylundecyl)dimethylammonium bromide (BFDMA) was synthesized according to methods published elsewhere.⁸⁰⁻⁸² Dodecyltrimethylammonium bromide (DTAB) was purchased from Acros Organics (Morris Plains, NJ). Dioleoylphosphatidylethanolamine (DOPE) was purchased from Avanti Polar Lipids (Alabaster, Alabama) in powdered form. Deionized water (18.2 M Ω) was used to prepare all buffers and salt solutions with the exception of samples for small angle neutron scattering (SANS), where deuterium oxide (D₂O) was used. Dulbecco's Modified Eagle's Medium (DMEM), OptiMEM cell culture medium, phosphate-buffered saline, fetal bovine serum (FBS), and bovine serum (BS) were purchased from Invitrogen (Carlsbad, CA). Plasmid DNA encoding enhanced green fluorescent protein (pEGFP-N1 (4.7 kbps, >95% supercoiled) and firefly luciferase (pCMV-Luc, >95% supercoiled) were purchased from Elim Biopharmaceuticals (San Francisco, CA). Bicinchoninic acid (BCA) protein assay kits were purchased from

Pierce (Rockford, IL). Glo Lysis Buffer and Steady-Glo Luciferase Assay kits were purchased from Promega Corporation (Madison, WI). All commercial materials were used as received without further purification unless otherwise noted.

2.2.2 Experimental methods

2.2.2.1 Preparation of reduced and oxidized BFDMA and BFDMA-DOPE solutions.

Solutions of reduced BFDMA were prepared by dissolving a desired mass of reduced BFDMA in chloroform at 10 mg/ml. Nitrogen gas was used to evaporate most of the chloroform from a clean glass tube containing the lipid. This partially dried sample was placed under vacuum in a desiccator overnight. Aqueous Li_2SO_4 (1 mM) was added and tip sonication was used to provide a homogeneous solution of 1 mM BFDMA. Solutions of BFDMA-DOPE were prepared in a similar way by dissolving a desired mass of DOPE into chloroform at 10 mg/ml. Chloroform-based solutions of BFDMA and DOPE at 10 mg/ml were then mixed to the desired molar ratio prior to drying with N_2 , desiccating overnight and reconstituting in Li_2SO_4 , as described above. Solutions of electrochemically oxidized BFDMA or oxidized BFDMA-DOPE were subsequently prepared by electrochemical oxidation of 1.0 mM reduced BFDMA solution at 75 °C, in the presence or absence of DOPE, using a bipotentiostat (Pine Instruments, Grove City, PA) and a three electrode cell to maintain a constant potential of 600 mV between the working electrode and a Ag/AgCl reference electrode, as described previously.⁵⁵ Platinum mesh (4.0 cm²) was

used as the working and counter electrodes. The extent of oxidation of BFDMA was followed by monitoring the current passed at the working electrode and by using UV/visible spectrophotometry.⁵⁵⁻⁵⁸

2.2.2.2 Preparation of lipoplexes for transfection assays.

Lipoplexes of reduced or oxidized BFDMA or BFDMA-DOPE were prepared in the following manner. A solution of plasmid DNA (24 $\mu\text{g}/\text{mL}$ in water) was added to a vortexing solution of aqueous Li_2SO_4 containing an amount of reduced or oxidized BFDMA or BFDMA-DOPE sufficient to give the final lipid concentration of 8 μM BFDMA for cell transfection experiments. This procedure resulted in the desired charge ratio of either BFDMA or BFDMA-DOPE and DNA in solution (where the charge ratio (CR) is defined as the mole ratio of the positive charges in the cationic lipid to negative charges of the DNA phosphate groups). The CRs investigated in this study were limited to 1.1:1 for BFDMA_{RED}-containing samples and 3.3:1 for BFDMA_{OX}-containing samples, selected for relevance to our past transfection experiments.⁵⁵⁻⁵⁷ We note that complexes formed from reduced BFDMA and DNA at a CR of 1.1:1 contain the same molar concentrations of BFDMA and DNA as complexes formed by oxidized BFDMA and DNA at a CR of 3.3:1,⁵⁸ and that DOPE is zwitterionic and therefore does not affect the final CR. The sample volume used for cell transfection experiments was 50 μL . Lipoplexes were allowed to stand at room temperature for 20 min before use.

2.2.2.3 Protocols for transfection and analysis of gene expression.

COS-7 cells used in transfection experiments were grown in clear or opaque polystyrene 96-well culture plates (for experiments using pEGFP-N1 and pCMV-Luc, respectively) at initial seeding densities of 15 000 cells/well in 200 μ L of growth medium (90% DMEM, 10% FBS, penicillin 100 units/mL, streptomycin 100 μ g/mL). After plating, all cells were incubated at 37 $^{\circ}$ C for 24 h. At approximately 80% confluence, the culture medium was aspirated and replaced with either 200 μ L of serum-free medium (OptiMEM), or a mixture of bovine serum (BS) and OptiMEM at different volume-based ratios up to 100% BS, followed by addition of 50 μ L of the lipoplex sample to achieve a final concentration of 8 μ M BFDMA in the presence of cells. We note that the addition of the 50 μ L sample of lipoplexes introduces a 20% dilution [$50 \mu\text{L}/(50 \mu\text{L} + 200 \mu\text{L}) * 100\%$] of the concentration of BS in the final solutions in which cells were bathed. Lipoplexes prepared as described above were added to assigned wells *via* pipette in replicates of three, and the cells were incubated for 4 h at 37 $^{\circ}$ C, at which point the lipoplex-containing medium was aspirated from all wells and replaced with 200 μ L of growth medium (composition given above). Samples were incubated for an additional 48 h prior to characterization of transgene expression. For experiments conducted using lipoplexes formed from pEGFP-N1, cell morphology and relative levels of EGFP expression were characterized using phase contrast and fluorescence microscopy. Luciferase protein expression was determined using a commercially available luminescence-based luciferase assay kit using the manufacturer's specified protocol. Samples were compared with signals

from control wells and/or normalized against total cell protein in each respective well using a commercially available BCA assay kit (Pierce). Luciferase protein expression data was analyzed for statistical significance using the Student's t-test with $\alpha = 0.05$. In the text below, when we refer to “significant differences” between our data, we are referring to the results of this test.

2.2.2.4 Preparation of lipoplexes for characterization by SAXS and SANS.

All samples characterized by SAXS and SANS were formulated using reduced or oxidized BFDMA, DOPE and plasmid DNA encoding EGFP (pEGFP-N1). Samples were prepared using 1 mM Li_2SO_4 in either D_2O for SANS or deionized water for SAXS. A stock solution of BFDMA and DOPE (1 mM BFDMA and relevant ϕ_{DOPE}) was diluted with a small volume of DNA stock solution (2.0 mg/ml in H_2O for SAXS and 2.9 mg/ml in D_2O for SANS resulting in a 10% and 13% dilution, respectively) and vortexed for 5 s. The CR used in all scattering experiments was 1.1:1, the same CR as used in the transfection experiments, as noted above. For SAXS analysis, samples of reduced BFDMA-containing lipoplexes, diluted in OptiMEM medium and 50% (v/v) BS, in the presence of and in the absence of DOPE ($\phi_{\text{DOPE}} = 0.71$ and 0, respectively), were also characterized. We note that the absolute concentrations of BFDMA used in the SANS and SAXS experiments (0.3 to 0.9 mM) were substantially higher than those of the transfection experiments (8 μM). These higher concentrations were necessary to obtain a sufficient intensity of scattered

neutrons or X-rays in SANS or SAXS experiments, respectively. All samples were also observed between crossed polars for evidence of optical birefringence.

2.2.2.5 Small-angle X-ray scattering (SAXS).

SAXS was performed using a 4m Rigaku small angle X-ray system with 2-d multi-wire detector. The energy of the incident beam was 40 W. As detailed elsewhere,⁸³ the samples characterized by SAXS were centrifuged using a Sorvall Biofuge Primo centrifuge (Thermo Scientific) at 2000 g for 10 minutes inside 1 mm diameter, 0.01 mm thick quartz capillary tubes (Hampton Research, Aliso Viejo, CA) to obtain a precipitate of lipoplexes. The detector was mounted at a distance of 0.55 m from the sample, allowing access to a q range of $0.066 - 4.0 \text{ nm}^{-1}$. To ensure statistically significant data, at least 10^6 counts were collected for each sample, resulting in an analysis time of between 4 and 12 h. The spectra were calibrated with silver behenate, which has a lamellar periodicity of 5.84 nm ⁸⁴ and angularly integrated by using the software SAXGUI (v2.02.09).

2.2.2.6 Small-angle neutron scattering (SANS).

SANS measurements were performed using the CG-3 Bio-SANS instrument at Oak Ridge National Laboratory (ORNL), Oak Ridge, TN. The incident neutron wavelength was 0.6 nm , with a spread in wavelength, $\Delta\lambda/\lambda$, of 15 %. Data were recorded at a range of sample-to-detector distances to provide a q range from $0.03 - 3.2 \text{ nm}^{-1}$. To ensure statistically significant data, at least 10^6 counts were collected for

each sample at each detector distance. The samples were contained in quartz cells with a 2 mm path length and placed in a sample chamber held at 25.0 ± 0.1 °C. The data were corrected for detector efficiency, background radiation, empty cell scattering, and incoherent scattering to determine the intensity on an absolute scale.⁵⁸ The background scattering from the solvent was subtracted. Samples of reduced BFDMA in 1 mM Li_2SO_4 with increasing levels of DOPE ($\phi_{\text{DOPE}} = 0$ to 1) were characterized. The processing of data was performed using Igor Pro (WaveMetrics, Lake Oswego, OR) with additional Igor Pro user procedures provided by ORNL. Guinier analysis and comparisons to previously published results⁵⁸ were used to interpret the scattering data.

2.3 Results and discussion

In the text below we use the abbreviations, $\text{BFDMA}_{\text{RED-DOPE/DNA}}$ and $\text{BFDMA}_{\text{OX-DOPE/DNA}}$ to describe the mixed-lipid-containing lipoplexes. The subscript “RED” refers to the reduced state of BFDMA and “OX” refers to the oxidized state of BFDMA. In addition, we define ϕ_{DOPE} to be the mole fraction of DOPE in lipoplexes formed from DOPE and BFDMA [$\phi_{\text{DOPE}} = \text{moles of DOPE}/(\text{moles of DOPE} + \text{moles of BFDMA})$]. Because we used measurements of the transfection of cells to identify lipid compositions (values of ϕ_{DOPE}) for detailed characterization by SAXS and SANS, below we present first the results of our transfection studies, and follow those results by descriptions of nanostructural characterization of the lipoplexes of highest interest.

2.3.1 Influence of DOPE on the transfection efficiency of lipoplexes containing reduced BFDMA (BFDMA_{RED}-DOPE/DNA).

To determine the ability of lipoplexes formed from mixtures of reduced BFDMA and DOPE to transfect cells in both serum-free and serum-containing cell culture media, we designed a series of qualitative gene expression experiments using the COS-7 mammalian cell line and a plasmid DNA reporter gene construct (pEGFP-N1) encoding enhanced green fluorescent protein (EGFP). For these experiments, lipoplexes prepared at four different molar ratios of BFDMA to DOPE ($\phi_{\text{DOPE}} = 0, 0.5, 0.71$ and 0.75 ; as described below, these compositions were selected to provide ratios above and below a maximum in cell transfection efficiency that was observed in initial experiments) were added to cells cultured in media containing a broad range of different concentrations (from 0 to 80%) of bovine serum (BS). For all ϕ_{DOPE} and BS levels tested, the final concentration of BFDMA in each well was $8 \mu\text{M}$ and the final concentration of DNA was $2.4 \mu\text{g/ml}$. These concentrations of BFDMA and DNA were selected to enable comparison to our past studies on the characterization of BFDMA/DNA lipoplexes.^{55-58, 61} The cells were incubated with lipoplexes in media containing various concentrations of BS for 4 h, followed by incubation in fresh growth medium containing 10% BS (see “Materials and Methods” for a detailed description of this assay) for an additional 44 h.

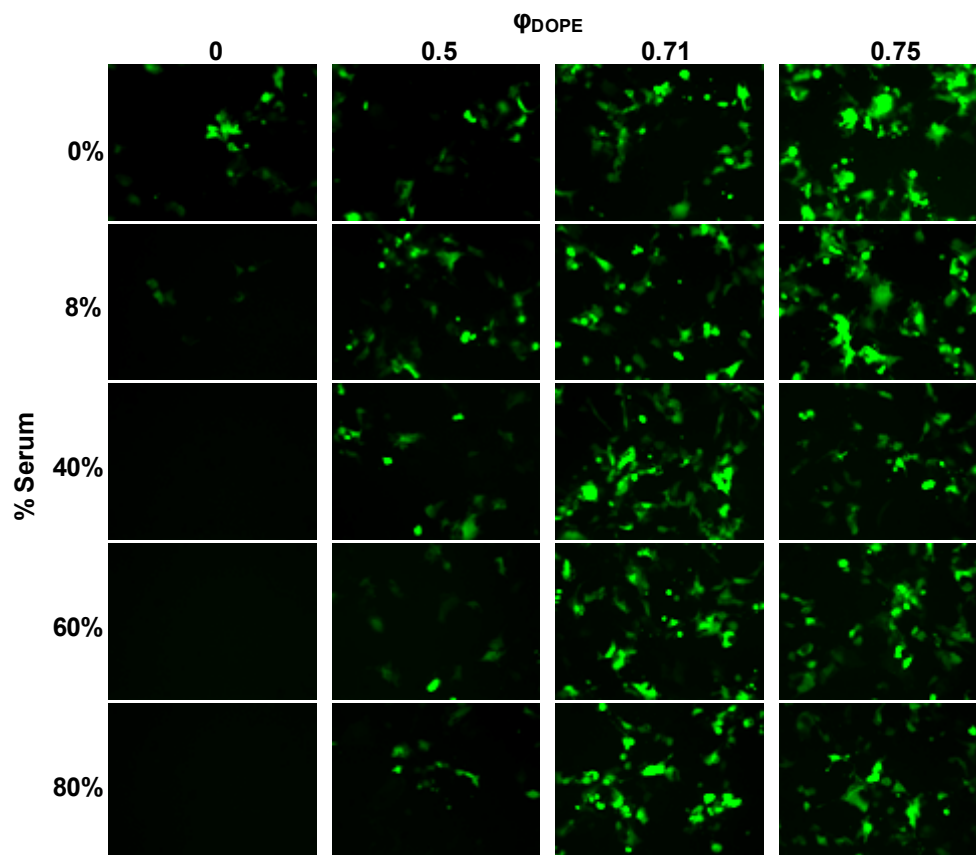


Figure 2.2. Influence of serum on EGFP expression in COS-7 cells treated with lipoplexes formed from pEGFP-N1 and mixtures of reduced BFDMA and DOPE for 4 h. The media used was pure OptiMEM or a mixture of OptiMEM and BS. All experiments were performed by adding 50 μL of lipid/DNA mixture in 1mM Li_2SO_4 solution to 200 μL of media in the presence of cells. Final BS concentrations are given down the left hand side of the figure. The overall concentrations of BFDMA and DNA in each lipoplex solution were 8 μM and 2.4 $\mu\text{g/ml}$, respectively, providing a charge ratio of 1.1:1 (+/-) for all samples as DOPE has a net charge of zero. Mole fractions of DOPE, $\phi_{\text{DOPE}} = \text{DOPE}/(\text{BFDMA}+\text{DOPE})$, are given across the top of the figure. Fluorescence micrographs (1194 μm by 895 μm) were acquired 48 h after exposure of cells to lipoplexes.

Figure 2.2 shows representative fluorescence micrographs of cells 48 h after exposure to the lipoplexes. These data demonstrate that lipoplexes containing BFDMA/DNA only were able to transfect cells growing in serum-free culture media (Figure 2.2, $\phi_{\text{DOPE}} = 0$; 0% BS), as indicated by the presence of cells expressing

EGFP. Further inspection of these data, however, reveals that these BFDMA/DNA-only lipoplexes ($\phi_{\text{DOPE}} = 0$) mediated qualitatively lower levels of transgene expression in media containing 8% serum, and that at higher levels of serum (*e.g.*, from 40% to 80% BS) no visible indication of transgene expression was observed (*e.g.*, absence of cells expressing visible levels of EGFP expression in the lower left column of Figure 2.2). These results confirm those of our past studies,^{55-57, 60} indicating that serum proteins have a deleterious effect on transfection of cells with BFDMA.

Further inspection of Figure 2.2, however, reveals that incorporation of DOPE into lipoplexes with BFDMA leads to qualitatively large increases in the extent of cell transfection when serum is present ($\phi_{\text{DOPE}} > 0$; columns 2, 3 and 4). In particular, we note that lipoplexes with $\phi_{\text{DOPE}} = 0.71$ and 0.75 mediated significant levels of transfection in cells growing in media containing up to 80% BS (see images in the lower right section of Figure 2.2). Overall, these results demonstrate that the addition of DOPE to BFDMA results in lipoplexes that promote high levels of cell transfection in the presence of serum.

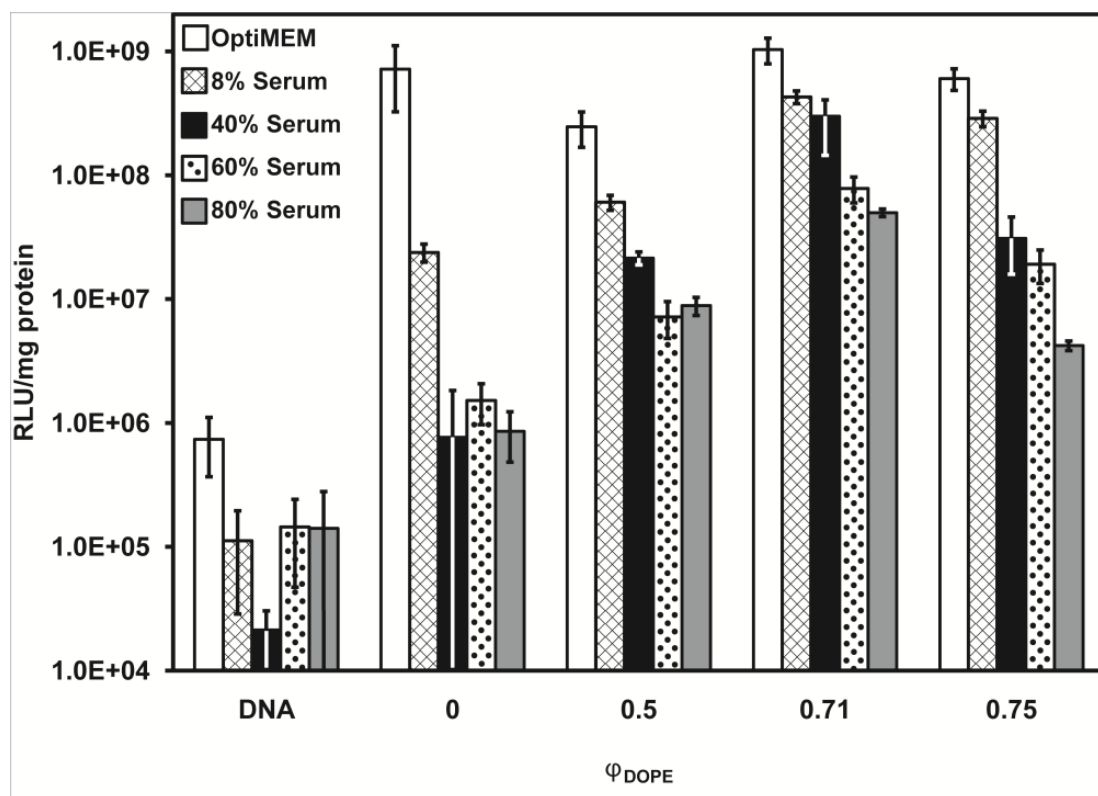


Figure 2.3. Influence of serum on normalized luciferase expression in COS-7 cells treated with lipoplexes formed from pCMV-Luc and mixtures of reduced BFDMA and DOPE for 4 h. The final concentration of BS is given in the legend. DNA was present at a concentration of 2.4 $\mu\text{g/ml}$ for all samples. “DNA” denotes a control with DNA only (no lipid). Molar fractions of DOPE, $\phi_{DOPE} = \text{DOPE}/(\text{BFDMA}+\text{DOPE})$, are given on the x-axis for each sample. The concentration of BFDMA in each sample was 8 μM . Luciferase expression was measured 48 h after exposure to lipoplexes. Error bars represent one standard deviation.

To quantify the differences in gene expression observed in Figure 2.2 using lipoplexes of BFDMA and DOPE, we conducted transfection experiments using lipoplexes formed using a plasmid DNA construct (pCMV-Luc) encoding firefly luciferase (Figure 2.3).

From the results shown in Figure 2.3, we make the following three observations. First, in serum-free cell culture medium (white bars), lipoplexes prepared with ϕ_{DOPE} ranging from 0.5 to 0.75 do not seem to differ significantly from

lipoplexes of BFDMA/DNA only ($\phi_{\text{DOPE}} = 0$) in their ability to efficiently transfect cells (all DOPE-containing transgene expression measurements have a mean within one standard deviation of lipoplexes of BFDMA/DNA). Second, in serum-containing cell culture media (all non-white bars in Figure 2.3), the efficiency of cell transfection does depend widely on the ratio of BFDMA to DOPE and on the concentration of BS present during transfection. For example, comparing changes in ϕ_{DOPE} , when the cell culture medium was supplemented with 80% BS (gray bars in Figure 2.3), cell transfection was measured to be significantly lower when DOPE is absent from the lipoplexes than when DOPE was present in the lipoplexes (*e.g.* protein expression was $8.6 \pm 3.7 \times 10^5$ RLU/mg protein at $\phi_{\text{DOPE}} = 0$ and $5.0 \pm 0.4 \times 10^7$ RLU/mg protein at $\phi_{\text{DOPE}} = 0.71$). Thus, we conclude that incorporation of DOPE into lipoplexes of BFDMA can increase levels of transgene expression by almost two orders of magnitude in serum-containing media.

The third and final observation regarding the results in Figure 2.3 is that the level of transgene expression goes through an apparent maximum as a function of ϕ_{DOPE} for all levels of serum present during cell transfection. This maximum occurs around a ratio of $\phi_{\text{DOPE}} = 0.71$. We also note here that when cells are treated with DOPE/DNA in the absence of BFDMA, low levels of transfection result (Figure 2.7† and Figure 2.8†) and, thus, the decrease in transfection efficiency observed at the highest values of ϕ_{DOPE} could reflect the dominating influence of DOPE in these DOPE- rich complexes. Overall, from the results shown in Figure 2.2 and Figure 2.3, we conclude that inclusion of DOPE in BFDMA/DNA lipoplexes leads to

compositions that are able to promote significant levels of transgene expression in the presence of high and physiologically relevant concentrations of serum.

2.3.2 Influence of DOPE on the physical properties and nanostructure of lipoplexes containing reduced BFDMA (BFDMA_{RED}-DOPE/DNA).

Past studies have demonstrated that, amongst a large number of factors that influence the ability of lipoplexes formed from cationic lipids to transfect cells, the size, zeta potential and nanostructure of the lipoplexes can be important.^{64, 85} Figure 2.9 to Figure 2.12 (see Supporting materials) show measurements of the sizes of BFDMA-containing lipoplexes under a range of conditions (obtained using DLS). With reference to the summary of key data presented in Figure 2.9, we make two observations. First, inspection of Figure 2.9A and B reveals that incorporation of DOPE into BFDMA lipoplexes in the absence of serum causes the intensity-weighted size distributions of the lipoplexes to increase from $\sim 680 \pm 280$ nm to $\sim 2900 \pm 2000$ nm (the corresponding number-weighted size distributions are $\sim 420 \pm 120$ nm to $\sim 750 \pm 300$ nm, respectively). These broad size distributions are typical of lipoplexes formed by cationic lipids and DNA, and they include a range of sizes of lipoplexes that are taken up by cells. Second, as evidenced by results shown in Figure 2.9C†, interpretation of DLS data obtained in the presence of serum is complicated because serum (without lipoplexes) contains a range of aggregates with sizes of ~ 80 nm \pm 20 nm (intensity-weighted). A comparison of Figure 2.9C with either Figure 2.9D or Figure 2.9E, however, reveals that, in the presence of serum, the size distributions of

BFDMA lipoplexes with and without DOPE exhibit a broad peak around $\sim 1 \mu\text{m}$ that is absent in the sample of serum only. In addition, comparison of DLS data measured after 20 minutes and 4 hours of incubation of the lipoplexes revealed no significant change in size, suggesting that DOPE does not lead to a change in colloidal stability (see Supporting materials, Figure 2.10 to Figure 2.12). We also measured zeta potentials of BFDMA lipoplexes containing DOPE (see ESI Figure 2.9 and Figure 2.13). Although we measured the presence of DOPE to change the zeta potentials of lipoplexes of BFDMA in the absence of serum, when serum was present, the zeta potentials of the lipoplexes were not measured to change significantly with addition of DOPE. Overall, our results obtained using DLS and zeta potential measurements indicate that, in the presence of serum, addition of DOPE to the lipoplexes of BFDMA causes a small increase in average size within a broad size distribution and no significant change in surface charge. We conclude, therefore, that the effect of DOPE on the size and charge of the lipoplexes is unlikely to be the origin of the influence of DOPE on transfection efficiency.

To determine how the presence of DOPE influences the nanostructure of lipoplexes formed by BFDMA_{RED} and DNA, and to determine whether the presence of serum impacts any nanostructures that do form, we next performed a series of SAXS and SANS experiments. In these experiments, pGFP-N1 DNA was used at a CR of 1.1:1 with BFDMA_{RED}, similar to the lipoplexes used in the cell transfection experiments described above.

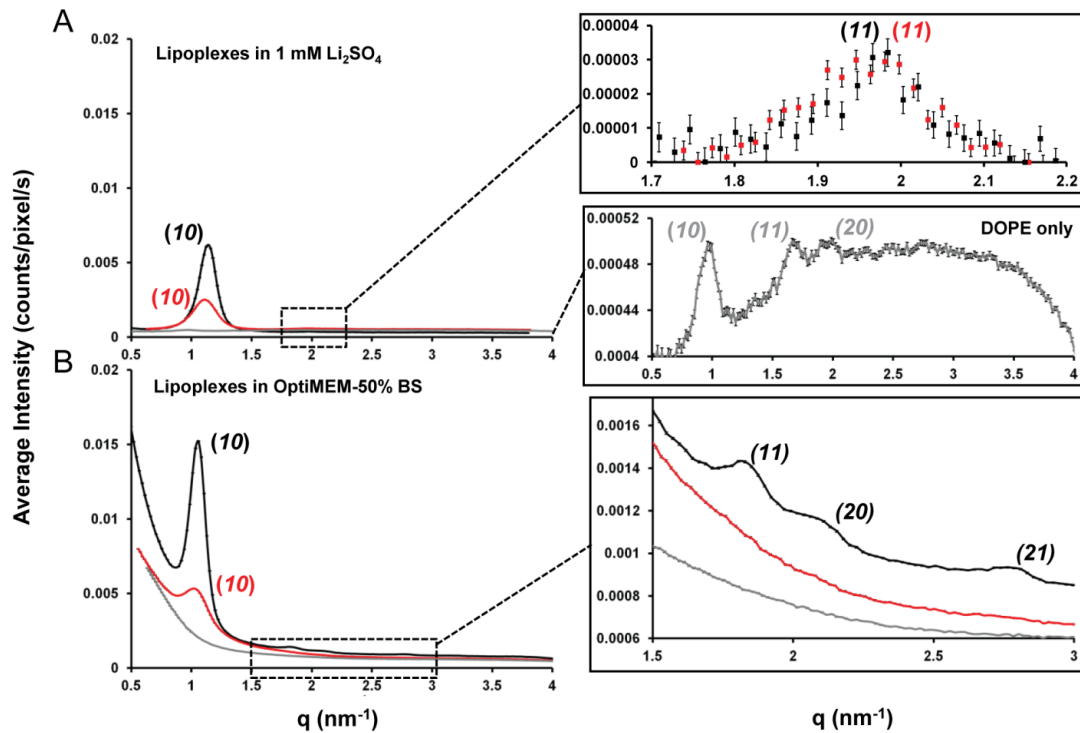


Figure 2.4. SAXS spectra obtained using BFDMA_{RED}-DOPE ($\phi_{\text{DOPE}} = 0.71$) (black), BFDMA_{OX}-DOPE ($\phi_{\text{DOPE}} = 0.71$) (red) or DOPE only (grey) containing lipoplexes in; **(A)** 1 mM Li₂SO₄, using lipid concentrations of 0.87 mM BFDMA and/or 2.17 mM DOPE; **(B)** OptiMEM with 50% (v/v) BS, using diluted lipid concentrations of 0.32 mM BFDMA and/or 0.8 mM DOPE; all in the presence of pEGFP-N1 (2.0 mg/ml) at a charge ratio of 1.1:1 or 3.3:1 (+/-) for reduced or oxidized BFDMA containing solutions respectively. Insets for both graphs are given on the right hand side. Bragg peaks are indicated on the graphs and color coded to their respective lipoplex.

The goal of our first scattering experiment was to use SAXS to characterize the impact of DOPE on the nanostructures of lipoplexes containing BFDMA_{RED} in a simple electrolyte solution (1 mM Li₂SO₄). For BFDMA_{RED}-DOPE/DNA lipoplexes at $\phi_{\text{DOPE}} = 0.71$ (Figure 2.4A, black data), Bragg peaks at $q_{10} = 1.12 \text{ nm}^{-1}$ and $q_{11} = 1.97 \text{ nm}^{-1}$ are observed, corresponding to a ratio $q_{10}/q_{11} = \sqrt{3}$ and thus a H_{II}^c nanostructure (hexagonal structures are characterized by a q_x/q_{10} spacing ratio of

1: $\sqrt{3}$: $\sqrt{4}$: $\sqrt{7}$).⁸⁶ As shown in Figure 2.1D, the periodicities of the 2D hexagonal structure are characterized by the unit cell spacing, $a = 4\pi/[(\sqrt{3})q_{10}] = 6.48 \pm 0.13$ nm in addition to the same d-spacing parameter described above, $d = 2\pi/q_{10}$ or $(\sqrt{3}/2)a = 5.61 \pm 0.11$ nm.⁷¹ We note here that, although one recent study has shown lipid-DNA mixtures can form cubic nanostructures,⁸⁷ we conclude that the nanostructures formed by DOPE, BFDMA_{RED} and DNA are not cubic because (i) all samples observed between crossed-polars are birefringent whereas cubic phases are optically isotropic (Figure 2.14), and (ii) the Bragg peak spacings for cubic phases are inconsistent with our SAXS data (see ESI for additional discussion). In contrast to lipoplexes formed by DOPE, BFDMA_{RED} and DNA, the scattering spectra of BFDMA_{RED} based lipoplexes without DOPE (as shown in Supporting materials, Figure 2.15A, black data) exhibited Bragg peaks at $q_{001} = 1.27$ nm⁻¹ and $q_{002} = 2.54$ nm⁻¹, corresponding to a ratio $q_{002}/q_{001} = 2$ and, therefore, a L_{α}^c nanostructure (lamellar structures are characterized by a q_x/q_{001} spacing ratio of 1:2:3:4).⁸⁶ The d-spacing periodicity (Figure 2.1C) was calculated as $d = 2\pi/q_{001} = 4.95 \pm 0.1$ nm.⁵⁸

We conclude, therefore, that the inclusion of DOPE in lipoplexes of BFDMA_{RED} (at $\phi_{\text{DOPE}} = 0.71$) causes the nanostructure of the lipoplexes to change from L_{α}^c to H_{II}^c (see Table 2.1 for a summary of these scattering results). We note here that lipoplexes of BFDMA and DOPE with $\phi_{\text{DOPE}} = 0.71$ possess a total lipid:DNA molar ratio of 3.9:1. In our past studies,⁵⁸ we observed lipoplexes of BFDMA_{RED} only, with lipid:DNA molar ratios as high as 4:1, to possess a multilamellar nanostructure. The 2D hexagonal nanostructure reported above in the

presence of DOPE is not, therefore, simply a result of a high total lipid:DNA molar ratio within the lipoplex, but rather, it reflects the tendency of DOPE to promote formation of inverse hexagonal nanostructure. The observation that DOPE induces formation of the H_{II}^c nanostructure with BFDMA is consistent with several past studies that have reported on the influence of DOPE on some (non-redox-active) cationic lipid formulations.^{63, 68-73} Furthermore, in light of the above-described transfection results, indicating that lipoplexes of BFDMA and DOPE lead to high levels of transfection in the presence of serum, the formation of the H_{II}^c phase in solution in the presence of DNA is potentially significant as the H_{II}^c nanostructure is thought to facilitate fusion of lipoplexes and cell membranes.^{72, 74-76}

Table 2.1. SAXS results; Bragg peak q_{hkl} positions (using Miller Indices), d-spacing and Bragg peak ratios, nanostructure, and unit cell spacing (a) for H_{II}^c phases, for lipoplexes of reduced or oxidized BFDMA/pGFP ($\phi_{DOPE} = 0$) and reduced or oxidized BFDMA-DOPE/pGFP ($\phi_{DOPE}=0.71$) with and without the presence of OptiMEM and 50% BS (v/v), and lipids of reduced BFDMA, reduced BFDMA-DOPE and DOPE. Errors are based on equipment calibration of 2% using a silver behenate standard.

Lipoplex	Bragg peak q_{hkl} position (nm^{-1})				Bragg peak ratios			Nano-structure	d or a^b (nm)
	1 st peak	2 nd peak	3 rd peak	4 th peak	2 nd /1 st	3 rd /1 st	4 th /1 st		
Lipoplexes in 1 mM Li_2SO_4									
BFDMA _{RED} /pGFP	$q_{001} = 1.27$	$q_{002} = 2.53$	-	-	1.99	-	-	L_α^c	4.95 ± 0.10
BFDMA _{RED} -DOPE/pGFP	$q_{10} = 1.12$	$q_{11} = 1.97$	-	-	1.76	-	-	H_{II}^c	6.48 ± 0.13
BFDMA _{OX} /pGFP	-	-	-	-	-	-	-	-	-
BFDMA _{OX} -DOPE/pGFP	$q_{10} = 1.12$	$q_{11} = 1.97$	-	-	1.76	-	-	H_{II}^c	6.48 ± 0.13
DOPE/pGFP	$q_{10} = 0.95$	$q_{11} = 1.67$	$q_{20} = 1.92$	-	1.75	2.00	-	H_{II}^c	7.63 ± 0.15
Lipoplexes in OptiMEM and 50% v/v BS									
BFDMA _{RED} /pGFP	$q_{001} = 1.13$	$q_{002} = 2.25$	-	-	1.99	-	-	L_α^c	5.56 ± 0.11
BFDMA _{RED} -DOPE/pGFP	$q_{10} = 1.04$	$q_{11} = 1.79$	$q_{20} = 2.08$	$q_{21} = 2.77$	1.72	2.00	2.66	H_{II}^c	6.97 ± 0.14
BFDMA _{OX} /pGFP	-	-	-	-	-	-	-	-	-
BFDMA _{OX} -DOPE/pGFP	$q_{10} = 1.04$	-	-	-	-	-	-	-	6.04 ± 0.12
DOPE/pGFP	-	-	-	-	-	-	-	-	-
Lipids only in 1 mM Li_2SO_4									
BFDMA _{RED}	-	-	-	-	-	-	-	-	-
BFDMA _{RED} -DOPE	$q_{10} = 1.05$	$q_{11} = 1.81$	$q_{20} = 2.12$	-	1.72	2.02	-	H_{II}	6.91 ± 0.14
DOPE	$q_{10} = 0.95$	$q_{11} = 1.69$	$q_{20} = 1.91$	-	1.78	2.01	-	H_{II}	7.63 ± 0.15

^a d-spacing, d given for lamellar L_α structure, $a=2/\sqrt{3}d$ given for hexagonal H_{II} structure (See Figure 2.1C and D).

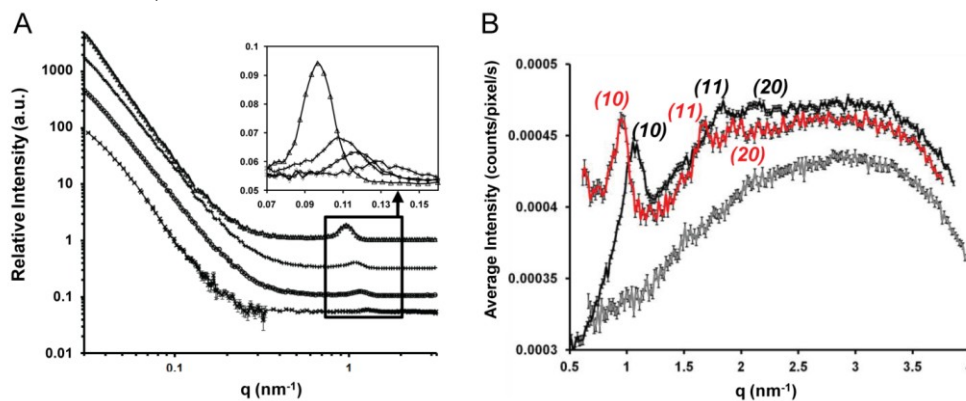


Figure 2.5. Evidence of association of BFDMA and DOPE in solution in the presence and absence of DNA; (A) SANS spectra measured using solutions of; (Δ) 1 mM DOPE ($\phi_{DOPE} = 1$); (+) 1 mM BFDMA and 1mM DOPE ($\phi_{DOPE} = 0.5$); (\circ) 1 mM BFDMA and 0.4 mM DOPE ($\phi_{DOPE} = 0.28$), (\times) 1 mM BFDMA ($\phi_{DOPE} = 0$), all in the presence of DNA (2.9 mg/ml) and, when BFDMA is present, at a charge ratio of 1.1:1 (+/-). The data are offset for clarity. The insert shows an expanded view of the Bragg peaks and has no offset in intensity between samples. (B) SAXS spectra obtained using lipid only solutions of; 1 mM BFDMA (grey); 2.5 mM DOPE (red); 1 mM BFDMA, 2.5 mM DOPE (black); all in 1 mM Li_2SO_4 (grey).

To provide further insight into the nanostructure of the lipoplexes of reduced BFDMA and DOPE, including the influence of serum on the nanostructure, we performed several additional experiments. First, we investigated the extent of mixing of the DOPE and BFDMA within the lipoplex formulations. To this end, we determined the periodicity of the nanostructures formed by mixtures of BFDMA and DOPE with compositions of $\phi_{\text{DOPE}} = 0, 0.28, 0.5$ and 1.0 to assess if a single periodicity corresponding to well-mixed lipoplexes was present (demixing of BFDMA and DOPE would be evidenced by multiple periodicities). SANS was used for these measurements to enable direct comparison to our past SANS studies of lipoplexes formed using BFDMA/DNA only ($\phi_{\text{DOPE}} = 0$).⁵⁸ All samples were prepared in 1 mM Li_2SO_4 using 100% D_2O . The results are shown in Figure 2.5A. Inspection of Figure 2.5A shows that only one Bragg peak is observed in each SANS spectrum, and that the location of each Bragg peak, and thus the corresponding periodicity, is dependent on the amount of DOPE in the sample. The measured periodicity ranges from $d = 4.95 \pm 0.10$ nm for lipoplexes of BFDMA_{RED} only (in agreement with SAXS analysis in Figure 2.4A and Table 2.1, as well as the results of past SANS studies),^{58, 61} increases with the incorporation of DOPE into the lipoplexes, and reaches $d = 6.50 \pm 0.13$ nm or $a = (2/\sqrt{3})d = 7.51 \pm 0.15$ nm (both values are in close agreement with past SAXS studies)^{71, 88} for solutions of DOPE/DNA only (in agreement with the SAXS result above, Figure 2.4A grey data). We note that past studies have reported that DOPE forms a H_{II} phase in the absence of DNA, and that in the presence of DNA there is little measurable association of the DNA and lipid.⁷¹ This general result is

consistent with our SANS measurements and transfection results shown in Figure 2.7† and Figure 2.8† in which levels of transfection mediated by mixtures of DOPE and DNA are comparable to those mediated by naked DNA (see also Figure 2.5B below). The key conclusion extracted from the appearance of a single Bragg peak in each of the scattering spectra is that DOPE is intimately mixed with BFDMA within the lipoplexes, and that increasing the relative amount of DOPE present in the lipoplex progressively increases the periodicity of the lipid-DNA complex. Thus we conclude that the transfection results obtained with mixtures of BFDMA and DOPE are likely the result of the activity of lipoplexes comprised of both BFDMA and DOPE (and not, for example, lipoplexes comprised predominantly of only one of the lipids in the formulation).

The results presented above indicate that the nanostructure of lipoplexes formed by BFDMA and DOPE is H_{II}^c . To determine if the presence of DNA is required to form the H_{II}^c phase, we used SAXS to characterize the nanostructure of DNA-free complexes containing BFDMA and DOPE (and also those free of DOPE). Inspection of Figure 2.5B reveals that complexes formed from BFDMA_{RED}-DOPE ($\phi_{DOPE} = 0.71$, black data) and DOPE only (red data) both show Bragg peaks with $1:\sqrt{3}:\sqrt{4}$ spacing, consistent with H_{II} nanostructure, with a positive shift in q_{10} of 0.13 nm^{-1} on incorporation of BFDMA_{RED}. In contrast, BFDMA_{RED} shows no Bragg peaks in the scattering (grey data). Together, these results indicate that formation of the inverse hexagonal structure, which we observe to correlate with the presence of high levels of transfection in the presence of serum proteins, is driven by the presence of

the DOPE. Specifically, we observe DOPE and BFDMA to mix in the absence of DNA to form the inverse hexagonal nanostructure.

The scattering results described above were obtained using simple electrolyte solutions. In a final set of scattering experiments, we investigated the influence of cell culture media and the presence of serum on the nanostructures of lipoplexes containing BFDMA_{RED} ($\phi_{\text{DOPE}} = 0$), BFDMA_{RED} with DOPE ($\phi_{\text{DOPE}} = 0.71$) and DOPE only ($\phi_{\text{DOPE}} = 1$). Lipoplexes of BFDMA only ($\phi_{\text{DOPE}} = 0$, see Supporting materials, Figure 2.15B, red data) were prepared in Li₂SO₄, and then diluted by the addition of OptiMEM and then 50% (v/v) BS. This dilution resulted in a 2.7-fold reduction of the concentration of lipid and DNA in solution. Our past studies⁵⁸ and the studies of others⁷¹ have revealed, however, that such dilution does not typically affect the type of nanostructure observed in solution. For these samples, we observed Bragg peaks at $q_{001} = 1.13 \text{ nm}^{-1}$ and $q_{002} = 2.25 \text{ nm}^{-1}$, corresponding to a L_{α}^c nanostructure (see Table 2.1 for periodicities). In contrast, as shown in Figure 2.4B (black data), the SAXS spectrum obtained using lipoplexes with $\phi_{\text{DOPE}} = 0.71$ (in 50% BS) exhibit four Bragg peaks: $q_{10} = 1.04 \text{ nm}^{-1}$, $q_{11} = 1.79 \text{ nm}^{-1}$, $q_{20} = 2.08 \text{ nm}^{-1}$, and $q_{21} = 2.77 \text{ nm}^{-1}$. The ratios of q_{hk}/q_{10} correspond to $\sqrt{3}$, $\sqrt{4}$ and $\sqrt{7}$, thus demonstrating that incorporation of DOPE into lipoplexes formed from DNA in the presence of 50% BS also causes the nanostructure of the lipoplexes to change from L_{α}^c (without DOPE) to H_{II}^c (with DOPE).

A comparison of Figure 2.15A and B with Figure 2.5A and B provides additional insight into the influence of cell culture media and serum proteins on the

nanostructures of these lipoplexes. Addition of serum to either BFDMA_{RED} only or BFDMA_{RED}-DOPE lipoplexes caused the Bragg peaks to move to lower q , corresponding to an increase in periodicity of 0.5-0.7 nm (shown for q_{001} in Figure 2.15A and B by a vertical dotted line at q_{001} , Figure 2.15B). This result indicates that the presence of serum causes the periodicity of the nanostructures (Figure 2.1C and D) to increase by 8-12%. This increase in periodicity has been seen in at least one other study (*i.e.*, on lipoplexes of DC-Cholesterol, DOPE and DNA),⁶⁴ where it was hypothesized that cationic lipids within lipoplexes containing DOPE associate with proteins⁸⁹ leading to the increased periodicity.^{66, 67} Here we note that the key conclusion extracted from our SAXS measurements is that the hexagonal nanostructure of the lipoplexes of DOPE and BFDMA survives exposure to high concentrations of serum proteins. This result is consistent with our measurement of high levels of transfection of cells in the presence of serum when using lipoplexes formed from mixtures of DOPE and BFDMA.

Here we also note that a number of past studies have reported that serum proteins can promote the disassembly of lipoplexes comprised of DNA and cationic lipids.^{60, 66, 90} These studies have also suggested that the destruction of the lipoplexes by serum proteins underlies the low levels of cell transfection measured in the presence of serum. In particular, in a study reported recently, cryo-TEM was used to characterize the nanostructures of BFDMA-containing lipoplexes (no DOPE) in the presence of serum and revealed that serum can promote dissociation of lipoplexes containing BFDMA.⁶⁰ Our SAXS-based characterization of the nanostructures of

lipoplexes of BFDMA_{RED} performed in the presence of serum (Figure 2.15B) suggests that addition of serum does not cause complete loss of the L_{α}^c nanostructure of the BFDMA_{RED} lipoplex. This result appears consistent with these prior cryo-TEM results,⁶⁰ which indicated that some intact multilamellar, L_{α}^c nanostructures also appeared to survive addition of serum under certain conditions. The results shown in Figure 2.15B which reveal that the periodicity of the multilamellar nanostructure changes upon addition of serum, also suggests an alteration of the physicochemical properties of the lipoplexes induced by association of proteins, rather than wholesale destruction and unraveling of the lipoplexes, which could also contribute to the lower levels of transfection promoted by lipoplexes formed using BFDMA/DNA only in the presence of serum.

2.3.3 Influence of oxidation state of BFDMA on the transfection efficiency, physical properties, and nanostructure of lipoplexes containing BFDMA and DOPE.

The key issue that we addressed next is whether the oxidation state of BFDMA influences the transfection efficiency of lipoplexes containing DOPE. Although our past studies using lipoplexes of BFDMA alone have revealed that the oxidation state of the BFDMA has a pronounced effect on transfection, because the nanostructures of lipoplexes formed by BFDMA only (multilamellar) and mixtures of DOPE and BFDMA (inverse hexagonal, see above) are different, we emphasize that it is not possible to anticipate the effects of changes in the oxidation state of BFDMA on

the transfection efficiency of lipoplexes containing BFDMA and DOPE on the basis of our past results using lipoplexes containing BFDMA only.

To enable studies of the effect of the oxidation state of BFDMA on the transfection efficiency and nanostructure of lipoplexes containing mixtures of BFDMA and DOPE, we first demonstrated that it was possible to oxidize BFDMA in the presence of DOPE (as shown in Supporting materials, Figure 2.16). Figure 2.6 presents the results of a quantitative gene expression assay, again using lipoplexes formed using the pCMV-Luc plasmid DNA construct, and shows the effects of oxidized BFDMA on cell transfection (both in the absence and presence of DOPE and as a function of the concentration of serum). Guided by the results presented in Figure 2.2 and Figure 2.3, the lipoplexes used in these experiments were prepared with $\phi_{\text{DOPE}} = 0.71$ (dotted and grey bars in Figure 2.6). Inspection of Figure 2.6 leads to two key observations. First, in the absence of serum (0% column), the levels of transgene expression mediated by lipoplexes formed using BFDMA_{OX}/DNA were approximately two orders of magnitude lower than levels mediated by lipoplexes formed using BFDMA_{RED}/DNA (*e.g.*, compare hashed bar to black bar). These differences were maintained, but were smaller (by approximately one order of magnitude), for DOPE-containing lipoplexes formed using reduced or oxidized BFDMA (compare dotted bar to grey bar). Second, when the cell culture medium contained 40% or 80% BS (Figure 2.6), relative to the high levels of cell transfection achieved using lipoplexes containing DOPE and reduced BFDMA (dotted bars, consistent with results in Figure 2.2 and Figure 2.3), the levels of transgene

expression decreased by at least two orders of magnitude when using lipoplexes formed from oxidized BFDMA and DOPE (compare dotted bars to grey bars). In particular, when we compare these two observations, we conclude that control of the oxidation state of BFDMA in lipoplexes of BFDMA and DOPE leads to larger changes in transfection efficiency in the presence of high concentrations of serum than in the absence of serum. Furthermore, inspection of Figure 2.6 reveals that transfection mediated by BFDMA_{OX}-DOPE/DNA in the presence of 80% BS is more than two orders of magnitude lower than levels mediated by BFDMA_{OX}-DOPE/DNA in the absence of serum. This result suggests that the presence of serum proteins may lead to substantial changes the structure and/or properties of lipoplexes of DOPE and oxidized BFDMA in ways that influence their activities, a point that we return to below.⁶⁰

We note here that we also confirmed the above conclusions regarding the impact of the oxidation state of BFDMA in the presence of DOPE on cell transfection by using qualitative fluorescence micrographs of cells expressing EGFP from experiments using lipoplexes formed from pGFP-N1 (as shown in Supporting materials, Figure 2.17). The results of additional live/dead cytotoxicity assays revealed that the lipoplex compositions described above do not lead to substantial cytotoxicity under the conditions used in the above experiments. Additional data and details of these cytotoxicity screens are included in Supporting materials, Figure 2.18 and Table 2.2.

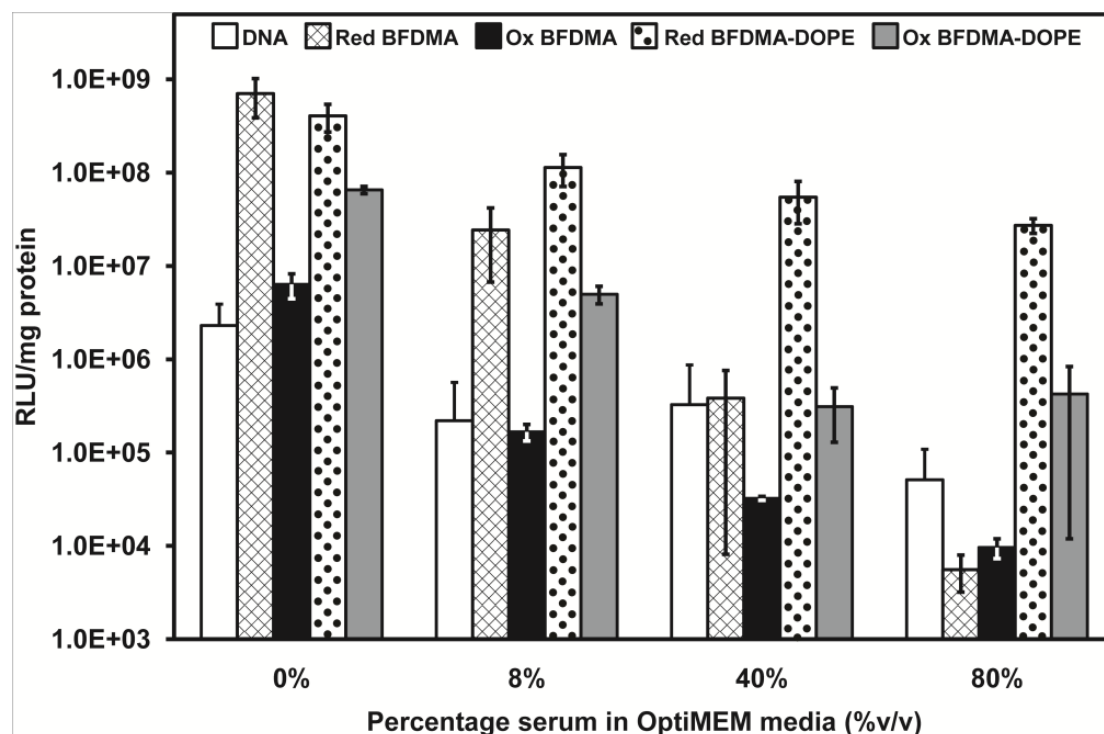


Figure 2.6. Influence of serum on the normalized luciferase expression in COS-7 cells treated with naked DNA (white bars), and lipoplexes of reduced BFDMA (hashed bars), oxidized BFDMA (black bars), reduced BFDMA and DOPE ($\phi_{\text{DOPE}} = 0.71$, dotted bars), and oxidized BFDMA and DOPE ($\phi_{\text{DOPE}} = 0.71$, gray bars) for 4 h. All experiments were performed by adding 50 μL of DNA/lipid mixture in 1mM Li_2SO_4 solution to 200 μL media in the presence of cells. The media was pure OptiMEM or a mixture of OptiMEM and BS. The final concentration of BS is indicated along the x-axis. DNA was present at a concentration of 2.4 $\mu\text{g}/\text{ml}$ in the presence of cells for all samples. 8 μM BFDMA was present in each BFDMA containing sample. Luciferase expression was measured 48 h after exposure to lipoplexes. Error bars represent one standard deviation.

To provide insight into the origin of the above-described influence of the oxidation state of BFDMA on the transfection efficiency of lipoplexes containing BFDMA and DOPE in the presence of serum, we measured the impact of changes in oxidation state of BFDMA on the sizes and zeta potentials of the lipoplexes (see Supporting materials, Figure 2.9E and F). Inspection of this data reveals that changes in the oxidation state of the BFDMA leads to no significant change in zeta potential

but a decrease in the number of aggregates with sizes of $\sim 1\mu\text{m}$ (i.e., sizes of aggregates of reduced BFDMA). We also performed SAXS measurements to determine if the oxidation state of BFDMA within the lipoplexes causes a change in nanostructure. Prior to performing these measurements, we confirmed that the scattering spectra of lipoplexes of BFDMA_{OX} (no DOPE; see ESI Figure 2.15A, red data) did not exhibit Bragg peaks (consistent with prior reports based on use of SANS and cryo-TEM⁵⁸ which show the absence of ordered lamellar structure within BFDMA_{OX}/DNA aggregates). For lipoplexes of BFDMA_{OX}-DOPE/DNA dispersed in Li₂SO₄ ($\phi_{\text{DOPE}} = 0.7$, Figure 2.4A, red data), Bragg peaks at $q_{10} = 1.12 \text{ nm}^{-1}$ and $q_{11} = 1.98 \text{ nm}^{-1}$ are observed, i.e. Bragg peaks at the same position as the lipoplex containing reduced BFDMA and DOPE (Figure 2.4A, black data), again, corresponding to a ratio $q_{10}/q_{11} = \sqrt{3}$ and thus a H_{II}^c nanostructure. However, the intensity of the q_{10} peak for the BFDMA_{OX}-DOPE/DNA sample is only 40% of the q_{10} peak for the BFDMA_{RED}-DOPE/DNA sample. This suggests that the fraction of the BFDMA and DOPE in the H_{II}^c nanostructural state is lower for the samples containing oxidized BFDMA and DOPE as compared to lipoplexes of reduced BFDMA and DOPE. Here we also note that DOPE/DNA mixtures (no BFDMA) were characterized by SAXS (Figure 2.4A, grey data). Even though three Bragg peaks are seen in the scattering at a $1: \sqrt{3}: \sqrt{4}$ periodicity indicating H_{II} nanostructure, shown in the insert of Figure 2.4A, the overall intensity of scattering from DOPE is significantly lower than BFDMA_{OX}-DOPE/DNA. This suggests that the Bragg peaks seen for the BFDMA_{OX}-DOPE/DNA data (Figure 2.4A, red data) do not arise from

the presence of DOPE alone and that BFDMA_{OX} must be integral to the BFDMA_{OX}-DOPE/DNA complex. Overall, the results presented above, when combined with our transfection measurements, serve to emphasize the correlation between the presence of H_{II}^c nanostructures in solution and the transfection efficiency of the BFDMA-DOPE lipoplexes.

We also investigated the influence of serum proteins on the nanostructure of the lipoplexes comprised of oxidized BFDMA and DOPE. Similar to the scattering data obtained using lipoplexes of oxidized BFDMA and DOPE in Li₂SO₄ (Figure 2.4A), BFDMA_{OX}-DOPE/DNA in 50% BS (Figure 2.4B, red data) generated a scattering spectrum with a first Bragg Peak at $q = 1.04$ but with only 18% of the intensity as BFDMA_{RED}-DOPE/DNA in 50% BS, (Figure 2.4B, black data). DOPE/DNA mixtures in 50% BS were also subjected to SAXS (Figure 2.4B, grey data). No Bragg peaks are seen in the scattering. Because the intensity of scattering for serum containing samples at $q < 1 \text{ nm}^{-1}$ is an order of magnitude higher than the Bragg peaks seen for DOPE/DNA in Li₂SO₄ (Figure 2.4A, grey data), any Bragg peaks generated by the DOPE lipid in this mixture are likely masked by the presence of serum. The Bragg peaks seen for the BFDMA_{OX}-DOPE/DNA data (Figure 2.4A, red data) suggests that the lipoplex nanostructure giving rise to the Bragg peaks cannot be attributed to the presence of DOPE alone and that BFDMA_{OX} must be helping the BFDMA_{OX}-DOPE/DNA complex to associate in a similar mechanism as for Li₂SO₄ based lipoplexes discussed above. Overall, the above result is significant because it reveals that the correlation between the presence of H_{II}^c nanostructures in

solution and the transfection efficiency of the BFDMA-DOPE lipoplexes is preserved in the presence of high concentrations of serum proteins.

2.4 Conclusions

A key result reported in this paper is that incorporation of DOPE into BFDMA-containing lipoplexes leads to a substantial increase in cell transfection efficiency in the presence of high concentrations of serum (up to 80% BS). This observation appears closely correlated with nanostructural characterization presented in this paper, which clearly shows that the incorporation of DOPE into the lipoplexes induces the formation of a H_{II}^c nanostructure. Although additional studies will be required to elucidate the precise mechanism of transfer of our DOPE-containing lipoplexes into cells, past studies have established that lipoplexes with a H_{II}^c nanostructure exhibit an increased propensity to fuse with cell membranes^{63, 68, 72, 74-76} (thus leading to a mechanism of uptake that is not generally thought to occur with lipoplexes that possess L_{α}^c nanostructures). It appears likely, therefore, that the high levels of cell transfection that we observe using lipoplexes of DOPE and BFDMA_{RED} in the presence of serum is the result of fusion of these lipoplexes with the cell membranes.

A second key result presented in this paper is that a change in the oxidation state of the BFDMA that is used to form the lipoplexes with DOPE substantially alters the efficiency with which lipoplexes of BFDMA and DOPE transfect cells (over a wide range of serum levels tested). When BFDMA is reduced, lipoplexes of BFDMA

and DOPE are highly efficient in transfecting cells. In contrast, when BFDMA is oxidized, lipoplexes of BFDMA and DOPE lead to levels of transgene expression that are two orders of magnitude lower than for lipoplexes containing reduced BFDMA. Complementary measurements using SAXS reveal that the low transfection efficiency of the lipoplexes of oxidized BFDMA and DOPE correlates with the presence of weak Bragg peaks corresponding to the H_{II}^c nanostructure and thus a low amount of this nanostructure in the solution. Our measurements of changes in physical properties of these lipoplexes (sizes, zeta-potentials and colloidal stability), as caused by incorporation of DOPE or oxidation of BFDMA, do not provide an alternative account for the influence of these key variables on the transfection efficiencies that are reported in this paper. We interpret our results to provide support for our hypothesis that DOPE-induced formation of the H_{II}^c nanostructure of the BFDMA-containing lipoplexes underlies the high cell transfection efficiency measured in the presence of serum, *and that the oxidation state of BFDMA within lipoplexes with DOPE substantially regulates the formation of the H_{II}^c nanostructure* and thus the ability of the lipoplexes to transfect cells with DNA.

Overall, the results described herein represent an important step toward the development of redox-active lipid materials that permit spatial and/or temporal control over the transfection of cells (*e.g.*, by the application of externally-applied electrochemical potentials or the spatially controlled delivery of chemical reducing agents). We conclude by noting that a major goal of synthetic DNA delivery vector research is to develop gene delivery materials that function in physiologically relevant

environments (*e.g.*, in the presence of high serum concentrations). A second major goal is to be able to achieve facile control over the location and timing of the delivery of DNA. The results reported in this paper represent a significant step toward the realization of gene delivery materials that possesses attributes that are relevant to both of these goals.

2.5 Acknowledgements

Financial support was provided by the National Institutes of Health (1 R21 EB006168 and AI092004), the National Science Foundation (CBET-0754921 and DMR-1121288) and the ARO (W911NF-11-1-0251). We acknowledge the support of Oak Ridge National Laboratory in providing the neutron facilities used in this work. We thank C. Jewell and X. Liu for many helpful discussions, S. Hata and H. Takahashi for assistance with synthesis of BFDMA, and V. Urban and D. Savage for help with the SANS and SAXS measurements, respectively.

2.6 References

‡ Portions of this chapter have been previously published as: J. P. E. Muller, B. S. Aytar, Y. Kondo, D. M. Lynn and N. L. Abbott, Incorporation of DOPE into Lipoplexes formed from a Ferrocenyl Lipid leads to Inverse Hexagonal Nanostructures that allow Redox-Based Control of Transfection in High Serum. *Soft Matter*, 2012, **8**, 2608-2619.

1. S. Patnaik, S. K. Tripathi, R. Goyal, A. Arora, K. Mitra, A. Villaverde, E. Vazquez, Y. Shukla, P. Kumar and K. C. Gupta, *Soft Matter*, **2011**, *7*, 6103-6112.
2. J. Ziauddin and D. M. Sabatini, *Nature*, **2001**, *411*, 107-110.

3. S. N. Bailey, R. Z. Wu and D. M. Sabatini, *Drug Discovery Today*, **2002**, 7, S113-S118.
4. F. H. Chang, C. H. Lee, M. T. Chen, C. C. Kuo, Y. L. Chiang, C. Y. Hang and S. Roffler, *Nucleic Acids Res.*, **2004**, 32, e33.
5. J. B. Delehanty, K. M. Shaffer and B. C. Lin, *Anal. Chem.*, **2004**, 76, 7323-7328.
6. F. Yamauchi, K. Kato and H. Iwata, *Nucleic Acids Res.*, **2004**, 32, e187.
7. F. Yamauchi, K. Kato and H. Iwata, *Biochim. Biophys. Acta, Gen. Subj.*, **2004**, 1672, 138-147.
8. Z. Bengali, A. K. Pannier, T. Segura, B. C. Anderson, J. H. Jang, T. A. Mustoe and L. D. Shea, *Biotechnol. Bioeng.*, **2005**, 90, 290-302.
9. M. Isalan, M. I. Santori, C. Gonzalez and L. Serrano, *Nat. Methods*, **2005**, 2, 113-118.
10. A. L. Hook, H. Thissen and N. H. Voelcker, *Biomacromolecules*, **2009**, 10, 573-579.
11. D. W. Green, S. Mann and R. O. C. Oreffo, *Soft Matter*, **2006**, 2, 732-737.
12. W. M. Saltzman and W. L. Olbricht, *Nat. Rev. Drug Discovery*, **2002**, 1, 177-186.
13. W. M. Saltzman, *Nature Biotechnology*, **1999**, 17, 534-535.
14. L. D. Shea, E. Smiley, J. Bonadio and D. J. Mooney, *Nat. Biotechnol.*, **1999**, 17, 551-554.
15. T. P. Richardson, M. C. Peters, A. B. Ennett and D. J. Mooney, *Nat. Biotechnol.*, **2001**, 19, 1029-1034.
16. T. P. Richardson, W. L. Murphy and D. J. Mooney, *Crit. Rev. Eukaryotic Gene Expression*, **2001**, 11, 47-58.
17. J. A. Shepard, A. Huang, A. Shikanov and L. D. Shea, *J. Controlled Release*, **2010**, 146, 128-135.

18. F. Yang, S. W. Cho, S. M. Son, S. R. Bogatyrev, D. Singh, J. J. Green, Y. Mei, S. Park, S. H. Bhang, B. S. Kim, R. Langer and D. G. Anderson, *Proc. Natl. Acad. Sci. U.S.A.*, **2010**, 107, 3317-3322.
19. S. Mandal, N. Rosso, C. Tiribelli, G. Scoles and S. Krol, *Soft Matter*, **2011**, 7, 9424-9434.
20. M. Guillot-Nieckowski, S. Eisler and F. Diederich, *New Journal of Chemistry*, **2007**, 31, 1111-1127.
21. M. Cavazzana-Calvo, S. Hacein-Bey, C. D. Basile, F. Gross, E. Yvon, P. Nusbaum, F. Selz, C. Hue, S. Certain, J. L. Casanova, P. Bousso, F. Le Deist and A. Fischer, *Science*, **2000**, 288, 669-672.
22. M. Cavazzana-Calvo, S. Hacein-Bey, F. Yates, J. P. de Villartay, F. Le Deist and A. Fischer, *J. Gene Med.*, **2001**, 3, 201-206.
23. M. Cavazzana-Calvo, A. Thrasher and F. Mavilio, *Nature*, **2004**, 427, 779-781.
24. W. J. Leonard, *Mol. Med. Today*, **2000**, 6, 403-407.
25. S. Hacein-Bey-Abina, F. Le Deist, F. Carlier, C. Bouneaud, C. Hue, J. De Villartay, A. J. Thrasher, N. Wulffraat, R. Sorensen, S. Dupuis-Girod, A. Fischer, M. Cavazzana-Calvo, E. G. Davies, W. Kuis, W. H. K. Lundlaan and L. Leiva, *N. Engl. J. Med.*, **2002**, 346, 1185-1193.
26. A. Fischer, S. Hacein-Bey and M. Cavazzana-Calvo, *Nat. Rev. Immunol.*, **2002**, 2, 615-621.
27. H. B. Gaspar, S. Howe and A. J. Thrasher, *Gene Ther.*, **2003**, 10, 1999-2004.
28. R. J. Kaufman, *Hum. Gene Ther.*, **1999**, 10, 2091-2107.
29. D. B. Kohn, *J. Intern. Med.*, **2001**, 249, 379-390.
30. D. Dimichele, F. G. Miller and J. J. Fins, *Haemophilia*, **2003**, 9, 145-152.
31. J. S. Chamberlain, *Hum. Mol. Genet.*, **2002**, 11, 2355-2362.
32. P. Gregorevic and J. S. Chamberlain, *Expert Opin. Biol. Ther.*, **2003**, 3, 803-814.

33. J. C. T. van Deutekom and G. J. B. van Ommen, *Nature Rev. Genet.*, **2003**, 4, 774-783.
34. M. Nishikawa and L. Huang, *Hum. Gene Ther.*, **2001**, 12, 861-870.
35. T. Niidome and L. Huang, *Gene Ther.*, **2002**, 9, 1647-1652.
36. D. Luo and W. M. Saltzman, *Nature Biotechnol.*, **2000**, 18, 33-37.
37. P. L. Felgner and G. M. Ringold, *Nature*, **1989**, 337, 387-388.
38. F. P. Kabanov AV, Seymour LW, *Self-Assembling Complexes for Gene Delivery: From Laboratory to Clinical Trial*, New York: John Wiley and Sons, 1998.
39. X. Guo and F. C. Szoka, *Acc. Chem. Res.*, **2003**, 36, 335-341.
40. F. X. Tang and J. A. Hughes, *Biochem. Biophys. Res. Commun.*, **1998**, 242, 141-145.
41. F. X. Tang and J. A. Hughes, *Bioconjugate Chem.*, **1999**, 10, 791-796.
42. F. X. Tang, W. Wang and J. A. Hughes, *J. Liposome Res.*, **1999**, 9, 331-347.
43. P. S. Ajmani, F. X. Tang, S. Krishnaswami, E. M. Meyer, C. Sumners and J. A. Hughes, *Neurosci. Lett.*, **1999**, 277, 141-144.
44. M. Balakirev, G. Schoehn and J. Chroboczek, *Chem. Biol.*, **2000**, 7, 813-819.
45. G. Byk, B. Wetzer, M. Frederic, C. Dubertret, B. Pitard, G. Jaslin and D. Scherman, *J. Med. Chem.*, **2000**, 43, 4377-4387.
46. B. Wetzer, G. Byk, M. Frederic, M. Airiau, F. Blanche, B. Pitard and D. Scherman, *Biochem. J.*, **2001**, 356, 747-756.
47. V. V. Kumar and A. Chaudhuri, *FEBS Lett.*, **2004**, 571, 205-211.
48. Z. H. Huang, W. J. Li, J. A. MacKay and F. C. Szoka, *Mol. Ther.*, **2005**, 11, 409-417.

49. V. Budker, V. Gurevich, J. E. Hagstrom, F. Bortzov and J. A. Wolff, *Nat. Biotechnol.*, **1996**, 14, 760-764.
50. O. V. Gerasimov, J. A. Boomer, M. M. Qualls and D. H. Thompson, *Adv. Drug Delivery Rev.*, **1999**, 38, 317-338.
51. P. Shum, J. M. Kim and D. H. Thompson, *Adv. Drug Delivery Rev.*, **2001**, 53, 273-284.
52. P. Meers, *Adv. Drug Delivery Rev.*, **2001**, 53, 265-272.
53. C. A. H. Prata, Y. X. Zhao, P. Barthelemy, Y. G. Li, D. Luo, T. J. McIntosh, S. J. Lee and M. W. Grinstaff, *J. Am. Chem. Soc.*, **2004**, 126, 12196-12197.
54. X. X. Zhang, C. A. H. Prata, J. A. Berlin, T. J. McIntosh, P. Barthelemy and M. W. Grinstaff, *Bioconjugate Chem.*, **2011**, 22, 690-699.
55. N. L. Abbott, C. M. Jewell, M. E. Hays, Y. Kondo and D. M. Lynn, *J. Am. Chem. Soc.*, **2005**, 127, 11576-11577.
56. C. M. Jewell, M. E. Hays, Y. Kondo, N. L. Abbott and D. M. Lynn, *J. Controlled Release*, **2006**, 112, 129-138.
57. C. M. Jewell, M. E. Hays, Y. Kondo, N. L. Abbott and D. M. Lynn, *Bioconjugate Chem.*, **2008**, 19, 2120-2128.
58. C. L. Pizzey, C. M. Jewell, M. E. Hays, D. M. Lynn, N. L. Abbott, Y. Kondo, S. Golan and Y. Talmon, *J. Phys. Chem. B*, **2008**, 112, 5849-5857.
59. M. E. Hays, C. M. Jewell, Y. Kondo, D. M. Lynn and N. L. Abbott, *Biophys. J.*, **2007**, 93, 4414-4424.
60. S. Golan, B. S. Aytar, J. P. E. Muller, Y. Kondo, D. M. Lynn, N. L. Abbott and Y. Talmon, *Langmuir*, **2011**, 27, 6615-6621.
61. B. S. Aytar, J. P. E. Muller, S. Golan, S. Hata, H. Takahashi, Y. Kondo, Y. Talmon, N. L. Abbott and D. M. Lynn, *Journal of Controlled Release*, **2012**, 157, 249-259.
62. M. E. Hays, C. M. Jewell, D. M. Lynn and N. L. Abbott, *Langmuir*, **2007**, 23, 5609-5614.

63. S. W. Hui, M. Langner, Y. L. Zhao, P. Ross, E. Hurley and K. Chan, *Biophys. J.*, **1996**, 71, 590-599.
64. G. Caracciolo, L. Callipo, S. C. De Sanctis, C. Cavaliere, D. Pozzi and A. Lagana, *Biochim. Biophys. Acta, Biomembr.*, **2010**, 1798, 536-543.
65. S. Audouy, G. Molema, L. de Leij and D. Hoekstra, *J. Gene. Med.*, **2000**, 2, 465-476.
66. O. Zelphati, L. S. Uyechi, L. G. Barron and F. C. Szoka, *Biochim. Biophys. Acta, Lipids Lipid Metab.*, **1998**, 1390, 119-133.
67. J. P. Yang and L. Huang, *Gene Ther.*, **1997**, 4, 950-960.
68. C. Marchini, M. Montani, A. Amici, H. Amenitsch, C. Marianecchi, D. Pozzi and G. Caracciolo, *Langmuir*, **2009**, 25, 3013-3021.
69. K. Ewert, N. L. Slack, A. Ahmad, H. M. Evans, A. J. Lin, C. E. Samuel and C. R. Safinya, *Curr. Med. Chem.*, **2004**, 11, 133-149.
70. M. W. Tate and S. M. Gruner, *Biochemistry*, **1987**, 26, 231-236.
71. I. Koltover, T. Salditt, J. O. Radler and C. R. Safinya, *Science*, **1998**, 281, 78-81.
72. A. D. Miller, *Angew. Chem., Int. Ed.*, **1998**, 37, 1769-1785.
73. M. Muñoz-Úbeda, A. Rodríguez-Pulido, A. Nogales, O. Llorca, M. Quesada-Pérez, A. Martín-Molina, E. Aicart and E. Junquera, *Soft Matter*, **2011**, 7, 5991-6004.
74. A. J. Verkleij, *Biochim. Biophys. Acta*, **1984**, 779, 43-63.
75. L. V. Chernomordik and J. Zimmerberg, *Curr. Opin. Struct. Biol.*, **1995**, 5, 541-547.
76. S. W. Hui, T. P. Stewart, L. T. Boni and P. L. Yeagle, *Science*, **1981**, 212, 921-923.
77. J. O. Rädler, I. Koltover, T. Salditt and C. R. Safinya, *Science*, **1997**, 275, 810-814.
78. D. Shier, J. Butler and R. Lewis, *Hole's Human Anatomy & Physiology*, McGraw-Hill, 2007.

79. N. S. Templeton, *Curr. Med. Chem.*, **2003**, 10, 1279-1287.
80. Y. Kakizawa, H. Sakai, K. Nishiyama, M. Abe, H. Shoji, Y. Kondo and N. Yoshino, *Langmuir*, **1996**, 12, 921-924.
81. Y. Kakizawa, H. Sakai, A. Yamaguchi, Y. Kondo, N. Yoshino and M. Abe, *Langmuir*, **2001**, 17, 8044-8048.
82. N. Yoshino, H. Shoji, Y. Kondo, Y. Kakizawa, H. Sakai and M. Abe, *J. Jpn. Oil Chem. Soc.*, **1996**, 45, 769-775.
83. X. Y. Liu and N. L. Abbott, *J. Phys. Chem. B*, **2010**, 114, 15554-15564.
84. T. C. Huang, H. Toraya, T. N. Blanton and Y. Wu, *J. Appl. Crystallogr.*, **1993**, 26, 180-184.
85. R. Koynova, B. Tenchov, L. Wang and R. C. MacDonald, *Mol. Pharmaceutics*, **2009**, 6, 951-958.
86. J. M. Seddon, *Biochim. Biophys. Acta*, **1990**, 1031, 1-69.
87. A. Bilalov, U. Olsson and B. Lindman, *Soft Matter*, **2009**, 5, 3827-3830.
88. J. Corsi, R. W. Hawtin, O. Ces, G. S. Attard and S. Khalid, *Langmuir*, **2010**, 26, 12119-12125.
89. S. Li, M. A. Rizzo, S. Bhattacharya and L. Huang, *Gene Ther.*, **1998**, 5, 930-937.
90. S. Li, W. C. Tseng, D. B. Stolz, S. P. Wu, S. C. Watkins and L. Huang, *Gene Ther.*, **1999**, 6, 585-594.

2.7 Supplemental Materials

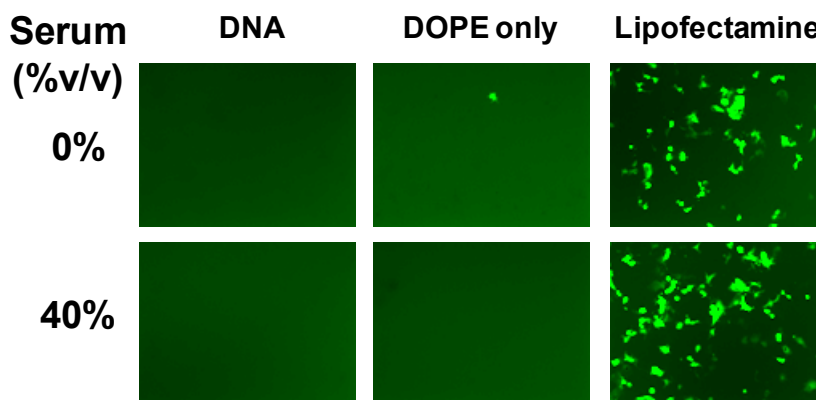


Figure 2.7. Influence of serum on EGFP expression in COS-7 cells treated with pEGFP-N1 only (DNA) or with pEGFP-N1 and 10 μM DOPE (DOPE only, ($\varphi_{\text{DOPE}} = 1$)) or with commercial transfection agent (Lipofectamine 2000). The overall concentration of DNA in each solution was 2.4 $\mu\text{g}/\text{ml}$. Cells were incubated with the DNA or lipoplex solutions in Opti-MEM or 50% OptiMEM and 50% adult bovine serum for 4 h. Final concentration of Serum (BS) includes a 20% dilution effect from addition of DNA or lipoplex solution to each well. Images were acquired at 48 h after exposure of cells to lipoplexes. The dimensions of each micrograph above are 1194 μm by 895 μm .

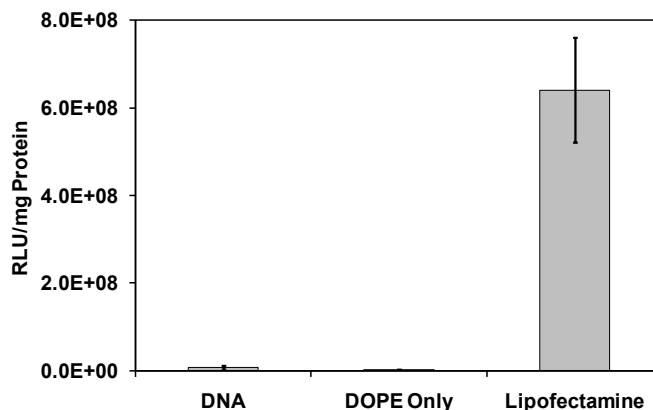


Figure 2.8. Extent of normalized luciferase expression in COS-7 cells treated with pEGFP-N1 only (DNA) or with pEGFP-N1 and 10 μM DOPE (DOPE only, ($\varphi_{\text{DOPE}} = 1$)) or with commercial transfection agent (Lipofectamine 2000) for 4 h. All experiments were performed by adding 50 μL of DNA/lipid mixture in 1mM Li_2SO_4 solution to 200 μL of OptiMEM with cells present. DNA was present at a concentration of 2.4 $\mu\text{g}/\text{ml}$ for all samples. Luciferase expression was measured 48 h after exposure to lipoplexes.

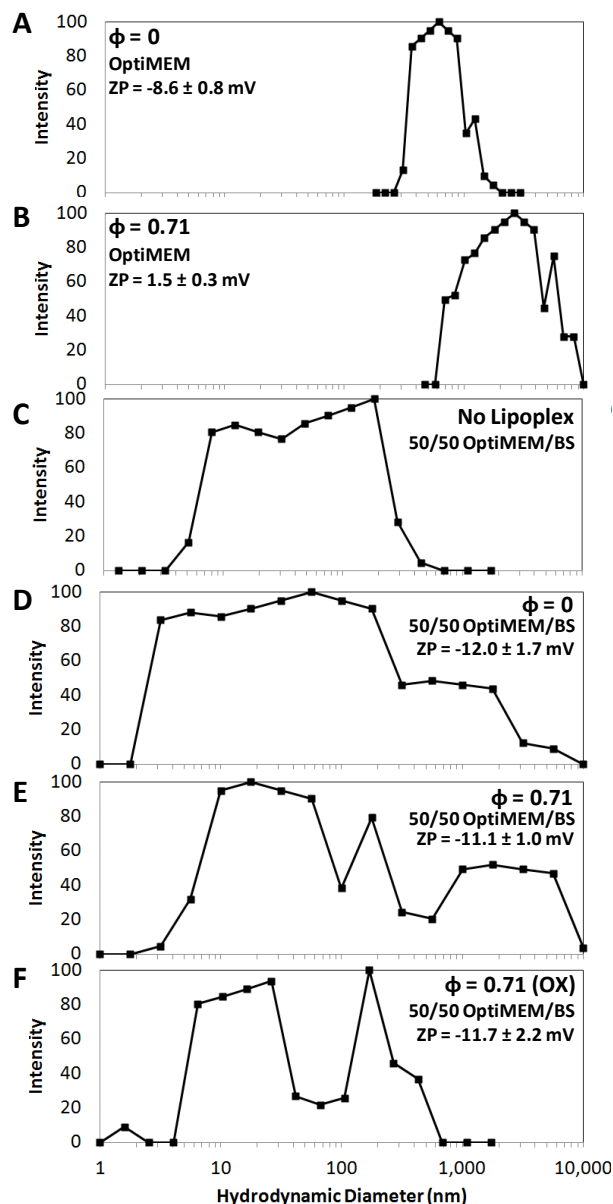


Figure 2.9. Hydrodynamic diameters (plotted as an intensity-weighted distribution) and zeta potentials of (A) lipoplexes of BFDMA_{RED} in OptiMEM, (B) lipoplexes of BFDMA_{RED} and DOPE in OptiMEM, (C) OptiMEM containing 50% (v/v) BS in the absence of any lipoplexes, (D) lipoplexes of BFDMA_{RED} in OptiMEM with 50% (v/v) BS, and (E) lipoplexes of BFDMA_{RED} and DOPE in OptiMEM with 50% (v/v) BS (F) lipoplexes of BFDMA_{OX} and DOPE in OptiMEM with 50% (v/v) BS; all lipoplexes were characterized after 20 minutes of incubation in the indicated media. Molar fractions of DOPE, $\phi_{\text{DOPE}} = \text{DOPE}/(\text{BFDMA} + \text{DOPE})$, are given in the legend of each graph. DNA was present at a concentration of 2.4 $\mu\text{g}/\text{mL}$ for all samples and the concentration of BFDMA in each sample was 8 μM . All experiments were repeated three times to confirm reproducibility of results.

Experiments designed to characterize the zeta potentials of lipoplexes, shown in Figure 2.9 and Figure 2.13, were conducted in the following general manner. Samples of lipoplexes formed from either BFDMA_{RED} or BFDMA_{RED}-DOPE, or BFDMA_{OX}-DOPE were prepared as described above and in the main manuscript. These samples were then diluted using OptiMEM or OptiMEM with 50% (v/v) BS. For each sample, 5 mL of lipoplex solution was injected into the inlet of a Zetasizer 3000HS instrument, and measurements were made at ambient temperature using an electrical potential of 150 V. The final BFDMA and plasmid DNA (pEGFP-N1) concentrations were 8 μ M and 24 mg/mL, respectively for all samples. These values are the same as those used in the cell transfection experiments described in the main manuscript. A minimum of five measurements was recorded for each sample, and the Henry equation was used to calculate zeta potentials from measurements of electrophoretic mobility. For this calculation, we assumed the viscosity of the solution to be the same as that of water.

Experiments designed to characterize the apparent size of lipoplexes, shown in Figure 2.9, Figure 2.10, Figure 2.11 and Figure 2.12, were conducted in the following general manner. A 100-mW, 532-nm laser (Compass 315M-100, Coherent, Santa Clara, CA) illuminated a temperature-controlled glass cell at 25 °C that was filled with a refractive-index matching fluid (decahydronaphthalene, Fisher Scientific, Pittsburgh, PA). The scattering of light was measured at an angle of 90°. The autocorrelation functions (ACFs) were obtained using a BI-9000AT digital autocorrelator (Brookhaven Instruments, Holtsville, NY). The ACFs were analyzed

using an intensity-based CONTIN analysis and then Stokes-Einstein relationship was used to yield hydrodynamic diameters as described previously (see Ref. 59 from the main manuscript). It is important to note that for lipoplexes with sizes greater than ~ 1 μm , the autocorrelation function can be influenced by rotational diffusion of the aggregates as well as internal degrees of freedom. For these reasons, the sizes of the larger complexes in Figure 2.9, Figure 2.10, Figure 2.11 and Figure 2.12 should be viewed as apparent hydrodynamic sizes.

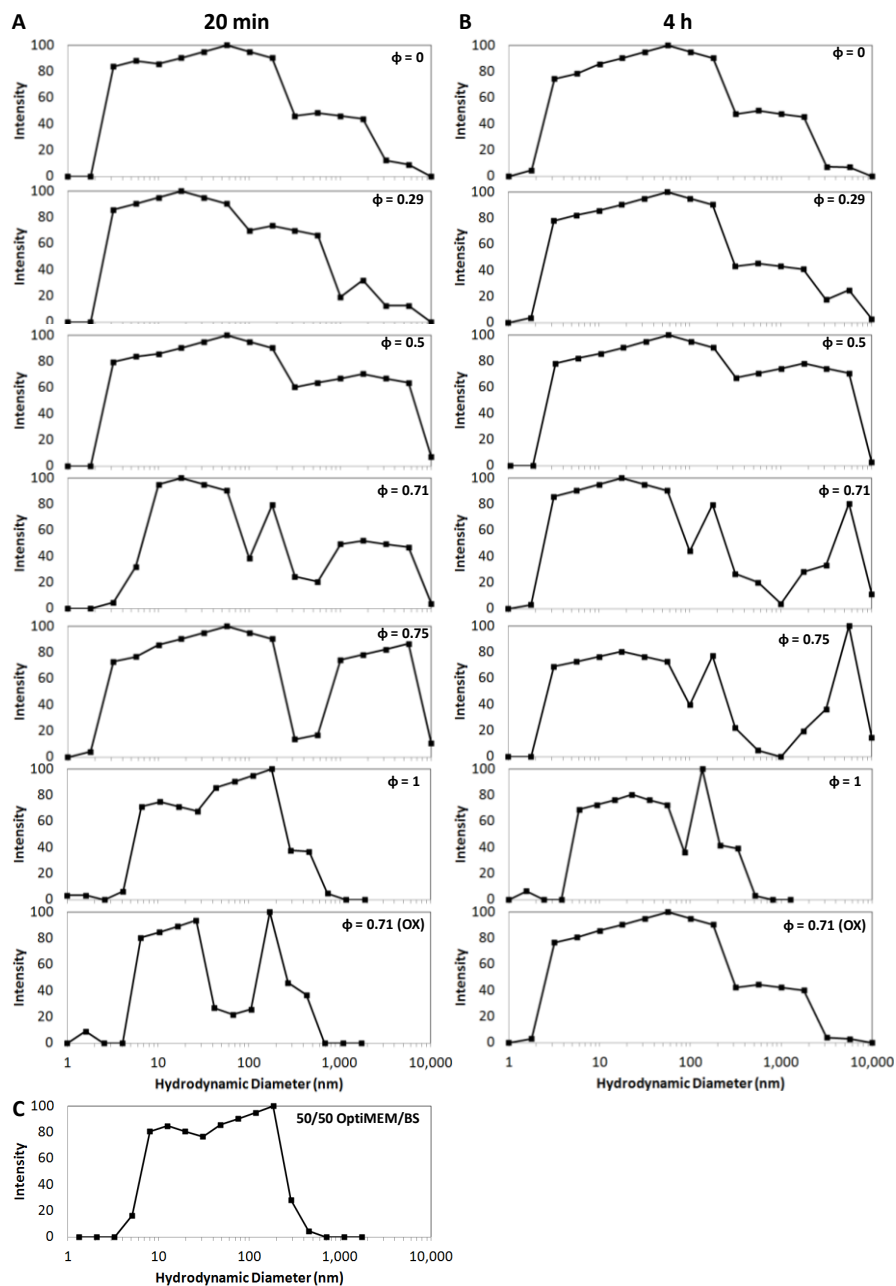


Figure 2.10. Hydrodynamic diameters of lipoplexes (plotted as intensity-weighted distributions) formed using solutions of DNA and lipid (BFDMA_{RED}, BFDMA_{OX} and/or DOPE), and incubated in OptiMEM with 50% (v/v) BS for (A) 20 minutes, (B) 4 hours. DNA was present at a concentration of 2.4 $\mu\text{g}/\text{mL}$ for all samples. Mole fractions of DOPE, $\phi_{\text{DOPE}} = \text{DOPE}/(\text{BFDMA} + \text{DOPE})$, are given in the legend of each graph. For $\phi < 1$, BFDMA_{RED} was used for all samples except where “(OX)” is indicated in the legend, denoting the presence of BFDMA_{OX}. The concentration of BFDMA in each sample was 8 μM . (C) Hydrodynamic diameters of aggregates found in OptiMEM with 50% (v/v) BS.

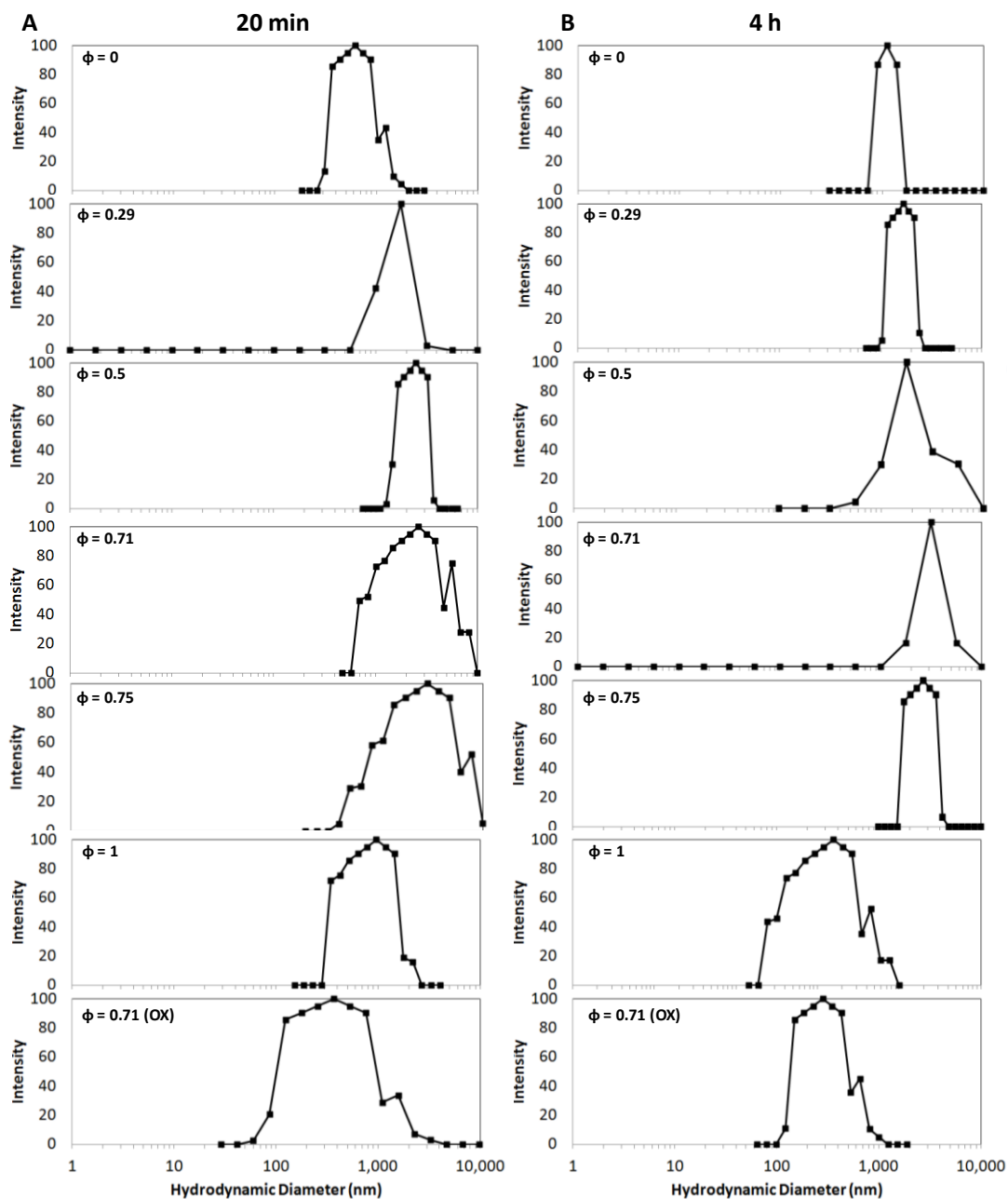


Figure 2.11. Hydrodynamic diameters of lipoplexes (plotted as intensity-weighted distributions) formed using solutions of DNA and lipid (BFDMA_{RED}, BFDMA_{OX} and/or DOPE), and incubated in OptiMEM for (A) 20 minutes, (B) 4 hours. DNA was present at a concentration of 2.4 $\mu\text{g/mL}$ for all samples. Mole fractions of DOPE, $\phi_{\text{DOPE}} = \text{DOPE}/(\text{BFDMA} + \text{DOPE})$, are given in the legend of each graph. For $\phi < 1$, BFDMA_{RED} was used for all samples except where “(OX)” is indicated in the legend, denoting the presence of BFDMA_{OX}. The concentration of BFDMA in each sample was 8 μM .

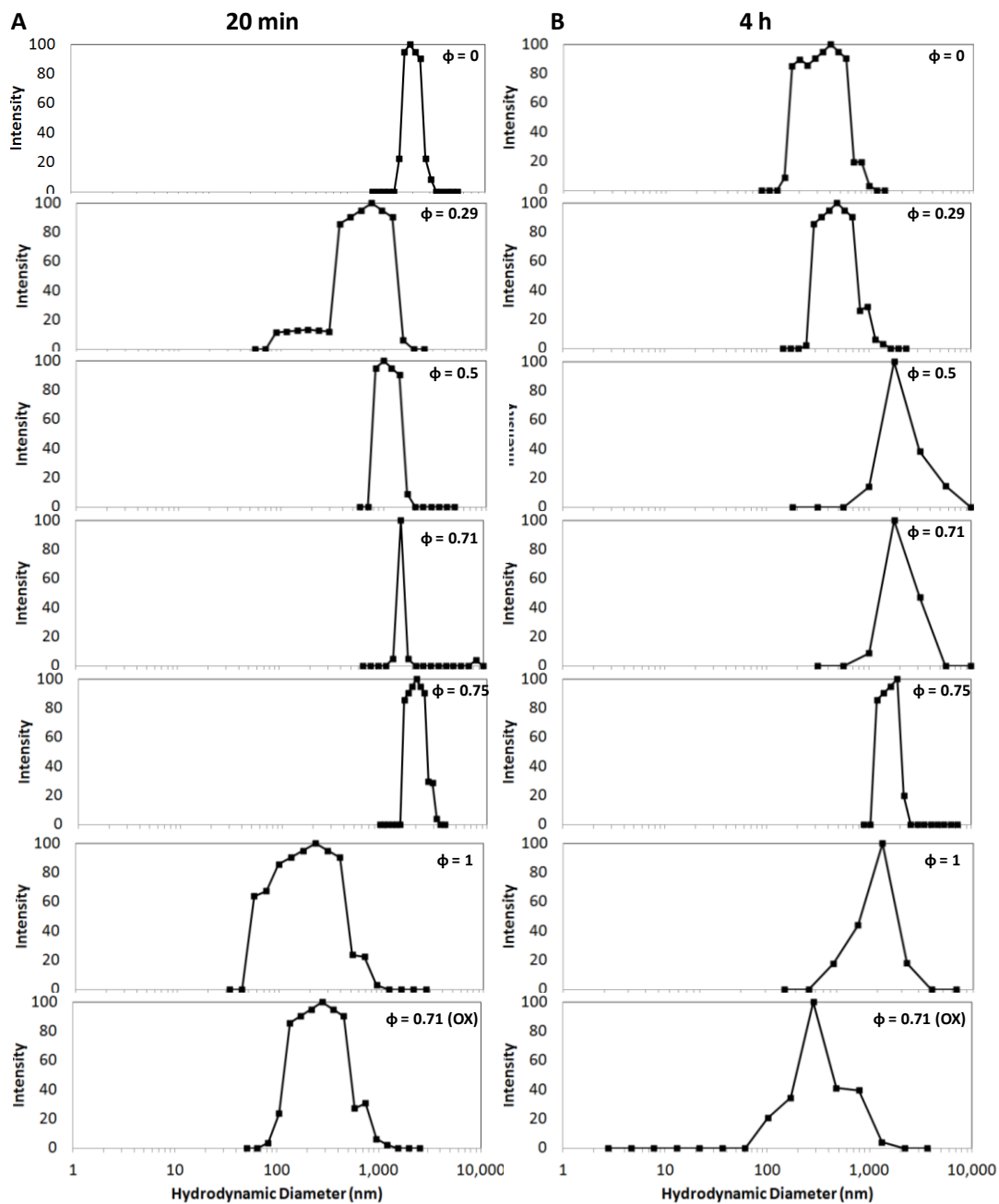


Figure 2.12. Hydrodynamic diameters of lipoplexes (plotted as intensity-weighted distributions) formed using solutions of DNA and lipid (BFDMA_{RED}, BFDMA_{OX} and/or DOPE), and incubated in 1 mM Li₂SO₄ for (A) 20 minutes, (B) 4 hours. DNA was present at a concentration of 2.4 μ g/mL for all samples. Mole fractions of DOPE, $\phi_{\text{DOPE}} = \text{DOPE}/(\text{BFDMA} + \text{DOPE})$, are given in the legend of each graph. For $\phi < 1$, BFDMA_{RED} was used for all samples except where “(OX)” is also indicated in the legend, denoting the presence of BFDMA_{OX}. The concentration of BFDMA in each sample was 8 μ M.

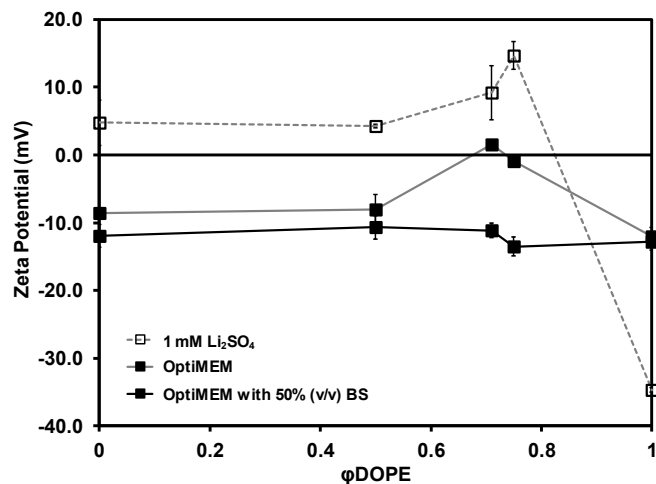


Figure 2.13. Zeta potentials of lipoplexes of BFDMA and/or DOPE and DNA, plotted as a function of mole fraction of DOPE (ϕ_{DOPE}). BFDMA is present at 8 μM and DNA at 2.4 $\mu\text{g}/\text{mL}$ resulting in a charge ratio of 1.1 for all samples with $\phi < 1$. The symbols correspond to different media, specified in the legend. Error bars represent the standard deviation of five measurements. Note that the zeta potential, when measured in OptiMEM containing 50% (v/v) BS, remains constant, around -11 ± 1 mV, for $\phi_{\text{DOPE}} = 0$ to 1.

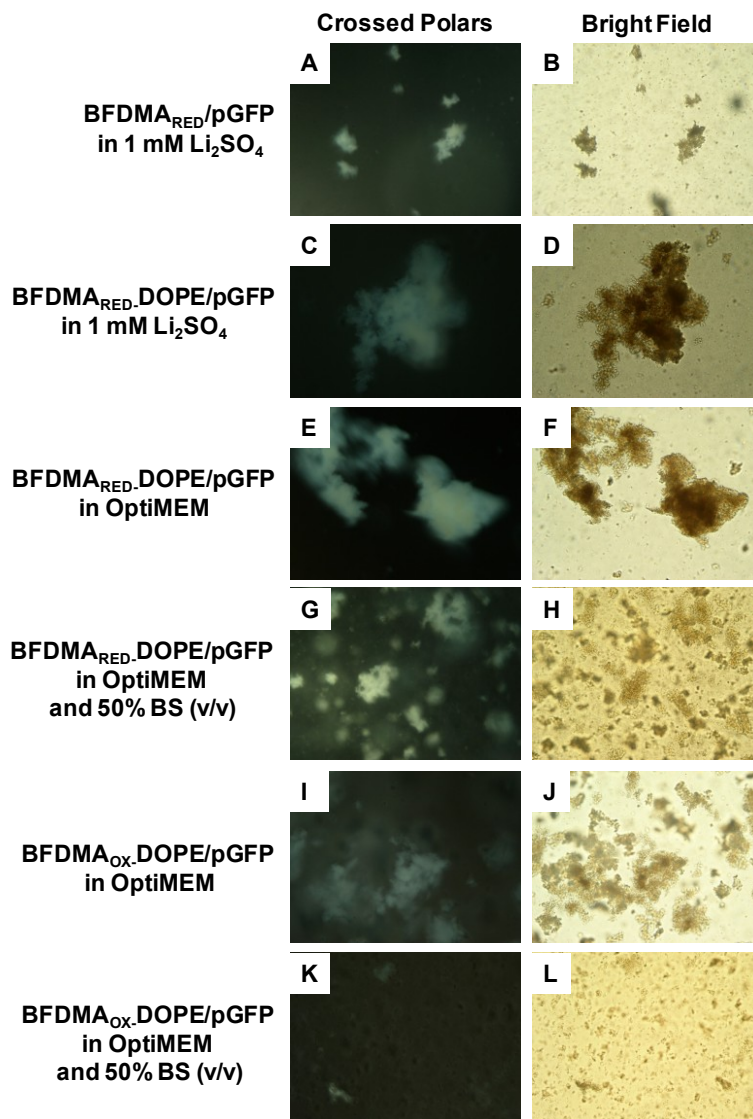


Figure 2.14. Optical images (crossed polars, left column and bright field, right column) of lipoplexes of either BFDMA alone ($\phi_{\text{DOPE}} = 0$) or BFDMA-DOPE ($\phi_{\text{DOPE}} = 0.71$) and pGFP DNA used to determine the presence of birefringence. The lipid concentrations in each sample are, **(A and B)** 0.87 mM BFDMA; **(C and D)** 0.87 mM BFDMA and 2.17 mM DOPE; **(E, F, I and J)** 0.64 mM BFDMA and 1.60 mM DOPE; **(G, H, K and L)** 0.32 mM BFDMA and 0.8 mM DOPE; all in the presence of pEGFP-N1 (2.0 mg/ml) at a charge ratio of 1.1:1 or 3.3:1 (+/-) for reduced or oxidized BFDMA containing solutions respectively. Media used for each sample is indicated on the left side of each figure. Width of each micrograph corresponds to 880 μm . Note that the concentrations of BFDMA in these samples are approximately 1000-fold higher than those used in transfection experiments, and thus the sizes of the aggregates in these images should not be used to indicate the sizes of lipoplexes that lead to cell transfection.

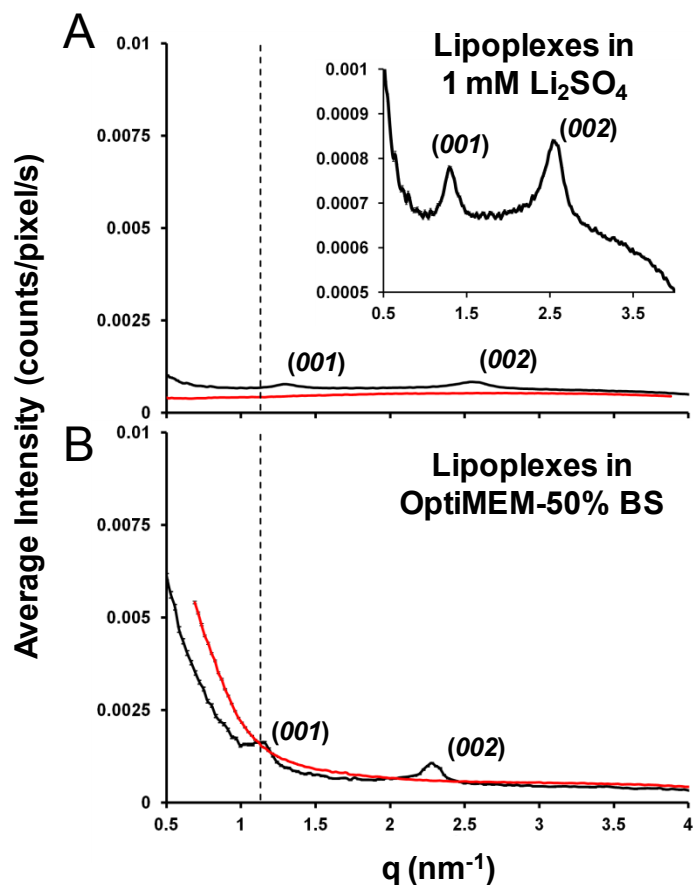


Figure 2.15. SAXS spectra obtained using reduced BFDMA (black) or oxidized BFDMA (red) containing solutions of; (A) 0.87 mM BFDMA in 1 mM Li₂SO₄; (B) 0.32 mM BFDMA in OptiMEM with 50% (v/v) BS, all in the presence of pEGFP-N1 (2.0 mg/ml) at a charge ratio of 1.1:1 or 3.3:1 (+/-) for reduced or oxidized BFDMA containing solutions respectively.

Comments regarding cubic nanostructures: Cubic phases reported in the literature include, (i) the space group Ia3d (Q230) with experimentally visible Bragg peaks at $\sqrt{6}$, $\sqrt{8}$, $\sqrt{14}$, $\sqrt{16}$, and $\sqrt{20}$. This is the most commonly observed bicontinuous cubic phases in surfactant and lipid systems.¹⁻⁶ Here we also note that Lindblom et al.² specify the Ia3d space group as $\sqrt{3}$, $\sqrt{4}$, $\sqrt{7}$, $\sqrt{8}$, etc. However, in International Tables (p. 345-346)⁷ no odd integer roots are allowed in the spacings, in disagreement with

ref 92. (ii) the space group Pn3m (Q224), a primitive cubic lattice with the spacing $\sqrt{2}$, $\sqrt{3}$, $\sqrt{4}$, $\sqrt{6}$, $\sqrt{8}$, $\sqrt{9}$, $\sqrt{10}$ etc., shown to exist, for example, in solutions containing DOPE-Me,⁸ (iii) the space group Im3m (Q229), a body-centred cubic lattice with the spacing $\sqrt{2}$, $\sqrt{4}$, $\sqrt{6}$, $\sqrt{8}$, $\sqrt{10}$, $\sqrt{12}$, $\sqrt{14}$ etc., a less common structure that has been observed in several lipid systems.^{2, 8}

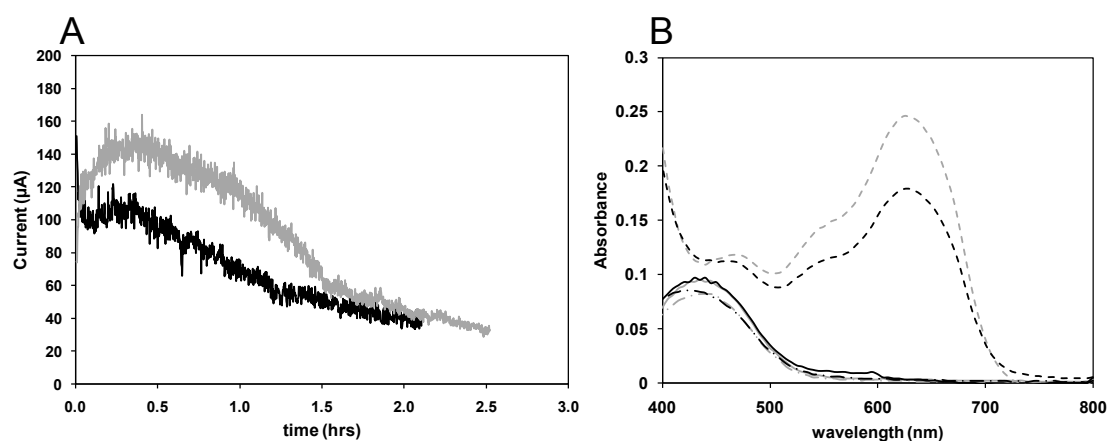


Figure 2.16. **(A)** Current passed over time at a potential of 600 mV during the electrochemical oxidation of 1 mM BFDMA, $\phi_{\text{DOPE}} = 0$ (light solid line) and 1 mM BFDMA in the presence of 2.5 mM DOPE, $\phi_{\text{DOPE}} = 0.71$ (dark solid line), in 1 mM Li₂SO₄; **(B)** UV/visible absorbance spectra for solutions of BFDMA only ($\phi_{\text{DOPE}} = 0$); reduced BFDMA (light line), electrochemically oxidized BFDMA (light dashed line), oxidized BFDMA treated with a 10 fold excess of ascorbic acid to chemically reduce an electrochemically oxidized sample (light dot-dashed line). The solutions were aqueous in 1 mM Li₂SO₄ containing 500 μM reduced or oxidized BFDMA respectively. UV/visible absorbance spectra for solutions of BFDMA and DOPE ($\phi_{\text{DOPE}} = 0.71$); reduced BFDMA/DOPE (dark line), electrochemically oxidized BFDMA/DOPE (dark dashed line), oxidized BFDMA/DOPE treated with a 10 fold excess of ascorbic acid (dark dot-dashed line). The solutions were aqueous in 1 mM Li₂SO₄ containing 500 μM reduced or oxidized BFDMA in the presence of 1.25 mM DOPE. For all samples, prior to absorbance measurements, DTAB was added to eliminate turbidity observed in the lipid solutions. DOPE, ascorbic acid and DTAB do not absorb light in the region of 400-800 nm.

To electrochemically oxidize BFDMA in the presence of DOPE for use in cell transfection experiments, we used a solution of 1 mM BFDMA and 2.5 mM DOPE in aqueous 1 mM Li₂SO₄ ($\phi_{\text{DOPE}} = 0.71$), a composition chosen on the basis of the

results shown in Figures 2 and 3. A platinum gauze electrode was immersed into the solution and held at a potential of 600 mV (vs. Ag/AgCl standard electrode) for 3 h at 75 °C. This elevated temperature was used because in past studies it has been found that the rate of oxidation of BFDMA alone is significantly enhanced at this temperature. Spectrophotometry was used to characterize the extent of oxidation of BFDMA in the resulting solution and the results were compared to previous studies (see Figure 2.16 above). In brief, spectrophotometric measurements confirmed that the presence of DOPE during electrochemical oxidation did not prevent the oxidation of BFDMA_{RED} to BFDMA_{OX} (see structure shown in Figure 1A). The absorbance spectrum of BFDMA_{RED} was similar to BFDMA_{RED}-DOPE and, upon electrochemical oxidation, the absorbance spectrum of BFDMA_{OX} was similar to BFDMA_{OX}-DOPE (Figure 2.16). We also note that subjecting a solution of 2.5 mM DOPE to a potential of 600 mV led to no significant passage of current over a period of 3 h. We conclude on the basis of these results that the procedure described above can be used to electrochemically oxidize BFDMA in the presence of DOPE.

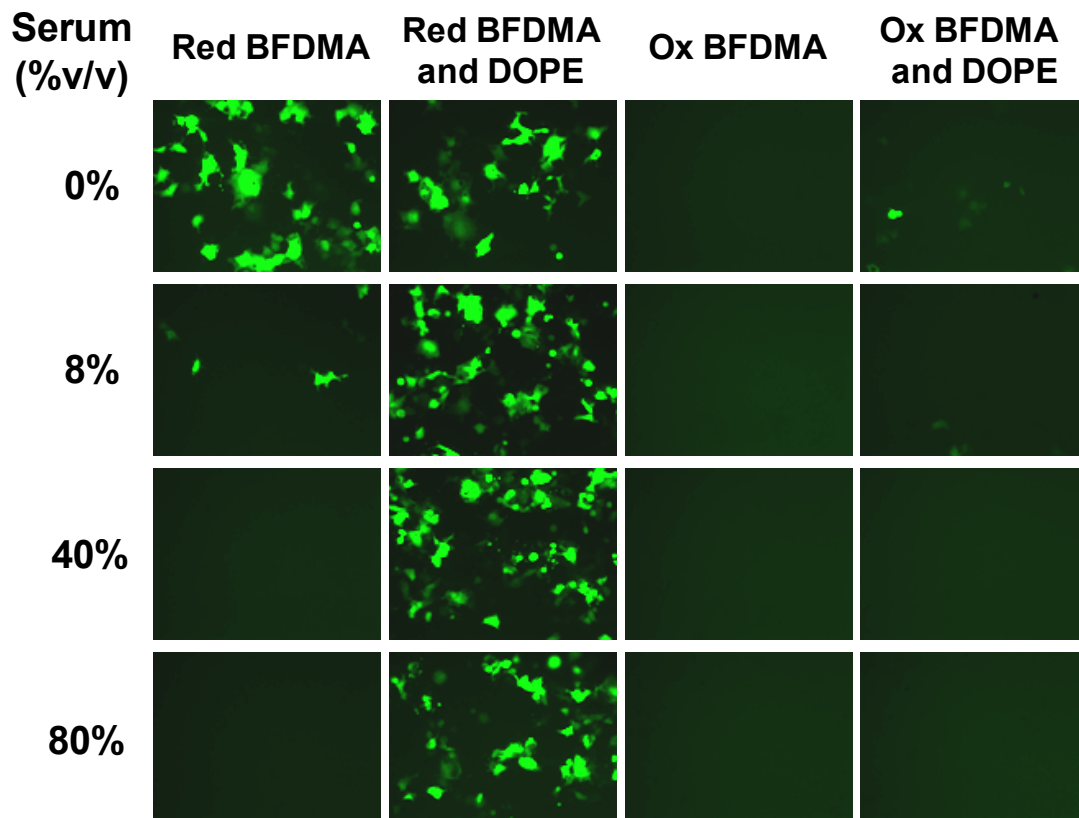


Figure 2.17. Influence of serum on EGFP expression in COS-7 cells treated with lipoplexes formed from pEGFP-N1 and reduced or oxidized BFDMA with ($\phi_{\text{DOPE}} = 0.71$) and without ($\phi_{\text{DOPE}} = 0$) DOPE for 4 h. Cells were incubated with the lipoplex solutions in Opti-MEM and different levels of BS (given down the left hand side of the figure). The overall concentrations of BFDMA and DNA in each lipoplex solution were $8 \mu\text{M}$ and $2.4 \mu\text{g/ml}$, respectively, providing a charge ratio of 1.1:1 (+/-) for all reduced BFDMA samples and 3.3 for oxidized BFDMA samples as DOPE has a net charge of zero. Fluorescence micrographs ($1194 \mu\text{m}$ by $895 \mu\text{m}$) were acquired 48 h after exposure of cells to lipoplexes. No evidence of cell transfection was seen for DOPE only containing lipoplexes (see Figure 2.7 and Figure 2.8).

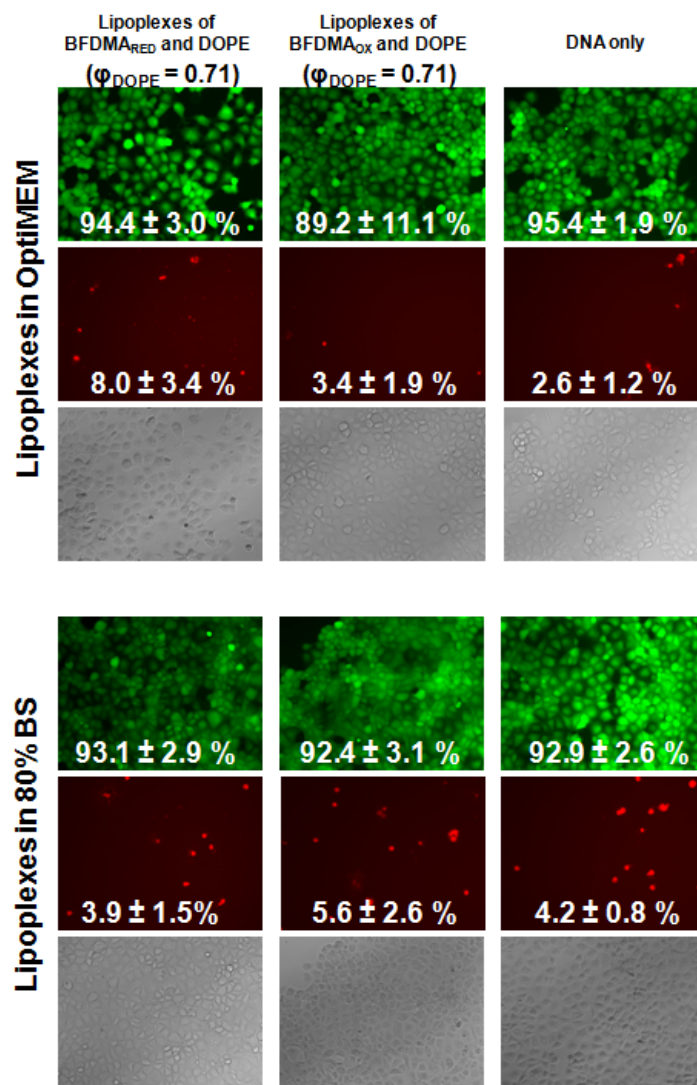


Figure 2.18. Results of live/dead cytotoxicity assays for COS-7 treated with lipoplexes formed from BFDMA_{RED}-DOPE, BFDMA_{OX}-DOPE, and DNA only (as a negative control). Plasmid DNA encoding luciferase was used to form the lipoplexes used in these experiments. Cells were exposed to lipoplexes for 4 h in OptiMEM (Top), or 80% BS (Bottom). Representative fluorescence and phase-contrast micrographs were captured 48 h after exposure to lipoplexes or DNA. Cells were stained with each of the following respective live/dead cell stains and allowed to sit for 30 minutes prior to imaging: Calcein AM was used to reveal live cells and appears as green fluorescence; EthD-1 was used to reveal dead cells and is shown as red fluorescence. Values for the percentage of live cells in each image were calculated using the number of Calcein AM-stained cells and the total number of cells determined by Hoechst (nuclear) stained cells (data not shown). The percentage of dead cells was calculated using the number of EthD-1-stained cells and the total number of Hoechst stained cells. These percentage values are shown in the figure above on each of the respective fluorescent micrographs. The error shown in the data is one standard deviation, n = 5.

Table 2.2. Results of live/dead cytotoxicity assays for COS-7 treated with lipoplexes formed from BFDMA_{RED}, BFDMA_{RED}-DOPE, BFDMA_{OX}-DOPE, and DNA only (as a negative control). Experiments were performed in OptiMEM media, or in OptiMEM containing increasing concentration of BS (8%, 40%, or 80% (v/v)). In each entry in the Table, “L” refers to the percentage of live cells, and “D” refers to the percentage of dead cells. For details of lipoplex preparation and methods used to determine the percentage of live and dead cells, see the caption to Figure 2.16.

	% Live cells (L) and % Dead cells (D)			
	OptiMEM	8% BS	40% BS	80% BS
BFDMA _{RED} + DNA	L: 90.8 ± 1.7 D: 6.2 ± 1.0	-	-	-
BFDMA _{RED} -DOPE+ DNA	L: 94.4 ± 3.0 D: 8.0 ± 3.4	L: 89.4 ± 8.0 D: 5.5 ± 4.4	L: 96.1 ± 2.8 D: 3.5 ± 2.5	L: 93.1 ± 2.9 D: 3.9 ± 1.5
BFDMA _{OX} -DOPE + DNA	L: 89.2 ± 11.1 D: 3.4 ± 1.9	L: 89.9 ± 4.4 D: 5.0 ± 2.3	L: 96.2 ± 3.4 D: 3.6 ± 1.4	L: 92.4 ± 3.1 D: 5.6 ± 2.6
DNA only	L: 95.4 ± 1.9 D: 2.6 ± 1.2	L: 90.1 ± 3.8 D: 3.1 ± 0.8	L: 88.2 ± 3.3 D: 5.0 ± 1.9	L: 92.9 ± 2.6 D: 4.2 ± 0.8

2.8 Supplemental materials references

1. P. Alexandridis, U. Olsson and B. Lindman, *Langmuir*, **1998**, 14, 2627-2638.
2. G. Lindblom and L. Rilfors, *Biochimica Et Biophysica Acta*, **1989**, 988, 221-256.
3. K. Fontell, *Colloid Polym. Sci.*, **1990**, 268, 264-285.
4. R. Ivanova, B. Lindman and P. Alexandridis, *Langmuir*, **2000**, 16, 3660-3675.
5. R. Ivanova, B. Lindman and P. Alexandridis, *Langmuir*, **2000**, 16, 9058-9069.
6. V. Luzzati and P. A. Spegt, *Nature*, **1967**, 215, 701-704.
7. International Tables for X-Ray Crystallography, 1, 2nd edn., The Kynoch Press, Birmingham, 1965.
8. S. M. Gruner, M. W. Tate, G. L. Kirk, P. T. C. So, D. C. Turner, D. T. Keane, C. P. S. Tilcock and P. R. Cullis, *Biochemistry*, **1988**, 27, 2853-2866.

Chapter 3: The Inverse Hexagonal Phase formed in Complexes of a Redox Active Ferrocenyl Amphiphile, DOPE and DNA is Observed Using cryo-TEM

3.1 Introduction

Data presented in this chapter build from Chapter 2 to demonstrate that the incorporation of dioleoylphosphatidylethanolamine (DOPE) into complexes of bis(11-ferrocenylundecyl)dimethylammonium bromide (BFDMA) and DNA (“lipoplexes”) results in the formation of inverse hexagonal (H_{II}^c) aggregates in solution (see Figure 2.1 in Chapter 2 of this thesis for the structure these molecules). While Chapter 2 reported use of quantitative small-angle x-ray scattering (SAXS), small-angle neutron scattering (SANS), birefringence, dynamic light scattering (DLS) and zeta potential analysis to characterize these mixed lipid-based lipoplexes, this chapter reports further characterization of the inverse hexagonal structure of this mixed lipid based lipoplex by direct nanoscale imaging using cryogenic transmission electron microscopy (cryo-TEM). SAXS is used in conjunction with cryo-TEM to provide quantitative information about these structures. Although previous studies have imaged the H_{II}^c phase within otherwise multilamellar (onion-like, layered) lipoplexes,¹ lipoplexes comprised largely of H_{II}^c nanostructure are described in this chapter.

In addition to characterization of the H_{II}^c structure, a second aim of the study reported in this chapter was to use cryo-TEM imaging and SAXS analysis to

characterize the effect that a chemical reducing agent, ascorbic acid (AA) has on the nanostructures of lipoplexes of oxidized BFDMA, DOPE and DNA. Previously, in the absence of DOPE, AA was used successfully to activate lipoplexes of oxidized BFDMA and DNA *in situ* with mammalian cells (i.e. reduction of the oxidized BFDMA within the formed lipoplexes led to the formation of a lipoplex of reduced BFDMA and DNA that transfected cells with significantly higher efficiency than lipoplexes of oxidized BFDMA).² The investigation reported in this chapter of the effect of AA on the nanostructures of BFDMA, DOPE and DNA aimed to determine if AA can be used to activate lipoplexes of oxidized BFDMA, DOPE and DNA.² We show that AA converts the nanostructures containing oxidized BFDMA into nanostructures that resemble those of reduced BFDMA. This conversion is more successful in the absence than in the presence of bovine serum. Finally, we use cell transfection assays to show that lipoplexes of oxidized BFDMA and DOPE treated with AA in the presence of cells in serum free media transfect cells with high efficiency. In contrast, when these lipoplexes are treated with AA in serum containing media, a significantly lower efficiency of cell transfection is observed, similar to that of lipoplexes of oxidized BFDMA and DOPE that were not treated with AA suggesting that efficiency of cell transfection is in some way related to the degree of ordering of the nanostructures of the lipoplexes in solution.

3.2 Experimental section

3.2.1 Materials

Bis-(11-ferrocenylundecyl)dimethylammonium bromide (BFDMA) was synthesized according to methods published elsewhere.³⁻⁵ Dioleoylphosphatidylethanolamine (DOPE) was purchased from Avanti Polar Lipids (Alabaster, Alabama) in powdered form. Ascorbic acid, and lithium sulfate monohydrate were purchased from Sigma Aldrich (St. Louis, MO). Deionized water (18.2 M Ω) was used to prepare all buffers and salt solutions. OptiMEM cell culture medium and bovine serum (BS) were purchased from Invitrogen (Carlsbad, CA). Plasmid DNA encoding enhanced green fluorescent protein (pEGFP-N1 (4.7 kbps, >95% supercoiled) was purchased from Elim Biopharmaceuticals (San Francisco, CA). All commercial materials were used as received without further purification unless otherwise noted.

3.2.2 Experimental methods

Preparation of reduced and oxidized BFDMA, and reduced and oxidized BFDMA-DOPE solutions was performed according to the procedure detailed in Chapter 2, section 2.2.2.1 of this thesis. We note here that, as in Chapter 2, we define ϕ_{DOPE} to be the mole fraction of DOPE in lipoplexes formed from DOPE and BFDMA [$\phi_{\text{DOPE}} = \text{moles of DOPE} / (\text{moles of DOPE} + \text{moles of BFDMA})$]. In the text below we use the abbreviations, BFDMA_{RED}-DOPE/DNA and BFDMA_{OX}-DOPE/DNA to describe the mixed-lipid-containing lipoplexes. The subscript “RED”

refers to the reduced state of BFDMA and “OX” refers to the oxidized state of BFDMA.

3.2.2.1 Preparation of lipoplexes for characterization by cryo-TEM and SAXS.

All samples characterized by Cryo-TEM and SAXS were formulated using reduced or oxidized BFDMA, DOPE and plasmid DNA encoding EGFP (pEGFP-N1). Samples were prepared using 1 mM Li_2SO_4 in deionized water. A stock solution of BFDMA and DOPE (1 mM BFDMA and relevant ϕ_{DOPE}) was diluted with a small volume of DNA stock solution (2.0 mg/ml in H_2O resulting in a 10% dilution) and vortexed for 5 s. The charge ratio (CR) used was 1.1:1 for reduced BFDMA containing lipoplexes and 3.3:1 for oxidized BFDMA containing lipoplexes, the same CRs as used in the transfection and characterization experiments in Chapter 2. Samples of reduced or oxidized BFDMA-containing lipoplexes were diluted in OptiMEM medium or OptiMEM medium and 10% (v/v) BS prior to characterization. We note that the absolute concentration of BFDMA was therefore between 0.57 to 0.71 mM across all samples analyzed. Where specified, an aqueous solution of 0.25 M ascorbic acid in 1 mM Li_2SO_4 was added to these lipoplex solutions at a ten times molar excess concentration (versus BFDMA) as a final step, after addition of media to the solution, and were allowed to incubate with the lipoplexes for ten minutes prior to vitrification for cryo-TEM analysis (see section 3.2.2.3 below).

3.2.2.2 Small angle x-ray scattering (SAXS).

SAXS was performed using the protocol described in detail in Chapter 2, section 2.2.2.5.

3.2.2.3 Cryogenic transmission electron microscopy (cryo-TEM).

Specimens of lipoplexes were prepared in a controlled environment vitrification (CEVS) system at 25 °C and 100% relative humidity, as previously described.⁶⁻¹⁰ Samples were examined using a Philips CM120 or in a FEI T12 G² transmission electron microscope operated at 120 kV, with Oxford CT-3500 or Gatan 626 cooling holders and transfer stations. Specimens were equilibrated in the microscope below -178 °C, and then examined in the low-dose imaging mode to minimize electron-beam radiation-damage. Images were recorded at a nominal underfocus of 1-2 μm to enhance phase contrast. Images were acquired digitally by a Gatan MultiScan 791 (CM120) or Gatan US1000 high-resolution (T12) cooled-CCD camera using the Digital Micrograph software package.

3.2.2.4 Cell transfection experiments and characterization of transgene expression

A luciferase assay was performed using the protocol described in detail in Chapter 2, section 2.2.2.3.

3.3 Results and discussion

3.3.1 Characterization of BFDMA-DOPE lipoplexes using cryo-TEM.

Figure 3.1 shows cryo-TEM micrographs of lipoplexes of BFDMA_{RED}-DOPE/DNA (Figure 3.1A), BFDMA_{OX}-DOPE/DNA (Figure 3.1B) and BFDMA_{OX}-DOPE/DNA with a 10 times molar excess of AA (versus the concentration of BFDMA), (Figure 3.1C and D), in OptiMEM medium.

BFDMA_{RED}-DOPE/DNA exhibited a predominantly H_{II}^c structure (Figure 3.1A, white arrows), in agreement with the observations reported in Chapter 2. No thread like structures outside of these highly ordered H_{II}^c structures, characteristic of free plasmid DNA,¹¹ were seen, suggesting a significant amount of the DNA is aggregated with the BFDMA and DOPE lipids in solution, and a stable, intact lipoplex of BFDMA_{RED}-DOPE/DNA describes the majority of species present within this sample. Conversely, the vitrified solution of BFDMA_{OX}-DOPE/DNA showed significantly less ordered, but highly aggregated structures (Figure 3.1B, black arrows). This result is again in agreement with the data presented in Chapter 2, specifically, the SAXS data, that showed a lower amount of ordered nanostructure within oxidized BFDMA-DOPE containing lipoplexes, when compared to lipoplexes of reduced BFDMA-DOPE (Chapter 2, Figure 2.4). Also, thread-like strands on free DNA are observed within this sample (inset of Figure 3.1B, black arrow heads). These results suggest that lipoplexes of BFDMA_{OX}-DOPE/DNA are significantly less ordered and less stable than lipoplexes of BFDMA_{RED}-DOPE/DNA.

Addition of AA to lipoplexes of BFDMA_{OX}-DOPE/DNA resulted in a highly ordered H_{II}^c structure (Figure 3.1C, white arrows), similar to those seen in BFDMA_{RED}-DOPE/DNA lipoplexes (Figure 3.1A, white arrows). However, also present within this vitrified sample, were areas of intact H_{II}^c structure, surrounded by a background solution within which a significant amount of free DNA (thread-like structures, Figure 3.1D, black arrow heads) and fragments of disordered structures (Figure 3.1D, black arrows) could be seen. Therefore, we interpret these results to suggest that the addition of AA to lipoplexes of BFDMA_{OX}-DOPE/DNA appears to be successful in forming H_{II}^c structures similar to lipoplexes of BFDMA_{RED}-DOPE/DNA, but the formation of these highly ordered structures is not complete (i.e. incorporation of DNA into these nanostructures is not complete).

To summarize observations from Figure 3.1, lipoplexes of BFDMA-DOPE/DNA in OptiMEM media have been successfully imaged using cryo-TEM as a function of the oxidation states of BFDMA, (including upon addition of AA to BFDMA_{OX}-DOPE/DNA lipoplexes). The images show the presence of a significant amount of H_{II}^c nanostructure within lipoplexes of BFDMA_{RED}-DOPE/DNA, a comparatively less ordered, less stable lipoplex nanostructure for BFDMA_{OX}-DOPE/DNA and, on subsequent addition of AA to these oxidized BFDMA-containing lipoplexes, partial reformation of the H_{II}^c nanostructure.

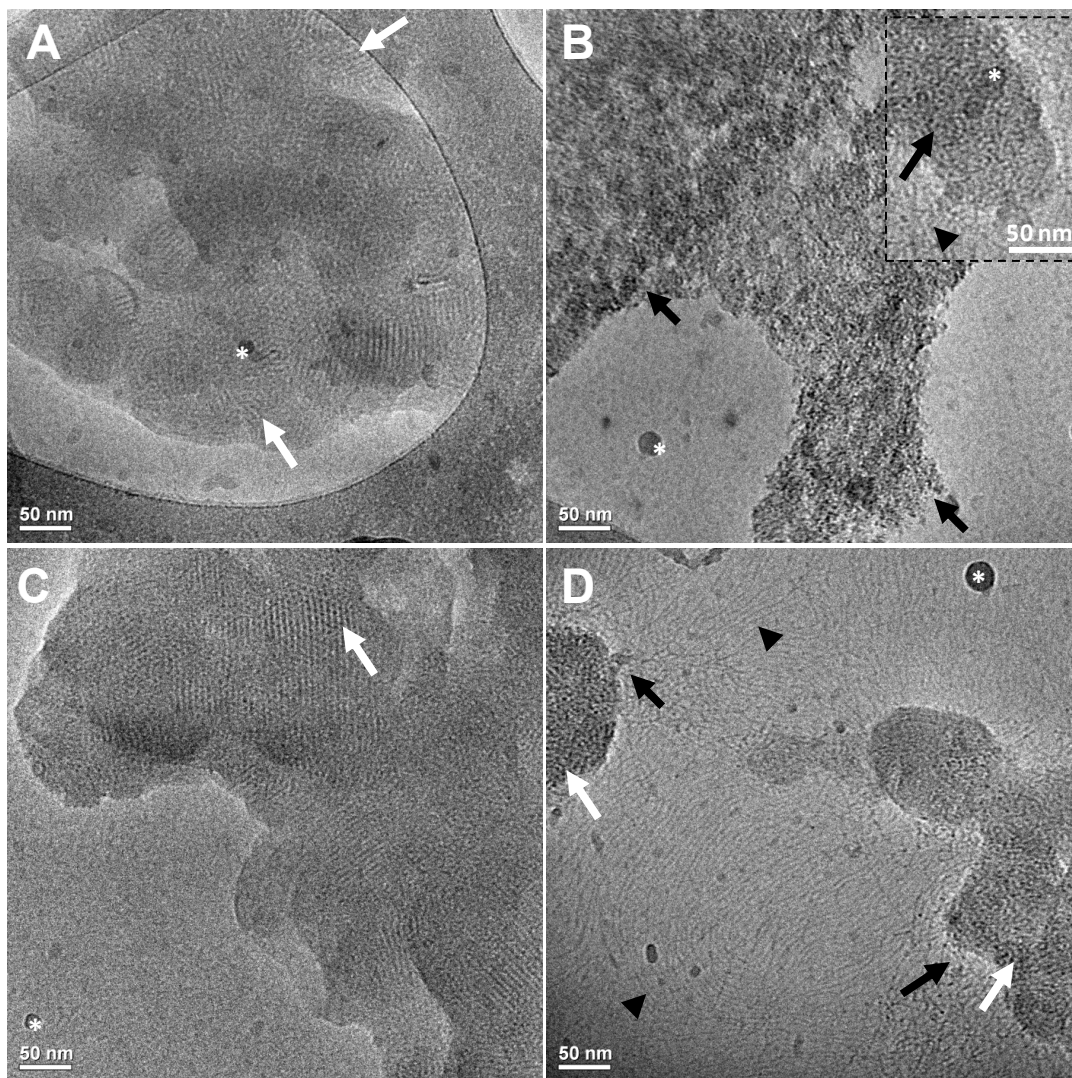


Figure 3.1. Cryo-TEM images of (A) lipoplexes of reduced BFDMA and DOPE, (B) lipoplexes of oxidized BFDMA and DOPE, and (C, D) lipoplexes of oxidized BFDMA and DOPE with AA, in OptiMEM. White arrows point to H_{II}^c structures, black arrows point to disordered structures, black arrow heads point to DNA threadlike structures, and white asterisks show ice formed during vitrification. The overall concentrations of BFDMA, DOPE and DNA in each solution prior to vitrification were 0.57 mM, 1.43 mM and 88 $\mu\text{g mL}^{-1}$ respectively, providing a charge ratio of 1.1:1 for all samples containing reduced BFDMA and 3.3:1 for all samples containing oxidized BFDMA. AA (5.7 mM final concentration) was added to the lipoplex 10 minutes before the sample was vitrified.

Next, we studied the influence of bovine serum (BS) on the nanostructures of the lipoplexes of BFDMA-DOPE/DNA, as a function of the oxidation states of BFDMA. Figure 3.2 displays the resulting cryo-TEM micrographs of lipoplexes of BFDMA_{RED}-DOPE/DNA (Figure 3.2A), BFDMA_{OX}-DOPE/DNA (Figure 3.2B) and BFDMA_{OX}-DOPE/DNA with a 10 times molar excess of AA (versus the concentration of BFDMA), (Figure 3.2C), all in OptiMEM medium with 10% (v/v) dilution in BS.

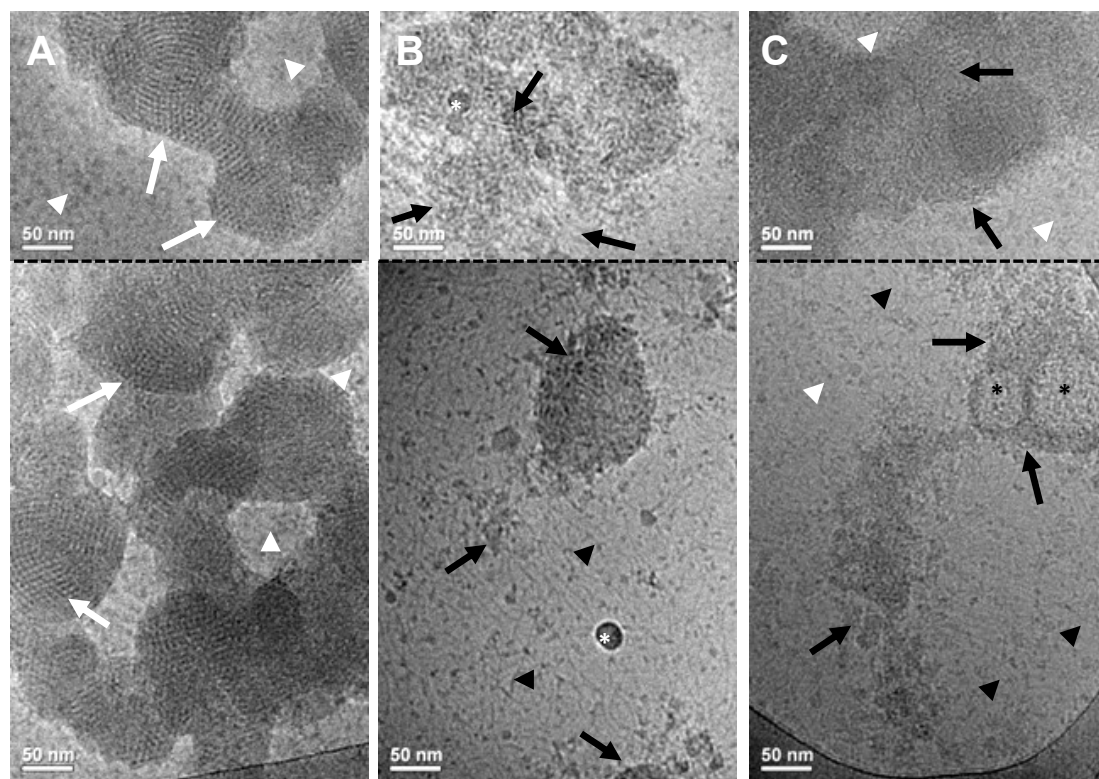


Figure 3.2. Cryo-TEM images of (A) lipoplexes of reduced BFDMA and DOPE, (B) lipoplexes of oxidized BFDMA and DOPE, and (C) lipoplexes of oxidized BFDMA and DOPE with AA, in OptiMEM and 10% BS. White arrows point to H_{II}^c structures, black arrows point to disordered structures, white arrow heads point to serum proteins, black arrow heads point to DNA threadlike structures, black asterisks show vesicles and white asterisks show ice formed during vitrification. The overall concentrations of BFDMA, DOPE and DNA in each solution prior to vitrification were 0.57 mM, 1.43 mM and 88 $\mu\text{g mL}^{-1}$ respectively, providing a charge ratio of 1.1:1 for all samples. AA (5.7 mM final concentration) was added to the lipoplex 10 minutes before the sample was vitrified.

BFDMA_{RED}-DOPE/DNA exhibited a predominantly H_{II}^c nanostructure in the presence of 10% (v/v) BS (Figure 3.2A, white arrows), with no evidence of free DNA (thread-like structures) occurring in the solution surrounding these structures. The increased grainy appearance of the background within this image compared to the images displayed in Figure 3.1 (Figure 3.2A, white arrow heads) is due to the presence of serum proteins, as discussed in detail, previously.¹¹ Similar to the case of no added BS (Figure 3.1A), this result is in agreement with the observations reported in Chapter 2. Specifically, the SAXS data in Figure 2.4 shows evidence of a significant amount of H_{II}^c nanostructure even at 50% (v/v) BS. Furthermore, in an equivalent concentration of BS, Golan et al. reported evidence of instability of multilamellar lipoplexes of BFDMA_{RED}/DNA (no DOPE), using cryo-TEM analysis.¹¹ Our results suggest, therefore, that DOPE significantly improves the stability of lipoplexes of BFDMA_{RED}-DOPE/DNA in 10% (v/v) BS.

In contrast, however, lipoplexes of BFDMA_{OX}-DOPE/DNA showed significantly less evidence of ordered nanostructure in the 10% (v/v) BS medium (Figure 3.2B) as compared to lipoplexes of BFDMA_{RED}-DOPE/DNA (Figure 3.2A). Disordered, loosely formed structures were the predominant type of aggregate observed within this sample (Figure 3.2B, black arrows) and free DNA was observed in the background (Figure 3.2B, black arrow heads). Closer inspection of Figure 3.1B and Figure 3.2B (no BS) hints that the overall level of aggregation of species is lower in the presence of 10% (v/v) BS, suggesting that constituents of the BS are interfering with the assembly of aggregates of BFDMA_{OX}, DOPE and DNA.

Finally, addition of AA to lipoplexes of BFDMA_{OX}-DOPE/DNA in the presence of 10% (v/v) BS (Figure 3.2C, black arrows) resulted in an increase in the level of aggregation when compared to lipoplexes of BFDMA_{OX}-DOPE/DNA (Figure 3.2B). However, the lipoplexes do not exhibit the highly ordered H_{II}^c structure seen in BFDMA_{OX}-DOPE/DNA lipoplexes with AA in the absence of 10% (v/v) BS (Figure 3.1C, white arrows). The presence of BS appears, therefore, to be at least partially preventing the reformation of the ordered H_{II}^c structure. Also present within the background of this vitrified sample were thread-like structures of free DNA (Figure 3.2C, black arrow heads), similar to those observed in the absence of BS (Figure 3.1D). Furthermore, lipid vesicles were seen (Figure 3.2D, black asterisks), whereas in the absence of BS, no vesicles were observed (Figure 3.1C and Figure 3.1D), consistent with weaker association of lipids and DNA in the presence of BS than in the absence of BS. Overall, these results suggest that addition of AA to lipoplexes of BFDMA_{OX}-DOPE/DNA in the presence of BS is less successful in reforming H_{II}^c nanostructure than in the absence of BS.

Overall, cryo-TEM analysis reported above provides insight into the nanostructure of lipoplexes of BFDMA-DOPE/DNA across oxidation states of BFDMA, and following addition of AA to lipoplexes of BFDMA_{OX}-DOPE/DNA, in the presence and the absence of BS. A highly ordered H_{II}^c structure was observed for lipoplexes of BFDMA_{RED}-DOPE/DNA both in the presence and in the absence of BS. In contrast, a significantly lower level of ordering was observed in equivalent lipoplexes containing oxidized BFDMA. Finally, addition of AA to lipoplexes

containing oxidized BFDMA in the absence of BS led to the appearance of the ordered H_{II}^c nanostructure of lipoplexes of BFDMA_{RED}-DOPE/DNA. However, the presence of BS appeared to prevent the reformation of the lipoplexes with H_{II}^c nanostructure.

3.3.2 Characterization of BFDMA-DOPE lipoplexes using SAXS.

Figure 3.3 and Table 3.1 show a summary of results from SAXS analysis performed on lipoplexes in a set of conditions identical to the cryo-TEM results reported above (Figure 3.1 and Figure 3.2). These experiments were performed to directly compare cryo-TEM images the Bragg peaks, as described in detail in Chapter 2, section 2.3.2.

Figure 3.3 shows SAXS data obtained from lipoplexes of BFDMA_{RED}-DOPE/DNA (black data), BFDMA_{OX}-DOPE/DNA (red data) and lipoplexes of BFDMA_{OX}-DOPE/DNA in the presence of AA (blue data), in OptiMEM media (Figure 3.3A) or OptiMEM with 10 % (v/v) BS (Figure 3.3B). These plots show a relatively high intensity of each first Bragg peak at approximately the same q for all three lipoplex solutions in both media. An analysis of the spacing between multiple Bragg peaks shown in the insets of Figure 3.3A and Figure 3.3B for BFDMA_{RED}-DOPE/DNA and BFDMA_{OX}-DOPE/DNA with AA, (Table 3.1) show H_{II}^c structure in both media (as described in detail in Chapter 2, section 2.3.2), in agreement with the cryo-TEM data above. Therefore, the position of the first Bragg peak for each lipoplex analyzed in Figure 3.3 can be used to calculate the “a” spacing of the H_{II}^c

structure (see Chapter 2, Figure 1D). BFDMA_{RED}-DOPE/DNA (black data) has an “a” spacing of 6.54 ± 0.13 nm in OptiMEM and 6.71 ± 0.13 nm in OptiMEM with 10% (v/v) BS. To compare these results to the distances shown in the micrographs in Figure 3.1, Image J software (v. 1.44p) was used to estimate the distances by taking a sample size of at least 15 gaps between repeat structures within the image across at least 3 separate regions of the image. For BFDMA_{RED}-DOPE/DNA, this analysis resulted in an equivalent “a” spacing of 6.2 ± 1.0 nm in OptiMEM and 6.5 ± 1.0 nm in OptiMEM with 10% (v/v) BS, respectively. Similarly, lipoplexes of BFDMA_{OX}-DOPE/DNA with AA (Figure 3.3, blue data) have an “a” spacing of 6.78 ± 0.14 nm in OptiMEM and 7.11 ± 0.14 nm in OptiMEM with 10% (v/v) BS from SAXS and 6.3 ± 1.0 nm in OptiMEM and 7.1 ± 1.0 nm in OptiMEM with 10% (v/v) BS from cryo-TEM and Image J analysis (Figure 3.1C). Therefore, the periodicity seen in SAXS and cryo-TEM is in good quantitative agreement. We note that lipoplexes of BFDMA_{OX}-DOPE/DNA (Figure 3.3, red data) did not show clear higher order Bragg peaks and so only the first Bragg peak is reported in Table 3.1. Consequently, it was not possible to use Image J to find gaps between repeat structures to measure the distances for lipoplexes of BFDMA_{OX}-DOPE/DNA in either media (Figure 3.1B and Figure 3.2B).

As initially discussed in detail in Chapter 2, the magnitude of the intensity of the first Bragg peaks for each lipoplex solution can be compared to give a qualitative comparison of the relative amount of ordered lipoplex in solution. While the magnitude of the first Bragg peak for lipoplexes of BFDMA_{OX}-DOPE/DNA with AA is similar to that of lipoplexes of BFDMA_{RED}-DOPE/DNA and significantly higher

than that of BFDMA_{OX}-DOPE/DNA in OptiMEM media (Figure 3.3A), in contrast, the magnitude of the first Bragg peak for lipoplexes of BFDMA_{OX}-DOPE/DNA with AA is similar to that of lipoplexes of BFDMA_{OX}-DOPE/DNA and significantly lower than that of BFDMA_{RED}-DOPE/DNA in OptiMEM media with 10% (v/v) BS (Figure 3.3B). This is in general agreement with the cryo-TEM data reported above, and suggests that the ability of AA to form highly ordered H_{II}^c structure is impeded by the presence of constituents within BS.

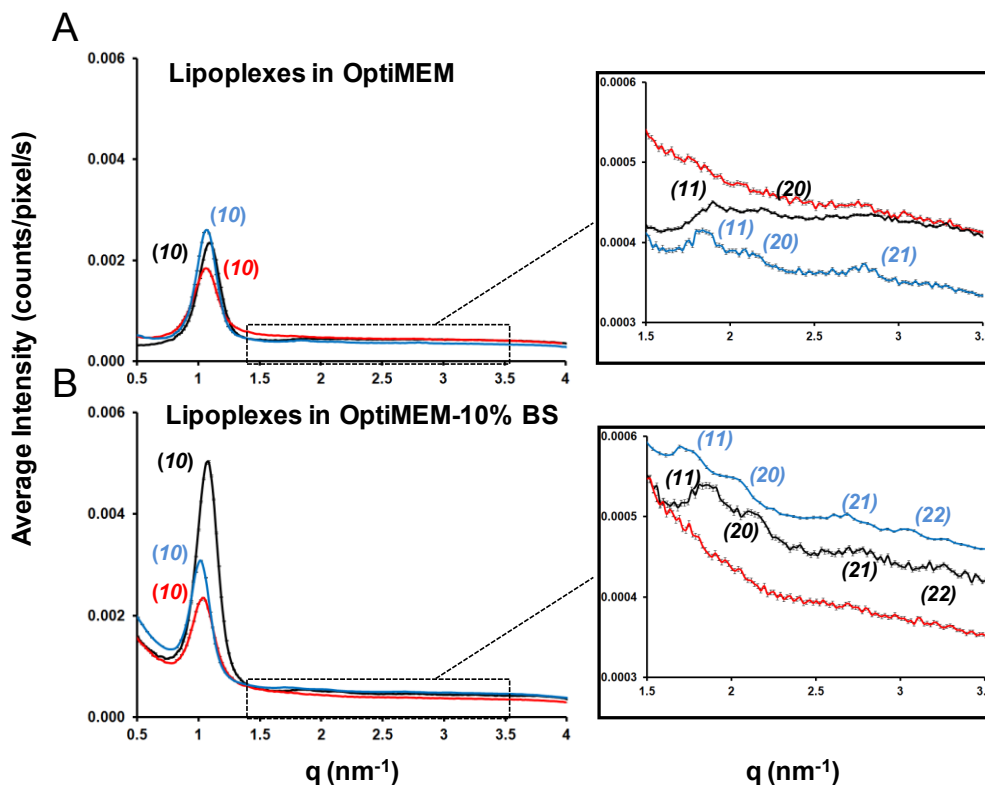


Figure 3.3. SAXS spectra obtained using BFDMA_{RED}-DOPE ($\phi_{\text{DOPE}} = 0.71$) (black), BFDMA_{OX}-DOPE ($\phi_{\text{DOPE}} = 0.71$) (red) or BFDMA_{OX}-DOPE and ten times molar excess of ascorbic acid ($\phi_{\text{DOPE}} = 0.71$) (blue) containing lipoplexes in; (A) OptiMEM, using lipid concentrations of 0.64 mM BFDMA and 1.59 mM DOPE; (B) OptiMEM with 10% (v/v) BS, using lipid concentrations of 0.57 mM BFDMA and/or 1.43 mM DOPE; all in the presence of pEGFP-N1 (2.0 mg/ml) at a charge ratio of 1.1:1 or 3.3:1 for reduced or oxidized BFDMA containing solutions respectively.

Table 3.1. SAXS results; Bragg peak q_{hkl} positions (using Miller Indices), and Bragg peak ratios, nanostructure, and unit cell spacing (a) for H_{II}^c phases, for lipoplexes of BFDMA_{RED}-DOPE/pGFP, BFDMA_{OX}-DOPE/pGFP and BFDMA_{OX}-DOPE/pGFP with 10 molar excess of AA ($\phi_{DOPE} = 0.71$) with and without the presence of 10% BS (v/v). Errors are based on equipment calibration of 2% using a silver behenate standard.

Lipoplex	Bragg peak q_{hkl} position (nm ⁻¹)					Bragg peak ratios				Nano-structure	a ^a (nm)
	1 st peak	2 nd peak	3 rd peak	4 th peak	5 th peak	2 nd /1 st	3 rd /1 st	4 th /1 st	5 th /1 st		
	(q ₁₀)	(q ₁₁)	(q ₂₀)	(q ₂₁)	(q ₂₂)						
Lipoplexes in OptiMEM											
BFDMA _{RED} -DOPE/pGFP	1.11	1.91	2.18	-	-	1.72	1.97	-	-	H _{II} ^c	6.54 ± 0.13
BFDMA _{OX} -DOPE/pGFP	1.07	-	-	-	-	-	-	-	-	-	-
BFDMA _{OX} -DOPE/pGFP +10x AA	1.07	1.86	2.13	2.82	-	1.74	1.99	2.62	-	H _{II} ^c	6.78 ± 0.14
Lipoplexes in OptiMEM and 10% v/v BS											
BFDMA _{RED} -DOPE/pGFP	1.08	1.89	2.16	2.82	3.26	1.75	2.00	2.61	3.02	H _{II} ^c	6.71 ± 0.13
BFDMA _{OX} -DOPE/pGFP	1.04	-	-	-	-	-	-	-	-	-	-
BFDMA _{OX} -DOPE/pGFP +10x AA	1.02	1.77	2.03	2.65	3.04	1.74	1.99	2.60	2.98	H _{II} ^c	7.11 ± 0.14

^a $a=2/\sqrt{3}d$ for hexagonal H_{II} structure

To summarise the observations from the SAXS analysis, in both OptiMEM and OptiMEM with 10% (v/v) BS media, lipoplexes of BFDMA_{RED}-DOPE/DNA and BFDMA_{OX}-DOPE/DNA with AA possess a highly ordered H_{II}^c nanostructure. In contrast, lipoplexes of BFDMA_{OX}-DOPE/DNA, while showing the presence of ordered nanostructure, exhibit a degree of ordering that is significantly lower than the other two lipoplex solutions. An analysis of the relative peak intensity of the first Bragg peaks observed for each lipoplex showed there to be a relatively lower abundance of H_{II}^c nanostructure in lipoplexes of BFDMA_{OX}-DOPE/DNA with AA when compared to lipoplexes of BFDMA_{RED}-DOPE/DNA in the presence of serum, but not so in the absence of serum. Therefore, observations from SAXS analysis are in general agreement with those from cryo-TEM above.

3.3.3 Characterization of BFDMA and BFDMA-DOPE using cryo-TEM.

It has been established via complementary cryo-TEM and SAXS analysis above, that lipoplexes of BFDMA_{RED}-DOPE/DNA form highly ordered H_{II}^c nanostructure in the presence or the absence of BS. As a final experiment, reduced BFDMA in OptiMEM (Figure 3.4A), and BFDMA_{RED}-DOPE in OptiMEM (Figure 3.4B) or OptiMEM with 10% (v/v) BS (Figure 3.4C) were imaged using cryo-TEM, in the absence of DNA, to investigate the origin of the inverse hexagonal nanostructure observed throughout these lipoplexes.

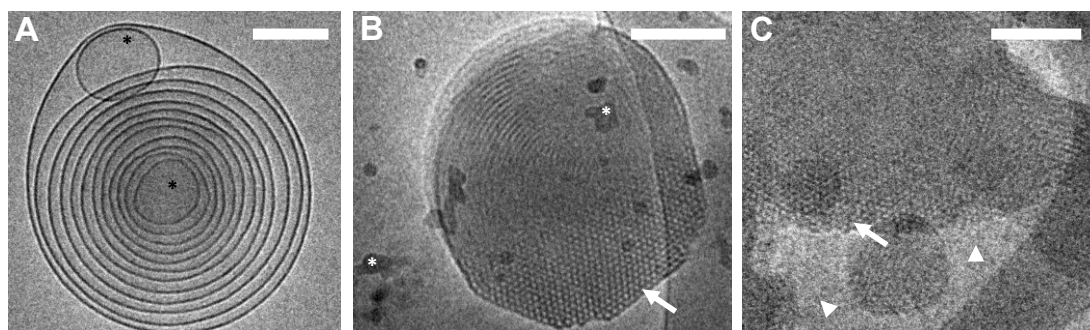


Figure 3.4. Cryo-TEM images of (A) 0.71 mM reduced BFDMA in OptiMEM, (B) 0.71 mM reduced BFDMA and 1.76 mM DOPE in OptiMEM, and (C) 0.63 reduced BFDMA and 1.57 mM DOPE, in OptiMEM and 10% BS. White arrows point to H_{II} structures, white arrow heads point to serum proteins, black asterisks show vesicles and white asterisks show ice formed during vitrification.

Reduced BFDMA, at concentrations on the order of 1 mM, form vesicles in solution (Figure 3.4A, black asterisks), as previously reported.^{3, 12} When a mixed lipid solution of BFDMA and DOPE ($\phi_{DOPE} = 0.71$) is formed, an inverse hexagonal structure spontaneously forms (Figure 3.4B, white arrow). Even in the presence of 10% (v/v) BS, this mixed lipid structure persists (Figure 3.4C, white arrow). From these

images, two interesting comparisons can be made to the lipoplex images reported earlier in this chapter.

First, comparison of Figure 3.4B, BFDMA_{RED}-DOPE and Figure 3.1A, lipoplexes of BFDMA_{RED}-DOPE/DNA, initially reveals the H_{II} structures formed to be qualitatively similar. However, a closer examination reveals that, in the absence of DNA (Figure 3.4B), the characteristic hexagonal structures have centers of low contrast with the rest of the aggregate and appear light or even hollow centered. Conversely, in the presence of DNA (Figure 3.1A), these centers have a high contrast and appear dark compared to the rest of the aggregated structure. This hints that in Figure 3.1A, we may be observing the position of DNA inside the centers of these hexagonal structures, as originally hypothesized by Koltover et al. using small angle neutron scattering (SANS) and geometric analysis.¹³

Second, whereas images of lipoplexes of BFDMA_{RED}-DOPE/DNA (Figure 3.1A) show only H_{II}^c structure, the image of BFDMA_{RED}-DOPE shows either a mixture of H_{II}^c structure and what appears to be multilamellar structure or a mixture of “end on” and “side on” H_{II}^c structures (Figure 3.4B). From the data reported in this chapter, however, it is not possible to determine which of the above combinations of structure is present.

3.3.4 Treatment of lipoplexes of oxidized BFDMA and DOPE with AA in the presence of cells.

Figure 3.5 shows a quantitative cell transfection assay using a plasmid DNA construct (pCMV-Luc) encoding firefly luciferase.

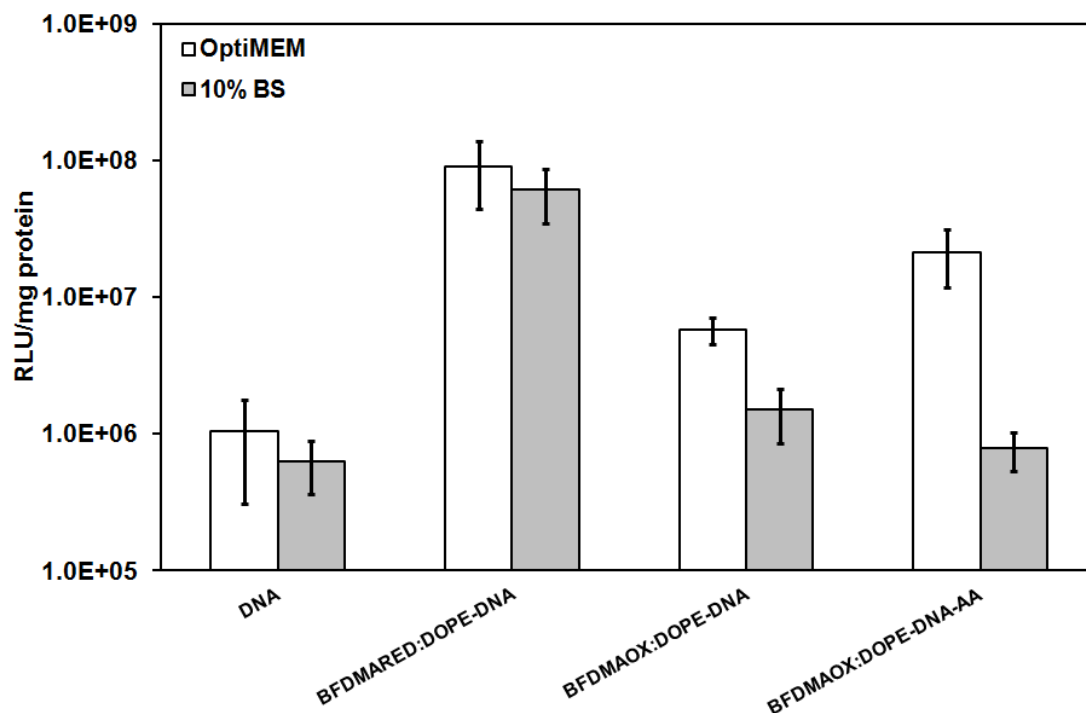


Figure 3.5. Normalized luciferase expression mediated by a DNA control (DNA), lipoplexes of reduced BFDMA and DOPE, lipoplexes of oxidized BFDMA and DOPE, or lipoplexes of oxidized BFDMA treated with AA in the presence of COS-7 cell lines in OptiMEM media (white bars) or OptiMEM with 10% (v/v) BS (grey bars). Error bars represent one standard deviation (n=6).

Lipoplexes formed from pCMV-Luc and DOPE with reduced BFDMA, oxidized BFDMA or oxidized BFDMA and ten times molar excess of ascorbic acid were incubated with cells for 4 h in either OptiMEM (Figure 3.5, white bars) or OptiMEM containing 10% (v/v) BS (Figure 3.5, grey bars). The overall concentrations of BFDMA, DOPE and DNA in each cell solution were 8 μ M, 20 μ M

and $2.4 \mu\text{g mL}^{-1}$ respectively, providing a charge ratio of 1.1:1 for all samples. Ascorbic acid was added immediately after lipoplexes were added to cells (10 μL of 2 mM ascorbic acid in 1 mM Li_2SO_4 added to cell solution giving a final concentration of 80 μM ascorbic acid). “DNA” denotes a control with DNA only (no lipid). Luciferase expression was measured 48 h after exposure to lipoplexes.

From the results shown in Figure 3.5, we can make the following main observations. First, lipoplexes of BFDMA_{RED}-DOPE and BFDMA_{OX}-DOPE both behave in a consistent way to similar results reported in Chapter 2, (Figure 2.3) that is, lipoplexes of BFDMA_{RED}-DOPE transfect cells with high efficiency, where are lipoplexes of BFDMA_{OX}-DOPE exhibit a significantly lower efficiency of transgene expression, both in the presence and in the absence of BS. Second, Figure 3.5 shows lipoplexes of BFDMA_{OX}-DOPE treated with AA to activate towards cell transfection in serum-free OptiMEM media (Figure 3.5, white bars) but not in the presence of BS (Figure 3.5, grey bars). This raises the hypothesis that the constituents of the serum that are effecting the ability of AA to reform highly ordered lipoplexes of $\text{H}_{\text{II}}^{\text{c}}$ nanostructure, as evidenced in both cryo-TEM (Figure 3.2) and SAXS (Figure 3.3) analysis above, are also prohibiting AA from successfully activating lipoplexes of BFDMA_{OX}-DOPE toward transfection. We note that this general result was also observed in the standard pEGFP-N1 based assay, where relative levels of EGFP expression in cells were characterized using fluorescence microscopy (Figure 3.6).

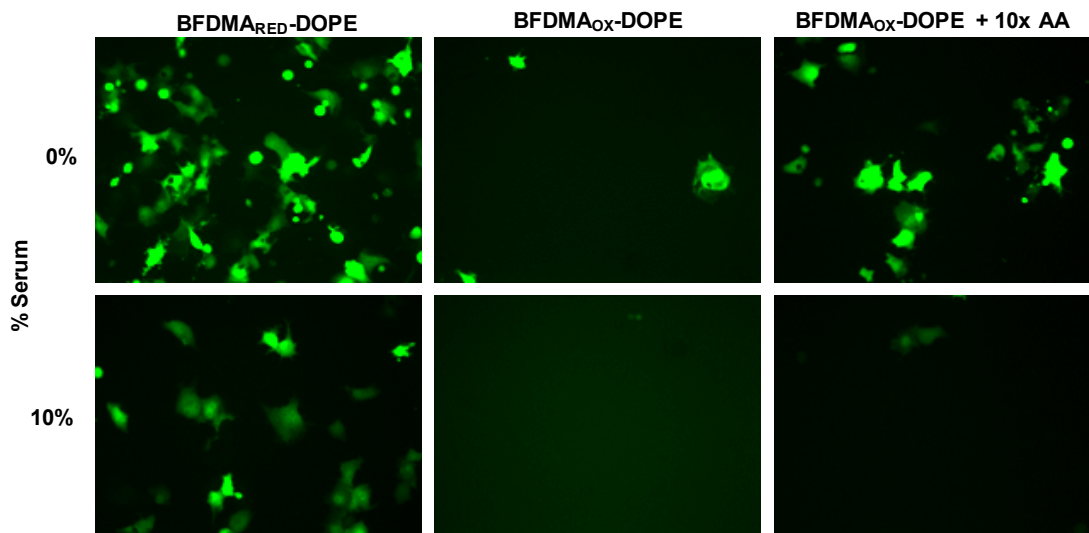


Figure 3.6. Representative fluorescence micrographs (100 \times mag; 1194 $\mu\text{m}\times 895 \mu\text{m}$) of confluent monolayers of COS-7 cells showing levels of EGFP expression mediated by lipoplexes of reduced BFDMA and DOPE, lipoplexes of oxidized BFDMA and DOPE or lipoplexes of oxidized BFDMA and DOPE treated with AA, in either OptiMEM or OptiMEM with 10% (v/v) BS.

3.4 Conclusions

This chapter reports cryogenic transmission electron microscopy images that show the presence of a highly ordered H_{II}^c structure in lipoplexes of BFDMA_{RED}-DOPE/DNA in both OptiMEM media and OptiMEM media with 10% (v/v) bovine serum. Analysis of lipoplexes of BFDMA_{OX}-DOPE/DNA, in contrast, show relatively poor ordering within the aggregates imaged in both media. Complementary small angle x-ray scattering analysis showed quantitative agreement with these cryo-TEM results in terms of the magnitude of the repeat structures within these ordered aggregates. Subsequent analysis of lipoplexes of BFDMA_{OX}-DOPE/DNA treated with a ten times molar excess of ascorbic acid showed a high degree of ordered H_{II}^c nanostructure in OptiMEM media, but significantly less ordering in OptiMEM media with 10% (v/v) bovine serum. Finally, a luciferase assay using COS-7 mammalian

cells compared the cell transfection efficiency between lipoplexes of BFDMA_{RED}-DOPE/DNA, lipoplexes of BFDMA_{OX}-DOPE/DNA and lipoplexes of BFDMA_{OX}-DOPE/DNA treated with a ten times molar excess of ascorbic acid, and showed that AA activates lipoplexes of BFDMA_{OX}-DOPE/DNA towards transfection in serum free media but not in media containing 10% (v/v) bovine serum. This result suggests that the constituents of bovine serum that are preventing reformation of the ordered H_{II}^c could also be leading to this difference in efficiency of transgene expression. Overall, these observations combine to provide cryo-TEM-based evidence of H_{II}^c nanostructure of lipoplexes of BFDMA and DOPE for the first time as well as initial characterization of lipoplexes of BFDMA_{OX}-DOPE/DNA with a chemical reducing agent, ascorbic acid. These results, when combined with previous studies using ascorbic acid to activate lipoplexes of BFDMA in the presence of cells, may provide a serum stable lipoplex, able to exhibit redox-mediated control over the efficiency of cell transfection.

3.5 Acknowledgements

Financial support was provided by the National Institutes of Health (1 R21 EB006168 and AI092004), the National Science Foundation (CBET-0754921 and DMR-1121288) and the ARO (W911NF-11-1-0251). All cryo-TEM analysis was carried out at the Technion Soft Matter Electron Microscopy Laboratory and represents collaboration with Yeshayahu Talmon, Judith Schmidt, Ellina Kesselman and co-workers. We thank Donald Savage for help with the SAXS measurements.

3.6 References

1. Y. S. Mel'nikova, S. M. Mel'nikov and J. E. Lofroth, *Biophys. Chem.*, **1999**, 81, 125-141.
2. B. S. Aytar, J. P. E. Muller, S. Golan, S. Hata, H. Takahashi, Y. Kondo, Y. Talmon, N. L. Abbott and D. M. Lynn, *Journal of Controlled Release*, **2012**, 157, 249-259.
3. Y. Kakizawa, H. Sakai, K. Nishiyama, M. Abe, H. Shoji, Y. Kondo and N. Yoshino, *Langmuir*, **1996**, 12, 921-924.
4. Y. Kakizawa, H. Sakai, A. Yamaguchi, Y. Kondo, N. Yoshino and M. Abe, *Langmuir*, **2001**, 17, 8044-8048.
5. N. Yoshino, H. Shoji, Y. Kondo, Y. Kakizawa, H. Sakai and M. Abe, *J. Jpn. Oil Chem. Soc.*, **1996**, 45, 769-775.
6. J. R. Bellare, H. T. Davis, L. E. Scriven and Y. Talmon, *Journal of Electron Microscopy Technique*, **1988**, 10, 87-111.
7. D. Danino, A. Bernheim-Groswasser and Y. Talmon, *Colloids and Surfaces a-Physicochemical and Engineering Aspects*, **2001**, 183, 113-122.
8. C. L. Pizzey, C. M. Jewell, M. E. Hays, D. M. Lynn, N. L. Abbott, Y. Kondo, S. Golan and Y. Tahnou, *Journal of Physical Chemistry B*, **2008**, 112, 5849-5857.
9. S. Golan, B. S. Aytar, J. P. E. Muller, Y. Kondo, D. M. Lynn, N. L. Abbott and Y. Talmont, *Langmuir*, **2011**, 27, 6615-6621.
10. B. S. Aytar, J. P. E. Muller, S. Golan, S. Hata, H. Takahashi, Y. Kondo, Y. Talmon, N. L. Abbott and D. M. Lynn, *J. Control. Release*.
11. S. Golan, B. S. Aytar, J. P. E. Muller, Y. Kondo, D. M. Lynn, N. L. Abbott and Y. Talmon, *Langmuir*, **2011**, 27, 6615-6621.
12. C. L. Pizzey, C. M. Jewell, M. E. Hays, D. M. Lynn, N. L. Abbott, Y. Kondo, S. Golan and Y. Talmon, *J. Phys. Chem. B*, **2008**, 112, 5849-5857.
13. I. Koltover, T. Salditt, J. O. Radler and C. R. Safinya, *Science*, **1998**, 281, 78-81.

Chapter 4: Presence of DOPE in Redox Active Ferrocenyl Amphiphile Containing Lipoplexes Provides a Fusogenic Internalization Capability to Redox-based Control of Cell Transfection

4.1 Introduction

Data presented in Chapters 2 and 3 have combined to provide insight into the effect of dioleoylphosphatidylethanolamine (DOPE) on the nanostructure and resulting increase in serum stability when added to complexes of bis(11-ferrocenylundecyl)dimethylammonium bromide (BFDMA) and DNA (“lipoplexes”). See Figure 2.1 in Chapter 2 of this thesis for the structure of these molecules. DOPE combines with BFDMA and DNA to force a change in nanostructure of the lipoplex from an “onion-like” multilamellar, L_{α}^c structure to an inverse hexagonal, H_{II}^c structure, as seen from both small angle x-ray scattering analysis and from imaging using cryogenic transmission microscopy.¹ These serum stable lipoplexes could lead to a wide range applications requiring the presence of serum. Separately, DOPE is known to promote membrane *fusion* through the H_{II}^c structure that it forces (i.e. the adherence and merging of cell membranes or intracellular membranes to each other through a variety of chemical and physical processes).²

Data presented in this chapter provides results that support the hypothesis that incorporation of DOPE into lipoplexes of BFDMA and DNA may lead to

internalization of the lipoplexes via a significantly increased level of membrane fusion, when compared to lipoplexes of BFDMA and DNA in the absence of DOPE. Fusion-based internalization is only one mechanism, of which there are many. Perhaps the most common type of mechanism is known as *endocytosis* (i.e. mechanisms involving uptake of cell material from the extra-cellular environment through invagination of the plasma membrane of cells). Past studies have claimed that internalization of lipoplexes via fusion has benefits in terms of speed of internalization,³⁻⁵ stability of the cell transfection vector in serum containing media,³ and the in providing the ability to by-pass the need for endosomal escape of internalized DNA^{4,5} over endocytotic mechanisms. Therefore, potential evidence that the mixed lipid lipoplex of DOPE and BFDMA promotes internalization via membrane fusion is significant, and may also provide insight into why these structures have been previously shown to be effective cell transfection vectors both in the presence and in the absence of serum (see Chapter 2 of this thesis).¹

A range of cell transfection assays have been used to characterize the fusion of lipoplexes with cell membranes.^{4, 6-8} In this chapter, we utilize one such method, namely, temperature-controlled cell transfection procedures between 4 °C, i.e. a non-physiological temperature, and 37 °C, i.e. a physiological temperature (the fusogenic method of cell transfection is known to not be highly temperature dependent^{6, 7} whereas endocytotic mechanisms typically require near-physiological temperature^{9, 10} in order to progress). Cell transfection efficiencies of lipoplexes of BFDMA, DOPE and DNA are compared and contrasted to a series of controls, namely, lipoplexes of

BFDMA and DNA in the absence of DOPE as well as other commonly used lipoplexes.

4.2 Experimental section

4.2.1 Materials

Bis-(11-ferrocenylundecyl)dimethylammonium bromide (BFDMA) was synthesized according to methods published elsewhere.¹¹⁻¹³ Dioleoylphosphatidylethanolamine (DOPE) and 1,2-dioleoyl-3-trimethylammonium-propane (DOTAP) were purchased from Avanti Polar Lipids (Alabaster, Alabama) in powdered form. Deionized water (18.2 M Ω) was used to prepare all buffers and salt solutions. Dulbecco's Modified Eagle's Medium (DMEM), OptiMEM cell culture medium, phosphate-buffered saline, fetal bovine serum (FBS), bovine serum (BS), and Lipofectamine 2000, were purchased from Invitrogen (Carlsbad, CA). Plasmid DNA encoding firefly luciferase (pCMV-Luc, >95% supercoiled) were purchased from Elim Biopharmaceuticals (San Francisco, CA). Bicinchoninic acid (BCA) protein assay kits were purchased from Pierce (Rockford, IL). Glo Lysis Buffer and Steady-Glo Luciferase Assay kits were purchased from Promega Corporation (Madison, WI). All commercial materials were used as received without further purification unless otherwise noted.

4.2.2 Experimental methods

4.2.2.1 Preparation of reduced BFDMA, reduced and oxidized BFDMA-DOPE and DOTAP-DOPE solutions.

Solutions of reduced BFDMA were prepared by dissolving a desired mass of reduced BFDMA in chloroform at 10 mg/ml. Nitrogen gas was used to evaporate most of the chloroform from a clean glass tube containing the lipid. This partially dried sample was placed under vacuum in a desiccator overnight to remove the remaining chloroform from the sample. An aqueous solution of Li_2SO_4 (1 mM) was added and tip sonication was used to provide a homogeneous solution of 1 mM BFDMA. Solutions of BFDMA-DOPE and DOTAP-DOPE were prepared using a similar method by dissolving a desired mass of DOPE or DOTAP into chloroform at 10 mg/ml as required. Chloroform-based solutions of BFDMA and DOPE or DOTAP and DOPE at 10 mg/ml were then mixed to the desired molar ratio prior to drying with N_2 , desiccating overnight and reconstituting in Li_2SO_4 , as described above.

4.2.2.2 Preparation of lipoplexes for transfection assays.

Lipoplexes of reduced BFDMA, BFDMA-DOPE or DOTAP-DOPE were prepared in the following manner. A solution of plasmid DNA (24 $\mu\text{g}/\text{mL}$ in water) was added to a vortexing solution of aqueous Li_2SO_4 containing an amount of reduced or oxidized BFDMA or BFDMA-DOPE sufficient to give the final lipid concentration of 8 μM BFDMA or 20 μM DOTAP for cell transfection experiments. This procedure resulted in the desired charge ratio of either BFDMA, BFDMA-DOPE or

DOTAP-DOPE and DNA in solution (where the charge ratio (CR) is defined as the mole ratio of the positive charges in the cationic lipid to negative charges of the DNA phosphate groups). The CRs investigated in this study were limited to 1.1:1 for BFDMA_{RED}-containing samples, and 2.8:1 for DOTAP-containing samples, selected for relevance to our past transfection experiments.^{1, 14-16} We note that that DOPE is zwitterionic and therefore does not affect the final CR. The sample volume used for cell transfection experiments was 50 μ L. Lipoplexes were allowed to stand at room temperature for 20 min before use.

4.2.2.3 Protocols for transfection and analysis of gene expression.

COS-7 cells used in transfection experiments were grown in opaque polystyrene 96-well culture plates at initial seeding densities of 15 000 cells/well in 200 μ L of growth medium (90% DMEM, 10% FBS, penicillin 100 units/mL, streptomycin 100 μ g/mL). After plating, all cells were incubated at 37 °C for 24 h. At approximately 80% confluence, the culture medium was aspirated and replaced with 200 μ L of serum-free medium (OptiMEM), followed by addition of 50 μ L of the lipoplex sample to achieve a final concentration of 8 μ M BFDMA or 20 μ M DOTAP in the presence of cells. Lipoplexes prepared as described above were added to assigned wells *via* pipette in replicates of six, and the cells were incubated for 4 h at either 4 °C or 37 °C, at which point the lipoplex-containing medium was aspirated from all wells and replaced with 200 μ L of growth medium (composition given above). Samples were incubated for an additional 48 h prior to characterization of transgene expression. Luciferase protein expression was determined using a

commercially available luminescence-based luciferase assay kit using the manufacturer's specified protocol. Samples were compared with signals from control wells and/or normalized against total cell protein in each respective well using a commercially available BCA assay kit (Pierce). Luciferase protein expression data was analyzed for statistical significance using the Student's t-test with $\alpha = 0.05$. In the text below, when we refer to "significant differences" between our data, we are referring to the results of this test.

4.3 Results and discussion

4.3.1 Transgene expression of lipoplexes at 4 °C and 37 °C.

Experiments were conducted to evaluate the relative extent of cell transfection at 4 °C (via incubation within a laboratory freezer) and 37 °C (via incubation within a standard incubator) of lipoplexes of reduced BFDMA and DOPE, at a molar ratio of 1 to 2.5 respectively and a CR of 1.1:1. This molar ratio was chosen as it was the optimum ratio between these lipids in terms of cell transfection efficiency, as reported previously (see Chapter 2 of this thesis).¹ Several controls were added to this experiment to compare to the cell transfection efficiency of the BFDMA-DOPE containing lipoplex;

(i) **Lipoplexes of reduced BFDMA**; these lipoplexes are known to form multilamellar, L_{α}^c aggregates in solution,¹⁷ in contrast to the inverse hexagonal aggregates of the reduced BFDMA-DOPE lipoplexes (see Chapter 2, Figure 2.4). The connection between lipoplex structure and method of internalization has been widely

documented in past studies within the field,^{4, 5, 8, 18, 19} and a general consensus is that inverse hexagonal structures promote predominantly fusogenic internalization whereas multilamellar structures promote predominantly endocytotic methods of internalization.^{4, 8, 18-20} Endocytotic methods of internalization rely on temperatures exceeding 4 °C as discussed above. Therefore, we expected to see comparatively less cell transfection at 4 °C for these lipoplexes than for the BFDMA-DOPE lipoplexes.

(ii) **Lipoplexes of DOTAP-DOPE;** DOTAP is a cationic lipid, commonly used as a vector for cell transfection. Here, we use a 1 to 2 molar ratio of DOTAP to DOPE at a CR of 2.8 to recreate a lipoplex used by Ewert et al.⁴ They show this lipoplex to be inverse hexagonal in structure, and to have fusogenic internalization characteristics with the cell membrane via laser scanning confocal microscopy. We use this lipoplex as a positive control to our experiment, aiming to understand the extent of transfection at 4 °C from a known fusogenic lipoplex and then to compare it with that of BFDMA-DOPE lipoplexes.

(iii) **Lipoplexes of Lipofectamine 2000;** Lipoplexes formed using Lipofectamine 2000 were used as a positive control and prepared according to the manufacturer's instructions. Although the exact formulation of this commercially available cell transfection vector is proprietary, it is known that DOPE is present in the formulation, therefore, it also has the potential to exhibit a significant level of cell transfection at 4 °C.

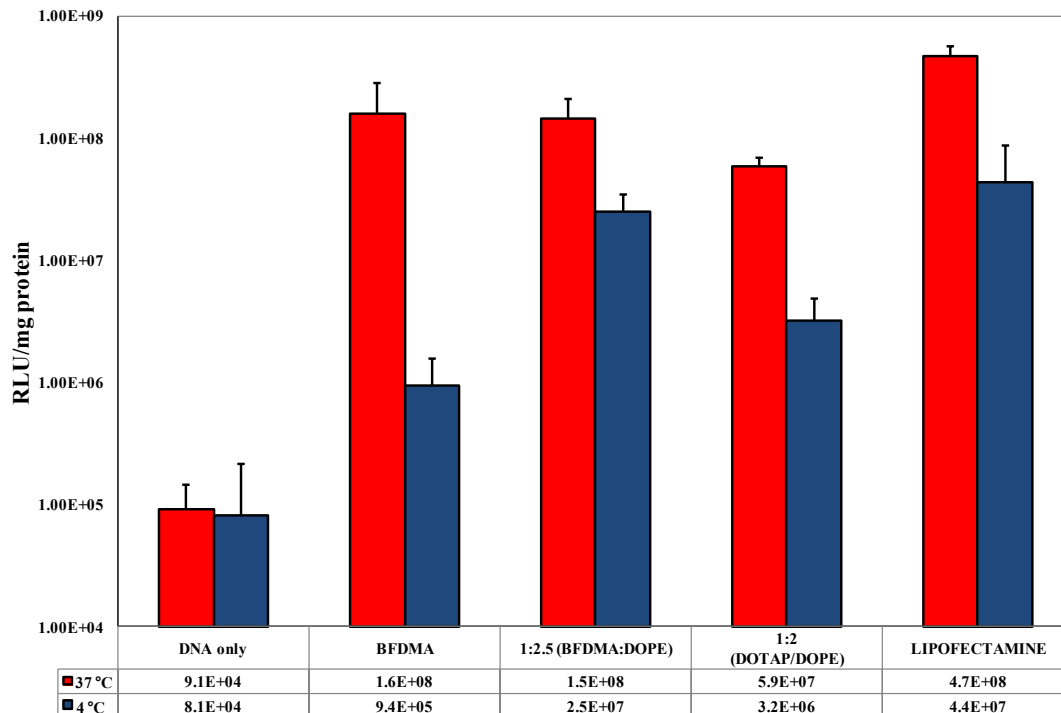


Figure 4.1. Influence of temperature on normalized luciferase expression in COS-7 cells treated with lipoplexes formed from pCMV-Luc and either 8 μ M reduced BFDMA (1.1 CR), a mixture of 8 μ M reduced BFDMA and 20 μ M DOPE (1.1 CR), a mixture of 20 μ M DOTAP and 40 μ M DOPE (2.8 CR) or Lipofectamine (see “Experimental section” for preparation details) for 4 h. The temperature at which cells were incubated with the lipoplexes is given in the legend (i.e. 37 °C - red bars, 4 °C - blue bars). DNA was present at a concentration of 2.4 μ g/ml for all samples. “DNA only” denotes a control with DNA alone (no lipid). Molar ratios are given on the x-axis for each mixed lipid sample. Luciferase expression was measured 48 h after exposure to lipoplexes. Mean relative light unit (RLU) per mg protein values are given in a table beneath each lipoplex tested. Error bars represent one standard deviation (n = 6).

Figure 4.1 shows levels of luciferase expression (expressed as relative light units normalized to total concentration of cell protein) mediated by the lipoplexes introduced above in the COS-7 cell line. The results of this experiment reveal that all lipoplexes incubated at 37 °C (red bars) mediate levels of transgene expression that are similar to each other (i.e. there is no significant difference in the level of expression, with the exception of the DOTAP-DOPE lipoplex, when compared to the

other three lipoplexes, where the expression is an order of magnitude lower at 5.9×10^7 RLU/mg protein). However, this is still three orders of magnitude higher than the expression from the incubation of DNA in the absence of any cationic lipid vector. Therefore, we conclude that all lipoplexes transfected COS-7 cells with high efficiency at 37 °C.

In contrast to the similar cell transfection efficiencies across all lipoplexes incubated at 37 °C, there were significant differences in the cell transfection efficiencies between the same set of lipoplexes incubated at 4 °C (Figure 4.1, blue bars). In fact, for each type of lipoplex reported in Figure 4.1, the cell transfection efficiency is significantly higher at 37 °C than at 4 °C. Therefore, there is some form (or forms) of a mechanism of internalization of DNA that is temperature dependent.

Next, we compare the efficiency of transgene expression between all lipoplexes and the negative control of DNA only (i.e. in the absence of any lipid vector) at 4 °C. With 95% confidence, using the Student's t-test, the only lipoplexes tested that did not show a significant difference in cell transfection efficiency to naked DNA were lipoplexes of reduced BFDMA and DNA. All other lipoplexes, (i.e. BFDMA-DOPE, DOTAP-DOPE and Lipofectamine 2000) all showed cell transfection efficiencies which were significantly higher than DNA only. We can conclude from this that these DOPE containing lipoplexes lead to significant levels of transfection of cells at 4 °C.

Finally, we compare the difference in cell transfection across temperature for lipoplexes of BFDMA and BFDMA-DOPE. Figure 4.1 shows the expression per mg

protein of Luciferase at both 4 °C and 37 °C for all lipoplexes. Lipoplexes of BFDMA only retain 0.6 ± 4.0 % expression at 4 °C in comparison to the level of cell transfection observed for the same lipoplex at 37 °C whereas lipoplexes of BFDMA-DOPE retain a significantly higher 16.6 ± 9.5 % expression at 4 °C when compared to expression using the same lipoplex at 37 °C (a level of retained expression higher than that of even the other positive controls, DOTAP-DOPE and Lipofectamine 2000). In other words, lipoplexes of BFDMA and DNA, in the absence of DOPE, only retain around 1% of their cell transfection efficiency at 4 °C in comparison to their performance at 37 °C. However, when DOPE is incorporated into these BFDMA containing lipoplexes, this retained transgene expression increases dramatically to around 20%, when comparing cell transfection at 4 °C and at 37 °C. When combined, these observations provide evidence to suggest that the presence of DOPE decreases the impact that the change in temperature from 37 °C to 4 °C has on the internalization of BFDMA-based lipoplexes to COS-7 cells, relative to DOPE-free lipoplexes. We hypothesize that this difference in temperature dependence of transgene expression is due to differences in the mechanism of internalization.

Finally, we note that other experimental approaches also exist to test for the relative proficiency of fusion-based internalization of DNA to cells. Two other examples are confocal microscopy, used to show the relative co-localization of DNA and endosomes and lysosomes after internalization of the cell transfection vector (or lipoplex) has occurred, and the use of inhibitors to prevent specific routes of internalization from occurring in controlled experiments. Fusion-based mechanisms

of cell transfection generally result in material entering the cell in the cytoplasm i.e. outside of the endosomes and lysosomes of the cell.^{4, 5} In contrast, endocytotic mechanisms result in material being initially trapped inside these regions of the cell. Therefore, all such techniques aim to exploit these differences in mechanism in order to define to what extent specific mechanisms are occurring in a given system. Initial confocal microscopy analysis has been attempted and preliminary results, looking at the overall presence and position of endosomes/lysosomes and DNA via specific staining of each type of species, suggest a higher co-localization of endosomes/lysosomes and DNA in cells incubated with multilamellar nanostructured (DOPE-free) lipoplexes of BFDMA than in cells incubated with inverse hexagonal nanostructured (DOPE containing) lipoplexes of BFDMA. Although more analysis is needed to be able to make any statements on significance in the differences seen from these initial studies, these initial results seem to tentatively co-operate with the results of the temperature dependent cell transfection assay detailed above.

4.4 Conclusions

Data presented in this chapter provides preliminary evidence that supports the hypothesis that the change of nanostructure of lipoplexes of reduced BFDMA and DNA upon incorporation of DOPE from L_{α}^c nanostructures to H_{II}^c nanostructures leads to an increase in the extent to which these lipoplexes are internalized by cells via the fusogenic mechanism of internalization. This is evidenced by measurement of

the relative cell transfection efficiencies at temperatures of 4 °C and 37 °C, and is supported by preliminary measurements of a directionally greater extent of co-localization of DNA and endosomes/lysosomes present inside the cell when DOPE is absent than when DOPE is present inside the lipoplex.

4.5 Acknowledgments

Financial support was provided by the National Institutes of Health (1 R21 EB006168 and AI092004), the National Science Foundation (CBET-0754921 and DMR-1121288) and the ARO (W911NF-11-1-0251). I thank S. Aytar for providing plates of cells for each experiment and for many helpful discussions, and S. Hata and H. Takahashi for assistance with synthesis of BFDMA.

4.6 References

1. J. P. E. Muller, B. S. Aytar, Y. Kondo, D. M. Lynn and N. L. Abbott, *Soft Matter*, **2012**, 8, 2608-2619.
2. Y. S. Mel'nikova, S. M. Mel'nikov and J. E. Lofroth, *Biophys. Chem.*, **1999**, 81, 125-141.
3. H. Mizuguchi, T. Nakagawa, M. Nakanishi, S. Imazu, S. Nakagawa and T. Mayumi, *Biochemical and Biophysical Research Communications*, **1996**, 218, 402-407.
4. K. Ewert, N. L. Slack, A. Ahmad, H. M. Evans, A. J. Lin, C. E. Samuel and C. R. Safinya, *Curr. Med. Chem.*, **2004**, 11, 133-149.
5. A. J. Lin, N. L. Slack, A. Ahmad, C. X. George, C. E. Samuel and C. R. Safinya, *Biophys. J.*, **2003**, 84, 3307-3316.
6. Y. Hu, Y. Jin and Y. Xia, *Drug Dev. Ind. Pharm.*, **2004**, 30, 135-141.

7. H. P. Zobel, F. Stieneker, S. A. A. Aziz, M. Gilbert, D. Werner, C. R. Noe, J. Kreuter and A. Zimmer, *Eur. J. Pharm. Biopharm.*, **1999**, 48, 1-12.
8. B. Kedika and S. V. Patri, *Mol. Pharm.*, 9, 1146-1162.
9. P. H. Weigel and J. A. Oka, *J. Biol. Chem.*, **1981**, 256, 2615-2617.
10. Z. Mamdouh, M. C. Giocondi, R. Laprade and C. LeGrimellec, *Biochim. Biophys. Acta-Biomembr.*, **1996**, 1282, 171-173.
11. Y. Kakizawa, H. Sakai, K. Nishiyama, M. Abe, H. Shoji, Y. Kondo and N. Yoshino, *Langmuir*, **1996**, 12, 921-924.
12. Y. Kakizawa, H. Sakai, A. Yamaguchi, Y. Kondo, N. Yoshino and M. Abe, *Langmuir*, **2001**, 17, 8044-8048.
13. N. Yoshino, H. Shoji, Y. Kondo, Y. Kakizawa, H. Sakai and M. Abe, *J. Jpn. Oil Chem. Soc.*, **1996**, 45, 769-775.
14. N. L. Abbott, C. M. Jewell, M. E. Hays, Y. Kondo and D. M. Lynn, *J. Am. Chem. Soc.*, **2005**, 127, 11576-11577.
15. C. M. Jewell, M. E. Hays, Y. Kondo, N. L. Abbott and D. M. Lynn, *J. Controlled Release*, **2006**, 112, 129-138.
16. C. M. Jewell, M. E. Hays, Y. Kondo, N. L. Abbott and D. M. Lynn, *Bioconjugate Chem.*, **2008**, 19, 2120-2128.
17. C. L. Pizzey, C. M. Jewell, M. E. Hays, D. M. Lynn, N. L. Abbott, Y. Kondo, S. Golan and Y. Talmon, *J. Phys. Chem. B*, **2008**, 112, 5849-5857.
18. I. Wrobel and D. Collins, *Biochim. Biophys. Acta-Biomembr.*, **1995**, 1235, 296-304.
19. C. Marchini, D. Pozzi, M. Montani, C. Alfonsi, A. Amici, S. C. De Sanctis, M. A. Digman, S. Sanchez, E. Gratton, H. Amenitsch, A. Fabbretti, C. O. Gualerzi and G. Caracciolo, *Cancer Gene Ther.*, **2011**, 18, 543-552.
20. I. Koltover, T. Salditt, J. O. Radler and C. R. Safinya, *Science*, **1998**, 281, 78-81.

Chapter 5: Chemical Oxidation of a Redox-Active, Ferrocene-Containing Cationic Lipid: Influence on Interactions with DNA and Characterization in the Context of Cell Transfection[‡]

5.1 Introduction

Cationic lipids are used widely to formulate lipid/DNA complexes (or lipoplexes) that promote delivery of DNA to cells.¹⁻⁵ Many properties of lipoplexes depend strongly on the nature of lipid-DNA interactions, and the ability to control or change the nature of these interactions is thus important in a range of contexts. Cationic lipids containing functional groups that respond to changes in stimuli present in intracellular environments, for example, can promote more effective trafficking of DNA and thus more efficient cell transfection.⁶⁻¹⁵ In contrast, lipids containing functionality that can be addressed, transformed, or activated using other, externally-applied stimuli¹⁶⁻¹⁸ could provide new opportunities to exert active or ‘on-demand’ control over the properties of lipoplexes (for example, methods that provide spatiotemporal control over the ‘activation’ of lipoplexes could lead to new approaches to active spatiotemporal control over the delivery of DNA to cells).

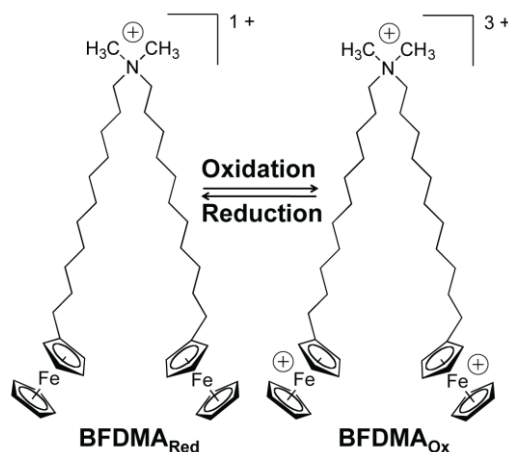


Figure 5.1. Structure of bis(11-ferrocenylundecyl)dimethylammonium bromide (BFDMA).

As a step toward the development of lipids that provide active control over the properties of lipoplexes, our group has investigated interactions between DNA and the redox-active, ferrocene-functionalized cationic lipid BFDMA [bis(11-ferrocenylundecyl) dimethylammonium bromide, Figure 5.1].¹⁹⁻²⁵ Our past studies demonstrate that lipoplexes formed using BFDMA can promote the delivery of DNA to cells, but that the ability to do so depends strongly on the oxidation state of the ferrocenyl groups of the lipid.^{19, 20, 23, 24} For example, whereas the reduced form of BFDMA (net charge of +1) can promote high levels of transgene expression, lipoplexes formed using oxidized BFDMA (net charge of +3) yield negligible or very low levels. Physical characterization experiments suggest that this oxidation-state dependence arises from differences in the nanostructures and other biophysical properties (e.g., differences in zeta potentials) that determine the extents to which the lipoplexes are internalized by cells.²¹⁻²⁴ The results of our past work also suggest that these differences in lipoplex properties that exert their primary influences in the

extracellular environment (i.e., by either promoting or almost completely preventing internalization, respectively^{23, 24}) rather than by influencing downstream events that occur in the intracellular environment.

Because ferrocenyl groups can be oxidized and reduced readily and reversibly (using either chemical or electrochemical methods),^{26, 27} BFDMA also offers a basis for active control over the ability of lipoplexes to transfect cells (e.g., by application of a chemical or electrochemical stimulus to transform the oxidation state of BFDMA). We have demonstrated that it is possible to reduce the BFDMA in lipoplexes of oxidized BFDMA by treatment with chemical reducing agents (e.g., glutathione or ascorbic acid),^{23, 24} and that these treatments can be used to influence physical properties that activate these lipoplexes toward transfection. A recent publication from our group also demonstrates that chemical reduction can be used to activate lipoplexes of oxidized BFDMA in culture media, in the presence of cells, to initiate transfection.²⁴

In our past studies, we synthesized reduced BFDMA directly and then obtained oxidized BFDMA by subsequent electrochemical oxidation.¹⁹⁻²⁴ While this electrochemical approach is useful, complete electrochemical oxidation of BFDMA generally requires long times (e.g., 2-3 hours) at high temperatures (75 °C). This current study sought to address these and other practical issues associated with electrochemical oxidation by investigating approaches to the chemical oxidation of BFDMA.

We report here that Fe(III)sulfate can be used to oxidize reduced BFDMA rapidly, quantitatively, and at ambient temperatures. However, lipoplexes formed using chemically oxidized BFDMA behaved differently than lipoplexes prepared using electrochemically oxidized BFDMA in the context of cell transfection (e.g., whereas the latter do not promote high levels of transfection, lipoplexes of chemically oxidized BFDMA do). The results of additional experiments reveal these differences to be a result of residual iron ions present in solutions of chemically oxidized BFDMA, and that treatment with an iron chelating agent (ethylenediaminetetraacetic acid, EDTA)²⁸ can be used to produce bulk samples of chemically oxidized BFDMA that do not promote cell transfection. We demonstrate further that (i) these EDTA-treated samples can be chemically reduced by treatment with ascorbic acid to produce samples of reduced BFDMA that do promote transfection, and (ii) lipoplexes formed using EDTA-treated samples can be chemically reduced to activate the lipoplexes and initiate transfection. Our results demonstrate that chemical approaches to the transformation of BFDMA can be used to preserve redox-based ‘on/off’ control over cell transfection demonstrated in past studies using electrochemical methods.

5.2 Experimental section

5.2.1 Materials

BFDMA was synthesized according to methods published previously.²⁹ Dodecyltrimethylammonium bromide (DTAB) and ethylenediaminetetraacetic acid (EDTA) were purchased from Acros Organics (Morris Plains, NJ). Fe(III)sulfate

($\text{Fe}_2(\text{SO}_4)_3 \cdot 5\text{H}_2\text{O}$; also referred to herein as Fe^{3+}) was purchased from Aldrich (St. Louis, MO) with a purity of at least 97%. Deionized water (18.2 M Ω) was used to prepare all buffers and salt solutions. Dulbecco's Modified Eagle's Medium (DMEM), Opti-MEM cell culture medium, phosphate-buffered saline (PBS), fetal bovine serum (FBS), and Lipofectamine 2000 were purchased from Invitrogen (Carlsbad, CA). Plasmid DNA encoding enhanced green fluorescent protein (pEGFP-N1, >95% supercoiled) and firefly luciferase (pCMV-Luc, >95% supercoiled) were purchased from Elim Biopharmaceuticals, Inc., San Francisco, CA. Bicinchoninic acid (BCA) protein assay kits were purchased from Pierce (Rockford, IL). Glo Lysis Buffer and Steady-Glo Luciferase Assay kits were purchased from Promega Corporation (Madison, WI). All commercial materials were used as received without further purification unless otherwise noted.

5.2.2 Experimental methods

5.2.2.1 Preparation of reduced and electrochemically oxidized BFDMA solutions.

Solutions of reduced BFDMA were prepared by dissolving a desired mass of reduced BFDMA in aqueous Li_2SO_4 (1 mM, pH 5.1) followed by dilution to a desired concentration. Solutions of electrochemically oxidized BFDMA were prepared by electrochemical oxidation of a 1 mM reduced BFDMA solution at 75 °C using a bipotentiostat (Pine Instruments, Grove City, PA) and a three electrode cell to maintain a constant potential of 600 mV between the working electrode and a Ag/AgCl reference electrode, as described previously.^{19-21, 23} Platinum mesh (2.5 cm²)

was used as the working and counter electrodes. For electrochemical oxidation of BFDMA in D₂O (used in SANS analyses described below), 1 mM sodium acetate was added to the BFDMA prior to oxidation to achieve full conversion of reduced BFDMA to oxidized BFDMA. The progress of oxidation was followed by monitoring current passed at the working electrode and by UV/visible spectrophotometry, as described previously.^{19, 20, 23}

5.2.2.2 Characterization of the transformation of reduced BFDMA upon addition of Fe³⁺.

Solutions of chemically oxidized BFDMA were prepared by chemical oxidation of solutions of 1 mM reduced BFDMA using a negligible volume (0.5-5 μ L) of a concentrated solution of Fe³⁺ (1.0 M) to obtain the BFDMA/Fe³⁺ molar ratios described in the text. Time-dependent characterization of chemical oxidation of reduced BFDMA upon addition of Fe³⁺ was conducted by measuring UV/vis absorbance spectra at wavelengths ranging from 400 to 800 nm. To this end, following the acquisition of an initial wavelength scan of reduced BFDMA solution, Fe³⁺ was added and the absorbance spectrum of the solution was monitored at predetermined time intervals until a constant absorbance at 630 nm (a wavelength characteristic of the absorbance of oxidized BFDMA) was observed. For experiments involving measurements made on solutions of reduced BFDMA, DTAB was added immediately prior to measurement of absorbance to eliminate clouding observed in BFDMA solutions at concentrations greater than 100 μ M. For experiments for which

Fe^{3+} was added to oxidize BFDMA, DTAB was added at the conclusion of each experiment before making an absorbance measurement. We note that DTAB does not absorb light in the visible region of interest (400-800 nm) in these experiments. For experiments in which iron chelating agents were used to investigate the influence of residual Fe^{2+} and Fe^{3+} species on the lipoplex activity (see text), solutions of chemically oxidized BFDMA were treated with a 1.5-fold molar excess of EDTA. Subsequent experiments investigating the chemical reduction of EDTA-treated samples of chemically oxidized BFDMA were performed using a 10-fold molar excess of ascorbic acid.

5.2.2.3 Preparation of lipoplex solutions.

Lipoplexes of reduced, electrochemically oxidized, or chemically oxidized BFDMA were prepared in the following general manner. A solution of plasmid DNA (24 $\mu\text{g}/\text{mL}$ in water) was added to a vortexing solution of aqueous Li_2SO_4 containing an amount of reduced or oxidized BFDMA sufficient to give the final lipid concentrations and BFDMA/DNA charge ratios (CRs) reported in the text. Total sample volume used for zeta potential and cell transfection experiments was 5 mL, and 50 μL , respectively. Lipoplexes were allowed to stand at room temperature for 20 min before use in subsequent experiments.

5.2.2.4 General protocols for transfection and characterization of gene expression.

COS-7 cells used in transfection experiments were grown in clear or opaque polystyrene 96-well culture plates (for experiments using pEGFP-N1 and pCMV-Luc, respectively) at initial seeding densities of 15×10^3 cells/well in 200 μ L of growth medium (90% Dulbecco's modified Eagle's medium, 10% fetal bovine serum, penicillin 100 units/mL, streptomycin 100 μ g/mL). After seeding, all cells were incubated at 37 °C for 24 h. At approximately 80% confluence, culture medium was aspirated and replaced with 200 μ L of serum-free medium (Opti-MEM), followed by addition of 50 μ L of a lipoplex solution (to yield a final concentration of 10 μ M BFDMA). After 4 h at 37 °C incubation, lipoplex-containing medium was aspirated from all wells and replaced with 200 μ L of serum-containing medium. Cells were incubated for an additional 48 h prior to characterization of transgene expression. For experiments conducted using lipoplexes formed from pEGFP-N1, cell morphology and relative levels of EGFP expression were characterized using phase contrast and fluorescence microscopy. For experiments conducted using lipoplexes formed from pCMV-Luc, levels of luciferase expression were characterized using a commercially available luminescence based luciferase assay kit, using the manufacturer's specified protocol. Luciferase expression data were normalized to total cell protein in each respective well using a commercially available BCA protein assay kit.

5.2.2.5 Characterization of zeta potentials of lipoplexes.

Experiments designed to characterize the zeta potentials of lipoplexes were conducted in the following general manner. Samples of lipoplexes formed from either reduced BFDMA, electrochemically oxidized BFDMA, or chemically oxidized BFDMA were prepared as described above. These samples were then diluted using 1 mM Li_2SO_4 (pH 5). For each sample, 5 mL of lipoplex solution was injected into the inlet of a Zetasizer 3000HS instrument, and measurements were made at ambient temperature using an electrical potential of 150 V. The final BFDMA and plasmid DNA (pEGFP-N1) concentrations were 10 μM and 24 mg/mL, respectively for all samples. These values are the same as those used in the cell transfection experiments described above. A minimum of five measurements was recorded for each sample, and the Henry equation was used to calculate zeta potentials from measurements of electrophoretic mobility. For this calculation, we assumed the viscosity of the solution to be the same as that of water.

5.2.2.6 Preparation of samples of lipoplexes for characterization by SANS and cryo-TEM.

Samples of lipoplexes formed from BFDMA and plasmid DNA (pEGFP-N1) were prepared in deuterated or aqueous Li_2SO_4 (1 mM) for SANS and cryo-TEM experiments, respectively. The 1 mM stock solution of BFDMA was diluted with DNA stock solution and vortexed for 5 s. Lipoplexes used in these experiments were formulated at CRs similar to those used in cell transfection experiments (see text), but

the absolute concentrations of BFDMA used in the SANS experiments (0.7 to 0.9 mM) were substantially higher than those used in transfection experiments (10 μ M). These higher concentrations were necessary to obtain sufficient intensities of scattered neutrons in SANS experiments. To be consistent with the concentrations used in the SANS measurements and also allow better sampling, cryo-TEM analyses of lipoplexes were also performed at these high lipid concentrations.

5.2.2.7 Characterization of lipoplexes by SANS.

SANS was performed using the CG-3 Bio-SANS instrument at Oak Ridge National Laboratory (ORNL), Oak Ridge, TN. The incident neutron wavelength was on average 6 \AA , with a spread in wavelength, $\Delta\lambda/\lambda$, of 15 %. Data were recorded at two different sets of sample-to-detector distances (0.3, 6, and 14.5 m or 1 and 14.5 m), giving q ranges from 0.360-0.030, 0.065-0.0065 and 0.03-0.003 \AA^{-1} or from 0.490-0.018 and 0.064-0.003 \AA^{-1} , respectively. The two different sets of sample-to-detector distances represent two separate trips to ORNL to perform these analyses. To ensure statistically relevant data, at least 10^6 counts were collected for each sample at each detector distance. The samples were contained in quartz cells with a 2 mm path length and placed in a sample chamber held at 25.0 ± 0.1 $^{\circ}\text{C}$. The data were corrected for detector efficiency, background radiation, empty cell scattering, and incoherent scattering to determine the intensity on an absolute scale ²². The background scattering from the solvent was subtracted. The processing of data was performed using Igor Pro (WaveMetrics, Lake Oswego, OR) with a program provided by ORNL.

Guinier analysis described in detail elsewhere^{22, 30} was used to interpret the scattering. Errors reported for d-spacing were calculated directly from q-values by assuming 2% experiment-to-experiment change in Bragg peak position versus q position (via calibration using silver behenate standards). $I(q) = n_p P(q) S(q)$

5.2.2.8 Characterization of lipoplexes by cryo-TEM.

Specimens of lipoplexes were prepared in a controlled environment vitrification (CEVS) system at 25 °C and 100% relative humidity, as previously described.^{22, 24, 25, 31, 32} Samples were examined using a Philips CM120 or in a FEI T12 G² transmission electron microscope operated at 120 kV, with Oxford CT-3500 or Gatan 626 cooling holders and transfer stations. Specimens were equilibrated in the microscope below -178 °C, and then examined in the low-dose imaging mode to minimize electron-beam radiation-damage. Images were recorded at a nominal underfocus of 1-2 μm to enhance phase contrast. Images were acquired digitally by a Gatan MultiScan 791 (CM120) or Gatan US1000 high-resolution (T12) cooled-CCD camera using the Digital Micrograph software package.

5.3 Results and discussion

5.3.1 Characterization of the chemical oxidation of reduced BFDMA using Fe³⁺

We selected Fe(III)sulfate (Fe³⁺) as a model chemical oxidizing agent on the basis of past studies demonstrating that Fe³⁺ can be used to oxidize ferrocenyl groups, including those present in single-tailed ferrocenyl surfactants.^{33, 34} In a series of initial

experiments, we characterized the rate and extent of the oxidation of the ferrocenyl groups in solutions of reduced BFDMA after addition of Fe^{3+} at ambient temperature (25 °C). For all experiments performed in this study, we used BFDMA solutions (0.5 mM) prepared using 1 mM aqueous Li_2SO_4 . Although chemical reduction can also be performed in biologically relevant media, we used this simple electrolyte solution to permit more direct comparisons between solutions of chemically oxidized BFDMA and electrochemically oxidized BFDMA^{19, 20, 22-24} (the latter of which requires the use of an electrolyte solution).

Figure 5.2A shows the UV/vis absorption spectra of solutions of reduced BFDMA (solid black line), electrochemically oxidized BFDMA (dotted black line), and a sample of reduced BFDMA to which Fe^{3+} was added (dashed black line; produced by treating solutions of reduced BFDMA with a 1.5-fold molar excess of Fe^{3+}). Inspection of these data reveals that upon treatment of the solution of reduced BFDMA with Fe^{3+} , the absorbance peak at 445 nm (characteristic of solutions of reduced BFDMA) disappeared, and that a new peak at 630 nm (characteristic of solutions of electrochemically oxidized BFDMA) appeared.

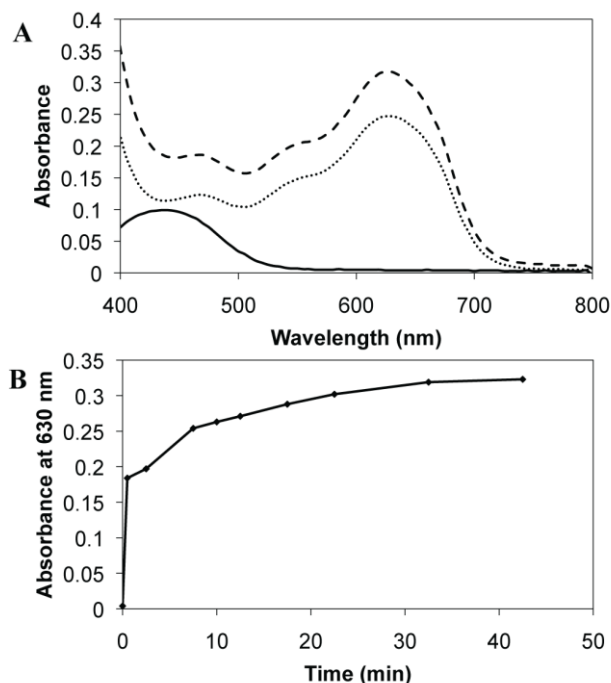


Figure 5.2. (A) UV/visible absorbance spectra of solutions of reduced BFDMA (solid black line), electrochemically oxidized BFDMA (dotted black line) or chemically oxidized BFDMA (dashed black line). (B) Increase in absorbance maximum (630 nm) of oxidized BFDMA vs time upon treatment of reduced BFDMA solution with 1.5-fold excess of Fe^{3+} (See Figure 5.9, Supplemental Materials for details of the kinetics of oxidation).

In general, the overall shape of the absorption spectrum of the solution of Fe^{3+} -treated BFDMA was similar to that of solutions of electrochemically oxidized BFDMA. We attribute the difference in the magnitudes of the absorbance values of solutions of electrochemically oxidized BFDMA (0.25) and chemically oxidized BFDMA (0.31) at 630 nm to (i) the loss of small amounts of the former during electrochemical oxidation (e.g., by adsorption of BFDMA to the electrode and salt bridge (glass frit) of the electrochemical cell during oxidation; evident by visual inspection) and (ii) the slightly higher turbidity of solutions of chemically oxidized BFDMA (even in the presence of DTAB, which was used to disrupt aggregates and

reduce the turbidity of the solution; these differences in absorbance are not the result of residual Fe^{3+} or Fe^{2+} species in solution.) Characterization of the time-dependent appearance of the peak in absorbance at 630 nm upon addition of Fe^{3+} to reduced BFDMA (Figure 5.2B; see also Figure 5.9) demonstrated that complete chemical oxidation of BFDMA can be achieved rapidly compared to electrochemical methods (e.g., oxidation is ~90% complete in less than 20 min). These results demonstrate that Fe^{3+} can be used to oxidize reduced BFDMA rapidly and quantitatively at ambient temperature. The observation that this transformation does not occur instantaneously upon the addition of Fe^{3+} may be a consequence of the fact that reduced BFDMA self-associates to form submicrometer-scale vesicles in aqueous media (i.e., sequestration of ferrocenyl groups within these assemblies could slow access of Fe^{3+} to the ferrocene).³⁵

5.3.2 Characterization of cell transfection mediated by lipoplexes of chemically oxidized BFDMA.

We performed cell-based experiments to determine how DNA lipoplexes formed using chemically oxidized BFDMA behave in the context of cell transfection. These experiments were performed using COS-7 cells and lipoplexes formed using plasmid DNA (pEGFP or pCMV-Luc) encoding enhanced green fluorescent protein (EGFP) or firefly luciferase to permit qualitative and quantitative characterization of levels of transgene expression, respectively. We selected COS-7 cells for use in these studies for two reasons. First, the use of this cell line allowed us to compare our

results to those of our past studies on BFDMA-mediated transfection using this cell line.^{19, 20, 23-25} Second, COS-7 cells are generally regarded as being relatively easy to transfect.³⁶ The use of this cell line in these experiments thus provides a more rigorous challenge with respect to characterization of the ability (or the inability) of oxidized BFDMA to transfect cells.

For the experiments described here, we used lipoplexes of reduced BFDMA and oxidized BFDMA (produced either by electrochemical or chemical oxidation) prepared at BFDMA/DNA charge ratios (CRs) of 1.4:1 and 4.2:1, respectively. We note that solutions of lipoplexes formed using oxidized BFDMA (net charge of +3) at a CR of 4.2:1 contain the same molar ratio of BFDMA and DNA as solutions of lipoplexes formed using reduced BFDMA (net charge of +1) at a CR of 1.4:1. These conditions were chosen on the basis of optimized protocols²⁰ demonstrating that lipoplexes formed using reduced BFDMA at a CR of 1.4:1 mediate high levels of cell transfection, but lipoplexes formed from electrochemically oxidized BFDMA at a CR of 4.2:1 lead to low levels of transfection. For all lipoplex formulations, the overall lipid concentration used for transfection experiments was 10 μ M.

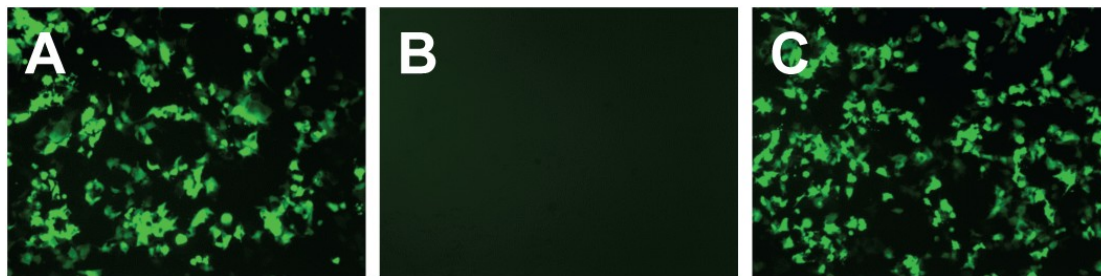


Figure 5.3. Representative fluorescence micrographs ($100\times$ original magnification, $1194\ \mu\text{m} \times 895\ \mu\text{m}$) of confluent monolayers of COS-7 cells showing EGFP expression mediated by lipoplexes of (A) reduced BFDMA, (B) electrochemically oxidized BFDMA and (C) chemically oxidized BFDMA. See text for additional information on lipid/DNA ratios and other experimental details.

Figure 5.3 shows fluorescence micrographs of EGFP expression in COS-7 cells treated with lipoplexes formed from (A) reduced BFDMA, (B) electrochemically oxidized BFDMA, and (C) chemically oxidized BFDMA produced as described above. Inspection of these images reveals that lipoplexes of reduced and electrochemically oxidized BFDMA mediated high and low levels of EGFP expression, respectively, consistent with the results of our past studies^{19, 20, 23, 24}. The image presented in Figure 5.3C, however, reveals that lipoplexes prepared using chemically oxidized BFDMA mediated high levels of transgene expression that were qualitatively similar to those using reduced BFDMA (Figure 5.3A). Figure 5.4 shows levels of luciferase expression (expressed as relative light units normalized to total cell protein) for cells treated with lipoplexes of reduced BFDMA, electrochemically oxidized BFDMA, or chemically oxidized BFDMA. These data also reveal that lipoplexes of chemically oxidized BFDMA mediated high levels of transgene expression similar to those promoted by lipoplexes of reduced BFDMA, consistent with the qualitative EGFP expression results discussed above (Figure 5.3).

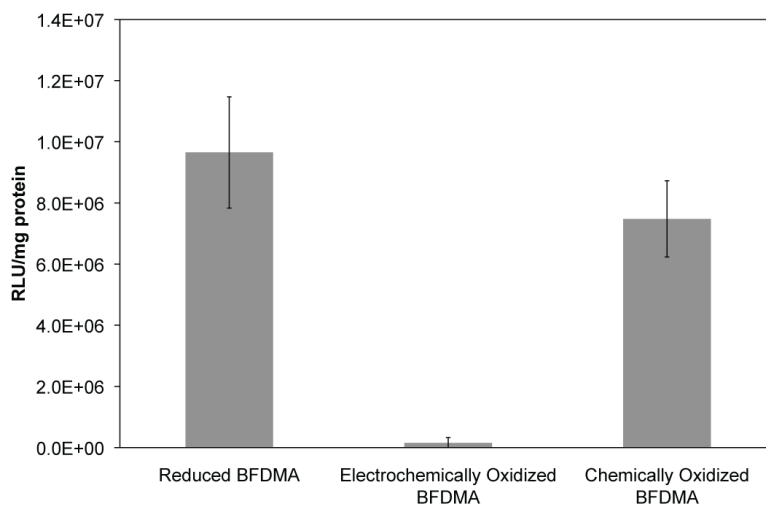


Figure 5.4. Normalized luciferase expression in COS-7 cells mediated by lipoplexes formed from reduced BFDMA, electrochemically oxidized BFDMA and chemically oxidized BFDMA. See text for additional information on lipid/DNA ratios and other experimental details.

Although the results presented in Figure 5.2 demonstrate that both electrochemical and chemical methods can be used to oxidize the ferrocenyl groups of BFDMA, it is clear from the results of these cell-based experiments that lipoplexes formed using these two different forms of oxidized BFDMA behave quite differently in the context of cell transfection. Below, we describe the results of characterization experiments that identify features and properties of these lipoplexes that could underlie these differences in cell transfection.

5.3.3 Characterization of the zeta potentials of lipoplexes of chemically oxidized BFDMA

The zeta potentials of lipoplexes can affect the efficiency with which lipoplexes are internalized by cells and, thus, influence levels of cell transfection significantly.^{37, 38} Our past studies suggested that large differences in the zeta potentials of lipoplexes of reduced and electrochemically oxidized BFDMA (discussed in more detail below) correlate to differences in the extent to which these lipoplexes are internalized by cells (an important first step in the overall cell transfection process).^{23, 24} We performed experiments to characterize and compare the zeta potentials of lipoplexes formed using electrochemically and chemically oxidized BFDMA (prepared as used in the cell transfection experiments above, i.e., at a BFDMA concentration of 10 μM and at BFDMA/DNA CRs of 1.4:1 and 4.2:1 for lipoplexes of reduced and oxidized BFDMA, respectively).

Table 5.1. Zeta Potentials of Lipoplexes.^a

Sample Type	Zeta Potentials (mV)
Lipoplexes of reduced BFDMA	-10 \pm 4
Lipoplexes of electrochemically oxidized BFDMA	-18 \pm 9
Lipoplexes of chemically oxidized BFDMA	+2 \pm 1
Lipoplexes of EDTA-treated chemically oxidized BFDMA	-20 \pm 7

^aLipoplexes were prepared in Li_2SO_4 and diluted into Li_2SO_4 so that the final concentration of BFDMA was 10 μM in all cases, and lipid/DNA charge ratios were fixed at 1.4:1 for lipoplexes of reduced BFDMA and 4.2:1 for lipoplexes of oxidized BFDMA (see text for additional details).

The results shown in Table 5.1 demonstrate that the average zeta potentials of lipoplexes prepared from electrochemically oxidized BFDMA (approximately -18 mV) were more negative than those of lipoplexes formed from reduced BFDMA (approximately -10 mV). These results are in general agreement with the results of past studies.^{21, 24} The average zeta potentials of lipoplexes formed from *chemically* oxidized BFDMA, however, were positive (approximately $+2$ mV) and, thus, substantially different from the zeta potentials of lipoplexes of both reduced and electrochemically oxidized BFDMA. We hypothesized that this positive zeta potential was the result of association of lipoplexes with residual Fe^{2+} and/or Fe^{3+} species present in solutions of chemically oxidized BFDMA (because a 1.5-fold molar excess of Fe^{3+} was used to oxidize BFDMA, both Fe^{2+} and Fe^{3+} species are present in solution at the end of the oxidation process; these species are not present in solutions of electrochemically oxidized BFDMA). It is possible that the small but positive zeta potentials of these lipoplexes could contribute to more favorable interactions with cell membranes and promote more efficient internalization (and, thus, contribute to higher levels of cell transfection than those promoted by lipoplexes of electrochemically oxidized BFDMA). We note, however, that other factors could also contribute to these observed differences, and we return to a discussion of the impact of changes in zeta potentials on cell transfection again in the discussion below.

5.3.4 Characterization of lipoplex nanostructures using SANS and cryo-TEM

We used SANS and cryo-TEM to provide insight into potential differences in the nanostructures of lipoplexes of electrochemically and chemically oxidized BFDMA that may underlie differences in cell transfection levels and zeta potentials described above. These experiments were performed in deuterated 1 mM Li_2SO_4 using lipoplexes formulated at BFDMA/DNA CRs of 1.1:1 and 3.3:1 for lipoplexes of reduced BFDMA and oxidized BFDMA, respectively. We note that these CRs do not correspond exactly to those used in the cell transfection experiments presented in Figures 3 and 4. The CRs used here were chosen to permit more direct comparisons to the results of our past SANS and cryo-TEM analyses of BFDMA lipoplexes,^{22, 24, 25} which were performed at these slightly different CRs. Those past studies suggested that the nanostructures of lipoplexes formed from BFDMA and DNA do not change substantially with small changes in the BFDMA/DNA CR (at least for lipoplexes formed from reduced BFDMA).²²

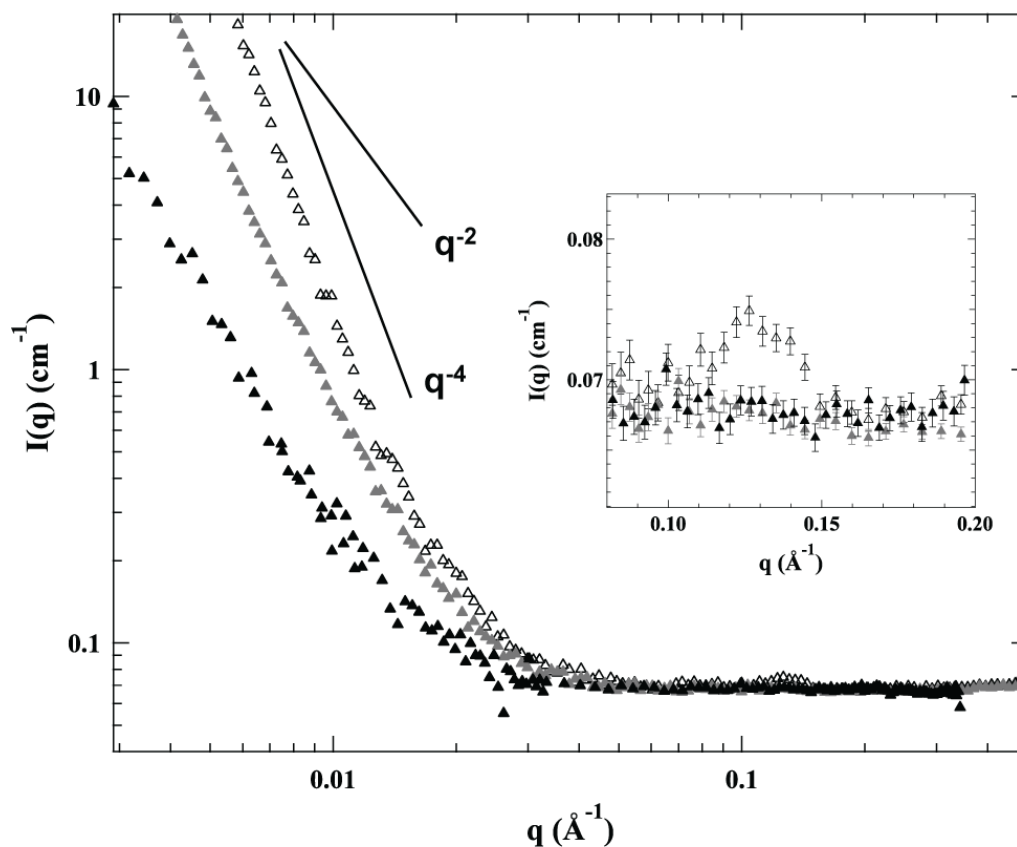


Figure 5.5. SANS spectra of lipoplexes of reduced BFDMA (open black triangles), lipoplexes of electrochemically oxidized BFDMA (solid gray triangles), and lipoplexes of chemically oxidized BFDMA (solid black triangles). The inset shows the Bragg peak observed at $q=0.12 \text{ \AA}^{-1}$.

Figure 5.5 shows SANS spectra of lipoplexes of reduced BFDMA (open black triangles), lipoplexes of electrochemically oxidized BFDMA (solid gray triangles), and lipoplexes of chemically oxidized BFDMA (solid black triangles). The inset in Figure 5.5 shows the Bragg peaks identified for these complexes. The SANS spectrum of the lipoplexes of reduced BFDMA exhibits a Bragg peak at $q=0.12 \text{ \AA}^{-1}$ (see also the inset in Figure 5.5). This peak corresponds to the periodicity of

multilamellar lipoplexes formed from BFDMA and DNA in which DNA (thickness of 2.7 nm) is intercalated between lipid bilayers (thickness of 2.5 nm).²² This model of lipoplex structure is also confirmed by the results of our cryo-TEM analyses (Figure 5.6, discussed below). Further inspection of the SANS data for lipoplexes of reduced BFDMA in the low q region of the spectrum reveals a q^{-4} dependence that is consistent with the presence of polydisperse multilamellar vesicles. Figure 5.5 also reveals that no Bragg peaks were observed for lipoplexes formed from either electrochemically or chemically oxidized BFDMA. This result indicates the absence of any measurable periodic nanostructures for either of these oxidized BFDMA lipoplex formulations. In addition, the SANS spectra of these complexes in the low q region follows a q dependence of q^{-3} , consistent with the presence of loose aggregate structures rather than a periodic multilamellar structure.

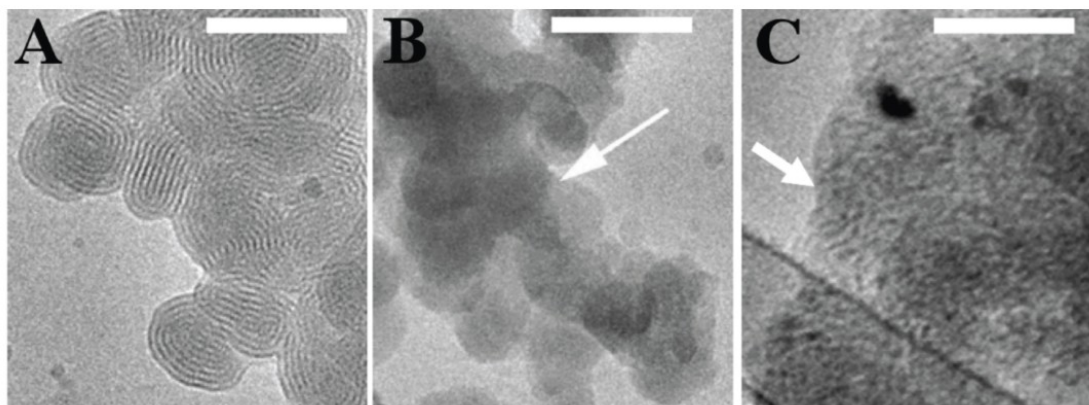


Figure 5.6. Cryo-TEM images of (A) lipoplexes of reduced BFDMA, (B) lipoplexes of electrochemically oxidized BFDMA (arrow points to amorphous, nonlamellar structures), and (C) lipoplexes of chemically oxidized BFDMA (arrow points to large aggregates composed of a stack of sheets, superimposed due to the two-dimensional nature of cryo-TEM optics). Scale bars are 100 nm in each image.

Cryo-TEM images of lipoplexes of reduced BFDMA (Figure 5.6A) revealed spherically-shaped multilamellar structures with a periodicity of 5.1 ± 0.2 nm, consistent with the above-described interpretation of our SANS results (Figure 5.5). Inspection of cryo-TEM images of lipoplexes of electrochemically oxidized BFDMA (Figure 5.6B) and chemically oxidized BFDMA (Figure 5.6C) reveals differences in overall morphology, but that both of these complexes form aggregates without any internal periodicity. In general, these observations are consistent with the q dependence of -3 in the low q region and the absence of a Bragg peak in the SANS spectrum of these lipoplexes (Figure 5.5). However, further inspection of the cryo-TEM images of these lipoplexes demonstrates that the aggregates formed using chemically oxidized BFDMA appear larger than those formed using electrochemically oxidized BFDMA. This difference in size or extent of aggregation was not detected in the SANS analyses (i.e. both complexes have a q dependence of -3 in the low q region). This may result from the fact that larger aggregates settle more rapidly to the bottom of the cuvettes used for SANS over the time scale of those longer measurements (and, thus, they reside largely out of the path of the incident neutron beam travelling through and being scattered by the sample).

We performed dynamic light scattering (DLS) experiments to further characterize differences in the sizes of aggregates formed using electrochemically or chemically oxidized BFDMA. These measurements were performed using lipoplexes prepared at the same BFDMA/DNA CRs used for SANS and cryo-TEM, but at a lower BFDMA concentration ($8 \mu\text{M}$) to permit characterization by DLS. These

experiments revealed the mean size of lipoplexes of electrochemically oxidized BFDMA to be ~190 nm, but that the average size of lipoplexes formed using chemically oxidized BFDMA was approximately 1500 nm (Figure 5.10, Supplemental Materials). These results provide further evidence of differences in the physical properties of lipoplexes formed from electrochemically and chemically oxidized BFDMA (and suggest that the apparent difference in the sizes of aggregates shown in Figure 5.6B-C is not the result of artifacts arising from the preparation of these samples for cryo-TEM analysis).

5.3.5 Investigation of potential influences of residual Fe^{2+} and Fe^{3+} on the properties and behaviors of lipoplexes of chemically oxidized BFDMA

The results above demonstrate that Fe^{3+} can oxidize the ferrocenyl groups of BFDMA rapidly and completely at ambient room temperature. However, our results also demonstrate that lipoplexes formed using samples of chemically oxidized BFDMA differ from lipoplexes prepared using electrochemically oxidized BFDMA in several important ways. Foremost among these differences (at least from a functional standpoint) is that lipoplexes of chemically oxidized BFDMA are able to promote high levels of cell transfection that are similar to those mediated by reduced BFDMA. Thus, although the use of Fe^{3+} presents a practical alternative to electrochemical oxidation, it also appears to have a significant influence on the levels of redox-based ‘on/off’ control over cell transfection that can be achieved using reduced and electrochemically oxidized BFDMA.

Lipoplexes formed using reduced and electrochemically oxidized BFDMA exhibit large differences in zeta potentials, a likely result of differences in the nanostructures of these lipoplexes (as discussed above and shown in Figures 5 and 6, lipoplexes of reduced BFDMA exhibit multilamellar nanostructures, while lipoplexes of electrochemically oxidized BFDMA are amorphous and devoid of periodic nanostructure). Our current results reveal differences in the zeta potentials of lipoplexes of chemically and electrochemically oxidized BFDMA that could also underlie the large differences in cell transfection observed in Figures 3 and 4. Interestingly, however, our current results suggest that these differences in zeta potential do not arise from substantial differences in the nanostructures of these complexes (e.g., as shown in Figures 5 and 6, lipoplexes of chemically and electrochemically oxidized BFDMA both possess amorphous, non-periodic nanostructures). As a final point of discussion, we note that the results of cryo-TEM and DLS experiments reveal that the average size of aggregates in solutions of lipoplexes of chemically oxidized BFDMA is substantially larger (~1500 nm) than the average size of aggregates present in solutions of lipoplexes of electrochemically oxidized BFDMA (~190 nm). The presence of these larger aggregates could arise from differences in the zeta potentials of these lipoplexes, and these larger structures could promote more effective physical delivery of DNA to cells during transfection experiments (e.g., by sedimentation). Although this latter possibility could potentially contribute to the higher levels of transfection observed using lipoplexes of chemically

oxidized BFDMA, we note that any fraction of larger aggregates capable of sedimenting more rapidly would also be less likely to be internalized by cells.

The samples of chemically oxidized BFDMA used in this study contain additional Fe^{2+} and Fe^{3+} species that are not present in solutions of electrochemically oxidized BFDMA. The presence of these species does not appear to influence the nanostructures of these lipoplexes. However, the presence and association of these ionic species with the surfaces of lipoplexes could influence surface charges (and thus zeta potentials). To investigate the potential influence of these species, we performed experiments using samples of chemically oxidized BFDMA treated with EDTA, a well known chelating agent used to sequester Fe^{2+} and Fe^{3+} ions.²⁸

In a first set of experiments, we performed the oxidation of reduced BFDMA using a 1.5-fold molar excess of Fe^{3+} (as described above), and then added a 1.5-fold molar excess of EDTA. Characterization of these samples using UV/vis spectrophotometry revealed that the addition of EDTA did not change the overall shape of the absorption spectrum (data not shown), suggesting that addition of EDTA does not promote significant degradation or destruction of ferrocenium ions under these conditions. DLS analysis of lipoplexes formed using EDTA-treated solutions of chemically oxidized BFDMA (Figure 5.10) revealed the average size of these lipoplexes to be large (~1800 nm) and similar to the average size of lipoplexes prepared using untreated samples of chemically oxidized BFDMA. However, characterization of the zeta potentials of lipoplexes formed using these EDTA-treated solutions revealed values that were substantially lower (more negative) than those

formed using untreated samples of chemically oxidized BFDMA (e.g., approximately -20 mV versus $+2$ mV for lipoplexes formed using untreated BFDMA; see Table 5.1). This substantially lower zeta potential is similar to that measured for lipoplexes prepared using electrochemically oxidized BFDMA (approximately -18 mV). This change in the zeta potentials of lipoplexes formed using EDTA-treated oxidized BFDMA reflects the affinity of Fe^{2+} and Fe^{3+} for EDTA relative to the lipoplexes, but these results do not distinguish potential differences in the relative contributions of these two species to the zeta potentials of lipoplexes in the presence or absence of EDTA.

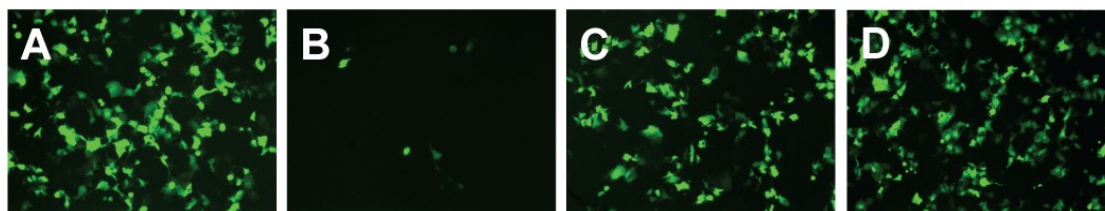


Figure 5.7. Representative fluorescence micrographs ($100\times$ original magnification, $1194\ \mu\text{m} \times 895\ \mu\text{m}$) of confluent monolayers of COS-7 cells showing EGFP expression mediated by (A) lipoplexes formed from chemically oxidized BFDMA (similar to the image shown in Figure 5.3C); (B) lipoplexes formed using chemically oxidized BFDMA treated with EDTA; (C) lipoplexes formed using EDTA-treated oxidized BFDMA treated with a 10-fold molar excess of ascorbic acid (prior to the formation of lipoplexes, see text); (D) lipoplexes formed using EDTA-treated oxidized BFDMA that were chemically reduced by the addition of a 10-fold molar excess of ascorbic acid in the presence of cells (i.e., ascorbic acid was added to lipoplexes after the lipoplexes had been placed in the presence of cells; see text).

These observations are consistent with the view that the presence of Fe^{2+} and Fe^{3+} could influence levels of cell transfection (i.e., help to promote it) through their influence on the zeta potentials of lipoplexes. More generally, these results also suggest a practical and straightforward route to the preparation of samples of

chemically oxidized BFDMA that can be used to prepare lipoplexes with properties that are more similar to those of lipoplexes formed using electrochemically oxidized BFDMA (that is, lipoplexes that *do not* transfect cells significantly). Figure 5.7A-B shows results of a cell transfection experiment using lipoplexes prepared using pEGFP and either chemically oxidized BFDMA or EDTA-treated samples of chemically oxidized BFDMA, respectively. These results demonstrate clearly that post-oxidation treatment of Fe^{3+} -oxidized BFDMA with EDTA can be used to prepare solutions of oxidized BFDMA that do function, in the context of cell transfection, in ways that ‘recover’ the functional properties of solutions of electrochemically oxidized BFDMA (i.e., to formulate BFDMA lipoplexes that are inactive toward transfection; similar to the results of experiments using electrochemically oxidized BFDMA shown in Figure 5.3B).

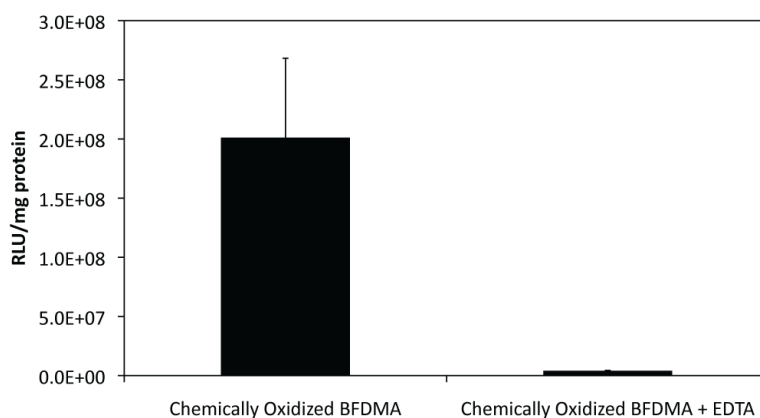


Figure 5.8. Normalized luciferase expression in COS-7 cells mediated by lipoplexes formed from chemically oxidized BFDMA and chemically oxidized BFDMA treated with EDTA. See text for additional information on lipid/DNA ratios and other experimental details.

Figure 5.8 shows levels of luciferase expression for populations of cells treated with otherwise identical lipoplexes prepared the pLuc plasmid and either chemically oxidized BFDMA or EDTA-treated chemically oxidized BFDMA. The results of these quantitative experiments confirm the large qualitative differences observed in EGFP expression shown in Figure 5.7.

Finally, as described in the Introduction, we recently demonstrated that treatment of lipoplexes of electrochemically oxidized BFDMA with the small-molecule chemical reducing agent ascorbic acid can be used to reduce BFDMA and “activate” these otherwise inactive lipoplexes toward cell transfection.²⁴ We performed experiments demonstrating that EDTA-treated solutions of chemically oxidized BFDMA can also be reduced by treatment with the chemical reducing agent ascorbic acid (as determined by UV/vis spectrophotometry; data not shown). The results of additional cell-based experiments also demonstrated that: (i) lipoplexes formed using these chemically reduced samples of BFDMA (Figure 5.7C) can promote high levels of cell transfection that are qualitatively similar to those promoted by fresh (as-synthesized) reduced BFDMA (Figure 5.3A), and (ii) that pre-formed lipoplexes formed using these EDTA-treated samples can be chemically reduced *in vitro*, in cell culture media and in the presence of cells, to activate lipoplexes toward transfection (e.g., Figure 5.7D). The results of these experiments, when combined, demonstrate that combinations of chemical oxidation and chemical reduction can be used to achieve levels of redox-based ‘on/off’ control of cell

transfection that are similar to those achieved in past studies^{23, 24} using electrochemical methods.

5.4 Conclusions

We have demonstrated that the ferrocenyl groups of the cationic, redox-active lipid BFDMA can be oxidized rapidly and quantitatively using a chemical oxidizing agent. This chemical approach to oxidation confers several practical advantages (including the ability to perform oxidation rapidly at ambient temperatures) compared to electrochemical oxidation methods used in past studies for the preparation of bulk samples of oxidized BFDMA. Subsequent experiments demonstrated that BFDMA/DNA lipoplexes prepared using samples of chemically oxidized BFDMA behaved very differently from lipoplexes formed using electrochemically oxidized BFDMA with respect to their ability to promote *in vitro* cell transfection. While lipoplexes of electrochemically oxidized BFDMA do not transfect cells efficiently, lipoplexes formed using chemically oxidized BFDMA promoted levels of transfection that were high and similar to levels mediated by lipoplexes of reduced BFDMA.

Physical characterization experiments revealed that lipoplexes of chemically and electrochemically oxidized BFDMA both have amorphous, non-periodic nanostructures, but that these lipoplexes differ significantly in terms of both size and zeta potential. The results of additional experiments suggested that these differences in zeta potential likely arise from the presence of residual Fe^{2+} and Fe^{3+} ions present in samples of chemically reduced BFDMA. In support of this hypothesis, we

demonstrated that the addition of EDTA to solutions of chemically oxidized BFDMA can be used as a practical and straightforward method to produce samples of chemically oxidized BFDMA that are functionally similar to samples of electrochemically oxidized BFDMA (e.g., to produce lipoplexes that do not transfect cells significantly). Finally, our results demonstrate that (i) EDTA-treated samples of chemically oxidized BFDMA can be reduced by treatment with a chemical reducing agent to produce samples of reduced BFDMA that do promote high levels of cell transfection, and (ii) lipoplexes formed using these EDTA-treated samples can be chemically reduced in the presence of cells to activate the lipoplexes and initiate transfection. Overall, the results of this study demonstrate that combinations of chemical oxidation and chemical reduction can be used to achieve levels of redox-based ‘on/off’ control of cell transfection that are similar to those achieved in past studies using electrochemical methods.

5.5 Acknowledgements

Financial support was provided by the NIH (1 R21 EB006168) and the National Science Foundation (CBET-0754921). We gratefully acknowledge S. Hata and H. Takahashi for assistance with the synthesis of BFDMA, and the support of the Oak Ridge National Laboratory in providing the neutron facilities use in this work. Cryo-TEM work was carried out at the Technion Soft Matter Electron Microscopy Laboratory with the financial support of the Technion Russell Berrie Nanotechnology Institute (RBNI).

5.6 References

‡ Portions of this chapter have been previously published as: J. P. E. Muller, B. S. Aytar, S. Golan, Y. Kondo, Y. Talmon, N. L. Abbott and D. M. Lynn, Chemical Oxidation of a Redox-Active, Ferrocene-Containing Cationic Lipid: Influence on Interactions with DNA and Characterization in the Context of Cell Transfection. *J. Colloid Interface Sci.*, **2012**, 387, 56-64.

1. P. L. Felgner, T. R. Gadek, M. Holm, R. Roman, H. W. Chan, M. Wenz, J. P. Northrop, G. M. Ringold and M. Danielsen, *Proceedings of the National Academy of Sciences of the United States of America*, **1987**, 84, 7413-7417.
2. J. Zabner, *Advanced Drug Delivery Reviews*, **1997**, 27, 17-28.
3. A. V. Kabanov, P. L. Felgner and L. W. Seymour, *Self-Assembling Complexes for Gene Delivery: From Laboratory to Clinical Trial*, John Wiley and Sons, New York, 1998.
4. L. Wasungu and D. Hoekstra, *Journal of Controlled Release*, **2006**, 116, 255-264.
5. C. T. de Ilarduya, Y. Sun and N. Duzgunes, *European Journal of Pharmaceutical Sciences*, **2010**, 40, 159-170.
6. F. X. Tang and J. A. Hughes, *Biochemical and Biophysical Research Communications*, **1998**, 242, 141-145.
7. B. Wetzer, G. Byk, M. Frederic, M. Airiau, F. Blanche, B. Pitard and D. Scherman, *Biochemical Journal*, **2001**, 356, 747-756.
8. X. Guo and F. C. Szoka, *Accounts of Chemical Research*, **2003**, 36, 335-341.
9. Z. H. Huang, W. J. Li, J. A. MacKay and F. C. Szoka, *Molecular Therapy*, **2005**, 11, 409-417.
10. V. Budker, V. Gurevich, J. E. Hagstrom, F. Bortzov and J. A. Wolff, *Nature Biotechnology*, **1996**, 14, 760-764.
11. O. V. Gerasimov, J. A. Boomer, M. M. Qualls and D. H. Thompson, *Advanced Drug Delivery Reviews*, **1999**, 38, 317-338.
12. J. Zhu, R. J. Munn and M. H. Nantz, *Journal of the American Chemical Society*, **2000**, 122, 2645-2646.

13. P. Meers, *Advanced Drug Delivery Reviews*, **2001**, 53, 265-272.
14. C. A. H. Prata, Y. X. Zhao, P. Barthelemy, Y. G. Li, D. Luo, T. J. McIntosh, S. J. Lee and M. W. Grinstaff, *Journal of the American Chemical Society*, **2004**, 126, 12196-12197.
15. X. X. Zhang, C. A. H. Prata, J. A. Berlin, T. J. McIntosh, P. Barthelemy and M. W. Grinstaff, *Bioconjugate Chemistry*, **2011**, 22, 690-699.
16. T. Nagasaki, A. Taniguchi and S. Tamagaki, *Bioconjugate Chemistry*, **2003**, 14, 513-516.
17. J. A. Wolff and D. B. Rozema, *Molecular Therapy*, **2008**, 16, 8-15.
18. Y. C. Liu, A. L. M. Le Ny, J. Schmidt, Y. Talmon, B. F. Chmelka and C. T. Lee, *Langmuir*, **2009**, 25, 5713-5724.
19. N. L. Abbott, C. M. Jewell, M. E. Hays, Y. Kondo and D. M. Lynn, *Journal of the American Chemical Society*, **2005**, 127, 11576-11577.
20. C. M. Jewell, M. E. Hays, Y. Kondo, N. L. Abbott and D. M. Lynn, *Journal of Controlled Release*, **2006**, 112, 129-138.
21. M. E. Hays, C. M. Jewell, Y. Kondo, D. M. Lynn and N. L. Abbott, *Biophysical Journal*, **2007**, 93, 4414-4424.
22. C. L. Pizzey, C. M. Jewell, M. E. Hays, D. M. Lynn, N. L. Abbott, Y. Kondo, S. Golan and Y. Tahnou, *Journal of Physical Chemistry B*, **2008**, 112, 5849-5857.
23. C. M. Jewell, M. E. Hays, Y. Kondo, N. L. Abbott and D. M. Lynn, *Bioconjugate Chemistry*, **2008**, 19, 2120-2128.
24. B. S. Aytar, J. P. E. Muller, S. Golan, S. Hata, H. Takahashi, Y. Kondo, Y. Talmon, N. L. Abbott and D. M. Lynn, *J. Control. Release*, **2012**, 157, 249-259.
25. S. Golan, B. S. Aytar, J. P. E. Muller, Y. Kondo, D. M. Lynn, N. L. Abbott and Y. Talmont, *Langmuir*, **2011**, 27, 6615-6621.
26. G. Wilkinson, M. Rosenblum, M. C. Whiting and R. B. Woodward, *Journal of the American Chemical Society*, **1952**, 74, 2125-2126.
27. A. J. Bard and L. R. Faulkner, *Electrochemical methods : fundamentals and applications*, Wiley, New York, 2001.

28. R. Prããibil, *Analytical applications of EDTA and related compounds*, Pergamon Press, Oxford, New York, 1972.
29. N. Yoshino, H. Shoji, Y. Kondo, Y. Kakizawa, H. Sakai and M. Abe, *Journal of Japan Oil Chemists' Society*, **1996**, 45, 769-775.
30. A. Guinier and G. Fournet, *Small Angle X-ray Scattering*, John Wiley & Sons, New York, 1955.
31. J. R. Bellare, H. T. Davis, L. E. Scriven and Y. Talmon, *Journal of Electron Microscopy Technique*, **1988**, 10, 87-111.
32. D. Danino, A. Bernheim-Groswasser and Y. Talmon, *Colloids and Surfaces a-Physicochemical and Engineering Aspects*, **2001**, 183, 113-122.
33. B. S. Gallardo, M. J. Hwa and N. L. Abbott, *Langmuir*, **1995**, 11, 4209-4212.
34. D. E. Bennett, B. S. Gallardo and N. L. Abbott, *Journal of the American Chemical Society*, **1996**, 118, 6499-6505.
35. Y. Kakizawa, H. Sakai, K. Nishiyama, M. Abe, H. Shoji, Y. Kondo and N. Yoshino, *Langmuir*, **1996**, 12, 921-924.
36. E. V. B. van Gaal, R. van Eijk, R. S. Oosting, R. J. Kok, W. E. Hennink, D. J. A. Crommelin and E. Mastrobattista, *J. Control. Release*, **2011**, 154, 218-232.
37. E. Tomlinson and A. P. Rolland, *Journal of Controlled Release*, **1996**, 39, 357-372.
38. F. Sakurai, R. Inoue, Y. Nishino, A. Okuda, O. Matsumoto, T. Taga, F. Yamashita, Y. Takakura and M. Hashida, *Journal of Controlled Release*, **2000**, 66, 255-269.

5.7 Supplemental materials

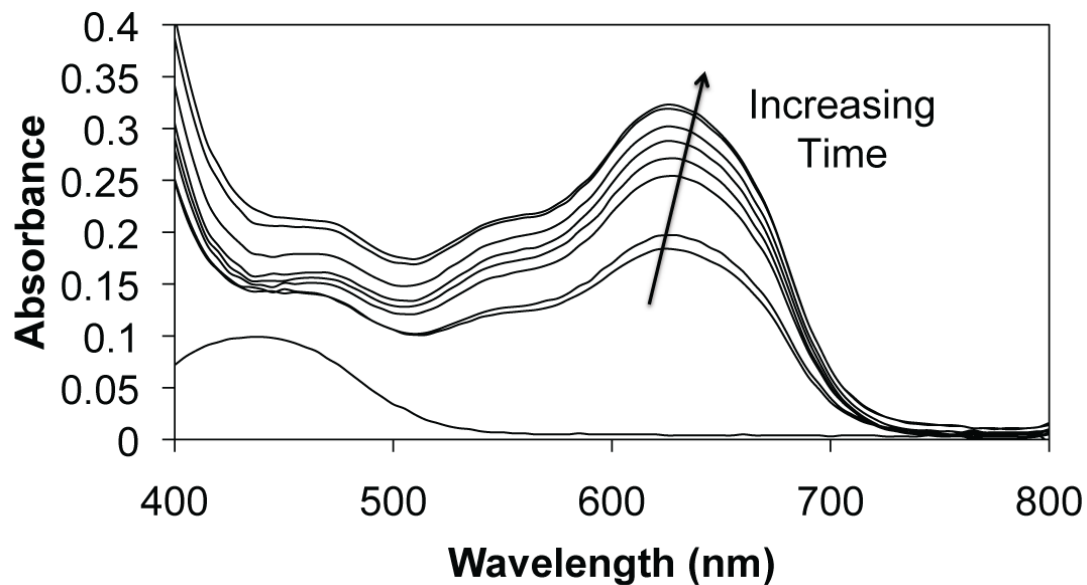


Figure 5.9. Time dependent changes of UV/visible absorbance spectra of a solution of reduced BFDMA upon treatment with a 1.5-fold molar excess of Fe^{3+} . Arrow indicates progressive time points acquired at time points of 30 sec, 2.5, 7.5, 12.5, 17.5, 22.5, 32.5, and 42.5 minutes. The initial solution was aqueous Li_2SO_4 containing 500 μM reduced BFDMA. Prior to individual absorbance measurements, DTAB was added to eliminate turbidity observed in lipid solutions. DTAB does not absorb light in the region of 400-800 nm.

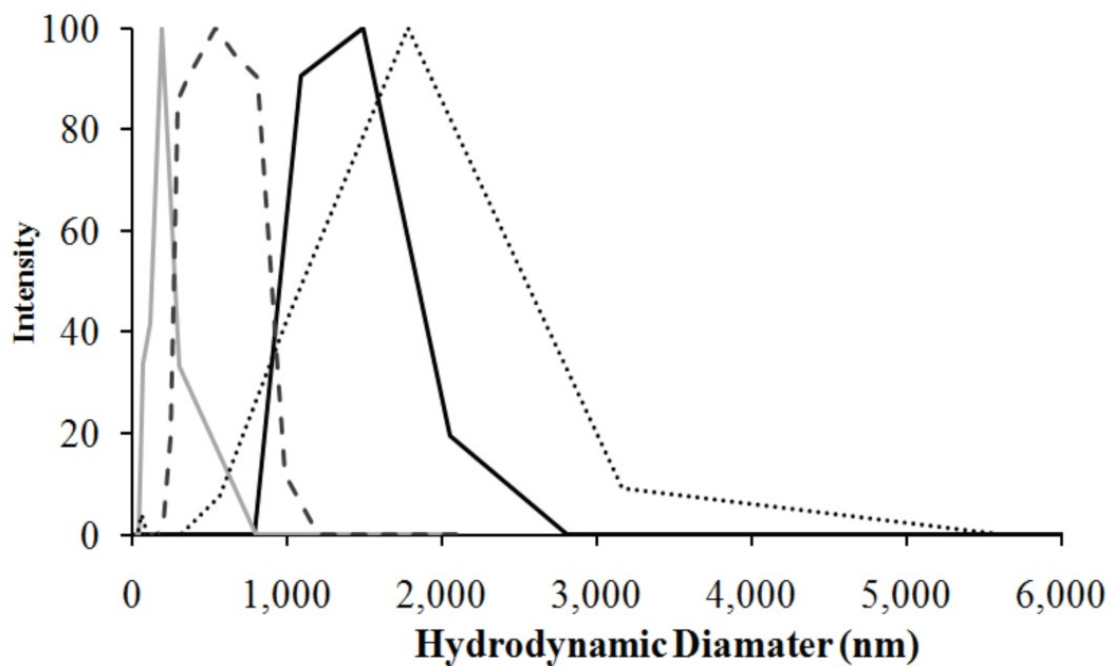


Figure 5.10. Hydrodynamic diameters of lipoplexes of reduced BFDMA (dashed black line), electrochemically oxidized BFDMA (solid gray line), chemically oxidized BFDMA (solid black line), and chemically oxidized BFDMA treated with EDTA (dotted black line). The final concentration of BFDMA was $8 \mu\text{M}$ in all cases, and lipid/DNA charge ratios were fixed at 1.1:1 for lipoplexes of reduced BFDMA and 3.3:1 for lipoplexes of oxidized BFDMA.

Chapter 6: Influence of the Phase State of Self-Assembling Redox-Active Mediators on their Electrochemical Activity

6.1 Introduction

Redox-active amphiphiles, when adsorbed at surfaces, can be used to modify interfacial electron transfer events in a wide range of contexts. For example, adsorbed surfactants can enable fast electron transfer through molecular bridges over large distances for use in biosensors,^{1, 2} organic light-emitting diodes³⁻⁵ and molecular electronic devices.^{6, 7} Alternatively, surfactants can block the surface of an electrode to inhibit corrosion^{8, 9} or poisoning an electrocatalyst.¹⁰ Finally, surfactants can change the surface of an electrode from being hydrophilic to hydrophobic and thereby increase in the potential for oxidation of water and provide a wider potential window for transformations of organic compounds.¹¹ In the majority of systems, a key underlying fundamental issue is how the organization of amphiphiles impacts interfacial electron transfer processes.

In an effort to understand how the organization of amphiphiles impacts electron transfer processes at interfaces, several prior studies have reported investigations of rates of electron transfer from electroactive groups (for example ferrocene (Fc)) held at a fixed distance from the surface of an electrode by using highly organized, self-assembled monolayers.¹²⁻¹⁶ Consistent with the so-called superexchange model,¹⁷ representing relatively fast single electron tunneling steps through purposefully designed molecular bridges, the rate constants for electron

transfer were measured in these studies to decrease exponentially with increasing distance over which electron transfer took place.^{18, 19} Alternatively, and of relevance to the study reported in this chapter, Rusling and coworkers have studied the distance dependence of electron-transfer rate constants using ferrocene and ferrocenyl amphiphiles coadsorbed with cetyltrimethylammonium bromide (CTAB) on the surfaces of electrodes. They interpreted their results to indicate that an increase in distance of approximately two Angstroms between the ferrocene and electrode resulted in an order of magnitude decrease in the rate of electron transfer.²⁰ Building from these prior studies, we report here an investigation of how the self-assembled states of amphiphilic redox mediators impact their interfacial electrochemical behaviors. Specifically, we compare and contrast the properties of two water-soluble amphiphiles, (11-ferrocenylundecyl)trimethylammonium bromide (FTMA) and bis(11-ferrocenylundecyl)dimethylammonium bromide (BFDMA) (Figure 6.1), that form significantly different self-assembled structures in solution, and as demonstrated in our study, at electrode surfaces.

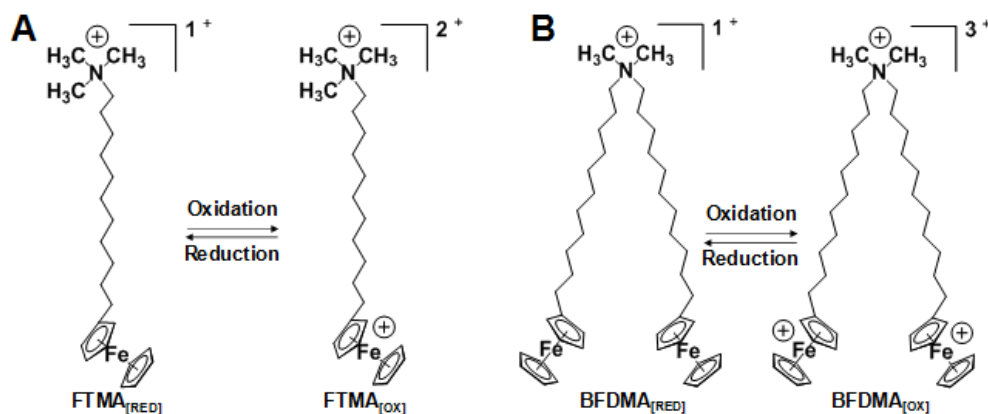


Figure 6.1. Structures of (A) FTMA ((11-ferrocenylundecyl)trimethylammonium bromide) and (B) BFDMA (bis(11-ferrocenylundecyl)dimethylammonium bromide).

The ferrocenyl amphiphiles used in our study have been investigated over the past decade as the basis of redox-active surfactant systems that can be placed under active control (i.e., enabling tuning of the amphiphilic nature of surfactants through cycling of the molecules between “on” and “off” redox states).²¹ In particular, the single-tailed redox-active ferrocenyl amphiphile, FTMA (Figure 6.1A) was used to demonstrate that changes in the oxidation state of ferrocene within the amphiphile can lead to large changes in surface tensions of aqueous solutions,^{22, 23} the reversible assembly and disassembly of micelles in solution²⁴ and active control over the interactions of surfactants with macromolecules.²⁵ In addition, the double-tailed redox-active amphiphilic surfactant, BFDMA (Figure 6.1B) has been shown to form complexes (or lipoplexes) with DNA that can deliver DNA to the nucleus of cells with an efficiency that depends strongly on the oxidation state of the ferrocenyl groups.²⁶⁻³³ While both of these amphiphiles have been investigated extensively in bulk solution, how their self-assembly at surfaces impacts their electrochemical activity has not been investigated in detail, particularly for BFDMA. Knowledge of the factors that control the rates of oxidation of these species at electrodes will be broadly useful in the rational design of systems containing self-assembling redox-active molecules. In this chapter, as a first step toward this goal, we compare and contrast the electrochemical characteristics of BFDMA and FTMA at a Pt electrode.

A central goal of the study reported in this chapter was to understand how the differences in the self-assembled states of amphiphilic redox-active species impacts the rate of oxidation and reduction of the amphiphiles at electrodes. Here we note that

we have previously observed that the rate of oxidation of BFDMA is slow relative to FTMA.^{24, 34-37} For FTMA, it has been proposed in past studies that, within the concentration boundary layer formed at an electrode held at oxidizing over-potentials, small globular micelles of FTMA present in bulk solution disassemble prior to arriving at the electrode.³⁵⁻³⁷ In contrast to FTMA, BFDMA forms large aggregates in solution even at low concentration.³¹ In addition, the dynamics of disassembly of BFDMA are expected to be much slower than FTMA. We hypothesized that the size and/or state of the assemblies formed by BFDMA relative to FTMA in solution in some way underlie their striking differences in electrochemical activity. To test this hypothesis, we report used cyclic voltammetry at both stationary and rotating disk electrode surfaces to provide insight into the physical processes occurring at electrodes incubated in aqueous solutions of BFDMA and FTMA. Our results reveal that the self-assembled states of the ferrocenyl amphiphiles do have a pronounced impact of the rates of electron transfer to and from electrodes. Overall, the results presented in this chapter hint that redox-active amphiphiles may offer the basis of self-assembling redox mediators that can be used to tune electron transfer events via changes in self-assembly (including redox-induced changes in self-assembly). Such principles have the potential to be broadly useful in designing interfacial charge transfer processes involved, for example, in energy storage and light-harvesting processes (e.g., photocatalytic splitting of water or solar cells).

6.2 Experimental section

6.2.1 Materials

The redox-active ferrocenyl amphiphile, FTMA was purchased from Dojindo Corporation (Gaithersburg, MD) and was used without further purification. The redox-active ferrocenyl amphiphile, BFDMA was synthesized according to methods published elsewhere.^{31, 32, 38} Dodecyltrimethylammonium bromide (DTAB) was purchased from Acros Organics (Morris Plains, NJ). Lithium sulfate monohydrate was purchased from Sigma-Aldrich (St. Louis, MO). Deionized water (18.2 M Ω) was used to prepare all salt solutions.

6.2.2 Experimental methods

6.2.2.1 Sample Preparation.

Each surfactant was dissolved in 20 mL aqueous 1 mM Li₂SO₄ (pH 5.1). 1 mM FTMA solutions dissolved readily but 1 mM BFDMA solutions required sonication for 20 minutes. Solutions were deoxygenated by bubbling argon for 30 min before use. An amphiphile concentration of 1 mM and electrolyte composition of 1 mM Li₂SO₄ was used for both BFDMA and FTMA throughout the experiments. These conditions were selected for relevancy to prior studies, where bulk oxidation of BFDMA was previously performed.^{27-30, 33, 39-41}

6.2.2.2 Bulk Electrolysis.

Bulk electrolysis was performed using an AFCBP1 Bipotentiostat (Pine Instrument Company, Grove City, PA). The working and counter electrodes were 25 mm x 25 mm platinum 45 mesh, woven from 0.198 mm diameter wire, 99.9%

(metals basis), folded twice into a 12.5 mm x 12.5 mm, four layered square (Alfa Aesar, Ward Hill, MA). Prior to use, the electrodes were polarized cathodically in 1.0 N H₂SO₄ to evolve H₂ by applying 200 potential sweeps of 0 to -1 V (vs a silver|silver chloride (Ag|AgCl) reference electrode (BASi, West Lafayette, IN)) to remove oxides from the surface of the electrodes.⁴² Bulk oxidation of FTMA and BFDMA was performed at either 0.4 V or 0.6 V, respectively (vs Ag|AgCl), at 25 °C with continuous stirring. The process of oxidation was stopped when a constant current was passed at the working electrode for at least 30 min. UV-vis spectrophotometry⁴³ and integration of the current-versus-time plots were used to determine the extent of oxidation of each amphiphile.

6.2.2.3 Cyclic voltammetry at stationary and rotating disk electrodes.

A 5 mm diameter disk working electrode (Pt) was used for all CV and RDE CV experiments. The electrode was polished using alumina polishing gamal, grade B (Fisher Chemical, Pittsburgh, PA) and degreased with acetone. Prior to use, the electrode was then polarized cathodically (as described above). These cleaning steps were performed as described in previous studies⁴² and they were found to provide reproducible results. CVs performed using a rotating disk electrode used an ASR Speed Control and an Analytical Rotator (Pine Instrument Company, Grove City, PA) to provide specific rotational speeds of the working electrode. Finally, prior to recording CVs, each electrode was swept from 0 mV to either 400 mV for FTMA or 600 mV for BFDMA (vs Ag|AgCl) at a scan rate of 100 mV/s until there was no further change in the magnitudes of anodic or cathodic Faradaic peak currents on

subsequent scans. This electrode conditioning step was found to be necessary to obtain consistent and reproducible results.

The peak cathodic and anodic currents (i_{peak}) measured in CVs obtained using the stationary disk electrode were analyzed to determine the rate-limiting electrode processes. For mass transfer limited, reversible processes at the electrode (no adsorption) the current passed at the electrode was fitted to the Randles-Sevcik equation,⁴⁴

$$i_{\text{peak,a_or_c}} = 0.4463n^{3/2} \left(\frac{F^3}{RT} \right)^{1/2} AD_0^{1/2} v^{1/2} C_0^* \quad (1)$$

where n is the number of electrons in the half cell reaction, R is the ideal gas constant, T is the temperature of the solution, F is Faraday's constant, A is the area of working electrode, D_0 is the diffusion coefficient of the dissolved electroactive species, C_0^* is the bulk concentration of the electroactive species, and v is the scan rate of the applied potential. According to equation 1, when mass transport is rate-limiting, i_{peak} is proportional to $v^{1/2}$. This relationship is true when sweeping the potential either anodically (producing a peak current, $i_{\text{peak,a}}$) or cathodically (producing a peak current, $i_{\text{peak,c}}$). Alternatively, if only adsorbed species lead to the current passed at the working electrode, the peak anodic or cathodic current, i_{peak} , becomes,⁴⁵

$$i_{\text{peak,a_or_c}} = \left(\frac{n^2 F^2}{4RT} \right) A v \Gamma_0^* \quad (2)$$

where Γ_o^* is the concentration of adsorbed electrochemically active species at the electrode surface. For this physical situation, i_{peak} is proportional to v . The CVs performed using a spinning disk electrode of known area, A , were analyzed using the Levich equation,^{46, 47}

$$i_{1,c} = 0.620nFAD_o^{2/3}\omega^{1/2}\nu^{-1/6}C_o^* \quad (3)$$

where ν is now the kinematic viscosity of the solution and the speed of the rotating disk electrode is ω .⁴⁷ Analysis of CVs obtained at both stationary and rotating disk electrodes were analyzed to provide estimates of the diffusion coefficient, D_o . The Stokes-Einstein equation was used to calculate the apparent hydrodynamic radius of the aggregates according to

$$D_o = \frac{k_B T}{6\pi\eta R_H} \quad (4)$$

where R_H is the apparent hydrodynamic radius, η is the viscosity, T is temperature and k_B is Boltzmann's constant.

6.2.2.4 Dynamic light scattering.

Dynamic light scattering (DLS) measurements of bulk solutions of 1 mM FTMA and 1 mM BFDMA were performed using a 100 mW, 532 nm laser (Coherent Compass 315M-100) and a BI-9000AT digital autocorrelator (Brookhaven Instruments Corporation, Holtsville, NY) at temperatures from 25 °C to 75 °C. The scattering of light was measured at 90°. The autocorrelation functions were analyzed using CONTIN.^{48, 49}

6.2.2.5 Differential scanning calorimetry.

Differential scanning calorimetry (DSC) measurements of bulk solutions of 1 mM FTMA and 1 mM BFDMA were performed using a Q100 Modulated Differential Scanning Calorimeter with Autosampler and Mass Flow Control (TA Instruments, New Castle, DE). 7 ± 1 mg samples, hermetically sealed in aluminum pans, were allowed to equilibrate at 25 °C before ramping the temperature at a rate of 1 °C/min up to 85 °C. The samples were held for 2 minutes at this temperature and then cooled at 1 °C/min to 25 °C.

6.3 Results and Discussion

6.3.1 Bulk electrolysis of BFDMA and FTMA

We begin by reporting an experiment that aimed to quantify differences in the rates of electrochemical oxidation of BFDMA and FTMA under the same experimental conditions (25 °C, 1 mM of amphiphile in 4.5 mL). As discussed in the Introduction, the pronounced differences that we measured in the rates of oxidation of these two ferrocenyl amphiphiles within this present experiment motivated the investigation that is reported in the remainder of this manuscript. This initial experiment involved application of an oxidizing potential of either 0.4 V or 0.6 V (vs Ag|AgCl) to Pt mesh electrodes immersed in solutions of FTMA or BFDMA, respectively. These oxidizing potentials were chosen on the basis of prior studies of FTMA^{34, 36} and BFDMA^{27, 28, 31-33} which showed that application of these respective

potentials lead to complete oxidation of each amphiphile. As detailed later in this chapter, under these conditions, the over-potential (applied potential minus formal potential, E°) applied to the Pt electrodes is similar (within 0.04 V) for the two amphiphiles, and therefore the driving force for oxidation of each amphiphile is similar (E° was determined for FTMA as 0.140 ± 0.010 V (vs Ag|AgCl) and for BFDMA as 0.305 ± 0.004 V (vs Ag|AgCl) from the CV experiments described below).

Figure 6.2 shows the current passed at a Pt mesh electrode, measured as a function of time, for both FTMA and BFDMA. Inspection of Figure 6.2 reveals striking differences in the behaviors of the two amphiphiles. First, the initial current passed during oxidation of FTMA was approximately 250 μ A, compared to only 32 μ A for BFDMA (see inset in Figure 6.2). Correspondingly, whereas the current passed at the electrode immersed into the solution of FTMA decayed over 3.6 h (Figure 6.2, black line), a sustained but smaller current was observed over almost 45 h when using BFDMA (Figure 6.2, grey line). Finally, the current passed during oxidation of FTMA drops gradually at a rate of approximately 50 μ A per hour over the duration of the experiment whereas, for BFDMA, the current dropped below 10 μ A within the first few minutes of application of the electrical potential. These initial observations provided the first hint that a barrier consisting of an adsorbed layer of BFDMA may be forming at the electrode immersed into the BFDMA solution.

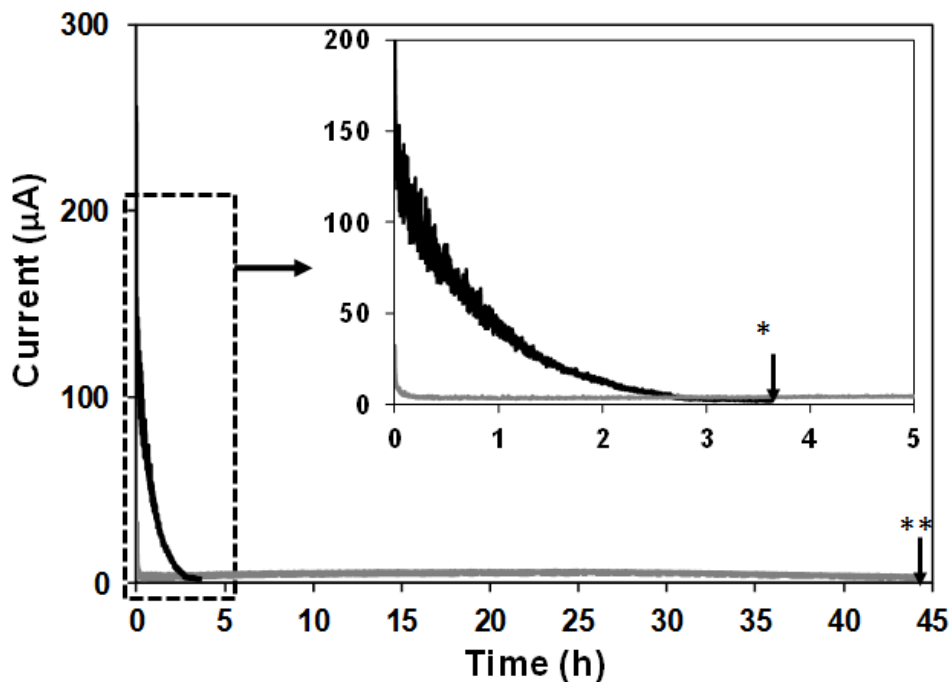


Figure 6.2. Current passed during electrochemical oxidation of 1 mM FTMA_{RED} (black line, at 0.4 V) or 1 mM BFDMA_{RED} (grey line, at 0.6 V) in 1 mM Li₂SO₄ pH 5 at ambient temperature. Platinum mesh working and counter electrodes, and a Ag|AgCl reference electrode were used. The volume of the solution was 4.5 mL.

To explore further the hypothesis that BFDMA was forming a barrier at the electrode, in an independent experiment that was otherwise identical to the experiment shown in Figure 6.2, a solution of BFDMA was incubated with the Pt mesh working electrode for one hour before applying an oxidizing potential of 0.6 V (vs Ag|AgCl, see Figure 6.10 of Supplemental materials). Although the initial current passed at the electrode was 32 μ A (unchanged from that measured above), the total charge passed over the first 400 s of the experiment was 30% less than that measured without pre-incubation of the electrode in the BFDMA solution (2.5 mC and 3.6 mC, respectively). This result provides further support for our hypothesis that BFDMA forms a barrier on the electrode surface that slows oxidation of the amphiphile.

We integrated the currents shown in Figure 6.2 over time to determine the total charge passed at the electrodes during the bulk electrolyses of FTMA and BFDMA and calculated the extent of oxidation of the ferrocenyl amphiphiles in solution. From these calculations, we determined that the charge passed at the electrode immersed into the FTMA solution was 0.396 C (corresponding to 91% of the theoretical charge for complete oxidation of all FTMA molecules in solution) and the charge passed at the electrode immersed into the BFDMA solution was 0.812 C (corresponding to 94% of the theoretical charge for complete oxidation of all BFDMA molecules in solution). We note also that the charge passed for BFDMA is approximately twice the value of FTMA for the same solution concentration, consistent with oxidation of both ferrocene groups of BFDMA. In summary, from these electrochemical measurements, we concluded that, although the oxidation of BFDMA is slower than FTMA, the oxidation of both amphiphiles was largely complete at the end of the experiments reported in Figure 6.2. This conclusion was supported additionally by measurements using UV-vis absorption spectrophotometry performed on each amphiphile solution before and after oxidation (See Supplemental materials, Figure 6.11).

In summary, we measured near complete oxidation of the ferrocenyl groups in aqueous solutions of each of 1 mM FTMA or 1 mM BFDMA. The rate of oxidation of BFDMA, however, was significantly lower than the rate of oxidation of FTMA. Furthermore, pre-incubation of the Pt electrode within a solution of BFDMA reduced the rate of oxidation of BFDMA further, suggesting that BFDMA is assembling into

an adsorbed layer on the electrode, thus creating a barrier to oxidation of additional BFDMA molecules. In contrast, we measured no such process for aqueous solutions of FTMA.

6.3.2 Cyclic voltammetry

To provide further insight into the physical processes that underlie the observations in Figure 6.2, we performed CV at a stationary Pt flag electrode immersed into solutions of either FTMA (Figure 6.3A and B) or BFDMA (Figure 6.3C and D). Similar to Figure 6.2, these measurements were performed in 1 mM Li_2SO_4 solution at room temperature. The range of potentials over which CVs were performed was 0 to 400 mV (vs Ag|AgCl) for FTMA and 0 to 600 mV (vs Ag|AgCl) for BFDMA (i.e. from 0 mV to the potential used for the bulk electrolysis of the amphiphiles (see Figure 6.2)). The voltage scan rates were increased from 10 mV/s to 200 mV/s to determine the dependence of the peak current on scan rate for each amphiphile (Figures 3B and 3D). Below we make three observations regarding the data reported in Figure 6.3.

First, for FTMA, we measured two cathodic and two anodic Faradaic current peaks at all scan rates (Figure 6.3A). The magnitude of the peak at the lowest potential (for scans in both directions) was found to depend on the scan rate with an exponent of 0.50 ± 0.01 (Figure 6.3B, peaks labeled a and c, correlation coefficient, $R^2 > 0.99$, $n = 2$). This result suggests that these peaks in the CV are caused by FTMA that is diffusing from solution to the electrode where it is oxidized (equation 1).

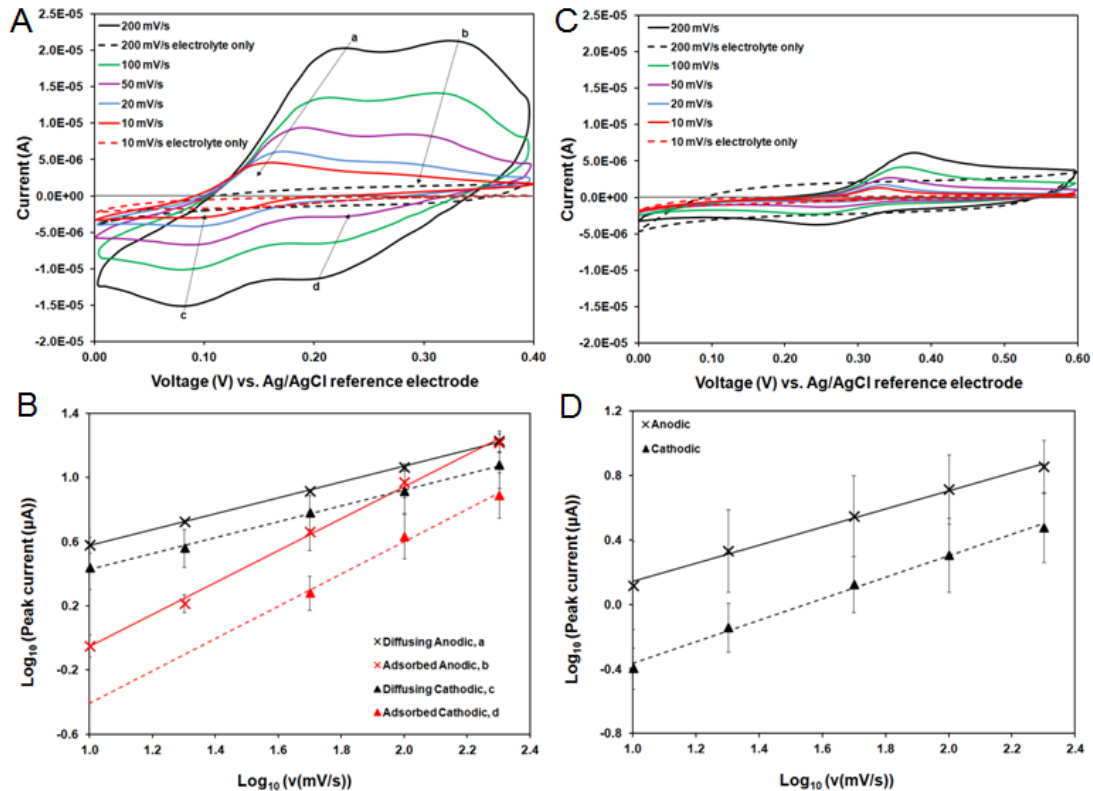


Figure 6.3. Cyclic voltammograms of aqueous solutions of (A) 1 mM reduced FTMA and (C) 1 mM reduced BFDMA, in 1 mM Li_2SO_4 pH 5. “Electrolyte only” refers to control experiments using 1 mM Li_2SO_4 free of amphiphile. A platinum disk working electrode (diameter of 5 mm), platinum mesh counter electrode, and a Ag|AgCl reference electrode were used. (B and D) Log-log plots of anodic or cathodic Faradaic peak currents versus v (correlation coefficient, $r^2 > 0.99$ for all fits). The dependence of the magnitude of the peak current on scan rate was characterized by an exponent of 0.50 ± 0.01 for each first (lines a and c) and 1.00 ± 0.01 for each second (lines b and d) anodic and cathodic peaks for FTMA ($n = 2$), and 0.57 ± 0.12 for the anodic peaks, and 0.67 ± 0.10 for the cathodic peaks of BFDMA ($n = 3$).

In contrast, the second peaks (at higher potential) in the CVs recorded for FTMA depend on the scan rate with an exponent of 1.00 ± 0.01 (Figure 6.3B, peaks labeled b and d, correlation coefficient, $R^2 > 0.99$, $n = 2$). These peaks in the CV, therefore, appear to be due to FTMA that is adsorbed at the electrode surface (equation 2). Overall, the occurrence of the second Faradaic peak current in both

anodic and cathodic scan directions (following the initial peak current corresponding to diffusing species, i.e., *postpeaks*) indicates that FTMA adsorption at the electrode surface causes a substantial change in the free energy required to change the oxidation state of the FTMA (relative to freely diffusing FTMA).⁵⁰ Specifically, with reference to the CV measured at a scan rate of 200 mV/s (black data, Figure 6.3A), the peak currents for the adsorbed species occur at 0.325 V (vs Ag|AgCl) in the anodic direction and 0.195 V (vs Ag|AgCl) in the cathodic direction. In contrast, the potentials at which the current peaks for the diffusing species are 0.226 V (vs Ag|AgCl) in the anodic direction and 0.081 V (vs Ag|AgCl) in the cathodic direction. By using the Nernst equation,⁵¹ the effect of adsorption on the free energy required to change the oxidation state of FTMA was estimated to be 3.9 ± 0.8 kT for the anodic scan direction, and 4.4 ± 0.8 kT for the cathodic scan direction at 200 mV/s. Similar conclusions are reached using the data presented in Figure 6.3A at other scan rates.

In contrast to FTMA, we measured only a single peak in the CVs for solutions of BFDMA (both scan directions). The dependence of the magnitude of the peak current on scan rate was characterized by an exponent of 0.57 ± 0.12 during oxidation and 0.67 ± 0.10 during reduction ($n=3$, Figure 6.3D), suggesting that the peak current contained contributions from both diffusing species and adsorbed species. We interpret these CVs of single peaks in either scan direction for solutions of BFDMA to indicate that the free energy required to change the oxidation states of the “bound” and “diffusing BFDMA species” are not measurably different. Here we note that

Kakizawa and coworkers,³² observed the presence of one peak only when oxidizing BFDMA at a Pt electrode (using 5 mM BFDMA in 0.1 M Li₂SO₄ at 20 mV/s), which they interpreted to indicate that both ferrocene groups on the BFDMA molecule are oxidized at similar potentials. In addition, we note that we previously characterized a similar surfactant to BFDMA, Fc(CH₂)₈N⁺(CH₃)₂(CH₂)₃-(CH₃)₂N⁺(CH₂)₈Fc 2Br⁻ at gold electrode by CV.⁵² Similar to the results reported in this chapter with BFDMA, we observed this surfactant to exhibit a single peak (in CVs), with a magnitude that varied with scan rate with an exponent of between 0.55 to 0.78 (dependent on concentration: 0.01 to 1 mM).

The second observation arising from Figure 6.3 is that an estimate for the formal potential, E⁰ for FTMA (0.140 ± 0.010 V, (vs Ag|AgCl)) calculated as the average of the anodic and cathodic peak potentials for diffusing species, i.e. E⁰ = (E_{peak,a} + E_{peak,c})/2 is lower than that of BFDMA (0.305 ± 0.004 V, (vs Ag|AgCl)), indicating that the free energy required to change the oxidation state of FTMA is less than BFDMA by 18.3 ± 0.7 kT, comparable to the difference in the free energy of aggregation between each amphiphile, 6.9 kT (calculated from the difference in free energy between a CMC of FTMA of 0.1 mM⁵³ and a CAC of BFDMA of 1x10⁻⁷ M³¹). In addition, for BFDMA, we note the separation of the peak potentials, E_{peak,a} and E_{peak,c} to be 0.043 V at a scan rate of 10 mV/s. Because the peak separation for a reversible electrode process should be 0.059 V/n, where n is the number of electrons transferred,⁵⁴ this result provides further evidence that both ferrocene groups on each molecule of BFDMA are being oxidized during the anodic scan (see Supplemental

materials for full discussion). We also note that the values of E° described above for FTMA and BFDMA are generally consistent with those reported previously for these ferrocenyl surfactants (under conditions that differed from those reported in this chapter). For example, for FTMA, Lui⁵⁵ reported CV data with an E° value of 0.13 to 0.14 V (vs Ag|AgCl) for FTMA (using a gold electrode and an electrolyte concentration of 0.1 M Li_2SO_4). For BFDMA, Kakizawa³² reported CV data with an E° value of approximately 0.31 V (vs Ag|AgCl, using platinum wire electrodes and an electrolyte concentration of 0.1 M Li_2SO_4).

The third key observation that we make regarding the CVs of FTMA and BFDMA is that the magnitudes of the anodic and cathodic peak currents obtained using BFDMA are lower than those of FTMA (e.g. at 200 mV/s, $i_{\text{peak,a}}$ is 6 μA for diffusing and adsorbed species of BFDMA but 19 μA for diffusing species of FTMA alone, see Figure 6.3A and 3C, solid black lines). If the currents were due solely to species diffusing from solution to the electrode, according to equation 1 this difference in current could be attributed to differences in the effective diffusion coefficients (D_o) (note that n is 1 for FTMA and 2 for BFDMA, Figure 6.1). By using the peak currents measured at 100 mV/s for both BFDMA and FTMA, we estimated the apparent diffusion coefficient, and thus the apparent hydrodynamic diameter (d_H , Table 6.1) of the assemblies diffusing to the electrodes.

Table 6.1. DLS analysis of hydrodynamic sizes of aggregates formed in aqueous solutions of 1 mM FTMA or 1 mM BFDMA in 1 mM Li₂SO₄. Calculation of hydrodynamic sizes of aggregates using peak currents in CVs performed at stationary electrodes (Figure 6.3) using the Randles-Sevcik equation (equation 1)^a or at rotating electrodes (Figure 6.5) using the Levich equation (equation 3)^b, followed by the use of Stokes-Einstein equation (equation 4) to calculate the hydrodynamic diameter.

Amphiphile	Hydrodynamic diameter, d_H (nm)		
	DLS	CV ^a via $i_{\text{peak,a}}$	RDE CV ^b via $i_{\text{l,c}}$
FTMA	10 ± 4	10	4
BFDMA	795 ± 250	700	n/a

We note that, while we analyzed the peak corresponding to diffusing species for FTMA, the peak analyzed for BFDMA necessarily included current arising from both diffusing and adsorbed species (see above). We emphasize, therefore, that the apparent size of the aggregates of BFDMA is a lower bound to the actual size of the aggregates in solution. For comparison, we also measured the hydrodynamic sizes of the aggregates using DLS (Table 6.1). Inspection of Table 6.1 reveals that values of d_H calculated from the peak anodic currents are in general agreement with the DLS data for each amphiphile (i.e., 10 ± 4 nm from DLS compared to 10 nm from $i_{\text{peak,a}}$ for FTMA, and 795 ± 250 nm from DLS compared to 700 nm from $i_{\text{peak,a}}$ for BFDMA).

Overall, the CVs shown in Figure 6.3 clearly establish that, for both FTMA and BFDMA, a population of each amphiphile is adsorbed to the electrodes and undergoes oxidation/reduction during the cycling of the electrode potential, with adsorbed and diffusing species separated during the voltage scan for FTMA but not for BFDMA. To provide information regarding the relative stability of the assemblies of adsorbed amphiphiles (FTMA or BFDMA) formed on the Pt electrode, we

measured CVs at Pt electrodes in solutions of either FTMA or BFDMA (as described above in the context of the electrode conditioning) and then transferred the electrodes to 1 mM Li_2SO_4 solutions that were free of dissolved amphiphiles. Figure 6.4 shows that, upon scanning of the potential of the pre-treated electrodes in the electrolyte solutions free of amphiphiles, Faradaic peaks were measured in both scan directions for BFDMA. In contrast, in a similar experiment performed with FTMA, no such current peaks were measurable (see Supplemental materials, Figure 6.12). We analyzed the magnitude of the anodic peaks for BFDMA in Figure 6.4. We then calculated the surface concentration of electroactive species of BFDMA (Γ_0) to be between 4.9 and 12.2 $\text{nm}^2/\text{molecule}$ using equation 2 (i.e., sub-monolayer coverage). The magnitudes of the anodic and cathodic Faradaic peaks associated with the adsorbed BFDMA (Figure 6.4) were approximately 33 to 40% of those measured when the CVs were recorded in the bulk solutions of BFDMA (equivalent scan rate data, Figure 6.3C). This result is consistent with our conclusion, based on the scan rate dependence of the peak current shown in Figure 6.3C, that the peak current measured in the bulk solution of BFDMA contained contributions from both adsorbed and diffusing species.

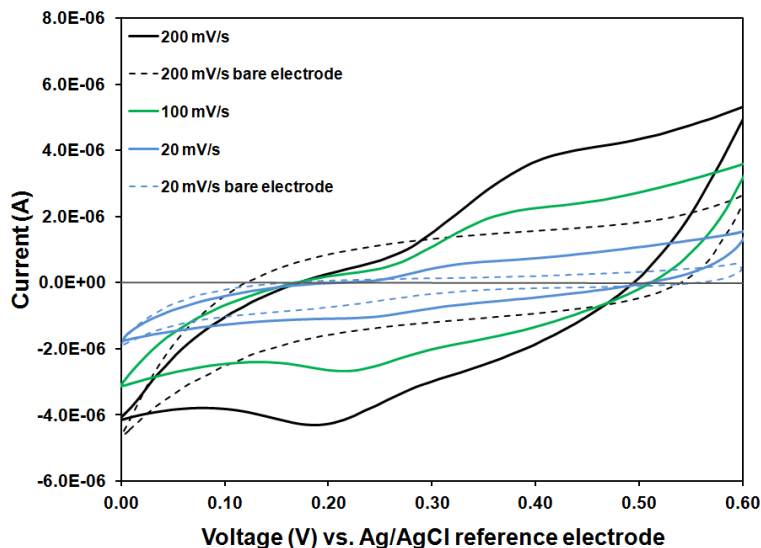
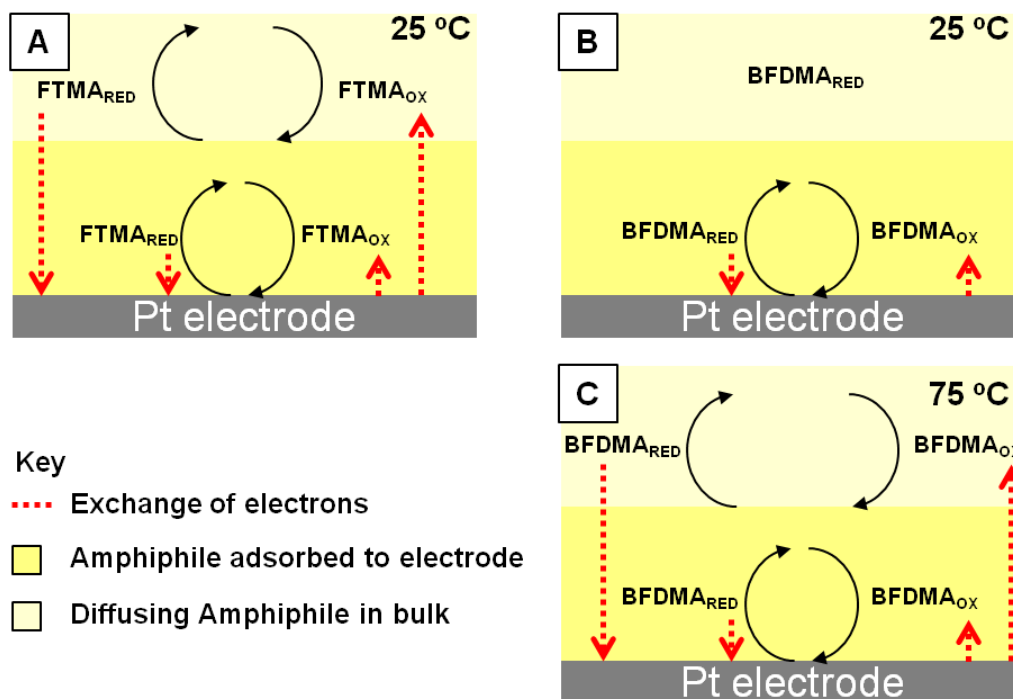


Figure 6.4. Cyclic voltammograms measured in aqueous 1 mM Li_2SO_4 after incubation of a Pt working electrode in a solution of 1 mM BFDMA in 1 mM Li_2SO_4 . Upon removal from the solution of BFDMA, the working electrode was gently rinsed with 1 mM Li_2SO_4 and immersed in the solution of 1 mM Li_2SO_4 . A platinum disc working electrode (diameter of 5 mm), platinum mesh counter electrode, and a Ag|AgCl reference electrode were used.

A surprising result, however, was obtained when the scan rate of the potential was varied in the experiment in Figure 6.4. We measured the magnitude of the peak current to change with scan rate with an exponent of 0.59 for $i_{\text{peak,a}}$, and 0.57 for $i_{\text{peak,c}}$, consistent with the presence of both diffusing species and adsorbed species. Because the BFDMA in bulk solution was removed in this experiment, we hypothesized that the flux of BFDMA to the electrode was influenced by the diffusion of BFDMA *within* an adsorbed layer of BFDMA that persists at the electrode, after rinsing and transfer to a solution of 1 mM Li_2SO_4 . In contrast, there is no evidence of FTMA at the surface of the electrode following an equivalent rinse.

6.3.3 Cyclic voltammetry at a rotating disc electrode

As discussed above, we interpreted the CVs obtained at a stationary electrode to indicate that both BFDMA and FTMA adsorb onto the electrode. The adsorbed layer of BFDMA appears to attenuate the contribution of BFDMA in bulk solution to the CV, although the scan-rate-dependence of the CV also suggests that BFDMA is mobile (diffusing) within the adsorbed layer at the electrode (Figures 3 and 4). In contrast, FTMA adsorbed to the electrode, while evident in the CV as a distinct peak, does not appear to block substantially the flux of FTMA to the electrode from bulk solution (see Scheme 6.1A). To provide an additional test of the physical picture that emerges from the CV at the stationary electrode, we performed CV at a rotating disc electrode (RDE).



Scheme 6.1. Electrochemical activity during a full CV scan for adsorbed and diffusing (A) FTMA at 25 °C (B) BFDMA at 25 °C and (C) BFDMA at 75 °C.

Figure 6.5 shows CVs of FTMA (Figure 6.5A) and BFDMA (Figure 6.5B) obtained at an electrode undergoing rotation at three speeds (600, 2900 and 6000 rpm). An initial inspection of the CVs in Figure 6.5A suggest that solutions of FTMA (Figure 6.5A) follow a typical Levich-type current behavior (equation 3), i.e., a mass transfer-limited rate of oxidation at the electrode. In brief, in this scenario, the fluid convection driven by the motion of the working electrode causes reactants of the half-cell reaction to be replenished at the surface of the electrode, thus avoiding any significant depletion of the concentration of redox species at the electrode (as occurs with a stationary electrode).⁵⁴ In addition, it is evident that the magnitude of the peak current increased with rotational speed of the working electrode.

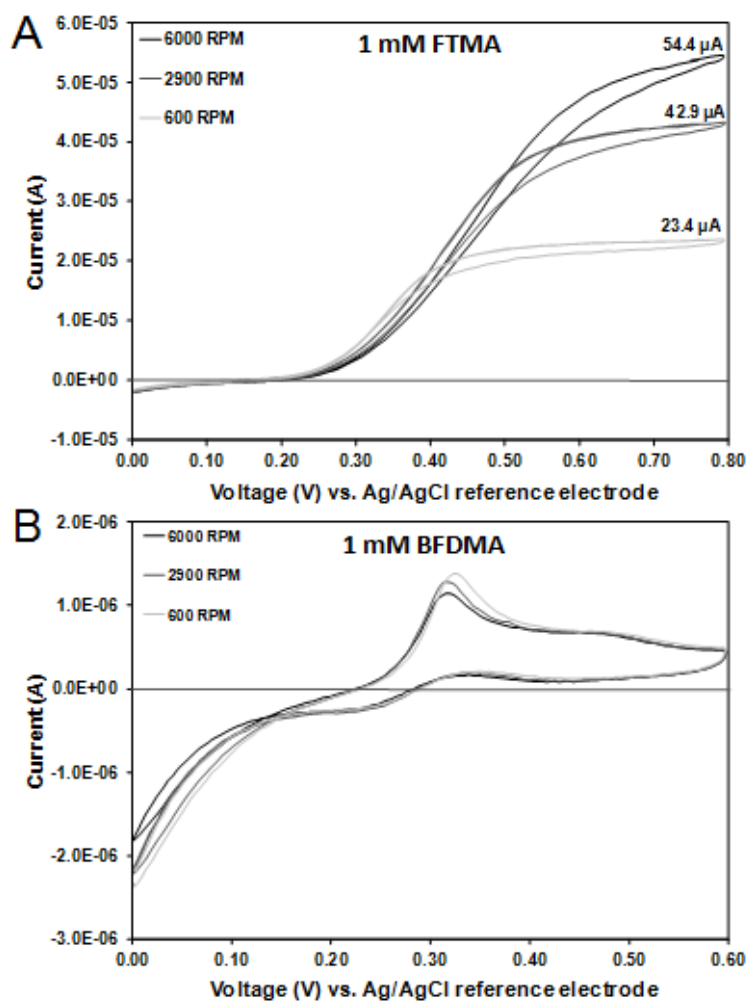


Figure 6.5. Cyclic voltammograms obtained at a RDE when using (A) 1 mM FTMA_{RED} and (B) 1 mM BFDMA_{RED}, in 1 mM Li₂SO₄ pH 5. The scan rate was 10 mV/s. A platinum disc working electrode (diameter of 5 mm), platinum mesh counter electrode, and a Ag|AgCl reference electrode were used.

In contrast to FTMA, solutions of BFDMA (Figure 6.5B) generated CVs at the RDE that possessed a Faradaic current peak during the anodic voltage scan. This peak was evident for all rotation speeds of the working electrode (i.e. from 600 to 6000 RPM). The presence of a peak current with increasing overpotential at the electrode, even though the electrode was rotating, indicates that the reduced BFDMA species in

bulk solution were not able to replenish the concentration of reduced BFDMA at the electrode during the anodic scan. This interpretation is consistent with the presence of an adsorbed layer of BFDMA that serves as a barrier against the ability of BFDMA from bulk solution to exchange electrons with the electrode (see Scheme 6.1B).

The magnitude of the Faradaic peak current in the anodic scan direction for BFDMA (Figure 6.5B) provides further insight to the effect of the adsorbed layer of BFDMA at the surface of the electrode. The peak current measured at the RDE was 1.0 to 1.3 μA , which is comparable to the peak current measured at the stationary electrode at the equivalent scan rate (1.0 μA for 10 mV/s; Figure 6.3C, red solid line). This observation again suggests that the Faradaic peak current is produced predominantly from electroactive species that are locally diffusing to and from the electrode within large aggregates of BFDMA (see Scheme 6.1B), as would be expected if the electrode were not rotating and forcing a constant supply of reactants to the surface of the electrode. In addition, we note that with increasing scan rate, the magnitude of the peak current in Figure 6.5B decreases. While we do not yet fully understand the origins of this phenomenon, we hypothesize that large aggregates of BFDMA (795 ± 250 nm, Table 6.1) may be loosely adsorbed to the electrode surface, adding to the localized population of slowly diffusing BFDMA molecules that contribute to the Faradaic current. As rotation speed increases, we speculate that the shear force imposed on these weakly adsorbed aggregates of BFDMA may increase, leading to their removal from the electrode and a lowering of the peak current.

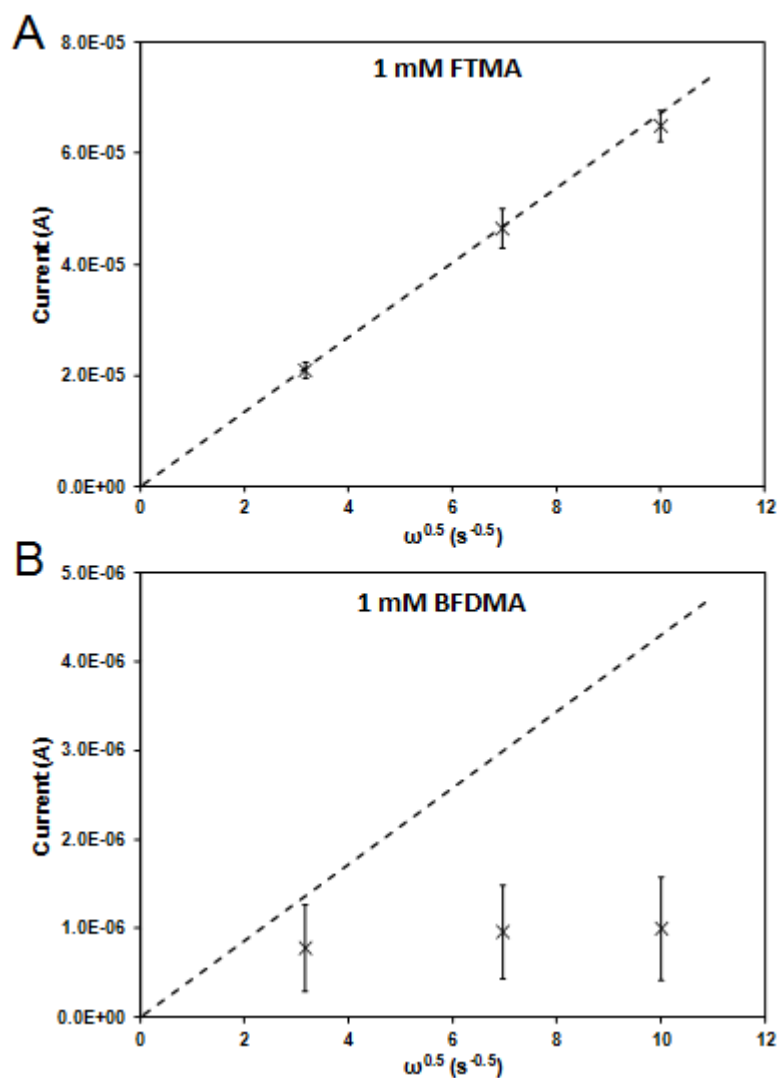


Figure 6.6. Peak anodic currents measured at RDEs using (A) 1 mM FTMA or (B) 1 mM BFDMA, in 1 mM Li_2SO_4 pH 5. For each graph, (x) represents the experimental data and the dotted line is the Levich current. See text for a full description of parameters used to model each analyte. The scan rate was 10 mV/s. A platinum disc working electrode (diameter of 5 mm), platinum mesh counter electrode, and a Ag|AgCl reference electrode were used. Error bars represent one standard deviation ($n = 3$).

Figure 6.6 shows the limiting anodic current passed at the RDE immersed into solutions of either FTMA or BFDMA plotted against $\omega^{1/2}$ (as per equation 3) to quantitatively compare each amphiphile to Levich-type behavior. For both

amphiphiles, the calculated Levich current is shown as a dotted line. The Levich current in Figure 6.6A (for FTMA) was calculated using a hydrodynamic diameter of 4 nm (similar to DLS data of 10 ± 4 nm, see Table 6.1). The agreement between the model and the experimental data (crosses, Figure 6.6A) is good, thus confirming that the rate of oxidation of FTMA is mass transfer-limited. For BFDMA (Figure 6.6B), the Levich current calculated assuming a hydrodynamic diameter of 700 nm (obtained from the DLS data in Table 6.1) greatly exceeds the experimentally determined currents at high potential.

In summary, our analyses of the CVs measured at the RDE lead to a physical picture that is consistent with that suggested by our measurements at the stationary electrode. Specifically, both sets of experiments support the proposition that the CVs obtained using BFDMA are dominated by BFDMA that is *within* an adsorbed layer at the surface of the electrode. Also, the RDE experiments suggest that diffusion of BFDMA from aggregates outside of the adsorbed layer plays little role in determining the current passed at the electrode (Scheme 6.1B). There does, however, appear to be a population of BFDMA aggregates that are weakly bound to the electrode and can be removed by shear. In contrast, CVs of FTMA obtained at RDEs show typical mass transfer-limited Levich-type behavior (Scheme 6.1A).

6.3.4 Investigation of the effects of heating BFDMA

To investigate further the physical state of the adsorbed layer of BFDMA that appears to regulate the rate of oxidation of BFDMA (see above), we investigated the effects of heating solutions of BFDMA. First, we performed measurements using differential scanning calorimetry (DSC) to determine if BFDMA exhibits evidence of a melting transition.

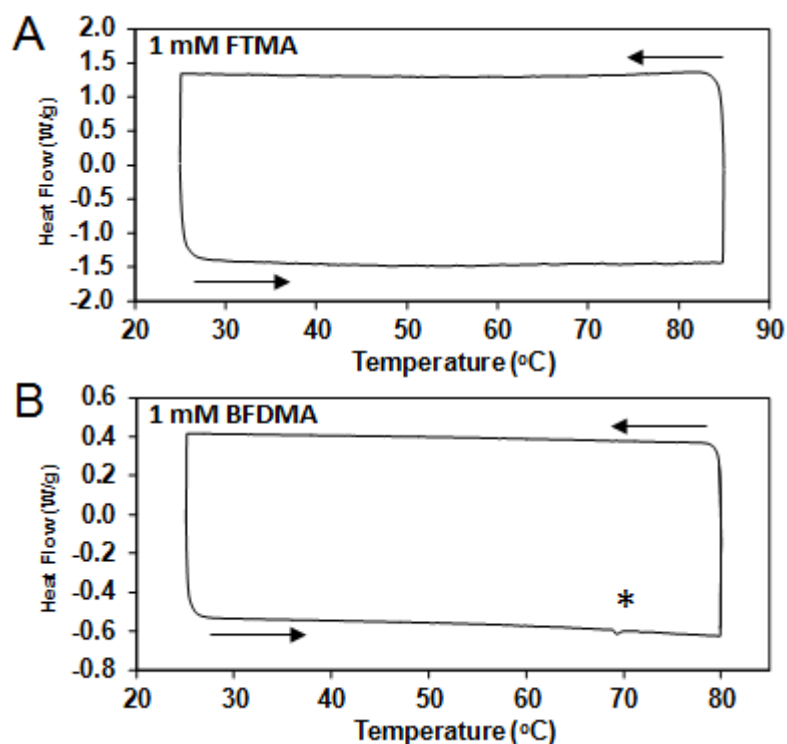


Figure 6.7. Thermograms obtained by DSC of aqueous solutions of (A) 1 mM FTMA or (B) 1 mM BFDMA, in 1 mM Li_2SO_4 . The temperature was changed at a rate of 1 °C/min in both scan directions. An asterisk, * shows a small endothermic peak upon heating of 1 mM BFDMA with an onset at 68.95 °C and a maximum at 69.33 °C.

Figure 6.7 shows the heat flow during a 1 °C/min ramp of solutions of either 1 mM FTMA or 1 mM BFDMA (between 25 °C and 85 °C or 80 °C respectively). While the scans obtained using FTMA were featureless (Figure 6.7A), an

endothermic event was recorded for BFDMA (asterisk, Figure 6.7B) during the up-scan in temperature. The peak started at a temperature of 68.95 °C, peaked at 69.33 °C and possessed an overall molar enthalpy of 96.7 kJ/mol of BFDMA. Past studies have shown that the magnitude of the molar enthalpy is comparable to a gel to liquid transition (45.9 kJ/mol at 44 °C) in vesicular dispersions of dioctadecyldimethylammonium bromide (DODAB).⁵⁶ We note that the structure of DODAB is comparable to BFDMA without the terminal ferrocene groups. We also measured the hydrodynamic size of the BFDMA as a function of temperature using DLS. The average hydrodynamic diameter of BFDMA at 75 °C was measured to be 565 ± 40 nm, a drop in size of 230 nm from that measured at 25 °C. These observations, when combined, suggest that the melting of the BFDMA aggregates is accompanied by reorganization of the molecules of BFDMA in solution. We also note that we did not detect an exothermic process (i.e., freezing) when a solution of BFDMA was cooled from 75 °C to 25 °C. We interpret this result to indicate that either the melting transition was not reversible on the time-scale of our experiments, or that a process of freezing does occur but that it occurs over a broad temperature range that makes it difficult to detect. The latter interpretation is supported by DLS analysis of a solution of 1 mM BFDMA, preheated to 75 °C for 2 h and then allowed to cool to room temperature. An analysis of the size distribution reveals an average mean diameter of 706 ± 20 nm, i.e. similar to a solution of 1 mM BFDMA that has not been preheated (795 ± 250 nm, Table 6.1), suggesting that the self-assembly processes occurring in solution upon heating are reversible.

To determine whether the above-described change in phase state of BFDMA has a measurable impact on the electrochemical activity of adsorbed and/or diffusing species of BFDMA, we measured CVs at stationary and rotating disk electrodes as a function of temperature. The CVs were measured at 60 °C and 75 °C, above or below the endothermic event observed in Figure 6.7B, in an experiment otherwise identical to that reported in Figure 6.3C. Table 6.2 shows the results of these experiments (see Figure 6.13, of the Supplemental materials for the CVs). Similar to the CVs reported at ambient temperature, at both elevated temperatures one Faradaic peak was observed in each scan direction. In addition, the peak currents changed with scan rate with an exponent between 0.5 and 1.0 (see Table 6.2 for calculated values), thus confirming the presence of adsorbed and diffusing electroactive species.

Table 6.2. Peak potentials and currents obtained from CVs of either 1 mM FTMA (lowest potential peaks in each scan direction only, Figure 6.3A) or 1 mM BFDMA (Figure 6.3C, and Figure 6.13 from Supplemental materials) in 1 mM Li₂SO₄ at a scan rate of 100 mV/s. Values of a_a and a_c were calculated from a range of scan rates between 10 and 200 mV/s. R^2 of a_a and a_c values are >0.99.

Amphiphile	Temperature (°C)	$E_{\text{peak,a}}$ (V)	$E_{\text{peak,c}}$ (V)	E° (V)	$i_{\text{peak,a}}$ (μA)	$i_{\text{peak,c}}$ (μA)	a_a	a_c
FTMA	25	0.21	0.08	0.15	12.0	-10.3	0.50	0.50
BFDMA	25	0.36	0.26	0.31	3.3	-1.1	0.57	0.67
	60	0.28	0.24	0.26	3.6	-2.0	0.55	0.78
	75	0.28	0.22	0.25	9.2	-5.0	0.59	0.85
	25 (preheated to 75 °C)	0.39	0.25	0.32	4.0	-2.7	0.51	0.58

However, increasing the temperature from 25 °C to 60 °C or 75 °C also led to several differences in the CV relative to what was observed at ambient temperatures.

First, the Faradaic peak currents measured in both scan directions increased significantly at 75 °C but not at 60 °C. For example, at 75 °C and at 100 mV/s, $i_{\text{peak,a}}$ increased from 3.3 μA to 9.2 μA , and $i_{\text{peak,c}}$ increased in magnitude from -1.1 μA to -5.0 μA when compared to CV measurements at 25 °C. In contrast, at 60 °C, the magnitude of the current peaks remained low, with an $i_{\text{peak,a}}$ of 3.6 μA and $i_{\text{peak,c}}$ of -2.0 μA . This result suggests that the rate of oxidation of BFDMA is higher at 75 °C than at ambient temperature or 60 °C. Second, we measured E° to decrease from 0.31 V (vs Ag|AgCl) at 25 °C to 0.26 V (vs Ag|AgCl) at 60 °C and to 0.25 V (vs Ag|AgCl) at 75 °C, i.e. the change in free energy required to change the oxidation state of BFDMA was measured to decrease at these higher temperatures and, the change in E° with temperature does not appear to be due to the difference in the phase state of the adsorbed BFDMA at the surface of the electrode. Third, we also performed CVs in 1 mM Li_2SO_4 solutions following pre-treatment of the electrode in 1 mM BFDMA at 75 °C to determine whether adsorbed BFDMA persists at the electrode at this temperature. The CV measured in the 1 mM Li_2SO_4 solution showed no evidence of a Faradaic peak in either scan direction (Figure 6.8), in contrast to the observation in Figure 6.4D where, in an otherwise identical experiment performed at 25 °C, an adsorbed layer of electroactive BFDMA molecules were present (Figure 6.4). This result is consistent with removal of the adsorbed layer of BFDMA upon transfer into the 1 mM Li_2SO_4 solution (similar to FTMA at ambient temperatures).

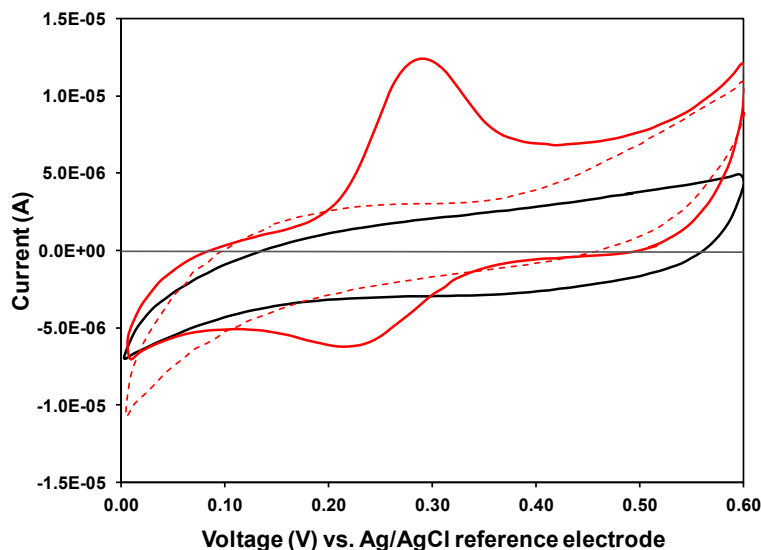


Figure 6.8. Cyclic voltammograms measured at a stationary electrode immersed into 1 mM Li_2SO_4 (dashed red line), then 1 mM reduced BFDMA in 1 mM Li_2SO_4 at 75 °C (red line), and then 1 mM Li_2SO_4 at 25 °C (black line), at a scan rate of 100 mV/s.

Next we performed CVs at a RDE at 60 °C and 75 °C (Figure 6.9 and Figure 6.14 of the Supplemental materials). At 75 °C, the peak currents measured with BFDMA followed a Levich current behavior with a corresponding hydrodynamic radius of 40 nm (using equation 3). This result is significantly lower than the hydrodynamic diameter of 795 ± 250 nm measured using DLS (Table 6.1). This may be evidence to suggest that the aggregates of BFDMA are reducing in size within boundary layer, approaching the surface of the electrode. In contrast, at 60 °C, the qualitative behavior of the peak currents was similar to that observed at 25 °C (Figure 6B). That is, the magnitudes of the anodic currents were not strongly dependent on rotational speed, and a peak in the current was seen during the anodic scan. These results support the conclusion emerging from the DSC that BFDMA undergoes a melting transition between 60 °C and 75 °C, and that the CVs of BFDMA measured at

25 °C are dominated by aggregates of BFDMA that adsorb to the surface of the electrode.

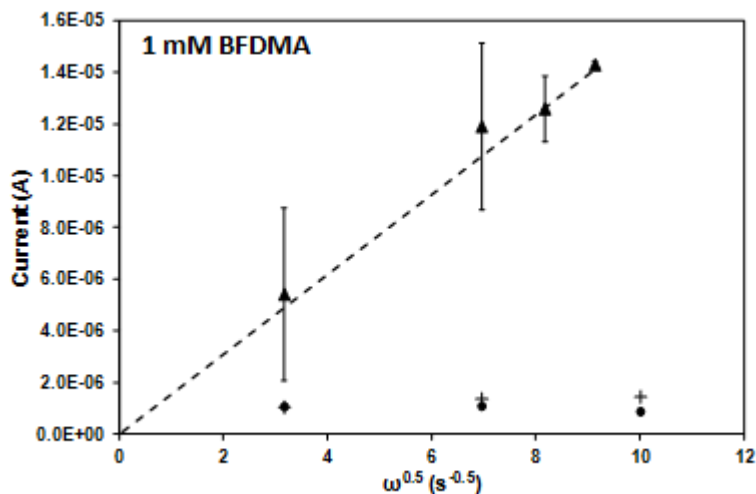


Figure 6.9. Peak anodic currents measured at a RDE immersed in aqueous 1 mM BFDMA containing 1 mM Li_2SO_4 pH 5 upon heating to 60 °C (+) or 75 °C (▲) and upon preheating to 75 °C (●) (2 h incubation) then cooling to 25 °C, respectively. The dotted line corresponds to a Levich current (see text for details). The scan rate was 10 mV/s. A platinum disc working electrode (diameter of 5 mm), platinum mesh counter electrode, and a Ag|AgCl reference electrode were used. Error bars represent one standard deviation ($n = 3$).

Finally, we performed bulk electrolysis of a solution of BFDMA at 75 °C at an oxidizing potential of 0.6 V (vs Ag|AgCl) in an otherwise identical electrochemical experiment to that reported in Figure 6.2. We measured a charge of 0.868 C (i.e. 100% conversion to oxidized BFDMA) to be passed at the electrode after 2.7 hours. This result, when compared to the data in Figure 6.2, reveals the rate of oxidation of BFDMA at 75 °C to be approximately 13 times faster than at 25 °C (and only 1.5 times slower than FTMA at 25 °C). This result supports our conclusion that at 75 °C, while BFDMA is still adsorbed to the surface of the working electrode, these adsorbed species do not block access of BFDMA from the bulk solution to the

electrode (see Scheme 6.1C). In contrast, at 60 °C, the adsorbed BFDMA influences electrode processes in a manner similar to that measured at 25 °C. The data collected at elevated temperatures on either side of the endothermic event identified via DSC (Figure 6.7B) show the pronounced effect of the phase state of the BFDMA assemblies on the electrochemical characteristics of redox-active amphiphiles.

Our results suggest that solution conditions (or cosurfactants) that change the phase state (e.g., salts, pH) of the amphiphiles may be exploited to dramatically impact electrode processes involving this amphiphile. Overall, this knowledge provides guidance to the design of self-assembling redox mediators that offer the potential for broad control of interfacial charge separation processes. The results also enable electrochemical approaches for control of surfactant-based phenomena using ferrocenyl amphiphiles, in general, including control of the formation of complexes between BFDMA and DNA in the context of development of methods that permit spatial and temporal control over the delivery of genes to cells.

6.4 Conclusions

In conclusion, this study provides insights into the influence of self-assembly of redox-active amphiphiles on their electrochemical activities. Specifically, we focused on comparing two ferrocene-containing amphiphiles that we reveal to exhibit strikingly different electrochemical signatures via CV at stationary and rotating electrodes. While both amphiphiles form interfacial assemblies on Pt electrodes at ambient conditions, the dynamics of the adsorbed FTMA are fast, and the interfacial

assembly of the surfactant has little impact on the access of FTMA in bulk solution to the electrode. The rate limiting process for this amphiphile at the RDE is mass transport from the bulk solution. In contrast, the behavior of BFDMA is more complex. Specifically, at ambient temperatures, there exists a bound layer of BFDMA that is not displaced from the surface by gentle rinsing. Measurements performed at the RDE indicate that the bound layer of BFDMA largely blocks the contributions of BFDMA in bulk solution to the current passed at the electrodes. However, CV performed at a stationary electrode as a function of scan rate reveals that BFDMA is diffusing within the adsorbed layer. Finally, DSC measurements indicated that BFDMA undergoes a melting transition of some type at 69 °C, and subsequent investigation revealed that the electrochemical traits of BFDMA above the melting transition were similar to that of FTMA (see Scheme 6.1). Overall, these results indicate that the phase state of assemblies formed by ferrocenyl amphiphiles can play a dominant role in determining their electrochemical activity.

6.5 Acknowledgements

Financial support was provided by the National Institutes of Health (AI092004), the National Science Foundation (CBET-0754921 and DMR-1121288) and the ARO (W911NF-11-1-0251).

6.6 References

1. M. Fedurco, *Coord. Chem. Rev.*, **2000**, 209, 263-331.
2. A. E. F. Nassar, J. F. Rusling and N. Nakashima, *J. Am. Chem. Soc.*, **1996**, 118, 3043-3044.
3. U. Mitschke and P. Bauerle, *J. Mater. Chem.*, **2000**, 10, 1471-1507.
4. P. Peumans, A. Yakimov and S. R. Forrest, *J. Appl. Phys.*, **2003**, 93, 3693-3723.
5. R. H. Friend, R. W. Gymer, A. B. Holmes, J. H. Burroughes, R. N. Marks, C. Taliani, D. D. C. Bradley, D. A. D. Santos, J. L. Bredas, M. Logdlund and W. R. Salaneck, *Nature*, **1999**, 397, 121-128.
6. J. Chen, M. A. Reed, A. M. Rawlett and J. M. Tour, *Science*, **1999**, 286, 1550-1552.
7. A. Malka and U. Peskin, *Israel Journal of Chemistry*, **2005**, 45, 217-225.
8. M. S. Morad and A. A. O. Sarhan, *Corrosion Sci.*, **2008**, 50, 744-753.
9. H. Y. Ma, S. H. Chen, B. S. Yin, S. Y. Zhao and X. Q. Liu, *Corrosion Sci.*, **2003**, 45, 867-882.
10. X. Wang and I. M. Hsing, *Electrochim. Acta*, **2002**, 47, 2981-2987.
11. T. C. Franklin and M. Ohta, *Surface Technology*, **1983**, 18, 63-76.
12. C. E. D. Chidsey, *Science*, **1991**, 251, 919-922.
13. H. D. Sikes, J. F. Smalley, S. P. Dudek, A. R. Cook, M. D. Newton, C. E. D. Chidsey and S. W. Feldberg, *Science*, **2001**, 291, 1519-1523.
14. K. Slowinski, H. K. Y. Fong and M. Majda, *J. Am. Chem. Soc.*, **1999**, 121, 7257-7261.
15. K. Slowinski, K. U. Slowinska and M. Majda, *J. Phys. Chem. B*, **1999**, 103, 8544-8551.

16. D. H. Charych, E. M. Landau and M. Majda, *J. Am. Chem. Soc.*, **1991**, 113, 3340-3346.
17. J. R. Miller and J. V. Beitz, *J. Chem. Phys.*, **1981**, 74, 6746-6756.
18. S. B. Sachs, S. P. Dudek, R. P. Hsung, L. R. Sita, J. F. Smalley, M. D. Newton, S. W. Feldberg and C. E. D. Chidsey, *J. Am. Chem. Soc.*, **1997**, 119, 10563-10564.
19. M. D. Newton, *Chem. Rev.*, **1991**, 91, 767-792.
20. A. P. Abbott, G. Gounili, J. M. Bobbitt, J. F. Rusling and T. F. Kumosinski, *J. Phys. Chem.*, **1992**, 96, 11091-11095.
21. X. Y. Liu and N. L. Abbott, *J. Colloid Interface Sci.*, **2009**, 339, 1-18.
22. B. S. Gallardo, V. K. Gupta, F. D. Eagerton, L. I. Jong, V. S. Craig, R. R. Shah and N. L. Abbott, *Science*, **1999**, 283, 57-60.
23. B. S. Gallardo, M. J. Hwa and N. L. Abbott, *Langmuir*, **1995**, 11, 4209-4212.
24. N. Aydogan and N. L. Abbott, *Langmuir*, **2001**, 17, 5703-5706.
25. M. E. Hays and N. L. Abbott, *Langmuir*, **2005**, 21, 12007-12015.
26. B. S. Aytar, J. P. E. Muller, S. Golan, S. Hata, H. Takahashi, Y. Kondo, Y. Talmon, N. L. Abbott and D. M. Lynn, *Journal of Controlled Release*, **2011**, 157, 249-259.
27. N. L. Abbott, C. M. Jewell, M. E. Hays, Y. Kondo and D. M. Lynn, *J. Am. Chem. Soc.*, **2005**, 127, 11576-11577.
28. C. M. Jewell, M. E. Hays, Y. Kondo, N. L. Abbott and D. M. Lynn, *J. Controlled Release*, **2006**, 112, 129-138.
29. C. M. Jewell, M. E. Hays, Y. Kondo, N. L. Abbott and D. M. Lynn, *Bioconjugate Chem.*, **2008**, 19, 2120-2128.
30. C. L. Pizzey, C. M. Jewell, M. E. Hays, D. M. Lynn, N. L. Abbott, Y. Kondo, S. Golan and Y. Talmon, *J. Phys. Chem. B*, **2008**, 112, 5849-5857.

31. Y. Kakizawa, H. Sakai, K. Nishiyama, M. Abe, H. Shoji, Y. Kondo and N. Yoshino, *Langmuir*, **1996**, 12, 921-924.
32. Y. Kakizawa, H. Sakai, A. Yamaguchi, Y. Kondo, N. Yoshino and M. Abe, *Langmuir*, **2001**, 17, 8044-8048.
33. J. P. E. Muller, B. S. Aytar, Y. Kondo, D. M. Lynn and N. L. Abbott, *Soft Matter*, **2012**, 8, 2608-2619.
34. D. E. Bennett, B. S. Gallardo and N. L. Abbott, *J. Am. Chem. Soc.*, **1996**, 118, 6499-6505.
35. C. A. Rosslee and N. L. Abbott, *Anal. Chem.*, **2001**, 73, 4808-4814.
36. X. Y. Liu and N. L. Abbott, *Anal. Chem.*, **2009**, 81, 772-781.
37. X. Y. Liu and N. L. Abbott, *Anal. Chem.*, **2011**, 83, 3033-3041.
38. N. Yoshino, H. Shoji, Y. Kondo, Y. Kakizawa, H. Sakai and M. Abe, *J. Jpn. Oil Chem. Soc.*, **1996**, 45, 769-775.
39. B. S. Aytar, J. P. E. Muller, S. Golan, S. Hata, H. Takahashi, Y. Kondo, Y. Talmon, N. L. Abbott and D. M. Lynn, *Journal of Controlled Release*, **2012**, 157, 249-259.
40. B. S. Aytar, J. P. E. Muller, S. Golan, Y. Kondo, Y. Talmon, N. L. Abbott and D. M. Lynn, *J. Colloid Interface Sci.*, **2012**, 387, 56-64.
41. M. E. Hays, C. M. Jewell, Y. Kondo, D. M. Lynn and N. L. Abbott, *Biophys. J.*, **2007**, 93, 4414-4424.
42. D. A. Szanto, S. Cleghorn, C. Ponce-De-Len and F. C. Walsh, *Aiche J.*, **2008**, 54, 802-810.
43. T. Takei, H. Sakai, Y. Kondo, N. Yoshino and M. Abe, *Colloid Surf. A-Physicochem. Eng. Asp.*, **2001**, 183, 757-765.
44. B. Faulkner, *Electrochemical Methods; Fundamentals and Applications*, 1 edn., John Wiley & Sons, Inc., New York, 1980, 231.
45. B. Faulkner, *Electrochemical Methods; Fundamentals and Applications*, 1 edn., John Wiley & Sons, Inc., New York, 1980, 591.

46. W. G. Cochran, *Mathematical Proceedings of the Cambridge Philosophical Society*, **1934**, 30, 365-375.
47. V. G. Levich, *Physicochemical hydrodynamics*, Prentice-Hall, Englewood Cliffs, N.J., 1962.
48. S. W. Provencher, *Comput. Phys. Commun.*, **1982**, 27, 213-227.
49. S. W. Provencher, *Comput. Phys. Commun.*, **1982**, 27, 229-242.
50. B. Faulkner, *Electrochemical Methods; Fundamentals and Applications*, 1 edn., John Wiley & Sons, Inc., New York, 1980, 596.
51. B. Faulkner, *Electrochemical Methods; Fundamentals and Applications*, 1 edn., John Wiley & Sons, Inc., New York, 1980, 36.
52. B. S. Gallardo and N. L. Abbott, *Langmuir*, **1997**, 13, 203-208.
53. B. S. Gallardo, K. L. Metcalfe and N. L. Abbott, *Langmuir*, **1996**, 12, 4116-4124.
54. B. Faulkner, *Electrochemical Methods; Fundamentals and Applications*, 1 edn., John Wiley & Sons, Inc., New York, 1980.
55. X. Y. Liu, M. D. Graham and N. L. Abbott, *Langmuir*, **2007**, 23, 9578-9585.
56. J. Cocquyt, U. Olsson, G. Ofsson and P. Van der Meeren, *Colloid Polym. Sci.*, **2005**, 283, 1376-1381.
57. O. Traverso and F. Scandola, *Inorganica Chimica Acta*, **1970**, 4, 493-498.
58. T. Saji, K. Hoshino and S. Aoyagui, *J. Am. Chem. Soc.*, **1985**, 107, 6865-6868.

6.7 Supplemental materials

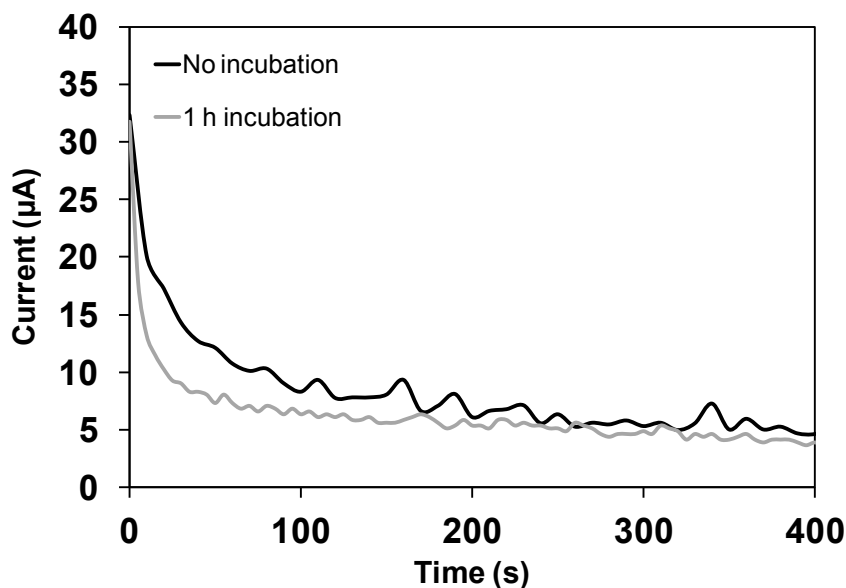


Figure 6.10. Bulk electrochemical oxidation of 4.5 mL of 1 mM BFDMA_{RED} in 1 mM Li₂SO₄ pH 5 after incubation with working electrode for 1 h (grey line) and 0 h (black line) prior to application of 0.6 V potential at ambient temperature. Charge passed over first 400 s for 1 mM BFDMA with no incubation time was 3.58 mC versus 2.49 mC for 1 mM BFDMA with 1 h incubation. Platinum mesh working and counter electrodes, and a Ag/AgCl reference electrode were used.

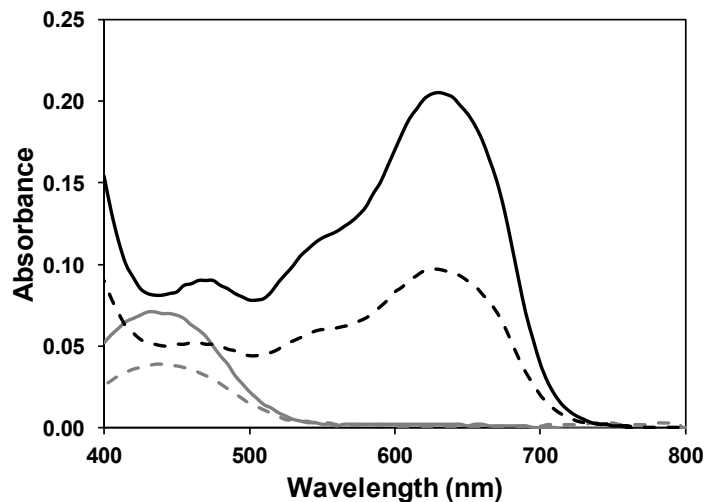


Figure 6.11. UV/visible absorbance spectra for solutions of FTMA; reduced FTMA (dotted grey line) and electrochemically oxidized FTMA (dotted black line) and BFDMA; reduced BFDMA (solid grey line), and electrochemically oxidized BFDMA (solid black line). All samples, prior to absorbance measurements, were diluted with an equal volume of 1 mM Li₂SO₄ to provide an amphiphile concentration of 500 μM .

Figure 6.11 shows the UV/vis absorption spectra of the FTMA solution before (dotted grey line) and after (dotted black line) bulk electrolysis for 3.6 h. Also shown in Figure 6.11 is the comparable data for the BFDMA solution before (solid grey line) and after (solid black line) bulk electrolysis as shown in Figure 6.2. Inspection of these data reveals that bulk electrolysis resulted in the disappearance of the absorbance peak at 435 nm (characteristic of solutions containing ferrocene groups),¹ and the appearance of a new peak at 630 nm (characteristic of solutions containing ferrocenium ions).¹ Past studies, showing UV-vis absorption spectrophotometry of reduced and oxidized BFDMA^{2,3} and FTMA⁴ are in good quantitative agreement with the data we report in Figure 6.11, thus providing additional support for our conclusion both BFDMA and FTMA can be oxidized to near completion (but at rates that differ by almost an order of magnitude). We also note that the magnitude of the peak absorbance of the solution of reduced FTMA at 435 nm is approximately half that of reduced BFDMA (see Figure 6.2, dotted grey line versus solid grey line). Similarly, the peak absorbance of the solution of oxidized FTMA at 630 nm is approximately half that of oxidized BFDMA (Figure 6.2, dotted black line versus solid black line). This result is consistent with oxidation of one ferrocene group per FTMA molecule and two ferrocene groups per BFDMA molecule.

6.7.1 Further discussion of Cyclic voltammetry results from Figure 6.3

Comparison of the position of Faradaic peaks associated with the diffusing species for each amphiphile provides further proof that both of BFDMA's ferrocene

groups are undergoing a change in redox state. The anodic and cathodic peak currents corresponding to the diffusing species of each amphiphile occur at different potentials, with a difference in potential, ΔE_p of 0.043 V to 0.135 V for BFDMA and 0.062 V to 0.186 V for FTMA, with ΔE_p increasing with increasing scan rate from 10 mV/s to 200 mV/s for both amphiphiles (calculated as $\Delta E_p = E_{pa} - E_{pc}$ at each scan rate measured). This is most likely due to the increasing scan rates causing the potential to change faster than the reactants near the surface of the electrode of each half cell reaction (i.e., in each scan direction) can be oxidized. For a fully reversible, diffusing redox species, this offset should be $0.059 \text{ V}/n$ where n is the number of electrons transferred. Therefore, it should be no smaller than 0.059 V for FTMA and 0.030 V for BFDMA. As at the slowest scan rate of 10 mV/s, ΔE_p is less than 0.059 V for BFDMA (i.e. 0.043 V), this is further evidence that both ferrocene groups are undergoing a change in redox state.

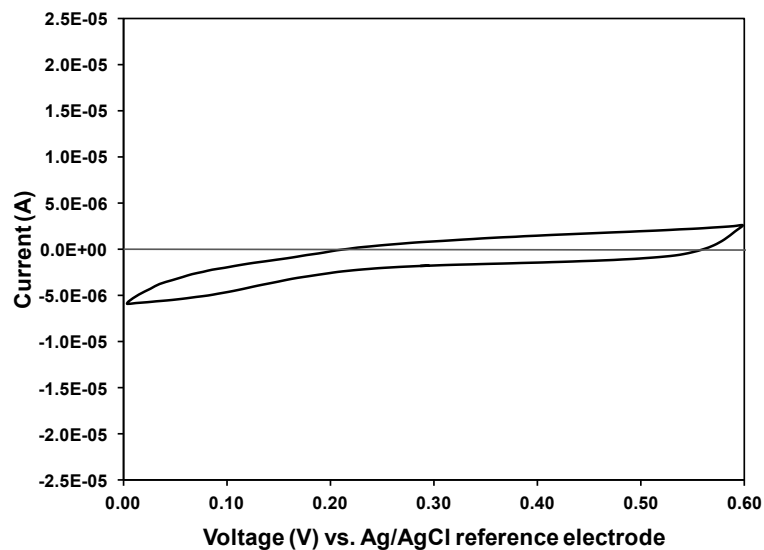


Figure 6.12. Cyclic voltammogram in a solution of 1 mM Li_2SO_4 after incubation of the working electrode in a solution of 1 mM FTMA in 1 mM Li_2SO_4 . Upon removal from the solution of FTMA, the working electrode was gently rinsed with 1 mM Li_2SO_4 and immersed in a solution of 1 mM Li_2SO_4 without any further cleaning before CVs were performed. A scan rate of 100 mV/s was used in a standard 50 mL glass beaker with 20 mL of solution. A platinum disc working electrode (diameter of 5 mm), platinum mesh counter electrode, and a Ag/AgCl reference electrode were used.

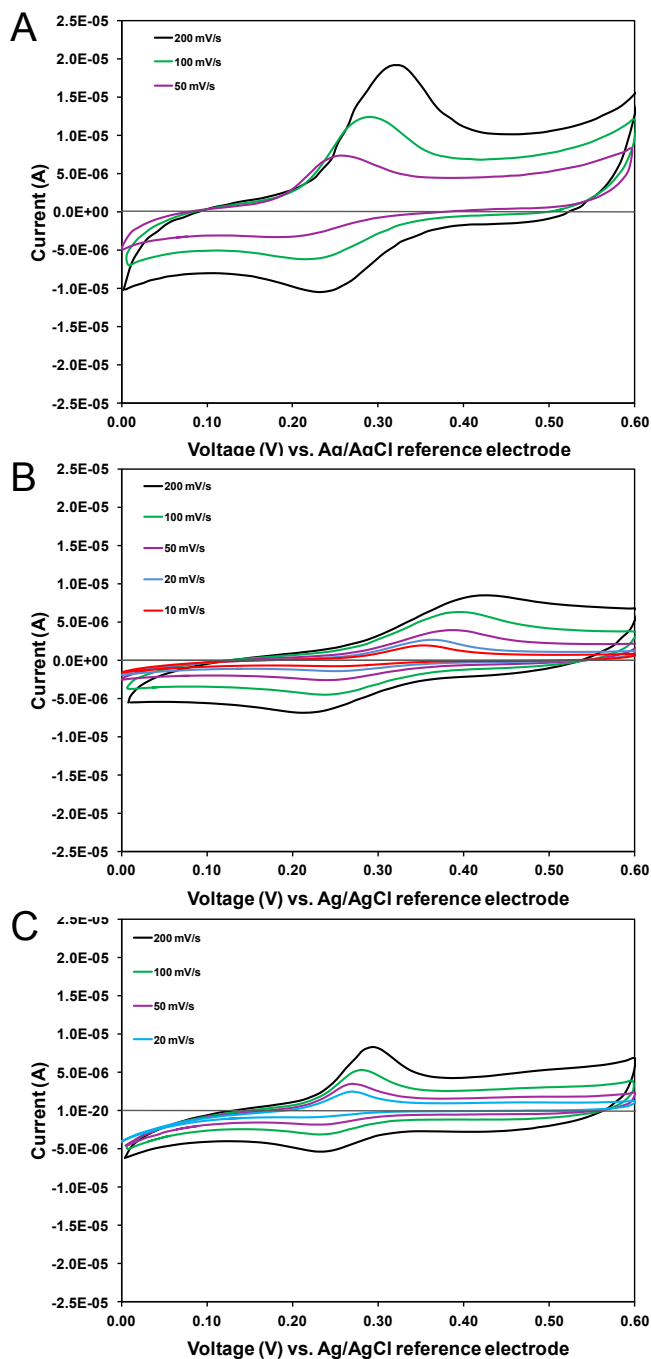


Figure 6.13. Cyclic voltammograms of 1 mM BFDMA at (A) 75 °C, (B) preheated to 75 °C then allowed to cool to ambient temperature before measurement, and (C) 60 °C, in 1 mM Li_2SO_4 pH 5. Scan rates from 200 to 10 mV/s were used in a standard 50 mL glass beaker with 20 mL of solution. A platinum disc working electrode (diameter of 5 mm), platinum mesh counter electrode, and a Ag/AgCl reference electrode were used. See Table 6.2 in the main manuscript for analysis of the peak currents observed in these CVs.

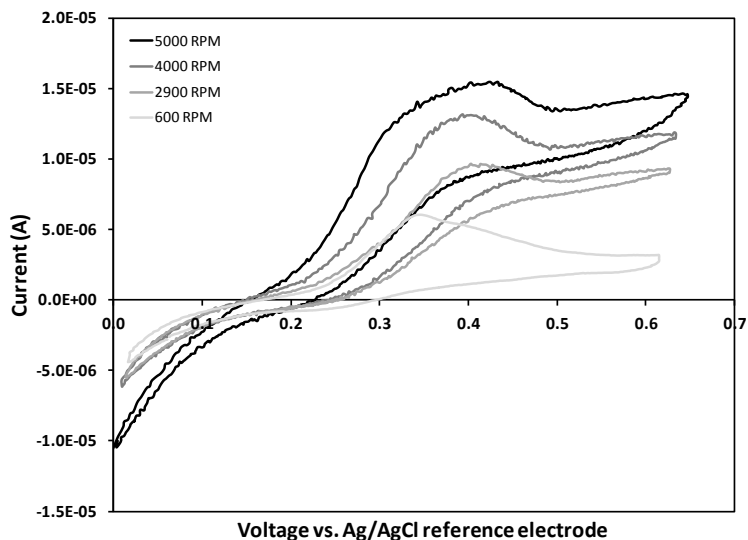


Figure 6.14. Rotating disc electrode cyclic voltammograms of 1 mM BFDMA_{RED}, in 1 mM Li₂SO₄ pH 5 at 75 °C. A scan rate of 10 mV/s was used in a standard 50 mL beaker with 20 mL of solution. A platinum disc working electrode (diameter of 5 mm), platinum mesh counter electrode, and a Ag/AgCl reference electrode were used. The rotational speed of the working electrode is given in the legend of each graph.

6.7.2 Investigation of the effects of preheating BFDMA

To test the conclusion that the melting event seen with DSC for 1 mM BFDMA is reversible, the electrochemical activity of BFDMA preheated to 75 °C was investigated. To this end, a solution of BFDMA was preheated to 75 °C, past the endothermic event seen in Figure 6.7B, for 2 hours, and then allowed to cool until it reached 25 °C before the following experiments were performed. Bulk oxidation, CV (Table 6.2 in the main manuscript, and Figure 6.12B), RDE CV and DLS of this solution were performed. The Faradaic peak currents and the formal potential are of a magnitude between those of the 25 °C solution that had not been preheated to 75 °C, from the experiments reported in Figures 2 and 3 and those of a solution at 75 °C (data shown in Table 6.2 for comparison). Also, bulk oxidation was performed on the

preheated sample, where 100% theoretical charge of 0.868C was passed after 20.7 h (data not shown), 1.7 times faster than a solution that had not been preheated to 75 °C but 7.7 times slower than bulk oxidation performed at 75 °C. Finally, from DLS analysis, the size of aggregates were 706 ± 22 nm as discussed previously, i.e. similar to a solution of 1 mM BFDMA that has not been preheated (795 ± 250 nm, Table 6.1). Finally, RDE CV data for a preheated sample of BFDMA, follows a similar kinetically limited behavior to that of BFDMA that has not been preheated (data not shown). Together, these results show that the step of preheating 1 mM BFDMA to 75 °C, and then allowing it to cool, while slightly improving the size of the Faradaic peaks on CV versus a solution of BFDMA that has not be preheated to 75 °C, results in a system similar to the original ambient system where the adsorbed species of BFDMA at the surface of the electrode are blocking the exchange of electrons with diffusing BFDMA species in bulk solution.

6.8 Supplemental materials references

1. O. Traverso, F. Scandola, *Inorganica Chimica Acta*, **1970**, *4*, 493-498.
2. J. P. E. Muller, B. S. Aytar, Y. Kondo, D. M. Lynn, N. L. Abbott, *Soft Matter*, **2012**, *8*, 2608-2619.
3. B. S. Aytar, J. P. E. Muller, S. Golan, Y. Kondo, Y. Talmon, N. L. Abbott, D. M. Lynn, *J. Colloid Interface Sci.*, **2012**, *387*, 56-64.
4. T. Saji, K. Hoshino, S. Aoyagui, *J. Am. Chem. Soc.*, **1985**, *107*, 6865-6868.

Chapter 7: Summary and Recommendations for Future Studies

7.1 Summary

The research described in this thesis has focused on characterization of the interactions between a redox-active ferrocenyl amphiphile, (11-ferrocenylundecyl)-dimethylammonium bromide (BFDMA), and nucleic acids (DNA) using a broad range of physicochemical techniques.

Chapter 2 reported that incorporation of DOPE into BFDMA-containing lipoplexes leads to a substantial increase in cell transfection efficiency in the presence of high concentrations of serum (up to 80% BS). This observation appears closely correlated with nanostructural characterization presented in this chapter, which clearly shows that the incorporation of DOPE into the lipoplexes induces the formation of a H_{II}^c nanostructure. Although additional studies will be required to elucidate the precise mechanism of transfer of our DOPE-containing lipoplexes into cells, past studies have established that lipoplexes with a H_{II}^c nanostructure exhibit an increased propensity to fuse with cell membranes¹⁻⁶ (thus leading to a mechanism of uptake that is not generally thought to occur with lipoplexes that possess L_{α}^c nanostructures). It appears possible, therefore, that the high levels of cell transfection that we observe using lipoplexes of DOPE and BFDMA_{RED} in the presence of serum is the result of fusion of these lipoplexes with the cell membranes. A second key result presented in Chapter 2 is that a change in the oxidation state of the BFDMA that is used to form

the lipoplexes with DOPE substantially alters the efficiency with which lipoplexes of BFDMA and DOPE transfect cells (over a wide range of serum levels tested). We interpret our results to provide support for our hypothesis that DOPE-induced formation of the H_{II}^c nanostructure of the BFDMA-containing lipoplexes underlies the high cell transfection efficiency measured in the presence of serum, *and that the oxidation state of BFDMA within lipoplexes with DOPE substantially regulates the formation of the H_{II}^c nanostructure* and thus the ability of the lipoplexes to transfect cells with DNA.

Chapter 3 reports cryogenic transmission electron microscopy images that show the presence of a highly ordered H_{II}^c structure in lipoplexes of BFDMA_{RED}-DOPE/DNA in both OptiMEM media and OptiMEM media with 10% (v/v) bovine serum. Analysis of lipoplexes of BFDMA_{OX}-DOPE/DNA, in contrast, show relatively poor ordering within the aggregates imaged in both media. Complementary small angle x-ray scattering analysis showed quantitative agreement with these cyro-TEM results in terms of the magnitude of the repeat structures within these ordered aggregates. Subsequent analysis of lipoplexes of BFDMA_{OX}-DOPE/DNA treated with a ten times molar excess of ascorbic acid showed a high degree of ordered H_{II}^c nanostructure in OptiMEM media, but significantly less ordering in OptiMEM media with 10% (v/v) bovine serum. Finally, a luciferase assay using COS-7 mammalian cells compared the cell transfection efficiency between lipoplexes of BFDMA_{RED}-DOPE/DNA, lipoplexes of BFDMA_{OX}-DOPE/DNA and lipoplexes of BFDMA_{OX}-DOPE/DNA treated with a ten times molar excess of ascorbic acid, and showed that

ascorbic acid activates lipoplexes of BFDMA_{OX}-DOPE/DNA towards transfection in serum free media but not in media containing 10% (v/v) bovine serum. This result suggests that the constituents of bovine serum that are preventing reformation of the ordered H_{II}^c may also be leading to this difference in efficiency of transgene expression. Overall, these observations combine to provide cryo-TEM-based evidence of H_{II}^c nanostructure of lipoplexes of BFDMA and DOPE as well as initial characterization of lipoplexes of BFDMA_{OX}-DOPE/DNA with a chemical reducing agent, ascorbic acid. These results, when combined with previous studies using ascorbic acid to activate lipoplexes of BFDMA in the presence of cells, may provide a serum stable lipoplex, able to exhibit redox-mediated control over the efficiency of cell transfection.

Chapter 4 provides preliminary evidence that supports the hypothesis that the hexagonal nanostructure of lipoplexes of reduced BFDMA and DOPE promotes internalization of the lipoplexes via fusion. This support is obtained by measurement of the relative cell transfection efficiencies at temperatures of 4 °C and 37 °C, and is supported by preliminary measurements of a directionally greater extent of co-localization of DNA and endosomes/lysosomes present inside the cell when DOPE is absent than when DOPE is present inside the lipoplex.

We report in Chapter 5 that Fe(III)sulfate can be used to oxidize reduced BFDMA rapidly, quantitatively, and at ambient temperatures. However, lipoplexes formed using chemically oxidized BFDMA behaved differently than lipoplexes prepared using electrochemically oxidized BFDMA in the context of cell transfection

(e.g., whereas the latter do not promote high levels of transfection, lipoplexes of chemically oxidized BFDMA do). The results of additional experiments revealed these differences to be a result of residual iron ions present in solutions of chemically oxidized BFDMA, and that treatment with an iron chelating agent (ethylenediaminetetraacetic acid, EDTA)⁷ can be used to produce bulk samples of chemically oxidized BFDMA that do not promote cell transfection. We demonstrated further that (i) these EDTA-treated samples can be chemically reduced by treatment with ascorbic acid to produce samples of reduced BFDMA that do promote transfection, and (ii) lipoplexes formed using EDTA-treated samples can be chemically reduced to activate the lipoplexes and initiate transfection. Our results demonstrated that chemical approaches to the transformation of BFDMA can be used to preserve redox-based ‘on/off’ control over cell transfection demonstrated in past studies using electrochemical methods.

Finally, in Chapter 6, this thesis reports an investigation of how self-assembly impacts the rate of electrochemical oxidation of BFDMA. BFDMA spontaneously adsorbs to Pt disk electrodes, forming an adsorbed layer that blocks the electrode from exchanging electrons with diffusing species in bulk solution. In contrast, a single tail analogue, (11-ferrocenylundecyl)trimethylammonium bromide (FTMA), a similarly Pt electrode adsorbing ferrocenyl amphiphile, allows exchange of electrons with species in bulk solution across the adsorbed layer. Differential scanning calorimetry and dynamic light scattering results combined to show that the phase state, not the

size of aggregates, dominates the interfacial electrochemical activity of these amphiphilic redox-mediators.

7.2 Future Studies: *In vivo* studies of lipoplexes of BFDMA_{RED}-DOPE and activation towards transgene expression in the presence of serum

Data reported in Chapters 2, 3 and 4 combined to provide characterization of a serum stable vector for cell transfection, BFDMA_{RED}-DOPE/DNA ($\phi_{\text{DOPE}} = 0.71$), via *in vitro* based mammalian cell transfection experiments using COS-7 cells. A natural direction to take based from this result would be to investigate whether this serum stable system can be successful as a vector for the delivery of DNA to cells in an *in vivo* context. Researchers have historically found it relatively difficult to design a lipoplex based *in vivo* gene delivery system, citing issues including morphology of the complexes, colloidal suspension, overall charge, half-life in circulation, biodistribution, and delivery to and dissemination throughout target tissues for example.⁸ In short, animal based experiments are significantly more complex to control than *in vitro* lab based assays.

As BFDMA in combination with DOPE is now proven to be serum stable, even in up to 80% (v/v) bovine serum, at least within the context of the previously reported *in vitro* cell assays in Chapter 2,⁹ and together with the unique property BFDMA has in terms of being able to mediate the efficiency of cell transfection through control over its oxidation state,¹⁰⁻¹⁴ it is clear to see way BFDMA is an

interesting candidate for use in *in vivo* studies. If it is possible to change the oxidation state of BFDMA and ultimately mediate the efficiency of cell transfection *in vivo*, then a common issue of reaching a concentration at which the vector becomes toxic to cells commonly occurs before a concentration of the vector required to produce a therapeutic benefit, can be alleviated by controlling the timing and location at which DNA is internalized (i.e. the focus on temporal and spatial control demonstrated previously for BFDMA in a serum-free context).¹⁰

Initial work to translate successful chemical activation of relatively inactive oxidized BFDMA containing lipoplexes in a serum free assay, into a serum containing assay has, however, been unsuccessful (see Chapter 3, Figure 3.5 and Figure 3.6). Here, even at a relatively low level of serum (10% (v/v)), and therefore at a significantly lower concentration than physiological concentrations of serum in blood, the oxidized BFDMA and DOPE containing lipoplexes cannot be activated using the chemical reducing agent. A range of conditions have already been tried, from changing the type of chemical reducing agent (e.g. glutathione and ascorbic acid), to altering the charge ratio between the cationic lipid, BFDMA and DNA, to altering the overall concentrations of lipoplexes. However, there are many more ways in which to progress this work. Reducing agents seem to readily interact and/or bind with constituents of serum. For example, ascorbic acid is known to readily bind with bovine serum albumin even at low serum concentrations, an effect that could be the reason underlying the inability to activate lipoplexes of oxidized BFDMA in the

presence of serum.¹⁵ Therefore, other chemical reducing agents should be used within these serum containing *in vitro* assays.

Research to date as focused on DOPE as the choice of lipid used in combination with BFDMA to form mixed lipid lipoplexes. Other “helper lipids” have been used in the field. One specific lipid, cholesterol, is of particular interest. Cholesterol is known to promote specific mechanisms of internalization, other than fusion.¹⁶ Therefore, a study comparing the cell transfection efficiency, physical characterization of the nanostructure using SAXS and attempts to activate lipoplexes of oxidized BFDMA in combination with cholesterol or with DOPE is recommended as a focus for future study. Cholesterol will likely form very different nanostructures with BFDMA than the inverse hexagonal structure reported in Chapters 2 and 3 for lipoplexes of BFDMA and DOPE. These different nanostructures and/or mechanisms of internalization may lead to different interactions between reducing agents, lipoplexes and constituents of serum, leading to successful reactivation towards transgene expression.

In parallel with further *in vitro* screening of reducing agents and/or lipoplex compositions and concentrations with the aim of activating lipoplexes in the presence of serum, *in vivo* assays to confirm whether active lipoplexes of reduced BFDMA and DOPE transfect cells within an animal with significant efficiency are recommended. Perhaps the optimum molar fraction of DOPE, ϕ_{DOPE} of 0.71 in mixed lipid lipoplexes of BFDMA and DOPE, found for *in vitro* based assays described in Chapter 2 is not the same in an *in vivo* context, for example. Therefore, confirming the range of

compositions of lipoplexes of BFDMA and DOPE that enable high efficiencies of transgene expression *in vivo* could help guide these *in vitro* activation experiments.

7.3 Future Studies: Specific ion effects on the electrochemical activity of BFDMA

Chapter 6 focused on the question of how self-assembly impacts the rates of oxidation of the ferrocenyl amphiphile (11-ferrocenylundecyl)trimethylammonium bromide (FTMA) and a double tailed analogue bis(11-ferrocenylundecyl)dimethylammonium bromide (BFDMA) at Pt electrodes in contact with aqueous electrolyte (1 mM Li₂SO₄). We measured the rates of oxidation of the two amphiphiles to differ by approximately one order of magnitude. The relatively slow rate of oxidation of BFDMA was attributed to the phase state of adsorbed BFDMA at the surface of the electrode. The adsorbed layer of BFDMA blocked the exchange of electrons with BFDMA in bulk solution. Our results suggest that solution conditions (or cosurfactants) that change the phase state (e.g., salts, pH) of the amphiphiles may be exploited to dramatically impact electrode processes involving this amphiphile. For example, a preliminary study performed in collaboration with Yutaka Takahashi from the Tokyo University of Science, investigated specific ion effects on the physical (solubility, Table 7.1) and electrochemical (cyclic voltammetry, Table 7.2) properties of BFDMA.

Table 7.1. BFDMA solution solubility, measured in the following types and concentrations of salt. Extensive sonication of 1 mM BFDMA was performed in each salt, followed by centrifugation at 1500 RPM for 10 minutes. The supernatant was collected and spectrophotometry was used to determine the peak absorbance at 425 nm. The magnitude of the absorbance at this peak position was compared to the absorbance of a solution of a known concentration of 1 mM BFDMA that had not been centrifuged (see Chapter 5, section 5.2.2.2 for details of this step) to obtain the final concentrations given below. All salt solutions were prepared at 5 pH.

	Li ₂ SO ₄	LiOAc	LiCl	LiBr	LiNO ₃	LiClO ₄
1 mM	0.24 mM	0.17 mM	0.07 mM	0.15 mM	0.09 mM	Insoluble
10 mM	Insoluble	0.36 mM	0.09 mM	0.19 mM	Insoluble	Insoluble
100 mM	Insoluble	0.35 mM	0.27 mM	Insoluble	Insoluble	Insoluble

Table 7.1 shows results of a solubility experiment, across a range of salts, spanning a Hofmeister series of anionics.¹⁷ Salts in Table 7.1 are ordered from most *kosmotropic* (“hard/small” ions) to most *chaotropic* (“soft/large” ions) from left to right. In Table 7.1, with the exception of the divalent SO₄²⁻ anion, the more kosmotropic the anion, the higher the solubility of BFDMA. In a review of the Hofmeister series, Kunz et al.¹⁷ explains that ionic interactions tend not to occur strongly when the ions are significantly different in size. The head group of BFDMA, is a relatively large (therefore chaotropic) quaternary amine N(CH₃)₄⁺. We may therefore tentatively suggest the following hypothesis based on the solubility results above; the small, kosmotropic, anions differ in size to the N(CH₃)₄⁺ group and therefore BFDMA does not strongly associate with the anions and thus stays in solution. The exception to this hypothesis is SO₄²⁻. Even though this anion is far on

the left hand side of the scale and therefore relatively small, it forms a divalent bond with two Li^+ ions, which could explain the relatively poor solubility reported in Table 7.1 (i.e. BFDMA is insoluble at Li_2SO_4 concentrations above 1 mM).

Solubility is relevant property to consider when the overall aim is to maximize the electrochemical activity of BFDMA (for example the rate of bulk oxidation) in a given electrolyte. Table 7.2 summarizes results of cyclic voltammetry performed across a range of scan rates.

Table 7.2. Summary of peak currents obtained from cyclic voltammetry performed on solutions of BFDMA between 10 mV/s and 200 mV/s across cyclic scans of 0 to 0.6 V (as per the protocol described in detail in Chapter 6, section 6.2.2.3) using 100 mM LiCl, 100 mM LiOAc and 1 mM Li_2SO_4 salts. Analysis was performed on solutions before and after the centrifugation step described in Table 7.1. “a” is the exponent describing the relationship between peak current and scan rate, R^2 is the correlation coefficient for the fit to estimate “a”. A platinum disk working electrode (diameter of 5 mm), platinum mesh counter electrode, and a Ag|AgCl reference electrode were used.

<i>electrolyte</i>	<i>Analyte</i>	<i>Scan direction</i>	<i>a</i>	R^2	<i>Peak current at 100 mV/s (μA)</i>	<i>Conc. from UV-vis (mM)</i>	<i>Peak current / Conc. BFDMA ($\mu\text{A}/\text{mM}$)</i>
100 mM LiCl	1 mM BFDMA	Anodic	0.71	0.99	10.6	1.06	10
		Cathodic	0.87	0.99	-5.4		-5.1
	1 mM BFDMA + centrifuge	Anodic	0.89	0.95	6.1	0.27	22.6
		Cathodic	0.91	0.98	-3.7		-13.7
100 mM LiOAc	1 mM BFDMA	Anodic	0.77	0.99	11.9	0.98	12.1
		Cathodic	0.91	1.00	-4.3		-4.4
	1 mM BFDMA + centrifuge	Anodic	0.75	0.95	6.7	0.35	19.1
		Cathodic	0.90	0.98	-3.3		-9.4
1 mM Li_2SO_4	1 mM BFDMA	Anodic	0.71	0.99	4.8	1.02	4.7
		Cathodic	0.67	1.00	-2.8		-2.7

The value of the exponent describing the dependence of scan rate on the Faradaic peak current is given for a range of salts, including 100 mM LiCl and 100 mM LiOAc (salts representing the highest solubility of BFDMA, from Table 7.1) and, for comparison, 1 mM Li₂SO₄ previously used for all previous BFDMA related research by our group.¹¹ The exponent, a , is between 0.5 and 1.0 for all salts and therefore shows that BFDMA is adsorbing to the electrode for all salts tested (See equations 1 and 2 of Chapter 6 for more background on this analysis). However, the phase state of BFDMA in these salts is not known from this experiment but, as discussed in detail in Chapter 6, is of great importance when interpreting whether BFDMA diffusing in bulk solution is able to exchange electrons with the Pt electrode surface, and therefore the overall contributions of the electrochemical activity of the system that BFDMA forms with the electrode. An interesting parameter to compare is the calculated value of peak current per concentration of BFDMA present in the experiment (right hand column, Table 7.2). It is clear that the more soluble salts from Table 7.1 are producing significantly (2 to 3 fold) higher peak currents than 1 mM Li₂SO₄. Furthermore, centrifuged salts (and therefore samples where the majority of BFDMA is dissolved in solution as opposed to being a mixture of suspended and dissolved) show an even higher value of peak current per concentration of BFDMA, i.e. around twice as high again as their respective non-centrifuged salt solution peak current values. While, with the present data set, it is unclear why the centrifugation step would increase the electrochemical activity of BFDMA in these salt solutions (when considering a “per concentration of BFDMA” basis), this preliminary study

suggests that a more detailed investigation of specific ion effects may provide important insights into the factors that govern the electrochemical activity of BFDMA.

Differential scanning calorimetry is recommended to determine the effect that different ions have on the melting temperature of BFDMA, for example. This would test the hypothesis that the higher electrochemical activity of BFDMA seen in the CV analysis in Table 7.1 for electrolytes of 100 mM LiCl or 100 mM LiOAc is due to the phase state of BFDMA being above the melting temperature of BFDMA when subjected to the conditions of the experiment (i.e. at ambient temperature).

7.4 Future Studies: Structural variations around BFDMA

Electrochemical methods can be used to further measure the effect that specific changes in structure have on the rate of electrochemical oxidation of ferrocenyl amphiphiles. Building from the study detailed in Chapter 6 which compared FTMA to BFDMA, a single chain surfactant molecule similar to BFDMA in terms of its amine head group, chain length and ferrocene tail, variants around the structure of BFDMA have been synthesized and should also be investigated. For example, short-chain homologues of BFDMA are expected to melt at lower temperatures than BFDMA, and thus should lead to high rates of electrochemical oxidation as lack of molecular mobility (i.e. the frozen aggregates of BFDMA seen at ambient temperatures, blocking the exchange of electrons from diffusing BFDMA in

bulk solution, see Scheme 6.1) has been proven to be a factor that leads to slow oxidation of BFDMA. Also, adding alkyl side chains to the ferrocene rings may introduce steric hindrance to the movement of these groups on the amphiphile molecules, leading to a different type of aggregate in solution and therefore, a different rate of diffusion and different electron transfer properties. Cyclic voltammetry at both a stationary and a rotating disk electrode should be performed using these structural variants of BFDMA to provide further insights into the factors that control the electrochemical activity of BFDMA.

7.5 References

1. A. D. Miller, *Angew. Chem., Int. Ed.*, **1998**, 37, 1769-1785.
2. A. J. Verkleij, *Biochim. Biophys. Acta*, **1984**, 779, 43-63.
3. L. V. Chernomordik and J. Zimmerberg, *Curr. Opin. Struct. Biol.*, **1995**, 5, 541-547.
4. S. W. Hui, T. P. Stewart, L. T. Boni and P. L. Yeagle, *Science*, **1981**, 212, 921-923.
5. C. Marchini, M. Montani, A. Amici, H. Amenitsch, C. Marianecchi, D. Pozzi and G. Caracciolo, *Langmuir*, **2009**, 25, 3013-3021.
6. S. W. Hui, M. Langner, Y. L. Zhao, P. Ross, E. Hurley and K. Chan, *Biophys. J.*, **1996**, 71, 590-599.
7. R. Prããibil, Pergamon Press, Oxford, New York, 1972.
8. N. S. Templeton, *Curr. Med. Chem.*, **2003**, 10, 1279-1287.
9. J. P. E. Muller, B. S. Aytar, Y. Kondo, D. M. Lynn and N. L. Abbott, *Soft Matter*, **2012**, 8, 2608-2619.

10. B. S. Aytar, J. P. E. Muller, S. Golan, S. Hata, H. Takahashi, Y. Kondo, Y. Talmon, N. L. Abbott and D. M. Lynn, *Journal of Controlled Release*, **2012**, 157, 249-259.
11. N. L. Abbott, C. M. Jewell, M. E. Hays, Y. Kondo and D. M. Lynn, *J. Am. Chem. Soc.*, **2005**, 127, 11576-11577.
12. B. S. Aytar, J. P. E. Muller, S. Golan, Y. Kondo, Y. Talmon, N. L. Abbott and D. M. Lynn, *J. Colloid Interface Sci.*, **2012**, 387, 56-64.
13. C. M. Jewell, M. E. Hays, Y. Kondo, N. L. Abbott and D. M. Lynn, *J. Controlled Release*, **2006**, 112, 129-138.
14. C. M. Jewell, M. E. Hays, Y. Kondo, N. L. Abbott and D. M. Lynn, *Bioconjugate Chem.*, **2008**, 19, 2120-2128.
15. S. Nafisi, G. B. Sadeghi and A. PanahYab, *J. Photochem. Photobiol. B-Biol.*, **2011**, 105, 198-202.
16. X. Hao, J. Z. Wu, Y. P. Shan, M. J. Cai, X. Shang, J. G. Jiang and H. D. Wang, *J. Phys.-Condes. Matter*, **2012**, 24, 7.
17. W. Kunz, *Curr. Opin. Colloid Interface Sci.*, **2010**, 15, 34-39.

Influence of Biological Media on the Structure and Behavior of Ferrocene-Containing Cationic Lipid/DNA Complexes Used for DNA Delivery

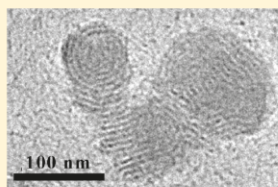
Sharon Golan,[†] Burcu S. Aydar,[‡] John P. E. Muller,[‡] Yukishige Kondo,[§] David M. Lynn,^{*,†} Nicholas L. Abbott,^{*,†} and Yeshayahu Talmon^{*,†}

[†]Department of Chemical Engineering, Technion-Israel Institute of Technology, Haifa 32000, Israel

[‡]Department of Chemical and Biological Engineering, University of Wisconsin—Madison, 1415 Engineering Drive, Madison, Wisconsin 53706-1607, United States

[§]Department of Industrial Chemistry, Tokyo University of Science, Tokyo, Japan

ABSTRACT: Biological media affect the physicochemical properties of cationic lipid–DNA complexes (lipoplexes) and can influence their ability to transfect cells. To develop new lipids for efficient DNA delivery, the influence of serum-containing media on the structures and properties of the resulting lipoplexes must be understood. To date, however, a clear and general picture of how serum-containing media influences the structures of lipoplexes has not been established. Some studies suggest that serum can disintegrate lipoplexes formed using certain types of cationic lipids, resulting in the inhibition of transfection. Other studies have demonstrated that lipoplexes formulated from other lipids are stable in the presence of serum and are able to transfect cells efficiently. In this article, we describe the influence of serum-containing media on lipoplexes formed using the redox-active cationic lipid bis(*n*-ferrocenylundecyl)dimethylammonium bromide (BFDMA). This lipoplex system promotes markedly decreased levels of transgene expression in COS-7 cells as serum concentrations are increased from 0 to 2, 5, 10, and 50% (v/v). To understand the cause of this decrease in transfection efficiency, we used cryogenic transmission electron microscopy (cryo-TEM) and measurements of zeta potential to characterize lipoplexes in cell culture media supplemented with 0, 2, 5, 10, and 50% serum. Cryo-TEM revealed that in serum-free media BFDMA lipoplexes form onionlike, multilamellar nanostructures. However, the presence of serum in the media caused disassociation of the intact multilamellar lipoplexes. At low serum concentrations (2 and 5%), DNA threads appeared to separate from the complex, leaving the nanostructure of the lipoplexes disrupted. At higher serum concentration (10%), disassociation increased and bundles of multilamellae were discharged from the main multilamellar complex. In contrast, lipoplexes characterized in serum-free aqueous salt (Li_2SO_4) medium and in OptiMEM cell culture medium (no serum) did not exhibit significant structural changes. The zeta potentials of lipoplexes in serum-free media (salt medium and cell culture medium) were similar (e.g., approximately -35 mV). Interestingly, the presence of serum caused the zeta potentials to become less negative (about -20 mV in OptiMEM and -10 mV in Li_2SO_4), even though serum contains negatively charged entities that have been demonstrated to lead to more negative zeta potentials in other lipoplex systems. The combined measurements of zeta potential and cryo-TEM are consistent with the proposition that DNA threads separate from the lipoplex in the presence of serum, resulting in a decrease in the net negative charge of the surface of the lipoplex.



INTRODUCTION

Cationic lipids are attractive as vectors for the nonviral delivery of DNA because they can interact with negatively charged DNA to form complexes (lipoplexes) that protect DNA from degradation by nucleases and facilitate internalization by cells. Despite these advantages and successes with a variety of different cationic lipid systems, many lipoplexes suffer from low transfection efficiencies, and the reasons for this remain poorly understood.^{1,2}

The factors that govern the transfection efficiency of cationic lipid systems can be divided into three major groups. The first one is the type (cationic, zwitterionic, etc.) and composition of the lipids used and the sizes and structures of the nucleic acid components (plasmids, oligonucleotides, etc.), both of which can influence the physicochemical properties of lipoplexes significantly. The second and third groups correspond to

solution conditions (ionic strength, pH, etc.) and interactions with biological species in extracellular and intracellular environments that can also impact and change the physicochemical properties of lipoplexes in important ways.³

Because lipoplexes can form different liquid-crystalline nanostructures, including the multilamellar $\text{L}\alpha^{\text{C}}$ phase and the inverted hexagonal $\text{H}_{\text{II}}^{\text{C}}$ phase,^{4–7} they can be extremely sensitive to changes in environmental conditions. Unfortunately, physical characterization of lipoplexes is often conducted in simple aqueous solutions of electrolyte (e.g., buffer) that do not accurately mimic the complexity of the biological media in which the lipoplexes will be used. After the lipoplexes are prepared, they are

Received: February 3, 2011

Published: May 02, 2011

introduced to biological media such as cell culture media and blood serum that may alter their structural and physicochemical properties significantly.^{4–8} To predict whether a certain lipidic system is suited for gene delivery applications, it should be characterized in the relevant biological medium or at least in the presence of serum-containing media to simulate biological conditions.

Simberg et al.⁹ studied the effect of blood serum on the structural and physicochemical properties of DOTAP-based (1,2-dioleoyl-3-trimethylammonium-propane) lipoplex systems. By using cryo-TEM, zeta potential, electrical surface potential Ψ_0 measurements, and FRET (fluorescence resonance energy transfer) techniques, they showed that DOTAP/cholesterol lipoplexes are stable (i.e., their nanostructure is not altered) in serum and lipoplexes formed using DOTAP and DOPE (dioleoyl phosphatidylethanolamine, which has been demonstrated to induce an inverse hexagonal phase) were unstable and disintegrated in the presence of serum. These authors suggested that serum proteins tend to adhere to the surfaces of the DOTAP/cholesterol lipoplexes and enlarge the aggregate size, rather than causing lipid–DNA disassociation.

Eliyahu et al.¹⁰ also studied the effect of serum on DOTAP/cholesterol lipoplexes and compared it to the effect of serum on dextran–spermine polyplexes. Using FRET, they showed that the addition of serum increased the lipid–DNA average molecular distance (from 5.25 to 5.79 nm) and decreased the polymer–DNA average distance (from 7.66 to 6.14 nm). However, FRET efficiency experiments showed that the serum proteins did not induce significant DNA disassociation from either complex, suggesting that DNA has a higher affinity than serum proteins for both cationic carriers. Their findings were in good agreement with the findings of Simberg et al.,⁹ showing that DOTAP/cholesterol lipoplexes preserved their shape and morphology after addition of serum, and that serum proteins did not penetrate into the vesicles, but associated only with the outer membranes.

In contrast to these studies, Li et al.¹¹ found via FRET and ethidium bromide (EtBr) intercalation assays that for several lipidic vectors of different compositions, serum induced the disintegration of lipoplexes and resulted in DNA release. They showed that DOTAP/DOPE lipoplexes disintegrated rapidly during serum incubation and exhibited low levels of transfection efficiency compared to DOTAP/cholesterol and DOTAP lipoplexes.

Yang and Huang¹² investigated the inhibition effect of serum on lipofection. They showed that serum has an inhibitory effect on transfection using DOTAP/DOPE, DC (3 β -[N-(N',N'-dimethylaminoethane)-carbamoyl]-cholesterol/DOPE, and lipofectamine lipoplex systems. However, in the DC-cholesterol- and DOTAP-containing systems, they found that inhibition could be overcome by optimizing the lipid-to-DNA charge ratio. To understand the reason for this serum inhibition, they removed the negatively charged proteins from the serum by DEAE–Sephacel chromatography, and the results showed that the inhibitory effect of the serum was eliminated. Therefore, one conclusion of this study was that the negatively charged proteins in the serum were responsible for the low transfection efficiency.

In spite of all of these past studies, the extents to which (and the mechanisms through which) the presence of serum can lead to lipoplex disruption and disintegration remain poorly understood. In this article, we report on the influence of biological media (e.g., both serum-free and serum-containing cell culture media) on the stability of lipoplexes formulated using a novel, ferrocene-containing cationic lipid.

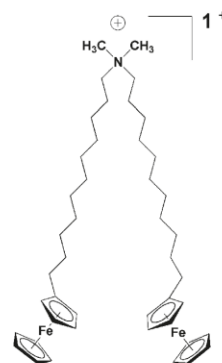


Figure 1. Molecular structure of BFDMA.¹⁵

We have demonstrated in past studies that the redox-active cationic lipid bis(*n*-ferrocenylundecyl)dimethylammonium bromide (BFDMA) is an effective cell transfection agent when it is used in its reduced state in a serum-free medium. Our past studies also demonstrate that the presence of serum can reduce levels of transfection significantly; for example, the efficiency in media containing 10% serum was found to be lower by an order of magnitude compared to levels of transfection observed when a serum-free medium is used.^{13,14}

This current study sought to investigate the influence of serum on the structures and properties of reduced BFDMA lipoplexes that could underlie these differences in cell transfection.

Pizzey et al.⁸ characterized the complexes that BFDMA forms with plasmid DNA using cryo-TEM and small-angle neutron scattering (SANS). The lipid in its reduced state exhibited well-defined multilamellar, onionlike lipoplexes in a large range of concentrations and lipid-to-DNA charge ratios. These past observations provide a basis from which to investigate changes in the structure of BFDMA/DNA lipoplexes that may occur upon the introduction of serum. We used cryo-TEM and measurements of zeta potential to characterize reduced BFDMA lipoplexes in (serum-free) OptiMEM cell culture medium, serum-containing OptiMEM cell culture medium, and serum-containing aqueous solutions of Li_2SO_4 . The structural and physicochemical properties of these lipoplexes were correlated to the results of transfection experiments using the COS-7 cell line and culture media containing increasing amounts of serum. Our results show that the presence of serum caused the disassociation of DNA from the lipid–DNA complexes. As the serum concentration increased, we observed enhanced levels of DNA disassociation that correlated with decreased levels of cell transfection. We use cryo-TEM to provide levels of detail regarding the lipoplex disassociation process that have not been reported previously.

EXPERIMENTAL SECTION

Materials. BFDMA was synthesized as described elsewhere.¹⁶ Adult bovine blood serum was purchased from Biological Industries Ltd. Kibbutz Beit Haemek, Israel or from Invitrogen (Carlsbad, CA). Plasmid DNA encoding enhanced green fluorescent protein (pEGFP-N1, 4.7 kb, >95% supercoiled) and firefly luciferase (pCMV-Luc, 6.2 kb, >90%

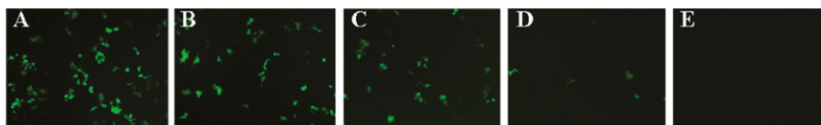


Figure 2. Representative fluorescence micrographs (100 \times magnification; 1194 μm \times 895 μm) showing relative levels of EGFP expression in a confluent layer of COS-7 cells 48 h after treatment with lipoplexes formed from reduced BFDMA. (A–E) Expression levels mediated in cell culture media supplemented with 0, 2, 5, 10, and 50% serum, respectively.

supercoiled) were purchased from Elim Biopharmaceuticals, Inc. (San Francisco, CA). OptiMEM cell culture medium, Dulbecco's Modified Eagle's Medium (DMEM), and fetal bovine serum (FBS) were purchased from Invitrogen (Carlsbad, CA). Bicinchoninic acid (BCA) protein assay kits were purchased from Pierce (Rockford, IL). Glo Lysis Buffer and Steady-Glo Luciferase Assay kits were purchased from Promega Corporation (Madison, WI). All salt solutions and buffers were prepared with deionized water (18.2 M Ω).

Preparation of Lipoplexes. Solutions of lipoplexes were prepared in the following manner. First, reduced BFDMA was dissolved in 1 mM Li₂SO₄ (pH 5), and the resulting solution was sonicated for about 15 min until all BFDMA was suspended in solution to produce a 1 mM reduced BFDMA solution. Then, to prepare lipoplexes in Li₂SO₄ solution, 2.9 mg/mL DNA in H₂O was added to the 1 mM reduced BFDMA lipid solution to produce a 0.905 mM BFDMA concentration with a 1.1:1 lipid-to-DNA charge ratio. The solution of BFDMA lipoplexes in Li₂SO₄ salt solution was added to the OptiMEM cell culture medium in a concentration that was 0.93 times the original purchased concentration. The final BFDMA concentration was 0.657 mM with a 1.1:1 lipid-to-DNA charge ratio. Serum solution was added to the lipoplex solutions (with or without OptiMEM cell culture medium) to produce solutions containing 2, 5, 10, and 50% (v/v) serum. Lipoplexes for zeta potential and transfection experiments were diluted to 40 and 8 μM BFDMA concentrations (respectively), and the DNA concentration was adjusted to maintain the 1.1:1 lipid-to-DNA charge ratio. The lipoplex concentrations and the lipid-to-DNA charge ratio were chosen on the basis of our previous studies demonstrating efficient transfection and consistency in morphology.^{8,13} We note that the pH of the OptiMEM-containing solutions and the serum-containing solution was about 7.5, and the pH of the Li₂SO₄-containing solution was about 5.

Transfection and Gene Expression Assays. Transfection experiments were conducted using COS-7 cells, which were grown in clear (for pEGFP-N1 expression) or opaque (for pCMV-Luc expression) polystyrene 96-well culture plates. The initial seeding densities of the cells were 15 000 cells/well in 200 μL of growth medium (90% Dulbecco's Modified Eagle's Medium, 10% fetal bovine serum, 100 units/mL penicillin, and 100 $\mu\text{g}/\text{mL}$ streptomycin). The cells were incubated at 37 $^{\circ}\text{C}$ for 24 h, and transfection experiments were conducted at approximately 80% confluence. The culture medium was replaced by 200 μL of OptiMEM with or without added serum, followed by the addition of 50 μL of a previously prepared lipoplex solution. After the addition of lipoplexes, the cells were incubated for 4 h at 37 $^{\circ}\text{C}$, after which time the lipoplex-containing medium was aspirated from all wells and replaced with 200 μL of fresh serum-containing medium. Samples were incubated for an additional 48 h, and then gene expression was characterized. EGFP expression was characterized using phase-contrast and fluorescence microscopy (Olympus IX70 fluorescence microscope with a MetaVue version 7.1.2.0 software package). Luciferase expression was determined using a commercially available luminescence-based luciferase assay kit according to the manufacturer's protocol. Samples were compared with signals from control wells and/or normalized against total cell protein in each respective well using a commercially available bicinchoninic acid (BCA) assay kit (Pierce).

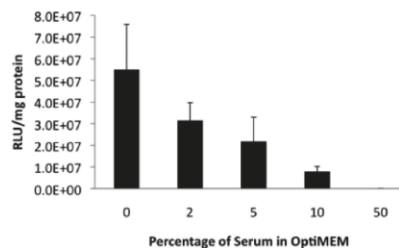


Figure 3. Luciferase expression in COS-7 cells (expressed as relative light units normalized to the total cell protein) mediated by lipoplexes formed from reduced BFDMA in the absence or presence of serum. Percentages of serum (v/v) correspond to conditions used to generate the data in Figure 2.

Cryogenic Transmission Electron Microscopy. Vitrified specimens of lipoplex solutions were prepared in the following manner. A drop of a lipoplex solution was applied to a perforated carbon film supported on a TEM copper grid in a controlled environment vitrification system (CEVS). The CEVS is a closed chamber, which allows the maintaining of a constant temperature (25 $^{\circ}\text{C}$ for our experiments) and 100% relative humidity to prevent evaporation of the solution from the grid. Then, the drop was blotted to create a thin film (<300 nm) and immediately plunged into liquid ethane at its freezing point (~ -183 $^{\circ}\text{C}$). Before cryo-TEM imaging, the vitrified specimens were stored in clean liquid nitrogen. The specimens were transferred to a Gatan 626 or to an Oxford CT-3500 cooling holder via their transfer station and equilibrated in the microscope at about -178 $^{\circ}\text{C}$. The samples were observed in a Philips CM120 or in a FEI T12 G2 transmission electron microscope operated in 120 kV, low-dose mode to minimize electron-beam radiation damage. We used a Gatan MultiScan 791 or a Gatan US 1000 high-resolution cooled-CCD camera to record the images at a nominal underfocus of 1 to 2 μm using the Digital Micrograph software package.

ζ -Potential Measurements. Five milliliters of lipoplex solution were injected into a Zetasizer 3000HS instrument (Malvern Instruments, Worcestershire, U.K.). Measurements were made using an applied voltage of 150 V at ambient temperature. The Henry equation was used to calculate ζ potentials from measurements of electrophoretic mobility.¹⁷ For every solution, five measurements were made; the viscosity was assumed to be the same as that of water.

RESULTS

Characterization of BFDMA-Mediated Transfection in the Presence of Serum. Gene expression levels were determined in OptiMEM cell culture medium containing 0, 2, 5, 10, and 50% serum. Levels of expression of pEGFP and luciferase are reported

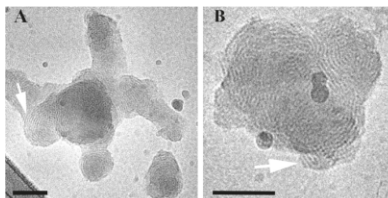


Figure 4. Cryo-TEM micrographs of reduced BFDMA lipid–DNA complexes in an aqueous Li_2SO_4 solution showing multilamellar nanostructures. The arrows point to multilamellar onionlike aggregates. The bars represent 100 nm.

in Figures 2 and 3, respectively. Figure 2 shows fluorescence micrographs of EGFP expression and permits the identification of qualitative trends. At low (0 and 2%) serum concentrations (Figure 2A,B), we observed high levels of expression; the difference in the levels of expression under these two conditions is not generally apparent in these data sets. However, at higher serum concentrations (5, 10, and 50%, Figure 2C–E), the EGFP expression levels decrease, with the presence of 10% serum concentration leading to very low expression levels. At 50% serum concentration (Figure 2E), no expression is visible. Additional transfection experiments using plasmid DNA encoding luciferase were conducted to quantify differences in these levels of gene expression. Figure 3 shows that the transfection efficiency decreased with increased serum concentration. The results show that the presence of 10% serum resulted in a one order of magnitude decrease in the gene expression level relative to controls performed in the absence of serum. However, the expression levels at low serum concentrations (0, 2, and 5%) are still on the order of 10^7 RLU/mg. At 50% serum concentration, the expression levels are very low, about 10^4 RLU/mg.

Characterization of Lipoplexes Using Cryo-TEM. Reduced BFDMA lipoplexes were prepared in an aqueous Li_2SO_4 salt solution (pH 5). The lipoplexes exhibited multilamellar nanostructures as reported previously by Pizzev et al.⁸ The majority of the nanostructures were onionlike multilamellar aggregates where the DNA is sandwiched between the lipid bilayers (Figure 4, arrows).

Figure 5 represents a cryo-TEM micrograph of the pEGFP-N1 plasmid DNA in water. The GFP plasmids, because of their supercoiled nature (more than 95% supercoiled) exhibited threadlike structures (not circular) that are thicker than the 2 nm diameter expected for a double-stranded DNA.

To mimic the conditions under which transfection is performed in vitro and thereby observe the effect of biological media on the nanostructure of the lipoplexes, we characterized reduced BFDMA lipoplexes in OptiMEM cell culture medium, serum-containing OptiMEM cell culture medium, and serum-containing aqueous salt solution.

Although the effect of the OptiMEM cell culture medium on the lipoplexes was modest, the lipoplexes did disassociate to some extent. The process is shown in Figure 6A, as indicated by some disassociation of the onionlike complexes releasing DNA threads, leaving the aggregate distorted (inset in Figure 6A). This process may occur because of the different ionic components of the OptiMEM cell culture medium. However, their effect on the

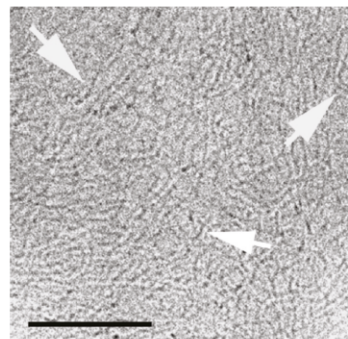


Figure 5. Cryo-TEM image of 2.9 mg/mL pEGFP-N1 plasmid DNA (4.7 kbps, >95% supercoiled) in water. The arrows point to threadlike structures that are formed by the DNA plasmids. The bar represents 100 nm.

morphology of the complexes is not dominant, and most of the multilamellar complexes are preserved (Figure 6B).

To understand the effect of blood serum on the nanostructures of the lipoplexes, we prepared solutions of the lipoplexes in OptiMEM containing 2, 5, 10, and 50% bovine blood serum. The results of the solution containing 5% serum showed similar behavior to the solution containing 2% serum and therefore are not presented here.

At 2% serum concentration, we observed DNA threads that were released from the onionlike aggregates (Figure 7). In Figure 7A, the arrowheads point to disassociating, distorted multilamellar aggregates and the arrows point to free DNA threads that probably disassociated from the complexes. Figure 7B shows at higher magnification a multilamellar aggregate in the process of disassociation.

At higher serum concentrations, the background in each image was grainier because of the high density of serum proteins (arrows in Figure 8). Figure 8 shows representative nanostructures observed in media containing 10% serum. Here, too, we observed the disassociation of lipoplexes. However, the disassociation process under these conditions was more severe. In 2% serum, disassociation occurs because of the release of DNA threads from the confined zone between two adjacent bilayers. At 10% serum, the DNA threads are not visible because of the high density of serum proteins. However, the disassociation of the lipoplexes is evident and appears to involve the simultaneous rupture of several lamellae (arrowheads in Figure 8A,B).

At higher serum concentrations (e.g., 50% serum), the multilamellar aggregates were almost completely absent. The few aggregates that we did observe were rather small (indicating a high extent of disassociation), and their multilamellar nature was not preserved. Figure 9B shows a representative example of such a distorted lipoplex. The arrowheads point to the edges of the aggregate, where traces of lamellae can be seen. In addition, we observed mostly empty liposomes that are represented in Figure 9A. Figure 9A shows that serum proteins tend to surround the BFDMA vesicle but do not penetrate or disassociate it.

We next sought to determine whether the presence of the cell culture medium itself contributed to the disassociation of the

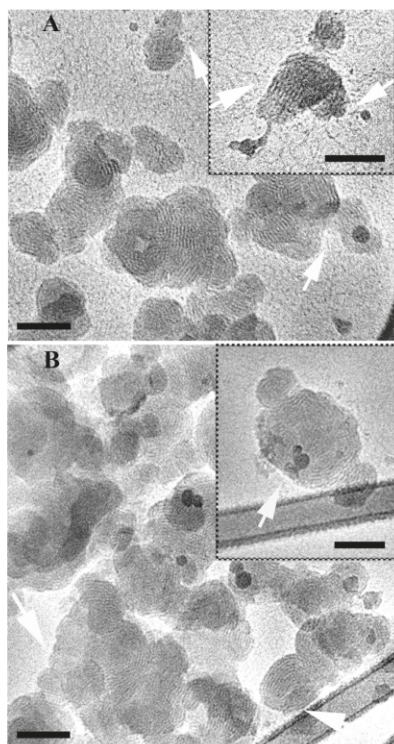


Figure 6. Cryo-TEM micrographs of reduced BFDMA lipid–DNA complexes in OptiMEM cell culture medium. (A) Arrows point to threadlike structures disassociated from the lipid–DNA complexes. (B) Arrows point to intact complexes (no disassociation features). The bars represent 100 nm.

lipid–DNA complexes. Therefore, we prepared solutions of the lipoplexes in 2, 5, and 10% serum in a Li_2SO_4 salt solution. In these samples, the extent of disassociation was similar to that of samples containing cell culture medium and serum, at the same serum concentration. Because we did not observe any difference in disassociation from the samples containing cell culture medium and serum, we show only representative results of the sample containing 5% serum (Figure 10).

Figure 10 shows lipid–DNA complexes during disassociation. In Figure 10A, the complex is distorted, DNA threads are released from the complex, and the multilamellar nature is not preserved. In Figure 10B, the extent of disassociation is moderate because we see just a few DNA threads being released from the aggregate; some of the original nanostructure is preserved. The complex in Figure 10C is almost intact, and only a few DNA threads are released from it. However, the aggregate is small and was probably detached from a larger lipoplex.

ζ -Potential Measurements. Zeta potential measurements of reduced BFDMA lipoplexes in Li_2SO_4 and in OptiMEM media

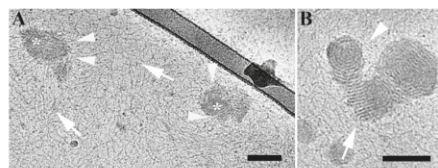


Figure 7. Cryo-TEM images of reduced BFDMA–DNA complexes in OptiMEM cell culture and 2% (v/v) serum. (A) Arrowheads point to threadlike structures disassociated from the edges of the lipid–DNA complexes. Arrows indicate free DNA threads, and asterisks decorate multilamellar complexes in the midst of the disassociation process. (B) The arrow points to the edge of a multilamellar complex, where the DNA threads are released into the solution. The arrowhead points to “leftovers” of the roundish onionlike lipoplex. The bars represent 100 nm.

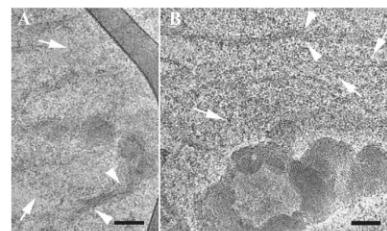


Figure 8. Cryo-TEM micrograph of reduced BFDMA–DNA complexes in OptiMEM cell culture medium and 10% (by volume) serum. (A, B) Arrowheads point to lamellae bundles that are released from lipoplex aggregates. Arrows point to serum proteins in the background. The bars represent 100 nm.

are summarized in Table 1. Table 1 shows that the zeta potential of the cationic reduced BFDMA lipid-only solution in Li_2SO_4 was positive, and complexes of reduced BFDMA lipid with plasmid DNA at a 1.1:1 lipid-to-DNA charge ratio exhibited zeta potentials that were negative in both Li_2SO_4 and in OptiMEM media. Also, the zeta potential values of lipoplexes in OptiMEM medium and in Li_2SO_4 aqueous medium without serum were comparable (approximately -35 mV). Interestingly, however, the presence of serum in both media caused the zeta potential to be less negative. For example, in the OptiMEM cell culture at 5, 10, and 50% serum concentrations, the zeta potential increased (became less negative) to values of approximately -20 mV (in the salt solution, values increased to approximately -10 mV).

DISCUSSION

Our results demonstrate that lipoplexes prepared using reduced BFDMA disassociate in the presence of biological media, particularly when serum proteins are added to cell culture media in which they are suspended. Lipoplexes in aqueous salt media (in Li_2SO_4) are multilamellar, roundish, and intact (Figure 4). Addition of the lipoplex solution to the OptiMEM cell culture medium does not alter the lipoplex structure (Figure 6) or the zeta potential value (around -35 mV for lipoplexes in both Li_2SO_4 and OptiMEM). However, the addition of serum to these solutions

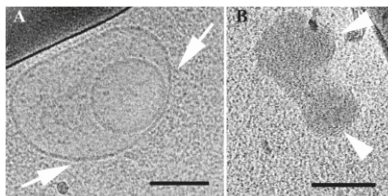


Figure 9. Cryo-TEM micrograph of reduced BFDMA lipid–DNA complexes in OptiMEM cell culture and 50% serum (by volume). The background looks grainy because of the high concentration of serum proteins. (A) The arrows point to the edge of a lipid vesicle, where serum proteins surround the outer surface of the lipid bilayers. (B) The arrowheads show a distorted multilamellar aggregate. The bars represent 100 nm.

caused significant changes in the physicochemical properties of the lipoplex aggregates, as determined by cryo-TEM and zeta potential measurements. Cryo-TEM revealed levels of lipoplex disassociation that varied with the level of serum added. At low serum concentrations (2 and 5%), both in Li_2SO_4 and OptiMEM media, we observed DNA threadlike structures that were released from the onionlike lipoplex aggregate (Figures 7 and 10). At higher serum concentrations (10 and 50%), lipoplex disassociation was more substantial. At 10% serum concentration (Figure 8), we observed bundles of multilamellae that disassociated from multilamellar lipoplexes. Because of the higher serum protein concentration (the grainy background in Figure 8), the proteins may interact with the lipoplex and tear away several lamellae from a larger multilamellar aggregate (which may explain the lamellae bundles that we observed in Figure 8).

At 50% serum concentration (Figure 9), the presence of the lipoplex aggregates was rare and the aggregates that we did observe seemed to be distorted (Figure 9B), indicating that most of the lipid–DNA complexes have already disassociated at such serum concentrations. In addition, we observed that serum proteins do not disintegrate the lipid bilayers because they do not penetrate the inner region of the vesicle but rather attach to the outer surface of it. That serum proteins do not penetrate or disassociate the lipid bilayers suggests that complex disassociation occurs because of DNA release rather than liposome bilayer disintegration. Therefore, lipoplex disassociation may occur because of the attachment of serum proteins to the positively charged lipids membrane, and by neutralizing the charge, DNA is released from the complex (i.e., effectively, an ion-exchange process on the surface of the lipoplex). In this physical scenario, the serum proteins and DNA are competing for the surface of the lipid bilayers.

Zeta potential results support the fact that serum causes structural changes. Blood serum contains mostly negatively charged entities (albumin). Thus, the zeta potential is expected to become more negative upon the introduction of positively charged lipoplexes to serum-containing media. Simberg et al.⁹ and Eliyahu et al.¹⁰ showed that for DOTAP-containing lipoplexes the zeta potential becomes more negative in the presence of serum, suggesting that serum proteins tend to coat the surface of the lipoplex and induce aggregation. In the BFDMA lipoplex system, that is not the case; instead of turning the zeta potential to a more

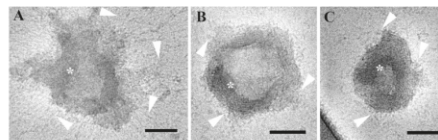


Figure 10. Cryo-TEM micrograph of reduced BFDMA lipid–DNA complexes in 5% serum (v/v, no cell culture OptiMEM medium). The arrowheads show that DNA threads disassociate from the lipoplex aggregate (asterisks). (A) High extent of disassociation (such as that in Figure 7A). (B) Moderate extent of disassociation. (C) Low extent of disassociation. The bars represent 100 nm.

Table 1. Zeta Potential Measurements of Reduced BFDMA Solutions

sample	1 mM Li_2SO_4 (mV)	OptiMEM (mV)
reduced BFDMA lipid	29.3 ± 1.1	
DNA only	-1.0 ± 2.7	
reduced BFDMA lipoplexes, 0% serum	-35.1 ± 1.5	-33.1 ± 2.0
reduced BFDMA lipoplexes, 2% serum	-15.1 ± 0.4	-24.9 ± 1.6
reduced BFDMA lipoplexes, 5% serum	-13.3 ± 0.3	-20.8 ± 1.2
reduced BFDMA lipoplexes, 10% serum	-9.5 ± 0.4	-18.5 ± 0.7
reduced BFDMA lipoplexes, 50% serum	-9.5 ± 1.1	-20 ± 1.9

negative value, the presence of serum causes the zeta potential to become less negative.

The combination of zeta potential measurements (Table 1) with cryo-TEM suggests that serum proteins cause DNA disassociation from the lipid–DNA complex. Serum proteins compete for the surface of the positively charged lipid bilayers, resulting in the disassociation of DNA from the complexes. Because of DNA release, there are less negatively charged entities associated in the complex; therefore, the zeta potential becomes less negative. Even if serum proteins replace the DNA, their charge density is lower than that of the DNA plasmids, thus causing the zeta potential to be less negative but still in the negative charge zone.

Transfection experiments and gene expression results show that levels of transfection mediated by reduced BFDMA lipoplexes are significantly lower in the presence of serum. As shown in Figures 2 and 3, levels of both EGFP and luciferase expression decrease as serum concentrations are increased. These decreases in expression levels correlate with changes in the physicochemical properties of the lipoplexes in the presence of serum that are revealed by our cryo-TEM and zeta potential measurements. Although it is difficult to determine the specific reasons for lower transfection on the basis of these current measurements, these large changes in structure and charge could potentially lead to changes in the extent to which DNA is internalized by cells (and thereby lead to lower overall levels of cell transfection). All of our findings show the ability of serum to disassociate the lipid–DNA complex. This is in contrast to other past reports that suggested that DNA is not released from lipoplexes based on other cationic lipids.^{9,10,18–20} Furthermore, Simberg et al.⁹ showed by cryo-TEM that serum proteins do not penetrate or disassociate DOTAP/cholesterol-based lipoplexes but rather adhere to the surface of the lipoplexes without causing them to disintegrate or

undergo other large changes in structure. These findings partially resemble ours. We also demonstrated in Figure 9A that serum proteins do not penetrate the lipid membrane. However, their results suggest that DNA does not disassociate from the lipoplex in the presence of serum. In our work, we observed DNA disassociation from lipoplexes in the presence of serum.

One wonders why the presence of blood serum causes DNA release from the cationic BFDMA lipid–DNA complexes whereas other cationic-based lipoplexes stay intact. Although the multi-lamellar morphology of lipoplexes based on reduced BFDMA is quite ordinary and resembles “standard” lipoplexes based on cationic lipids, the structure of this lipid is different in several ways from lipids investigated in the past studies noted above. Standard cationic lipids used for gene delivery are composed of a cationic polar headgroup and two hydrocarbon tails. Similarly, the reduced BFDMA lipid is composed of a cationic headgroup and double hydrocarbon tail. However, reduced BFDMA contains, at the end of each hydrocarbon tail, a ferrocene group. We note that past studies²¹ of monolayers of ferrocene-containing surfactants concluded that the ferrocene group substantially changes the conformation of the surfactant molecules at the surface of water. Similarly, the ferrocene groups of BFDMA may perturb the packing of the lipid within the bilayer structure, making it less stable and resulting in weaker electrostatic interactions between the lipid bilayers and the DNA. When serum is added, negatively charged proteins might interact with the positively charged lipid membrane and neutralize it. When some parts of the lipid membrane are neutralized, the interactions with the DNA are weakened and DNA may be released. Another secondary effect that may weaken the lipid–DNA interactions is the hydrophobic interactions between the hydrophobic domains of the serum proteins and the hydrophobic segments of the BFDMA lipids. In standard cationic lipids, the lipid bilayers may be stable and may be packed better (because their hydrophobic tails contain only hydrocarbon chains), allowing stronger electrostatic interactions with DNA.

CONCLUSIONS

We have demonstrated that lipoplexes formed using reduced BFDMA, when exposed to biological media, can undergo significant disassociation. The disassociation process and its extent depend on the type of medium and its concentration. OptiMEM cell culture medium induced some lipoplex disassociation but did not affect the zeta potential. In contrast, the addition of serum caused lipoplexes to disassociate, resulting in structural changes and changes in the zeta potential. We used cryo-TEM to characterize how the lipoplexes disassemble in the presence of serum and correlated these observations to the transfection efficiency, which demonstrated that as the serum concentration increased, transfection levels decreased.

AUTHOR INFORMATION

Corresponding Author

* (D.M.L.) Tel: 608-262-1086. E-mail: dlynn@engr.wisc.edu. (N.L.A.) Tel: 608-265-5278. E-mail: abbott@engr.wisc.edu. (Y.T.) Tel: +972-4-8292007. E-mail: ishi@tx.technion.ac.il.

ACKNOWLEDGMENT

Financial support was provided by the Technion Russell Berrie Nanotechnology Institute (RBNI) and the Technion Soft Matter Electron Microscopy Laboratory. In addition, support

from the U.S. National Science Foundation (CBET 075921) and the National Institutes of Health (1 R21 EB006168) is gratefully acknowledged.

REFERENCES

- (1) Verma, I. M.; Weitzman, D. *Annu. Rev. Biochem.* **2005**, *74*, 711–738.
- (2) Patil, S. D.; Rhodes, D. G.; Burgess, D. J. *AAPS J.* **2005**, *07*, E61–E77.
- (3) Boktov, J.; Hirsch-Lerner, D.; Barenholz, Y. *J. Gene. Med.* **2007**, *9*, 884–893.
- (4) Koltover, I.; Salditt, T.; Radler, J. O.; Safinya, C. R. *Science* **1998**, *281*, 78–81.
- (5) Koltover, I.; Salditt, T.; Safinya, C. R. *Biophys. J.* **1999**, *77*, 915–924.
- (6) Safinya, C. R.; Ewert, K.; Ahmad, A.; Evans, H. M.; Raviv, U.; Needleman, D. J.; Lin, A. J.; Slack, N. L.; George, C.; Samuel, C. E. *Philos. Trans. R. Soc., A* **2006**, *364*, 2573–2596.
- (7) Weisman, S.; Hirsch-Lerner, D.; Barenholz, Y.; Talmon, Y. *Biophys. J.* **2004**, *87*, 609–614.
- (8) Pizzey, C. L.; Jewell, C. M.; Hays, M. E.; Lynn, D. M.; Abbott, N. L.; Kondo, Y.; Golan, S.; Talmon, Y. *J. Phys. Chem. B* **2008**, *112*, 5849–5857.
- (9) Simberg, D.; Weisman, S.; Talmon, Y.; Faerman, A.; Shoshani, T.; Barenholz, Y. *J. Biol. Chem.* **2003**, *278*, 39858–39865.
- (10) Eliyahu, H.; Joseph, A.; Schillemans, J. P.; Azzam, T.; Domb, A. J.; Barenholz, Y. *Biomaterials* **2007**, *28*, 2339–2349.
- (11) Li, S.; Tseng, W.-C.; Stoltz, D. B.; Wu, S.-P.; Watkins, S. C.; Huang, L. *Gene Ther.* **1999**, *6*, 585–594.
- (12) Yang, J.-P.; Huang, L. *Gene Ther.* **1997**, *4*, 950–960.
- (13) Jewell, C. J.; Hays, M. E.; Kondo, Y.; Abbott, N. L.; Lynn, D. M. *J. Controlled Release* **2006**, *112*, 129–138.
- (14) Abbott, N. L.; Jewell, C. J.; Hays, M. E.; Kondo, Y.; Lynn, D. M. *J. Am. Chem. Soc.* **2005**, *127*, 11576–11577.
- (15) Kakizawa, Y.; Sakai, H.; Nishiyama, K.; Abe, M. *Langmuir* **1996**, *12*, 921–924.
- (16) Yoshino, N.; Shoji, H.; Kondo, Y.; Kakizawa, Y.; Sakai, H.; Abe, M. *J. Jpn. Oil Chem. Soc.* **1996**, *45*, 769.
- (17) Hunter, R. J. *Zeta Potential in Colloid Science*; Academic Press: New York, 1981.
- (18) Marchini, C.; Montani, M.; Amici, A.; Amenitsch, H.; Marianecchi, C.; Pozzi, D.; Caracciolo, G. *Langmuir* **2009**, *25*, 3013–3021.
- (19) Gao, X.; Kim, K.-S.; Liu, D. *AAPS J.* **2007**, *9*, E92–E104.
- (20) Madeira, C.; Loura, L. M. S.; Prieto, M.; Fedorov, A.; Aires-Barros, M. R. *BMC Biotechnol.* **2008**, *8*, 20.
- (21) Gallardo, B. S.; Metcalfe, K. L.; Abbott, N. L. *Langmuir* **1996**, *12*, 4116–4124.



Contents lists available at SciVerse ScienceDirect

Journal of Controlled Release

journal homepage: www.elsevier.com/locate/jconrel

Addition of ascorbic acid to the extracellular environment activates lipoplexes of a ferrocenyl lipid and promotes cell transfection

Burcu S. Aytar ^a, John P.E. Muller ^a, Sharon Golan ^b, Shinichi Hata ^c, Hiro Takahashi ^c, Yukishige Kondo ^c, Yeshayahu Talmon ^{b,*}, Nicholas L. Abbott ^{a,**}, David M. Lynn ^{a,***}

^a Department of Chemical and Biological Engineering, University of Wisconsin - Madison, 1415 Engineering Drive, Madison, WI 53706, United States

^b Department of Chemical Engineering, Technion-Israel Institute of Technology, Haifa 32000, Israel

^c Dept. of Industrial Chemistry, Tokyo University of Science, Tokyo, Japan

ARTICLE INFO

Article history:

Received 29 July 2011

Accepted 15 September 2011

Available online 22 September 2011

Keywords:

Ferrocenyl lipid
Lipoplexes
Transfection
Nanostructure
Ascorbic acid
External stimulus

ABSTRACT

The level of cell transfection mediated by lipoplexes formed using the ferrocenyl lipid bis(11-ferrocenylundecyl) dimethylammonium bromide (BFDMA) depends strongly on the oxidation state of the two ferrocenyl groups of the lipid (reduced BFDMA generally mediates high levels of transfection, but oxidized BFDMA mediates very low levels of transfection). Here, we report that it is possible to chemically transform inactive lipoplexes (formed using oxidized BFDMA) to “active” lipoplexes that mediate high levels of transfection by treatment with the small-molecule reducing agent ascorbic acid (vitamin C). Our results demonstrate that this transformation can be conducted in cell culture media and in the presence of cells by addition of ascorbic acid to lipoplex-containing media in which cells are growing. Treatment of lipoplexes of oxidized BFDMA with ascorbic acid resulted in lipoplexes composed of reduced BFDMA, as characterized by UV/vis spectrophotometry, and lead to activated lipoplexes that mediated high levels of transgene expression in the COS-7, HEK 293T/17, HeLa, and NIH 3T3 cell lines. Characterization of internalization of DNA by confocal microscopy and measurements of the zeta potentials of lipoplexes suggested that these large differences in cell transfection result from (i) differences in the extents to which these lipoplexes are internalized by cells and (ii) changes in the oxidation state of BFDMA that occur in the extracellular environment (i.e., prior to internalization of lipoplexes by cells). Characterization of lipoplexes by small-angle neutron scattering (SANS) and by cryogenic transmission electron microscopy (cryo-TEM) revealed changes in the nanostructures of lipoplexes upon the addition of ascorbic acid, from aggregates that were generally amorphous, to aggregates with a more extensive multilamellar nanostructure. The results of this study provide guidance for the design of redox-active lipids that could lead to methods that enable spatial and/or temporal control of cell transfection.

© 2011 Elsevier B.V. All rights reserved.

1. Introduction

Cationic lipids have been investigated broadly as non-viral agents for the delivery of DNA to cells [1–6]. Early studies demonstrated that significant levels of cell transfection could be achieved by formulating cationic lipid/DNA complexes (lipoplexes) using lipids with relatively simple molecular structures (e.g., a simple cationic head group and several hydrophobic tails) [7, 8]. Over time, however, the structures and properties of lipids used for cell transfection have evolved to include chemical functionality designed to overcome or address a variety of intracellular barriers that limit cell transfection efficiency. For example, lipids have been designed to form lipoplexes that are stable

in complex extracellular environments (including in the presence of serum proteins) [9–11] and/or release their cargo (DNA) in response to intracellular stimuli, including the presence of reducing agents [12–16] (e.g., glutathione), changes in pH [15, 17–19], or the presence of specific enzymes [20, 21]. The design of lipids that promote more efficient intracellular trafficking of internalized DNA has contributed significantly to the development of lipoplex-based approaches to DNA delivery.

In contrast to efforts to design functional lipids that promote the intracellular trafficking of DNA, relatively few studies have reported on the design of lipids that can be transformed (or “activated” toward transfection) in response to externally-controlled stimuli applied in *extracellular* environments (e.g., so as to influence extents to which complexes are either internalized or not internalized by cells) [22–24]. This latter approach could provide lipoplexes that enable control over the timing of the delivery of DNA to cells (i.e., “temporal control” of transfection) or, alternatively, allow delivery of DNA to sub-populations of cells within a larger population (i.e., “spatial control” of transfection

* Corresponding author.

** Corresponding author. Tel.: +1 608 265 5278.

*** Corresponding author. Tel.: +1 608 262 1086.

E-mail addresses: ishi@tx.technion.ac.il (Y. Talmon), abbott@engr.wisc.edu (N.L. Abbott), dlynn@engr.wisc.edu (D.M. Lynn).

by spatially-controlled delivery of an activating agent). The design of lipids that offer the ability to achieve external control over the timing and the locations at which DNA is available to cells could potentially find use in a broad range of applications, ranging from basic biomedical research (e.g., the design of transfected cell arrays) [25–29], engineering of tissues with complex tissue architectures [30–33], and, potentially, for the development of new gene-based therapies. In this current study, we report a step toward the realization of general and facile principles for spatial and temporal control over the lipoplex-mediated delivery of DNA to cells. Our approach is based on the use of a redox-active ferrocene-containing cationic lipid.

The study reported in this paper exploits the physicochemical properties of the redox-active ferrocene-containing lipid bis(11-ferrocenylundecyl)dimethylammonium bromide (BFDMA, Fig. 1) [34–36]. This lipid can be reversibly cycled between its reduced state (net charge of +1) and its oxidized state (net charge of +3) by either oxidation or reduction of the ferrocene groups present at the end of each hydrophobic chain [35–41]. Our past studies have demonstrated that the oxidation state of BFDMA significantly affects the interaction of this lipid with DNA [39, 40] and the efficiency with which lipoplexes of BFDMA and DNA transfect cells [37, 38, 41]. In particular, our past studies have identified a range of lipid concentrations over which lipoplexes formed from reduced BFDMA mediate high levels of transgene expression *in vitro*, whereas lipoplexes formed from oxidized BFDMA (over the same range of concentrations) yield negligible levels of transgene expression [37, 38, 41]. Our previous physical characterization experiments also reveal that the oxidation state of BFDMA influences the zeta potentials and nanostructures of lipoplexes formed from BFDMA [39, 40].

The oxidation state of ferrocene-containing surfactants and lipids can be transformed readily and reversibly using electrochemical methods or by using chemical oxidizing and reducing agents [34–46]. In a recent study, we reported the use of glutathione (GSH) to chemically reduce the ferrocenium groups within lipoplexes formed using DNA and oxidized BFDMA (in 1 mM aqueous Li_2SO_4 solution at pH 5.1) [41]. We demonstrated that when these transformed lipoplexes were subsequently introduced to COS-7 cells *in vitro*, they mediated high levels of transgene expression (i.e., levels that were comparable to the levels of transgene expression mediated by lipoplexes formed from reduced BFDMA and DNA). This past study demonstrated that “inactive” lipoplexes of oxidized BFDMA and DNA can be activated by treatment with a chemical reducing agent. However, while these past studies represent a significant step toward the realization of principles that could be used to exert spatial and temporal control over transfection using

ferrocene-containing lipids, a number of important issues remain to be addressed. First, as mentioned above, in our previous studies chemical reduction was performed (i) in a simple electrolyte solution (1 mM aqueous Li_2SO_4 , as opposed to cell culture media) and (ii) prior to the introduction of the lipoplexes to cells [41]. Second, we also observed that a large molar excess of GSH was required to achieve rapid transformation of oxidized BFDMA within lipoplexes (transformation occurred over ~90 min in the presence of a 10-fold molar excess of GSH, but within seconds to minutes in the presence of a 50-fold molar excess of GSH).

We also note, in this context, that while GSH served as a useful model reducing agent in our initial studies, this molecule is produced in significant concentrations inside cells and is also present at lower concentrations in extracellular environments [47, 48]. In the study reported in this paper, we demonstrate that the rapid and efficient chemical reduction of oxidized BFDMA within lipoplexes can be achieved at significantly lower concentrations using ascorbic acid (vitamin C) as a chemical reducing agent. Ascorbic acid (AA) is a well-known and biologically important chemical reducing agent, but in contrast to GSH it is not synthesized naturally by humans or primates [49]. Below, we demonstrate using cell-based experiments and physicochemical methods of characterization that AA can be used to chemically transform lipoplexes of oxidized BFDMA (via reduction of ferrocenium groups) to “activate” these lipoplexes both in cell culture media and *in the presence of cells* (i.e., by adding small amounts of AA to lipoplex-containing media in which cells are already growing).

2. Materials and methods

2.1. Materials

BFDMA was synthesized using methods described previously [35]. Ascorbic acid, heparin, and lithium sulfate monohydrate were purchased from Sigma Aldrich (St. Louis, MO). Dodecyltrimethylammonium bromide (DTAB) was purchased from Acros Organics (Morris Plains, NJ). Plasmid DNA constructs encoding enhanced green fluorescent protein [pEGFP-N1 (4.7 kb), >95% supercoiled] and firefly luciferase [pCMV-Luc, >95% supercoiled] were purchased from Elim Biopharmaceuticals, Inc. (San Francisco, CA). Dulbecco's modified Eagle's medium (DMEM), Opti-MEM cell culture medium, phosphate-buffered saline (PBS), fetal bovine serum (FBS), Lipofectamine 2000, LysoTracker Red, Wheat germ agglutinin (WGA)-Alexa Fluor 488, and Hoechst 34580 were purchased from Invitrogen (Carlsbad, CA). Bicinchoninic acid (BCA) protein assay kits were purchased from Pierce (Rockford, IL). Glo Lysis Buffer and Steady-Glo Luciferase Assay kits were purchased from Promega Corporation (Madison, WI). Cy5 Label-IT nucleic acid labeling kits were purchased from Mirus Bio (Madison, WI). Glass inset dishes used for laser scanning confocal microscopy (LSCM) were purchased from MatTek (Ashland, MA). Deionized water (18 M Ω) was used to prepare all buffers and salt solutions. All commercial materials were used as received without further purification, unless otherwise noted.

2.2. General considerations

Electrochemical oxidation of BFDMA was performed as described previously [37–39, 41]. UV/vis absorbance values of lipoplex solutions were monitored using a Beckman Coulter DU520 UV/vis Spectrophotometer (Fullerton, CA). Zeta potential measurements were performed using a Zetasizer 3000HS instrument (Malvern Instruments, Worcestershire, UK). Fluorescence microscopy images used to evaluate the expression of enhanced green fluorescent protein (EGFP) in cell transfection experiments were recorded using an Olympus IX70 microscope and were analyzed using the MetaVue version 7.1.2.0 software package (Molecular Devices; Toronto, Canada). Luminescence and absorbance measurements used to characterize luciferase expression and total cell protein were performed using a PerkinElmer EnVision multilabel plate reader (Luciferase: Em, 700 nm cutoff; BCA: Abs 560 nm). For LSCM experiments, DNA was

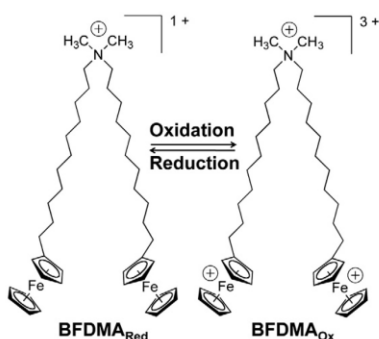


Fig. 1. Molecular structure of bis(11-ferrocenylundecyl)dimethylammonium bromide (BFDMA).

labeled using a Label-IT nucleic acid labeling kit according to the manufacturer's protocol (labeling density ~100 labels per plasmid). Labeled DNA was purified by ethanol precipitation, and labeling densities were determined using a UV/vis spectrophotometer, as described by the manufacturer. LSCM was performed using a Nikon A1R confocal microscope. LSCM images were processed using ImageJ 1.43u (National Institutes of Health; Washington, DC) and Photoshop CS5 (Adobe Systems; San Jose, CA).

2.3. Preparation of lipid and lipoplex solutions

Reduced BFDMA solutions (1 mM) were prepared by dissolving reduced BFDMA in aqueous Li_2SO_4 (1 mM, pH 5.1). Oxidized BFDMA solutions were prepared by electrochemical oxidation of solutions of reduced BFDMA. To prepare lipoplex solutions, a solution of plasmid DNA (24 $\mu\text{g}/\text{ml}$ in water) was added slowly to the aqueous Li_2SO_4 solution containing an amount of reduced or oxidized BFDMA sufficient to give the final lipid concentrations (and also lipid/DNA charge ratios, CRs) reported in the text. Lipoplex solutions were incubated at room temperature for 20 min before their use in subsequent experiments.

2.4. Characterization of the chemical reduction of lipoplexes of oxidized BFDMA upon treatment with AA

For experiments designed to characterize the reduction of oxidized BFDMA within lipoplexes, lipoplexes were diluted in Opti-MEM cell culture medium to a final lipid concentration of 250 μM , and a 10-fold molar excess of AA solution was added. The time-dependent transformation of lipoplexes of oxidized BFDMA upon treatment with AA was monitored by measuring UV/vis absorption spectra at wavelengths ranging from 400 to 800 nm, in analogy to methods described previously [41]. To facilitate measurements of absorbance, lipoplexes were prepared using a high concentration of BFDMA (250 μM) at lipid/DNA CRs of 1.4:1 and 4.2:1 (for lipoplexes of reduced or oxidized BFDMA, respectively). To eliminate the clouding of solutions of lipoplexes of reduced and oxidized BFDMA or lipoplexes of oxidized BFDMA that were treated with AA, DTAB was added prior to absorption measurements. We note here that DTAB does not absorb light in the range of wavelengths used in these experiments.

2.5. Cell transfection experiments and characterization of transgene expression

COS-7, HEK 293T/17, HeLa, and NIH 3T3 cells used in cell transfection experiments were grown in clear or opaque polystyrene 96-well culture plates (for experiments using pEGFP-N1 and pCMV-Luc, respectively) at initial seeding densities of 15×10^3 , 50×10^3 , 24×10^3 , and 6×10^3 cells/well, respectively, in 200 μL of growth medium. For each different cell type, the medium used was as follows: 90% DMEM, 10% fetal bovine serum for COS-7 and HEK 293T/17 cells; 90% MEM, 10% fetal bovine serum for HeLa cells, and 90% DMEM, 10% calf bovine serum for NIH 3T3 cells; 100 units/ml penicillin and 100 $\mu\text{g}/\text{ml}$ streptomycin were added to media for all cases. After plating, cells were incubated at 37 °C until the cell populations were ~80% confluent. For cell transfection experiments, serum-containing cell culture medium was aspirated and replaced by 200 μL of serum-free medium (Opti-MEM) followed by the addition of 50 μL of lipoplex solutions. After 4 h of incubation at 37 °C, lipoplex-containing medium was aspirated and replaced with 200 μL of fresh serum-containing medium. Cells were incubated for an additional 48 h and then analyzed for gene expression. For experiments where pEGFP-N1 was used, relative levels of EGFP expression in cells were characterized using fluorescence microscopy. For experiments where pCMV-Luc was used, luciferase protein expression measurements were conducted using luminescence-based luciferase assay kits, according to the manufacturer's specified protocol. Luciferase expression data were normalized against total cell protein in each

respective well using a commercially available BCA protein assay kit. All cell transfection experiments were conducted in replicates of six.

2.6. Characterization of internalization of lipoplexes using LSCM

COS-7 cells were grown in glass inset confocal microscopy dishes at an initial seeding density of 2.5×10^5 cells/dish in 2 mL of growth medium. Cells were allowed to grow overnight to approximately 80% confluence. Growth medium was then replaced with 2.0 mL of serum-free cell culture medium (Opti-MEM), and 500 μL of lipoplex solutions formulated from BFDMA and pEGFP-N1 (mixture of unlabeled pEGFP-N1 and 20% (w/w) of a pEGFP-N1 labeled with Cy-5) were added. Cells were incubated with lipoplex solutions at 37 °C for 4 h. Lipoplex solutions were aspirated and then cells were rinsed with 50 U/ml of a heparin solution (in PBS) to promote the removal of extracellular membrane-associated lipoplexes. Cells were then stained with solutions of Hoechst 34580 (nuclear stain), LysoTracker Red (endosome/lysosome stain), and WGA-Alexa Fluor 488 (membrane stain). Internalization of Cy5-labeled DNA was then characterized using LSCM. LSCM images were acquired using a 60 \times /1.40 NA oil immersion objective. Hoechst 34580, WGA-Alexa Fluor 488, LysoTracker Red, and Cy5-labeled DNA were excited using laser lines at 408, 488, 561 and 638 nm, respectively. Fluorescence emission signals were collected for four individual channels and merged to create four-color images.

2.7. Characterization of the zeta potentials of lipoplexes

The zeta potentials of lipoplexes were characterized using a Zetasizer 3000HS (Malvern Instruments, Worcestershire, UK). The analysis of 3 mL samples of lipoplex solutions was performed at ambient temperatures using an electrical potential of 150 V. Five measurements were performed for each lipoplex solution. The Henry equation was used to calculate the zeta potentials from measurements of electrophoretic mobility. In these calculations, the viscosity of the lipoplex solutions was assumed to be same as that of water.

2.8. Preparation of samples of lipoplexes for characterization by SANS and cryo-TEM

Stock solutions of BFDMA (1 mM) were prepared in 1 mM Li_2SO_4 . Lipoplex solutions were prepared by adding pEGFP-N1 to stock solutions of BFDMA and then diluting in Opti-MEM cell culture medium. Lipoplexes formed from reduced BFDMA and DNA were prepared at a charge ratio of 1.1:1, and contained the same molar concentrations of BFDMA as complexes formed by oxidized BFDMA and DNA at a charge ratio of 3.3:1. Although these charge ratios were chosen to be close to those used in cell transfection experiments, the absolute concentrations of BFDMA used in the SANS and cryo-TEM measurements (620 to 660 μM) were substantially higher than those used in the transfection experiments. These higher concentrations were necessary to obtain sufficient intensities of scattered neutrons in SANS experiments. To be consistent with the concentrations used in these SANS measurements and also allow for better sampling, cryo-TEM analyses of BFDMA lipoplexes were also performed at these high lipoplex concentrations.

2.9. Characterization of lipoplexes by small-angle neutron scattering

SANS measurements were performed using the CG-3 Bio-SANS instrument at the Oak Ridge National Laboratory (ORNL), Oak Ridge, TN. The incident neutron wavelength was on average 6 Å, with a spread in wavelength, $\Delta\lambda/\lambda$, of 15%. Data were recorded at two different sample-to-detector distances (1 and 14.5 m), giving q ranges from 0.490 to 0.018 and 0.064 to 0.003 Å⁻¹, respectively. To ensure statistically relevant data, at least 10^6 counts were collected for each sample at each detector distance. The samples were

contained in quartz cells with a 2 mm path length and placed in a sample chamber held at 25.0 ± 0.1 °C. The data were corrected for detector efficiency, background radiation, empty cell scattering, and incoherent scattering to determine the intensity on an absolute scale [40]. The background scattering from the solvent was subtracted. The processing of data was performed using Igor Pro (WaveMetrics, Lake Oswego, OR) with a program provided by ORNL. Guinier analysis described in detail elsewhere [40, 50] was used to interpret the scattering. Errors reported for d-spacings were calculated directly from q values by assuming a 2% experiment-to-experiment change in Bragg peak position versus q position (via calibration using silver behenate standards).

2.10. Characterization of lipoplexes by cryo-TEM

Specimens of lipoplexes used for characterization by cryo-TEM were prepared in a controlled environment vitrification (CEVS) system at 25 °C and 100% relative humidity, as previously described [51, 52]. Samples were examined using a Philips CM120 or in a FEI T12 G2 transmission electron microscope, operated at 120 kV, with Oxford CT-3500 or Gatan 626 cooling holders and transfer stations. Specimens were equilibrated in the microscope below -178 °C, and then examined in the low-dose imaging mode to minimize electron beam radiation damage. Images were recorded at a nominal underfocus of 1–2 μm to enhance phase contrast. Images were acquired digitally by a Gatan MultiScan 791 (CM120) or a Gatan US1000 high-resolution (T12) cooled-CCD camera using the DigitalMicrograph software package.

3. Results and discussion

3.1. Transformation of lipoplexes of oxidized BFDMA by treatment with ascorbic acid

We first conducted experiments to evaluate the extent and rate of reduction of lipoplexes of oxidized BFDMA upon treatment with AA in cell culture medium. For these studies, we selected the serum-free cell culture medium Opti-MEM (pH 7.4), because (i) this culture medium is widely used in *in vitro* cationic lipid-based cell transfection assays, and (ii) our previous cell transfection and physical characterization experiments were also performed using this medium [37–39, 41]. For the experiments presented in this section, we used lipoplexes of reduced or oxidized BFDMA prepared at BFDMA/DNA charge ratios (CRs) of 1.4:1 and 4.2:1, respectively. (We note here that lipoplexes of reduced and oxidized BFDMA prepared at these CRs contain the same molar ratio of BFDMA and DNA, owing to differences in the net charges of reduced (+1) and oxidized (+3) BFDMA.) These CRs were chosen on the basis of our past studies revealing that lipoplexes of reduced BFDMA at a CR of 1.4:1 yield high levels of cell transfection, but that lipoplexes of oxidized BFDMA at a CR of 4.2:1 mediate significantly lower levels of transfection [38, 41].

Fig. 2A shows UV/vis absorption spectra of solutions of lipoplexes of reduced BFDMA (black solid line), lipoplexes of oxidized BFDMA (black dashed line), and lipoplexes of oxidized BFDMA treated with a 10-fold molar excess of AA (gray dashed line) in Opti-MEM cell culture medium. Inspection of these data reveals that upon treatment of lipoplexes of oxidized BFDMA with AA, the absorbance peak at 630 nm, characteristic of oxidized BFDMA, disappeared, and a new maximum in absorbance at 430 nm (characteristic of the maximum absorbance of reduced BFDMA) appeared. The overall shape of the absorption spectrum of lipoplexes of oxidized BFDMA treated with AA was similar to that of lipoplexes of reduced BFDMA. Additional characterization of the time dependent disappearance of the peak in absorbance at 630 nm demonstrated that the AA-mediated reduction of lipoplexes occurred over a period of ~1 min (Fig. 2B). These observations demonstrate that AA can be used to reduce the ferrocenium

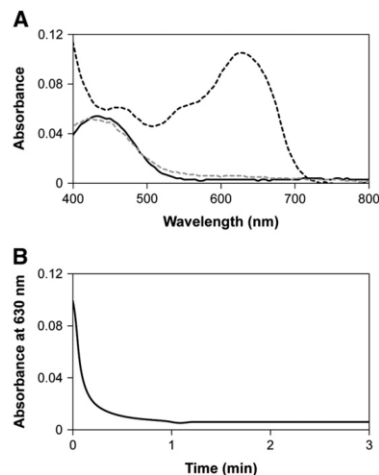


Fig. 2. (A) UV/visible absorbance spectra for solutions of lipoplexes of reduced BFDMA (black solid line), lipoplexes of oxidized BFDMA (black dashed line) or lipoplexes of oxidized BFDMA treated with AA (gray dashed line) in Opti-MEM cell culture medium. (B) Decrease in absorbance maximum (630 nm) of lipoplexes of oxidized BFDMA vs time upon treatment with a 10-fold molar excess of AA in Opti-MEM cell culture medium.

groups of oxidized BFDMA in lipoplexes at rates that are significantly higher than those that are possible using GSH (e.g., reduction occurred over ~90 min in the presence of 10-fold molar excess of GSH [41]).

3.2. Treatment of lipoplexes of oxidized BFDMA with AA in the presence of cells activates lipoplexes toward transfection

In our previous study, we demonstrated that GSH could be used to chemically transform inactive lipoplexes of oxidized BFDMA to lipoplex solutions capable of mediating levels of transgene expression comparable to those promoted by lipoplexes of reduced BFDMA (at several lipid/DNA CRs) [41]. In that study, chemical transformations of oxidized BFDMA lipoplexes were performed in 1 mM aqueous Li_2SO_4 prior to the introduction of the lipoplexes to cells [41]. In this current study, we sought to determine whether it was possible to perform the chemical transformation and, thus, the activation of inactive lipoplexes of oxidized BFDMA in cell culture media (Opti-MEM) and directly in the presence of cells. Here, we note that Opti-MEM differs from the Li_2SO_4 solutions used in our past studies in two important ways. First, the Li_2SO_4 solutions used in our past studies were prepared at pH 5.1 (this pH was chosen based on conditions required for the bulk electrolysis of BFDMA), but Opti-MEM is at physiological pH (pH 7.4). Second, Opti-MEM is a far more complex medium (e.g., it contains salts, trace elements, growth factors, and proteins) than aqueous Li_2SO_4 solution.

On the basis of these differences, we first sought to determine whether the addition of AA to lipoplexes of oxidized BFDMA in Opti-MEM cell culture medium and the presence of cells would lead to the activation of lipoplexes and result in high levels of cell transfection. To this end, we performed a series of qualitative gene expression assays using the COS-7 cell line and lipoplexes prepared from BFDMA and a plasmid DNA construct (pEGFP-N1) encoding enhanced green fluorescent protein (EGFP). For these experiments, we used lipoplexes prepared at BFDMA/DNA CRs that were identical to those

used in the experiments described above (i.e., BFDMA/DNA CRs of 1.4:1 and 4.2:1 for lipoplexes of reduced and oxidized BFDMA, respectively), but at lower overall BFDMA concentrations (10 μM). (See Materials and methods for additional details regarding these cell transfection experiments). Immediately following the introduction of lipoplexes of oxidized BFDMA to cells incubated in Opti-MEM, AA was added to the media and stirred gently using a pipette.

Fig. 3 shows representative fluorescence micrographs of COS-7 cells 48 h after incubation with either lipoplexes of (A) reduced BFDMA, (B) oxidized BFDMA, or (C) lipoplexes of oxidized BFDMA treated with AA. Inspection of these images reveals that lipoplexes of reduced BFDMA mediated high levels of EGFP expression, while lipoplexes of oxidized BFDMA yielded significantly lower levels of expression. These results are consistent with those of our past studies [37, 38, 41]. Further inspection of Fig. 3C, however, reveals that the lipoplexes of oxidized BFDMA that were treated with AA after addition to cells mediated levels of transgene expression that were qualitatively similar to those mediated by lipoplexes of reduced BFDMA. When combined, these results suggest that the addition of AA to the extracellular environment can be used to transform otherwise inactive lipoplexes of oxidized BFDMA into active lipoplexes that mediate high levels of transfection.

To confirm the results above and characterize relative levels of transgene expression quantitatively, we performed a second series of transfection experiments using lipoplexes formulated using BFDMA and a plasmid encoding firefly luciferase (pCMV-Luc) over a range of lipid concentrations (e.g., from 8 to 40 μM). These lipid concentrations correspond to lipid/DNA CRs ranging from 1.1:1 to 5.5:1 (for lipoplexes of reduced BFDMA) and 3.3:1 to 16.5:1 (for lipoplexes of oxidized BFDMA). These BFDMA concentrations (and thus BFDMA/DNA CRs) were chosen to permit comparisons to broader ranges of lipid concentrations used in our previous studies [37, 38, 41].

Fig. 4A shows levels of luciferase expression (expressed as relative light units normalized to total concentration of cell protein) mediated by lipoplexes of BFDMA in the COS-7 cell line. The results of this experiment (Fig. 4A) reveal that lipoplexes of reduced BFDMA (black bars) mediate significantly higher levels of transgene expression than lipoplexes of oxidized BFDMA (gray bars) at all of the BFDMA concentrations investigated. These results are generally similar to the results of our past studies [37, 38, 41]. Inspection of the luciferase expression data corresponding to lipoplexes of oxidized BFDMA treated with AA (white bars), however, reveals that these lipoplexes are able to mediate levels of transgene expression that are significantly higher than those mediated by lipoplexes of oxidized BFDMA (gray bars), particularly at BFDMA concentrations of 10 and 20 μM . The relative decrease in the level of expression of luciferase that is measured when using 40 μM BFDMA is due to the cytotoxicity of BFDMA at this higher concentration, as detailed in our past studies [38, 41]. We also note here that control experiments using (i) solutions of AA alone or (ii) mixtures of AA

and DNA in the absence of BFDMA did not result in levels of transgene expression comparable to those mediated by lipoplexes of oxidized BFDMA treated with AA (data not shown). Furthermore, the addition of a 10-fold molar excess of AA to lipoplexes of reduced BFDMA did not affect the level of transgene expression mediated by these lipoplexes.

These results, when combined, suggest that the increased levels of cell transfection that are observed to accompany the addition of AA to lipoplexes of oxidized BFDMA are due to the reduction of oxidized BFDMA within lipoplexes (and that this is not the result of other potential influences of AA on cell behavior). In conclusion, the results shown in Figs. 3 and 4A demonstrate that AA is able to transform (or activate) lipoplexes of oxidized BFDMA in the presence of cells, and that this transformation leads to lipoplexes that promote high levels of transgene expression in the COS-7 cell line. Finally, we note that levels of transgene expression mediated by lipoplexes of oxidized BFDMA treated with AA are lower than those mediated by lipoplexes of reduced BFDMA. Physicochemical factors and differences in lipoplex structure that could underlie these differences in levels of cell transfection are discussed in additional detail below.

We selected COS-7 cells for use in the initial studies above for two important reasons. First, the use of COS-7 cells allowed us to compare the results of this current study to those of our past investigations using this cell line [37, 38, 41]. Second, this cell line is generally considered to be easy to transfect, and, as such, provides a more challenging test of lipoplex “inactivity” (that is, our results demonstrate that lipoplexes of oxidized BFDMA (i.e., in an “off” state) transfect very poorly using a cell line that is otherwise regarded to be relatively easy to transfect [53]). We performed additional experiments similar to those described above to investigate the ability of lipoplexes of BFDMA to transfect three additional cell lines (HEK 293T/17, HeLa, and NIH 3T3 cells) used widely for the characterization of non-viral gene delivery systems. Quantitative luciferase-based transfection experiments were conducted in these additional cell lines using concentrations of BFDMA, lipid/DNA CRs, and other conditions identical to those used for transfection assays using COS-7 cells above.

Fig. 4B–D show plots of normalized luciferase expression in (B) HEK 293T/17, (C) HeLa and (D) NIH 3T3 cells after treatment with lipoplexes of reduced BFDMA (black bars), oxidized BFDMA (gray bars), or lipoplexes of oxidized BFDMA treated with AA (white bars). Inspection of these data reveals that lipoplexes of reduced BFDMA (black bars) were able to mediate significant levels of transfection in these cell lines at lipid concentrations ranging from 8 μM to 20 μM (albeit at absolute levels of expression that were different for each cell type; we return to these observations again below). In contrast, lipoplexes of oxidized BFDMA (gray bars) mediated levels of transfection that were significantly lower than those mediated by lipoplexes of reduced BFDMA. These results are generally consistent with the results of our current (Fig. 4A) and past studies using COS-7 cells [37, 38, 41], and lead to two important conclusions: (i) that the

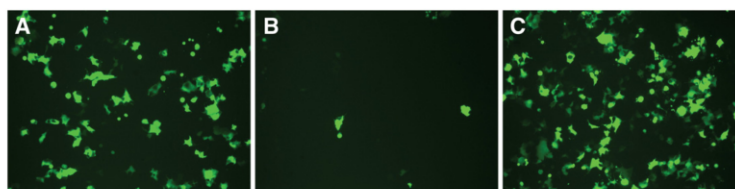


Fig. 3. Representative fluorescence micrographs (100 \times mag; 1194 μm \times 895 μm) of confluent monolayers of COS-7 cells showing levels of EGFP expression mediated by (A) lipoplexes of reduced BFDMA, (B) lipoplexes of oxidized BFDMA or (C) lipoplexes of oxidized BFDMA treated with AA.

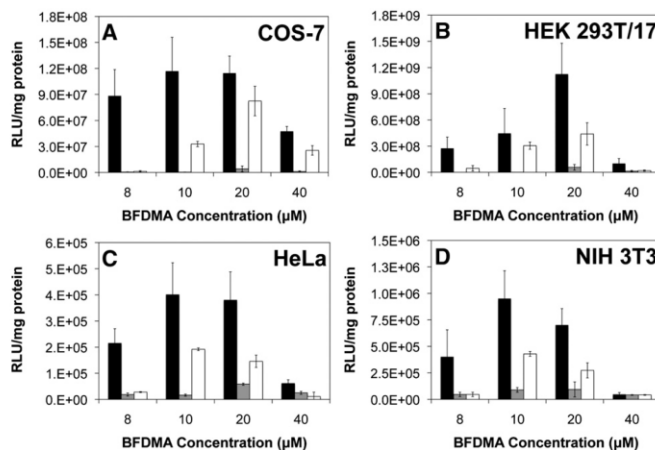


Fig. 4. Normalized luciferase expression mediated by lipoplexes of reduced BFDMA (black bars), lipoplexes of oxidized BFDMA (gray bars), or lipoplexes of oxidized BFDMA treated with AA (white bars) in (A) COS-7, (B) HEK 293T/17, (C) HeLa and (D) NIH 3T3 cell lines.

ability of reduced BFDMA to transfect cells is not limited to transfection of the COS-7 cell line, and (ii) that the large differences in transfection observed between lipoplexes of reduced and oxidized BFDMA are maintained across a more diverse panel of cell types. Finally, these results also reveal that the addition of AA can be used to transform lipoplexes of oxidized BFDMA (gray bars) to lipoplexes (white bars) that are able to mediate significantly higher levels of cell transfection at BFDMA concentrations of 10 and 20 μM .

As described above, the absolute levels of luciferase expression mediated by lipoplexes of reduced BFDMA and lipoplexes of oxidized BFDMA treated with AA varied considerably for each cell type. The data presented in Fig. 4, for example, demonstrate that levels of luciferase expression observed in the COS-7 and HEK 293T/17 cell lines were much higher (on the order of 10^7 – 10^9 RLU/mg protein, depending on BFDMA concentration) compared to levels of expression in HeLa and NIH 3T3 cells (e.g., on the order of 10^5 RLU/mg protein under otherwise identical conditions). These results are consistent with the results of other past studies demonstrating that levels of gene expression in HeLa and NIH 3T3 cells are lower than those in COS-7 and HEK 293T/17 cells [25, 28, 54]. Although many different factors could contribute to these large variations in transgene expression, the higher levels of expression observed in the COS-7 and HEK 293T/17 cells here also likely arise, at least in part, from the fact that these two transformed cell lines express the SV40 large T antigen [55, 56]. Expression of this antigen is known to result in increased expression of gene products of plasmids that contain the SV40 origin of replication (as contained in the two plasmid constructs used in this study) [55]. We note also that these current experiments were designed to investigate and screen the ability of BFDMA to transfect cells over a broad range of lipid concentrations. It is likely, however, that additional optimization studies could lead to formulations and experimental conditions that lead to higher absolute levels of transfection in these four cell types. In the context of this current study, however, we note that the primary significance of the results reported here lies not in comparisons of absolute levels of transgene expression, but in the observations that both (i) the fundamental influence of the redox state of BFDMA on cell transfection and (ii) the ability to chemically transform this redox state in a useful way by treatment with AA are preserved across a broader range of different cell types.

3.3. Characterization of cellular internalization and zeta potentials of lipoplexes of oxidized BFDMA treated with AA

We used laser scanning confocal microscopy (LSCM) and lipoplexes prepared using plasmid DNA labeled with a Cy-5 fluorescent label to characterize differences in the extents to which the lipoplexes reported above were internalized by COS-7 cells. Guided by the results of our transfection experiments, the concentration of BFDMA used in these experiments was 10 μM . The cells were incubated with lipoplexes of (i) reduced BFDMA, (ii) oxidized BFDMA, or (iii) lipoplexes of oxidized BFDMA treated with AA immediately after addition to cells. After a 4 h incubation period, cells were rinsed extensively with a solution of heparin (50 U/ml) to promote the removal of lipoplexes associated with (i.e., bound to) cell membranes. Fig. 5 shows LSCM images of the cells in these experiments. In these images blue, green, red and gray signals correspond to LysoTracker Red (endosome/lysosome stain), WGA-Alexa Fluor 488 (membrane stain), Cy5-labeled DNA, and Hoechst 34580 (nuclear stain), respectively. Membrane-associated red structures correspond to lipoplexes associated with cell membranes that were not removed by rinsing steps mentioned above.

The image in Fig. 5A shows cells incubated with lipoplexes of reduced BFDMA for 4 h. Inspection of this image reveals significant internalization of lipoplexes, and that DNA is present (i) as large aggregates which appear to be associated with the cell membrane (e.g., thick white arrows), (ii) inside the cells either in endosomes and/or lysosomes (e.g., thin white arrows; when blue signal corresponding to endosomes and/or lysosomes is merged with the red signal corresponding to Cy-5 labeled DNA, magenta spots are formed), and (iii) inside cells but not in acidic endosomes and/or lysosomes (e.g., white arrowheads). In contrast, inspection of the representative image in Fig. 5B, corresponding to cells treated with lipoplexes of oxidized BFDMA for 4 h, shows very low levels of internalized DNA (e.g., white arrowhead). The image in Fig. 5C, which corresponds to cells incubated with lipoplexes of oxidized BFDMA that were subsequently treated with AA, reveals high levels of internalized DNA and that the internalized DNA is located either in endosomes and/or lysosomes (e.g., thin white arrows) or in the cytosol (e.g., white arrowheads). A comparison of these results to the image shown in

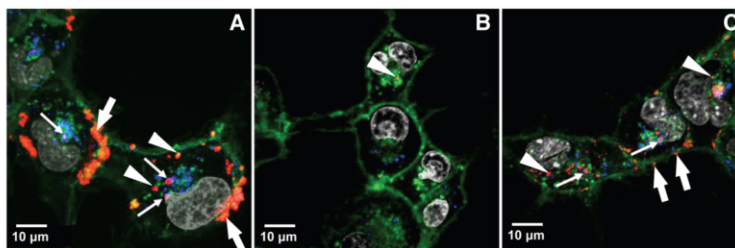


Fig. 5. Representative confocal fluorescence micrographs showing internalization of DNA by COS-7 cells treated with (A) lipoplexes of reduced BFDMA, (B) lipoplexes of oxidized BFDMA or (C) lipoplexes of oxidized BFDMA treated with AA. Fluorescence signals correspond to Lysotracker Red (endosome/lysosome stain; blue signal), WGA-Alexa Fluor 488 (membrane stain; green signal), Cy5 (labeled DNA; red), and Hoechst 34580 (nuclear stain; gray signal). Thick white arrows point to lipoplexes that appear to be associated with cell membranes, thin white arrows point to internalized lipoplexes located in endosomes and/or lysosomes, and white arrow heads point to lipoplexes that are not located in acidic endosomes or lysosomes.

Fig. 5A also reveals that fewer large aggregates are associated with the cell membrane (although several smaller membrane-associated aggregates are observed; Fig. 5C, e.g., white arrows). The results shown in Figs. 5A and B are in general agreement with the results of our past studies [41] and demonstrate that redox state of BFDMA significantly influences levels of cell transfection by changing the extents to which lipoplexes are internalized (or not internalized) by cells. The observation that lipoplexes of oxidized BFDMA treated with AA are internalized readily by cells correlates with the observation of higher levels of transfection (e.g., Figs. 3 and 4) and provides additional support for the view that lipoplexes of oxidized BFDMA can be activated toward transfection by the chemical reduction or transformation of the lipoplexes in the extracellular environment (and prior to internalization by cells).

Past studies have demonstrated that the efficiency with which lipoplexes are internalized by cells tends to increase with increases in the zeta potentials of the lipoplexes [57, 58]. To provide insight into changes in the physical properties of BFDMA lipoplexes that could underlie the changes in internalization and transgene expression described above, we performed a series of experiments to characterize the zeta potentials of BFDMA lipoplexes in Opti-MEM cell culture medium. These experiments were conducted using lipoplexes formed at lipid concentrations and BFDMA/DNA CRs identical to those used in the transfection and internalization experiments described above (i.e., at a BFDMA concentration of 10 μM and at a BFDMA/DNA CR of 1.4:1 and 4.2:1 for lipoplexes of reduced and oxidized BFDMA, respectively).

Table 1 shows the results of zeta potential measurements of either lipoplexes of reduced BFDMA, oxidized BFDMA, or lipoplexes of oxidized BFDMA treated with AA in Opti-MEM cell culture medium. These data reveal that the average zeta potential of lipoplexes of reduced BFDMA (which mediated high levels of internalization and transfection in the above experiments) was approximately -17 mV under these conditions. In contrast, the average zeta potential of lipoplexes of oxidized BFDMA (which were not internalized readily and

did not mediate high levels of cell transfection) was considerably more negative (approximately -34 mV). The average zeta potential of lipoplexes of oxidized BFDMA that were treated with AA (approximately -21 mV), however, was less negative than that of lipoplexes of oxidized BFDMA and, in general, closer in magnitude to that of lipoplexes of reduced BFDMA. We note that while the zeta potentials of lipoplexes of reduced BFDMA and lipoplexes of oxidized BFDMA treated with AA were not measured to be positive under these conditions (e.g., in Opti-MEM), these two types of lipoplexes did result in high levels of transfection and internalization in the experiments above. It is possible that the less-negative zeta potentials of these lipoplexes contribute to more efficient internalization and transfection by facilitating more favorable electrostatic interactions with negatively charged cell membranes, although we note that these current results do not rule out other factors that could lead to differences in internalization. In the section below, we describe the results of other physicochemical and nanostructural characteristics that could also contribute to observed differences in internalization and/or transfection.

3.4. Characterization of lipoplexes using SANS and cryo-TEM

We used SANS and cryo-TEM to provide additional insight into changes in the nanostructures of lipoplexes of oxidized BFDMA that could occur upon the addition of AA. These characterization experiments were performed in Opti-MEM cell culture medium using lipoplexes formulated at BFDMA/DNA CRs used in the transfection analyses described above (i.e., at a BFDMA/DNA CR of 1.1:1 and 3.3:1 for lipoplexes of reduced BFDMA and oxidized BFDMA, respectively). However, as described above in the Materials and Methods section, these experiments were performed at higher overall lipoplex concentrations to obtain sufficient intensities of scattered neutrons in SANS experiments. We note that these CRs do not correspond to those that lead to the highest levels of cell transfection in Fig. 4; these CRs were chosen to permit comparison to the SANS and cryo-TEM results reported in our past study on the characterization of lipoplexes of BFDMA and DNA at these CRs in 1 mM Li_2SO_4 [40]. The results of this past study demonstrated that the nanostructures of lipoplexes of BFDMA did not change substantially as CRs were varied (at least for lipoplexes of reduced BFDMA).

Fig. 6 shows SANS spectra of lipoplexes of reduced BFDMA (solid black triangles), lipoplexes of oxidized BFDMA (solid gray triangles), and lipoplexes of oxidized BFDMA that were treated with AA (open black triangles). The inset in Fig. 6 shows the Bragg peaks observed at $q = 0.12 \text{ \AA}^{-1}$ for these solutions. In both plots, the SANS spectra corresponding to solutions of lipoplexes of oxidized BFDMA and lipoplexes of oxidized BFDMA treated with AA were offset by a scale factor of 1.2 to facilitate comparison to the spectrum of lipoplexes of

Table 1
Zeta potentials of lipoplexes^a.

Sample	Zeta potentials (mV)
Lipoplexes of reduced BFDMA	-16.8 \pm 1.5
Lipoplexes of oxidized BFDMA	-33.7 \pm 1.4
Lipoplexes of oxidized BFDMA treated with AA	-20.6 \pm 1.2

^a Lipoplexes were prepared in Li_2SO_4 solution and then diluted in Opti-MEM cell culture medium so that the final concentration of BFDMA was 10 μM in all cases, and lipid/DNA charge ratios were fixed at 1.4:1 for lipoplexes of reduced BFDMA and 4.2:1 for lipoplexes of oxidized BFDMA. Lipoplexes of oxidized BFDMA were treated with 10-fold molar excess of AA following their dilution into Opti-MEM cell culture medium.

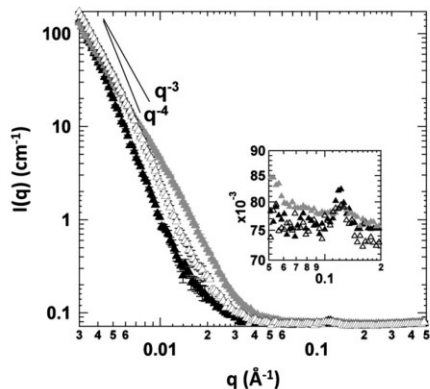


Fig. 6. SANS spectra of lipoplexes of reduced BFDMA (solid black triangles), lipoplexes of oxidized BFDMA (solid gray triangles) or lipoplexes of oxidized BFDMA treated with AA (open black triangles). The inset shows the Bragg peaks observed at 0.12 \AA^{-1} . The data corresponding to solutions of lipoplexes of oxidized BFDMA and lipoplexes of oxidized BFDMA treated with AA were offset by a scale factor of 1.2 to facilitate direct comparison to the SANS spectrum of reduced BFDMA lipoplexes.

reduced BFDMA. The SANS spectrum of the lipoplexes of reduced BFDMA (solid black triangles) exhibits a single peak at $q = 0.12 \text{ \AA}^{-1}$ (see Fig. 6 inset), which corresponds to a nanostructure with a periodicity of 5.2 nm. This periodicity is the same as that determined previously by us to correspond to multi-lamellar complexes of BFDMA and DNA [40], and is consistent with a model (informed by cryo-TEM images; see Fig. 7A, below) in which double-stranded DNA and D_2O (combined thickness of 2.5 nm) are intercalated between lipid bilayers (lipid thickness is estimated to be 2.7 nm). The presence of a single Bragg peak suggests that this periodic nanostructure does not extend over large distances. We also note here that these results obtained in Opti-MEM cell culture medium are similar to SANS results reported previously by our group using lipoplexes of BFDMA prepared in 1 mM Li_2SO_4 (i.e., in the absence of Opti-MEM) [40]. This result indicates that the periodicity of the nanostructure formed by reduced BFDMA and DNA in simple electrolytes is not disrupted by the higher ionic strength and more complex composition of Opti-MEM cell culture medium. Further inspection of the SANS data for these lipoplexes (solid black triangles) in the low q region of the spectrum reveals a q^{-4} dependence that is consistent with the presence of polydisperse multilamellar vesicles [40].

Next, we used SANS to characterize the nanostructures of lipoplexes of oxidized BFDMA in Opti-MEM cell culture medium (Fig. 6, solid gray triangles). For the solutions of lipoplexes of oxidized BFDMA, a Bragg peak with a low intensity was obtained (see Fig. 6 inset, solid gray triangles) at the same value of q (0.12 \AA^{-1}) at which the Bragg peak of the lipoplexes of reduced BFDMA was observed. The low intensity of this Bragg peak suggests that relatively few periodic structures are present in solution and/or that

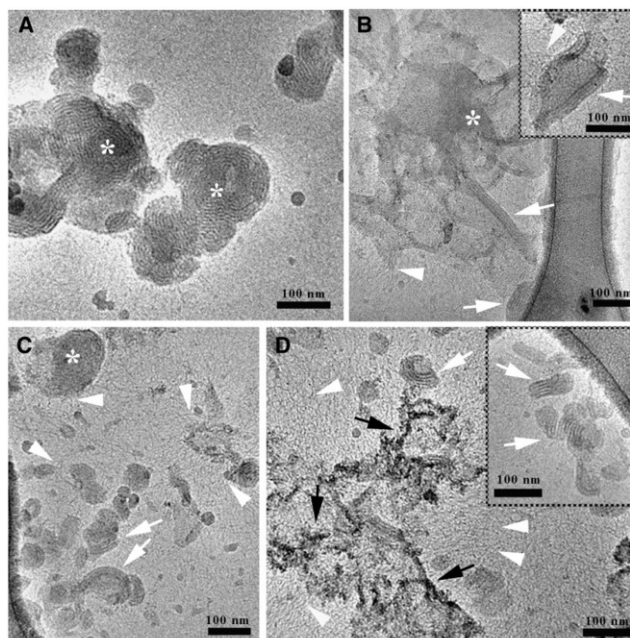


Fig. 7. Cryo-TEM images of (A) lipoplexes of reduced BFDMA (asterisks show onion-like lipoplexes), (B) lipoplexes of oxidized BFDMA (asterisk shows dense amorphous aggregate), or (C,D) lipoplexes of oxidized BFDMA treated with AA in Opti-MEM (asterisk shows onion-like lipoplexes). White arrows point to lamellar structures, arrowheads show DNA threadlike structures, and black arrows indicate high contrast amorphous aggregates.

the range of ordering of the periodic structures is short (as compared to lipoplexes of reduced BFDMA). In our previous study, in which we analyzed lipoplexes of oxidized BFDMA in 1 mM Li_2SO_4 (i.e., in the absence of Opti-MEM), no Bragg peak was observed in the SANS spectrum, indicating the absence of detectable periodic nanostructure in the solutions of the lipoplexes of oxidized BFDMA in 1 mM Li_2SO_4 [40]. However, the development of a Bragg peak for the lipoplexes of oxidized BFDMA in Opti-MEM cell culture medium suggests that the high ionic strength and/or the other components of Opti-MEM promote formation of ordered nanostructures (see cryo-TEM images of lipoplexes of oxidized BFDMA (Fig. 7B), which demonstrates the formation of nanostructures with short range of ordering at the edges of loose aggregate structures). We also note that the SANS spectrum of lipoplexes of oxidized BFDMA in the low q region follows a q dependence of $q^{-2.8}$, consistent with the presence of loose aggregate structures [40, 59]. These data, when combined, suggest that lipoplexes of oxidized BFDMA in Opti-MEM cell culture medium form both loose aggregates and periodic nanostructures with a short range of ordering.

Fig. 6 also shows the SANS spectrum of lipoplexes of oxidized BFDMA that were treated with AA (open black triangles). These data reveal a Bragg peak at the same position as the peak for lipoplexes of reduced or oxidized BFDMA ($q=0.12 \text{ \AA}^{-1}$; see Fig. 6 inset). In contrast to the spectrum observed for lipoplexes of oxidized BFDMA, the height of the Bragg peak following treatment with AA was similar to the height of the Bragg peak observed for lipoplexes of reduced BFDMA. This result suggests that the periodicity of the nanostructures of the lipoplexes of reduced BFDMA and lipoplexes of oxidized BFDMA treated with AA are similar. Furthermore, scattering from lipoplexes of oxidized BFDMA treated with AA in the low q region of the spectrum has a q dependence that is close to $q^{-3.5}$, a dependence that is close to that observed for lipoplexes of reduced BFDMA.

We also performed cryo-TEM experiments to provide complementary insight into differences in the nanostructures of these lipoplexes (Fig. 7). Cryo-TEM characterization of lipoplexes of reduced BFDMA (Fig. 7A) revealed spherically shaped, onion-like multilamellar structures (white asterisks) and a physical picture of the nanostructures of these lipoplexes that was generally consistent with the results of SANS measurements described above. We also observed partially disassociated structures and DNA threadlike structures, however their presence was rare and the majority of the lipoplexes were intact onion-like multilamellar structures with varying numbers of shells per aggregate. The disassociation could result from additional competitive interactions of lipoplexes with components of Opti-MEM cell culture medium. The structural characteristics of the lipoplexes of reduced BFDMA were consistent with the presence of a Bragg peak and also a q dependence of -4 in the low q region in the SANS spectrum of these complexes (Fig. 6, solid black triangles).

Cryo-TEM characterization of lipoplexes of oxidized BFDMA (Fig. 7B) revealed the presence of large amorphous aggregates (asterisk) and few isolated lamellar structures, sometimes located at the edges of these aggregates (white arrows). In general, these results are consistent with the q dependence of -2.8 in the low q region and the presence of a low intensity Bragg peak, respectively, in the SANS spectrum of these lipoplexes. Most of these lamellar structures (composed of 2–3 layers of lamellae) did not form onion-like spheres. We note again that these amorphous nanostructures are different from those observed by cryo-TEM of lipoplexes of oxidized BFDMA in Li_2SO_4 [40] (the cryo-TEM images of lipoplexes of oxidized BFDMA in Li_2SO_4 show predominantly dense amorphous aggregates without any periodic nanostructures). Finally, arrowheads in Fig. 7B point to fuzzy edges of the lamellar aggregates, where DNA threadlike structures emerge. This may also indicate dissociation of DNA from these aggregates in Opti-MEM cell culture medium.

Cryo-TEM images of lipoplexes of oxidized BFDMA treated with AA (Fig. 7C and D) reveal the coexistence of amorphous

structures, multilamellar aggregates, and DNA threadlike structures. The multilamellar aggregates are either non-spherical (Fig. 7C and D; white arrows), or consist of small spherical onion-like structures (Fig. 7C, asterisk). The non-spherical multilamellar structures were composed of several layers of lamellae, and were curved (in contrast to the structures observed in oxidized BFDMA lipoplexes). The presence of multilamellar nanostructures (Fig. 7C and D) is consistent with the presence of a Bragg peak in the SANS spectrum of these lipoplexes. Similar to the samples of lipoplexes of oxidized BFDMA described above, DNA threadlike structures (Fig. 7C and D, arrowheads) were also observed in areas near the lipoplexes. In both cases, we also observed DNA threads dispersed in the solution in areas that did not contain other aggregates (e.g., see Figure S1 of the Supplementary Data). In contrast, the amorphous structures (Fig. 7D, black arrows) observed for lipoplexes of oxidized BFDMA treated with AA differ from those observed in the samples of lipoplexes of oxidized BFDMA; they are less dense, and show better contrast and order.

In conclusion, the results of SANS and cryo-TEM analyses (Figs. 6 and 7) demonstrate that lipoplexes of reduced and oxidized BFDMA, or lipoplexes of oxidized BFDMA treated with AA, form nanostructures with different characteristics in Opti-MEM cell culture medium. The lipoplexes of reduced BFDMA form mostly onion-like multilamellar structures. In contrast, lipoplexes of oxidized BFDMA form mostly amorphous aggregates, although some lamellar structures (composed of 2–3 layers of lamellae) at the edges of the amorphous structures were observed. The formation of these lamellar structures could be triggered by the pH or the components of Opti-MEM, since in our previous cryo-TEM analysis of lipoplexes of oxidized BFDMA in 1 mM aqueous Li_2SO_4 , we did not observe these ordered structures at the edges of amorphous aggregates. Finally, we observed that the treatment of lipoplexes of oxidized BFDMA with AA in Opti-MEM cell culture medium leads to formation of small onion-like and curved multilamellar structures (i.e., a nanostructure that is similar to lipoplexes of reduced BFDMA).

4. Conclusions

We have demonstrated that AA can be used as a chemical reducing agent to activate otherwise inactive lipoplexes of oxidized BFDMA in the presence of cells. Our results establish that treatment with AA results in the rapid reduction of the ferrocenium groups of oxidized BFDMA, and that the resulting lipoplexes of reduced BFDMA mediate significant levels of cell transfection in a panel of several different cell lines (COS-7, HEK 293T/17, HeLa, and NIH 3T3 cell lines). Characterization by confocal microscopy and measurements of the zeta potentials of lipoplexes suggested that the large differences in cell transfection mediated by lipoplexes of oxidized BFDMA and lipoplexes of oxidized BFDMA treated with AA resulted from significant differences in the extents to which these lipoplexes were internalized by cells. Our results also demonstrate that these differences in transfection are a result of changes in the oxidation state of BFDMA that occur in the extracellular environment (that is, prior to the internalization of lipoplexes by cells). Additional characterization by SANS and cryo-TEM measurements revealed changes in the nanostructures of lipoplexes of oxidized BFDMA upon treatment with AA from aggregates that were generally amorphous to aggregates with a more extensive multilamellar nanostructure. When combined, the results of this study provide guidance for the design of redox-active lipids for cell transfection, and provide the basis of an approach for the extracellular activation of lipoplexes that could lead to new methods for exerting spatial and/or temporal control over the transfection of cells *in vitro*.

Acknowledgments

Financial support was provided by the NIH (1 R21 EB006168) and the National Science Foundation (CBET-0754921). We thank Lance

Rodenkirch, and the W. M. Keck Center for Biological Imaging at the UW-Madison for access to and assistance with confocal microscopy facilities. We gratefully acknowledge the support of the Oak Ridge National Laboratory in providing the neutron facilities. The cryo-TEM work was carried out at the Technion Soft Matter Electron Microscopy Laboratory with the financial support of the Technion Russell Berrie Nanotechnology Institute (RBNI).

Appendix A. Supplementary data

Supplementary data to this article can be found online at doi:10.1016/j.jconrel.2011.09.074.

References

- [1] P.L. Felgner, T.R. Gadek, M. Holm, R. Roman, H.W. Chan, M. Wenz, J.P. Northrop, G.M. Ringold, M. Danielsen, Lipofection – a highly efficient, lipid-mediated DNA-transfection procedure, *Proc. Natl. Acad. Sci. U.S.A.* 84 (1987) 7413–7417.
- [2] J. Zabner, Cationic lipids used in gene transfer, *Adv. Drug Deliv. Rev.* 27 (1997) 17–28.
- [3] A.V. Kabanov, P.L. Felgner, L.W. Seymour, Self-assembling complexes for gene delivery: from laboratory to clinical trial, John Wiley and Sons, New York, 1998.
- [4] M.C.P. de Lima, S. Neves, A. Filipe, N. Duzgunes, S. Simoes, Cationic liposomes for gene delivery: from biophysics to biological applications, *Curr. Med. Chem.* 10 (2003) 1221–1231.
- [5] L. Wasungu, D. Hoekstra, Cationic lipids, lipoplexes and intracellular delivery of genes, *J. Control. Release* 116 (2006) 255–264.
- [6] C.T. de Iarduya, Y. Sun, N. Duzgunes, Gene delivery by lipoplexes and polyplexes, *Eur. J. Pharm. Sci.* 40 (2010) 159–170.
- [7] D.D. Lasic, N.S. Templeton, Liposomes in gene therapy, *Adv. Drug Deliv. Rev.* 20 (1996) 221–266.
- [8] S.B. Zhang, Y.M. Xu, B. Wang, W.H. Qiao, D.L. Liu, Z.S. Li, Cationic compounds used in lipoplexes and polyplexes for gene delivery, *J. Control. Release* 100 (2004) 165–180.
- [9] J.G. Lewis, K.Y. Lin, A. Kothavale, W.M. Flanagan, M.D. Matteucci, R.B. DePrince, R.A. Mook, R.W. Hendren, R.W. Wagner, A serum-resistant cytotectin for cellular delivery of antisense oligodeoxynucleotides and plasmid DNA, *Proc. Natl. Acad. Sci. U.S.A.* 93 (1996) 3176–3181.
- [10] J.J. Wheeler, L. Palmer, M. Ossanlou, I. MacLachlan, R.W. Graham, Y.P. Zhang, M.J. Hope, P. Scherrer, P.R. Cullis, Stabilized plasmid-lipid particles: construction and characterization, *Gene Ther.* 6 (1999) 271–281.
- [11] M.F.M. Mustapa, S.M. Grosse, L. Kudsiyova, M. Elbs, E.A. Raiber, J.B. Wong, A.P.R. Brain, H.E.J. Armer, A. Warley, M. Keppler, T. Ng, M.J. Lawrence, S.L. Hart, H.C. Hailes, A.B. Tabor, Stabilized integrin-targeting ternary lipid (lipopolyplex) vectors for gene delivery designed to disassemble within the target cell, *Bioconjug. Chem.* 20 (2009) 518–532.
- [12] B. Wetzter, G. Byk, M. Frederic, M. Airiau, F. Blanche, B. Pitard, D. Scherman, Reducible cationic lipids for gene transfer, *Biochem. J.* 356 (2001) 747–756.
- [13] F.X. Tang, J.A. Hughes, Introduction of a disulfide bond into a cationic lipid enhances transgene expression of plasmid DNA, *Biochem. Biophys. Res. Commun.* 242 (1998) 141–145.
- [14] F.X. Tang, J.A. Hughes, Use of dithiodiglycolic acid as a tether for cationic lipids decreases the cytotoxicity and increases transgene expression of plasmid DNA in vitro, *Bioconjug. Chem.* 10 (1999) 791–796.
- [15] X. Guo, F.C. Szoka, Chemical approaches to triggerable lipid vesicles for drug and gene delivery, *Acc. Chem. Res.* 36 (2003) 335–341.
- [16] Z.H. Huang, W.J. Li, J.A. MacKay, F.C. Szoka, Thiocholesterol-based lipids for ordered assembly of bioresponsive gene carriers, *Mol. Ther.* 11 (2005) 409–417.
- [17] V. Budker, V. Gurevich, J.E. Hagstrom, F. Bortzov, J.A. Wolff, pH-sensitive, cationic liposomes: a new synthetic virus-like vector, *Nat. Biotechnol.* 14 (1996) 760–764.
- [18] O.V. Gerasimov, J.A. Boomer, M.M. Qualls, D.H. Thompson, Cytosolic drug delivery using pH- and light-sensitive liposomes, *Adv. Drug Deliv. Rev.* 38 (1999) 317–338.
- [19] J. Zhu, R.J. Munn, M.H. Nantz, Self-cleaving ortho ester lipids: a new class of pH-vulnerable amphiphiles, *J. Am. Chem. Soc.* 122 (2000) 2645–2646.
- [20] P. Meers, Enzyme-activated targeting of liposomes, *Adv. Drug Deliv. Rev.* 53 (2001) 265–272.
- [21] C.A.H. Prata, Y.X. Zhao, P. Barthelemy, Y.G. Li, D. Luo, T.J. McIntosh, S.J. Lee, M.W. Grinstaff, Charge-reversal amphiphiles for gene delivery, *J. Am. Chem. Soc.* 126 (2004) 12196–12197.
- [22] T. Nagasaki, A. Taniguchi, S. Tamagaki, Photoenhancement of transfection efficiency using novel cationic lipids having a photocleavable spacer, *Bioconjug. Chem.* 14 (2003) 513–516.
- [23] J.A. Wolff, D.B. Rozema, Breaking the bonds: non-viral vectors become chemically dynamic, *Mol. Ther.* 16 (2008) 8–15.
- [24] Y.C. Liu, A.L.M. Le Ny, J. Schmidt, Y. Talmon, B.F. Chmelka, C.T. Lee, Photo-assisted gene delivery using light-responsive cationic vesicles, *Langmuir* 25 (2009) 5713–5724.
- [25] J. Ziauddin, D.M. Sabatini, Microarrays of cells expressing defined cDNAs, *Nature* 411 (2001) 107–110.
- [26] F. Yamauchi, K. Kato, H. Iwata, Micropatterned, self-assembled monolayers for fabrication of transfected cell microarrays, *Biochim. Biophys. Acta, Gen. Subj.* 1672 (2004) 138–147.
- [27] F.H. Chang, C.H. Lee, M.T. Chen, C.C. Kuo, Y.L. Chiang, C.Y. Hang, S. Roffler, Surfacection: a new platform for transfected cell arrays, *Nucleic Acids Res.* 32 (2004) e33.
- [28] M. Isalan, M.L. Santori, C. Gonzalez, L. Serrano, Localized transfection on arrays of magnetic beads coated with PCR products, *Nat. Methods* 2 (2005) 113–118.
- [29] A.L. Hook, H. Thissen, N.H. Voelcker, Advanced substrate fabrication for cell microarrays, *Biomacromolecules* 10 (2009) 573–579.
- [30] W.M. Saltzman, Delivering tissue regeneration, *Nat. Biotechnol.* 17 (1999) 534–535.
- [31] L.D. Shea, E. Smiley, J. Bonadio, D.J. Mooney, DNA delivery from polymer matrices for tissue engineering, *Nat. Biotechnol.* 17 (1999) 551–554.
- [32] J.A. Shepard, A. Huang, A. Shikanov, L.D. Shea, Balancing cell migration with matrix degradation enhances gene delivery to cells cultured three-dimensionally within hydrogels, *J. Control. Release* 146 (2010) 128–135.
- [33] F. Yang, S.W. Cho, S.M. Son, S.R. Bogatyrev, D. Singh, J.J. Green, Y. Mei, S. Park, S.H. Bhang, B.S. Kim, R. Langer, D.G. Anderson, Genetic engineering of human stem cells for enhanced angiogenesis using biodegradable polymeric nanoparticles, *Proc. Natl. Acad. Sci. U.S.A.* 107 (2010) 3317–3322.
- [34] Y. Kakizawa, H. Sakai, K. Nishiyama, M. Abe, H. Shoji, Y. Kondo, N. Yoshino, Solution properties of double-tailed cationic surfactants having ferrocenyl groups in their hydrophobic moieties, *Langmuir* 12 (1996) 921–924.
- [35] N. Yoshino, H. Shoji, Y. Kondo, Y. Kakizawa, H. Sakai, M. Abe, Syntheses of cationic surfactants having two ferrocenylalkyl chains, *J. Jpn. Oil Chem. Soc.* 45 (1996) 769–775.
- [36] Y. Kakizawa, H. Sakai, A. Yamaguchi, Y. Kondo, N. Yoshino, M. Abe, Electrochemical control of vesicle formation with a double-tailed cationic surfactant bearing ferrocenyl moieties, *Langmuir* 17 (2001) 8044–8048.
- [37] N.L. Abbott, C.M. Jewell, M.E. Hays, Y. Kondo, D.M. Lynn, Ferrocene-containing cationic lipids: Influence of redox state on cell transfection, *J. Am. Chem. Soc.* 127 (2005) 11576–11577.
- [38] C.M. Jewell, M.E. Hays, Y. Kondo, N.L. Abbott, D.M. Lynn, Ferrocene-containing cationic lipids for the delivery of DNA: oxidation state determines transfection activity, *J. Control. Release* 112 (2006) 129–138.
- [39] M.E. Hays, C.M. Jewell, Y. Kondo, D.M. Lynn, N.L. Abbott, Lipoplexes formed by DNA and ferrocenyl lipids: effect of lipid oxidation state on size, internal dynamics, and zeta-potential, *Biophys. J.* 93 (2007) 4414–4424.
- [40] G.L. Pizzey, C.M. Jewell, M.E. Hays, D.M. Lynn, N.L. Abbott, Y. Kondo, S. Colan, Y. Talmon, Characterization of the nanostructure of complexes formed by a redox-active cationic lipid and DNA, *J. Phys. Chem. B* 112 (2008) 5849–5857.
- [41] C.M. Jewell, M.E. Hays, Y. Kondo, N.L. Abbott, D.M. Lynn, Chemical activation of lipoplexes formed from DNA and a redox-active, ferrocene-containing cationic lipid, *Bioconjug. Chem.* 19 (2008) 2120–2128.
- [42] T. Saji, K. Hoshino, S. Aoyagui, Reversible formation and disruption of micelles by control of the redox state of the head group, *J. Am. Chem. Soc.* 107 (1985) 6865–6868.
- [43] B.S. Gallardo, M.J. Hwa, N.L. Abbott, In-situ and reversible control of the surface-activity of ferrocenyl surfactants in aqueous-solutions, *Langmuir* 11 (1995) 4209–4212.
- [44] D.E. Bennett, B.S. Gallardo, N.L. Abbott, Dispensing surfactants from electrodes: Marangoni phenomenon at the surface of aqueous solutions of [11-ferrocenylnonyl]trimethylammonium bromide, *J. Am. Chem. Soc.* 118 (1996) 6499–6505.
- [45] B.S. Gallardo, V.K. Gupta, F.D. Egerton, L.L. Jong, V.S. Craig, R.R. Shah, N.L. Abbott, Electrochemical principles for active control of liquids on submillimeter scales, *Science* 283 (1999) 57–60.
- [46] C.A. Rosslee, C. Khripin, T.M.D. Foley, N.L. Abbott, Using “prosurfactants” to enhance rates of delivery of surfactants, *AIChE J.* 50 (2004) 708–714.
- [47] A. Meister, M.E. Anderson, Glutathione, *Annu. Rev. Biochem.* 52 (1983) 711–760.
- [48] F.Q. Schafer, G.R. Buettner, Redox environment of the cell as viewed through the redox state of the glutathione disulfide/glutathione couple, *Free Radic. Biol. Med.* 30 (2001) 1191–1212.
- [49] G. Banhegyi, L. Braun, M. Csala, F. Puskas, J. Mandl, Ascorbate metabolism and its regulation in animals, *Free Radic. Biol. Med.* 23 (1997) 793–803.
- [50] A. Guinier, G. Fournet, *Small Angle X-Ray Scattering*, John Wiley & Sons, New York, 1955.
- [51] J.R. Bellare, H.T. Davis, L.E. Scriven, Y. Talmon, Controlled environment vitrification system – an improved sample preparation technique, *J. Electron Microsc. Tech.* 10 (1988) 87–111.
- [52] D. Danino, A. Bernheim-Groszasser, Y. Talmon, Digital cryogenic transmission electron microscopy: an advanced tool for direct imaging of complex fluids, *Colloids Surf. A: Physicochem. Eng. Asp.* 183 (2001) 113–122.
- [53] E.V.B. van Gaal, R. van Eijk, R.S. Oosting, R.J. Kok, W.E. Hennink, D.J.A. Crommelin, E. Mastrobattista, How to screen non-viral gene delivery systems in vitro? *J. Control. Release* 154 (2011) 218–232.
- [54] J.P. Vigneron, N. Oudrhiri, M. Fauquet, L. Vergely, J.C. Bradley, M. Basseville, P. Lehn, J.M. Lehn, Guanidinium-cholesterol cationic lipids: efficient vectors for the transfection of eukaryotic cells, *Proc. Natl. Acad. Sci. U.S.A.* 93 (1996) 9682–9686.
- [55] Y. Gluzman, SV40-transformed simian cells support the replication of early SV40 mutants, *Cell* 23 (1981) 175–182.
- [56] W.S. Pear, G.P. Nolan, M.L. Scott, D. Baltimore, Production of high-titer helper-free retroviruses by transient transfection, *Proc. Natl. Acad. Sci. U.S.A.* 90 (1993) 8392–8396.

- [57] E. Tomlinson, A.P. Rolland, Controllable gene therapy – pharmaceuticals of non-viral gene delivery systems, *J. Control. Release* 39 (1996) 357–372.
- [58] F. Sakurai, R. Inoue, Y. Nishino, A. Okuda, O. Matsumoto, T. Taga, F. Yamashita, Y. Takakura, M. Hashida, Effect of DNA/liposome mixing ratio on the physicochemical characteristics, cellular uptake and intracellular trafficking of plasmid DNA/cationic liposome complexes and subsequent gene expression, *J. Control. Release* 66 (2000) 255–269.
- [59] M. Cardenas, C.A. Dreiss, T. Nylander, C.P. Chan, T. Cosgrove, B. Lindman, SANS study of the interactions among DNA, a cationic surfactant, and polystyrene latex particles, *Langmuir* 21 (2005) 3578–3583.